

# DISTINCTIVE

1<sup>st</sup> Annual Meeting, Millennium Gallery, Sheffield, UK

15<sup>th</sup> – 16<sup>th</sup> April 2015

## DISTINCTIVE

Decommissioning,  
Immobilisation and  
Storage solutions for  
NuClear waste InVENTories

A university consortium funded  
by the Research Councils  
UK Energy programme



**A university consortium funded by the:**



**Thank you to our key project partners for their support and significant contribution to the programme:**



**A special thank you to our event sponsors:**



Nuclear  
Decommissioning  
Authority



# Welcome

On behalf of the DISTINCTIVE Leadership Team, I welcome you to the Millennium Gallery, Sheffield, for the 1<sup>st</sup> Annual Meeting of the University Consortium.

DISTINCTIVE (Decommissioning, Immobilisation and Storage solutions for Nuclear waste Inventories) was formed following a call for proposals in the area of “Decommissioning, Immobilisation and Management of Nuclear Waste” from the Engineering and Physical Sciences Research Council in May 2013. I would like to take this opportunity to acknowledge funding from the Research Councils UK Energy Programme (EP/L014041/1). I would also like to thank our key project partners, NNL, NDA and Sellafield Ltd., for their support and significant contribution to the project through the sponsorship of PhD students.

The programme follows on from the highly successful DIAMOND Consortium, which ran from August 2008 to March 2013. Again, DISTINCTIVE is led by the University of Leeds, and our partners now include Lancaster University, University of Bristol, University of Strathclyde and University of Birmingham, in addition to Imperial College London, University of Manchester, University of Sheffield, Loughborough University and University College London. This broadened academic collaboration strengthens the UK’s nuclear research capability, and increases the multi-disciplinary nature of the project group.

The challenge of decommissioning and nuclear waste management is highly complex and requires a diverse range of skills and knowledge to be brought together. Over the duration of the programme, we will train the next generation of nuclear researchers so that they have the expertise and skill set that are required in the civil nuclear industry to address these issues.

The consortium has grown significantly since it started in February 2014. It now links 47 research projects (10 PDRA, 22 original PhD and 15 associated PhD) across four technical themes. We believe that our R&D community, including academics with a track-record of innovation and problem solving, is unrivalled both within the UK and internationally. As such, we aim to establish the UK industry as a leader in the nuclear waste management and decommissioning field.

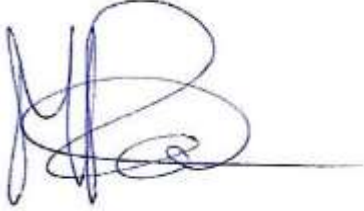
Industrial engagement remains a priority of the consortium, and it’s great to see so many supporters of the DIAMOND consortium at this event. We welcome our new guests and hope that you find the event invaluable for exploring how links between DISTINCTIVE and your organisation can be formed for mutual benefit.

Over the next two days you will gain an improved personal knowledge of the individual research projects and their importance to the UK’s nuclear decommissioning programme. Please take the opportunity to foster existing relationships, and to form new ones by interacting with representatives from academia, industry, government and the regulatory authorities.

I look forward to introducing you to our Keynote Speakers, Prof. Eric McFarland (University of Queensland, Australia) and Prof. Ian Pegg (Catholic University of America, USA) and thank them for contributing to this event. Thank you also to representatives from our industry partners, NNL, NDA and Sellafield Ltd., for agreeing to open and chair our technical sessions.

Finally, I would like to say a special thank you to our event sponsors, NNL and NDA, for their ongoing support to the consortium. Please take the opportunity to meet with them throughout the event.

I hope that you enjoy the event.

A handwritten signature in blue ink, appearing to be 'MF', with a horizontal line extending to the right.

Prof. Michael Fairweather

Principal Investigator



**DISTINCTIVE**

[www.distintiveconsortium.org](http://www.distintiveconsortium.org)

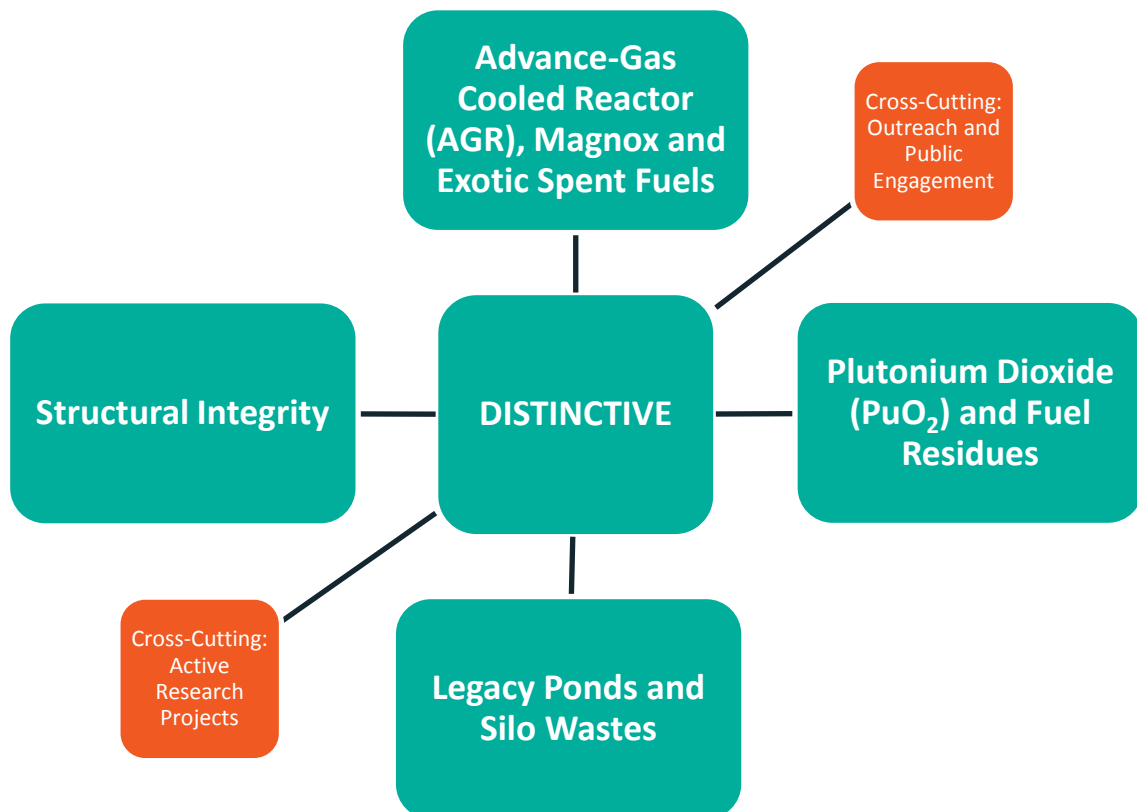
# Programme Overview

The structure of this world-class research programme has been aligned with the strategic needs of the UK industry in the area of nuclear waste management and decommissioning.

The aims of the consortium are:

- To carry out internationally leading science and engineering research in the area of decommissioning and nuclear waste management.
- To support research that provides routes to innovative technology developments that can be applied to decommissioning and nuclear waste management.
- To foster and develop new multi-disciplinary research partnerships between academic and industry researchers.
- To train the next generation of UK researchers, equipping them with skills and experiences relevant to nuclear waste management and decommissioning issues.
- To provide a focal point for government, industry and academics through which current and future R&D issues associated with nuclear waste and decommissioning can be discussed.
- To provide a route for public understanding of the underlying research and development needs opportunities and solutions to nuclear waste and decommissioning.

All 47 research projects fall into one of four technical themes which were co-identified with our industrial partners; NNL, NDA and Sellafield Ltd.



## Theme 1 - AGR, Magnox and Exotic Spent Fuels

**Aim:** To provide technical underpinning to the options for the management of the UK's AGR, Magnox and Exotic Spent Fuels

**Objectives:**

- To understand the evolution of Magnox and exotic SNF during recovery from aqueous storage, drying and repackaging.
- To develop spectroscopic methods for improved determination of SNF dissolution and corrosion rates in water.
- To determine the optimum drying conditions for AGR fuels and the subsequent surface reactivity and alteration of unclad UO<sub>2</sub> in dry storage.
- To determine the consequences of radiation damage in SNF, cladding and other wastefoms for safe long term storage.
- To determine suitable waste management options for spent carbide fuels.

## Theme 2 – PuO<sub>2</sub> and Fuel Residues

**Aim:** To provide technical underpinning to the options for the UK's civil Plutonium inventory

**Objectives:**

- To understand how the structure and properties of PuO<sub>2</sub> change with time in the presence of H<sub>2</sub>O.
- To understand the roles these processes play in gaseous product evolution from PuO<sub>2</sub> in storage.
- To understand radiation induced amorphisation and dissolution kinetics of Pu wastefoms.
- To develop novel, fast neutron based radiometric methods for the quantification, isotopic composition assessment and remote imaging of Pu bearing materials.

## Theme 3 – Legacy Ponds and Silo Wastes

**Aim:** To develop innovative technical approaches to clean up UK legacy wastes.

**Objectives:**

- To understand durability of heterogeneous ILW glass/ceramic wastefoms from LP&S wastestreams.
- To develop improved ways to remove radionuclides (RNs) from solution, both novel inorganic ion exchange solids and tailored binding superparamagnetic nanoparticles, to treat complex and variable effluents.
- To develop new micro- and ultra-filtration methods for use with sludges.
- To provide three-dimensional modelling and simulation for sludge disturbance, mobilisation and transport, with supportive experimental studies, and manipulation planning for removing corroding nuclear materials.

- To develop a better understanding of gas hold-up in sludges.
- To develop improved techniques for remote monitoring of sludges and heterogeneous wastes.

## Theme 4 – Structural Integrity

**Aim:** To develop reliable systems for infrastructure characterisation, restoration and preservation, that minimise current, and future, radiation exposure to the workforce whilst providing economically viable technological solutions.

### Objectives:

- To develop in-situ ground barriers that could act as a ‘second skin’ surrounding on-site structures, such as silos and ponds, for prevention of subsurface radionuclide migration.
- To develop smart solutions for remote crack detection, infrastructure health prediction and building preservation that can be retrofitted to existing sites.
- To develop autonomous systems with increased functionality and to coordinate them through a CAD-based real-time management system, to facilitate planning and execution of decommissioning works.

## Cross-Cutting Themes

The Leadership Team will continue to identify common themes across the research projects to maximise collaboration, training and knowledge/technology transfer across the consortium.

Two cross-cutting themes currently exist; Active Research Projects, and Outreach and Public Engagement.

### Active Research Projects

A key component of the DISTINCTIVE programme is the use of world-class active research facilities, both within the UK and internationally. Prof. Simon Pimblott is responsible for ensuring that the consortium receives excellent advice and support in this area, especially relating to the technical needs and duration of the work.

### Outreach and Public Engagement

The consortium has identified three distinct groups of non-academic beneficiaries from consortium activities; site license companies and the associate industrial supply chain; Government, regulators and implementation authorities; and, society and stakeholders groups. Over the duration of the programme, DISTINCTIVE will deliver a variety of activities, led by Prof. Neil Hyatt, which will have impact in four key domains:

- Knowledge
- People
- Economy
- Society

## The Leadership Team

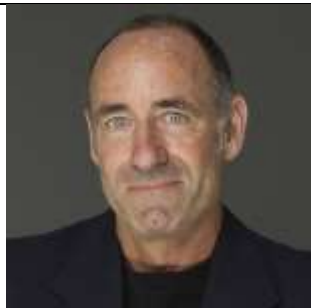
	<p><b>Prof. Michael Fairweather</b> Principal Investigator</p>		<p>School of Chemical and Process Engineering University of Leeds +44 (0)113 3432419 m.fairweather@leeds.ac.uk</p>
	<p><b>Dr Tom Scott</b> Theme 1 Lead</p>		<p>School of Physics University of Bristol +44 (0) 117 3311176 t.b.scott@bristol.ac.uk</p>
	<p><b>Dr Nick Evans</b> Theme 1 Lead</p>		<p>Department of Chemistry Loughborough University +44 (0) 1509 222564 N.D.M.Evans@lboro.ac.uk</p>
	<p><b>Prof. Colin Boxall</b> Theme 2 Lead</p>		<p>Department of Engineering Lancaster University +44 (0)1524 593109 c.boxall@lancaster.ac.uk</p>
	<p><b>Prof. Nik Kaltsoyannis</b> Theme 2 Lead</p>		<p>Department of Chemistry University College London +44 (0)20 7679 4670 n.kaltsoyannis@ucl.ac.uk</p>

## The Leadership Team

	<p><b>Prof. Bill Lee</b> Theme 3 Lead</p>		<p>Department of Materials Imperial College London +44 (0)20 7594 6733 w.e.lee@imperial.ac.uk</p>
	<p><b>Dr Joe Hriljac</b> Theme 3 Lead</p>		<p>School of Chemistry University of Birmingham +44 (0) 121 414 4458 j.a.hriljac@bham.ac.uk</p>
	<p><b>Prof. Rebecca Lunn</b> Theme 4 Lead</p>		<p>Department of Civil and Environmental Engineering University of Strathclyde +44 (0)141 548 2826 rebecca.lunn@strath.ac.uk</p>
	<p><b>Prof. Simon Pimblott</b> Cross-Cutting Champion – Active Research Projects</p>		<p>School of Chemistry University of Manchester +44 (0) 161 275 1325 simon.pimblott@manchester.ac.uk</p>
	<p><b>Prof. Neil Hyatt</b> Cross-Cutting Champion – Outreach and Public Engagement</p>		<p>Department of Materials Science and Engineering University of Sheffield +44 (0) 114 222 5470 n.c.hyatt@sheffield.ac.uk</p>

## Introducing the Keynote Speakers

### **Prof. Eric McFarland (The University of Queensland, Australia)**



Prof. Eric McFarland studied nuclear engineering at MIT where he received his PhD. He was a Professor of Nuclear Engineering at MIT and Chemical Engineering at the University of California, Santa Barbara. McFarland is presently the Director of the Dow Centre for Sustainable Engineering Innovation at the University of Queensland and the Dow Chemical Chair, Professor of Chemical Engineering. Eric has an international reputation for his research, which over the last ten years has been in catalysis and fundamental chemical science related to energy and chemical conversions. Eric has worked extensively with industry and has started and led several technology companies based on university research, among them Symyx Technologies and Gas Reaction Technologies.

### **Prof. Ian I. Pegg (Catholic University of America, USA)**



Dr. Ian L. Pegg is Professor of Physics and Director of the Vitreous State Laboratory (VSL) at The Catholic University of America. His research has spanned various areas of materials science including the optimization of processes and glass compositions for use in nuclear waste disposal, geopolymers, nano-materials, and thermoelectrics. Dr. Pegg has led numerous vitrification R&D programs involving the development and characterization of glass formulations and the demonstration and scale-up of Joule-heated melting processes. Dr. Pegg has served as a technical team member on several successful multi-billion-dollar treatment facility proposals, including the WTP privatization at Hanford and the AMWTP privatization at Idaho. Dr. Pegg directs the Hanford WTP vitrification research and technology support effort at VSL, which supports the design, construction, and operation of what will be the world's largest nuclear waste vitrification facility. Dr. Pegg also directs similar R&D efforts for the Defense Waste Processing Facility at the Savannah River Site and for the Rokkasho vitrification facility at Rokkasho, Japan. Dr. Pegg has been a frequent participant on expert review teams for the US Department of Energy. He is the co-founder of three advanced materials companies. He previously held positions at the National Institute for Standards and Technology and in the Department of Chemistry and Biochemistry at UCLA. He holds a PhD in physical chemistry from The University of Sheffield as well as MBA and BSc degrees.

## PhD Student Awards

A £250 prize will be awarded for best oral and best poster presentation given by a DISTINCTIVE PhD student.

Our industry delegates (only) are invited to register their vote at the Reception Desk by **14:55 on Thursday 16<sup>th</sup> April**. A voting sheet can be collected from the desk (or from Abby Ward) at any time.

The awards for each category will be presented by Rick Short on behalf of the NDA, who kindly sponsored these awards, at the end of the event.



# Agenda

Wednesday 15 <sup>th</sup> April		
Time	Title	Presenter
10:00	Delegate Registration, Poster Board Set Up, Coffee/Tea/Pastries	
11:00	Introduction and Housekeeping	Michael Fairweather ( <i>Session Chair</i> ) University of Leeds
11:20	Chemicals: Creating a Compelling Nuclear Value Proposition Through Co-production	Prof. Eric McFarland University of Queensland
<b>Theme 1 - AGR, Magnox and Exotic Spent Fuels</b>		
12:00	Decisions, Decisions... How Research Supports the NDA's Spent Fuel Strategies	Danny Fox ( <i>Session Chair</i> ) NDA
12:20	Layers of Complexity; A Thin Film Approach to Spent Nuclear Fuel	James Darnbrough (PDRA) University of Bristol
12:40	Lunch, Coffee/Tea/Juice, Posters	
13:40	Corrosion of Nuclear Fuel: Radiolysis Driven Dissolution at the UO <sub>2</sub> /Water Interface	Sophie Rennie (PhD) University of Bristol
14:00	Uranium Measurements by Time Resolved Laser Induced Fluorescence Spectroscopy	Oliver Preedy (PDRA) Loughborough University
<b>Theme 2 – PuO<sub>2</sub> and Fuel Residues</b>		
14:20	PuO <sub>2</sub> Storage - Chemistry in a Can. What Does the Industry Need?	Howard Sims ( <i>Session Chair</i> ) NNL
14:40	CaUTi <sub>2</sub> O <sub>7</sub> Ceramics for Actinide Disposition	Shi-Kuan Sun (PDRA) University of Sheffield
15:00	The Development of Glass-Ceramic Wasteforms by Hot Isostatic Pressing for Actinide Immobilisation	Stephanie Thornber (PhD) University of Sheffield
15:20	Afternoon Break, Coffee/Tea/Biscuits, Posters	
15:50	Crystal Microbalance Investigation of the Interaction of Water with Plutonium Oxide Analogues	Dominic Laventine (PDRA) Lancaster University
16:10	Towards Water Adsorption on Actinide Oxide Surfaces	Bengt Tegner (PDRA) UCL
<b>Cross-Cutting Themes</b>		
16:30	Engagement and Impact with a Distinctive Edge	Neil Hyatt ( <i>Session Chair</i> ) University of Sheffield
16:50	An Overview of the U.S. Department of Energy's Office of Environmental Management	Rodrigo Rimando U.S. Department of Energy

17:10	A Life Cycle Approach as a Decision Tool for Nuclear Waste Management	Andrea Paulillo (PhD) UCL
17:30	Break	
18:30	Drinks and Canapé Reception	
19:30	Evening Dinner	
22:00	End of Day	

<b>Thursday 16th April</b>		
<b>Time</b>	<b>Title</b>	<b>Presenter</b>
9:00	Delegate Registration, Poster Board Set Up, Coffee/Tea/Pastries	
9:30	Introduction and Housekeeping	Michael Fairweather ( <i>Session Chair</i> ) University of Leeds
9:40	Overview of Immobilization R&D Programs at the Vitreous State Laboratory	Prof. Ian I. Pegg Catholic University of America
<b>Theme 3 – Legacy Ponds and Silo Wastes</b>		
10:20	Legacy Ponds and Silos – Key Challenges for Waste Disposal	Cristiano Padovani ( <i>Session Chair</i> ) RWM NDA
10:40	In-line Rheometry and Flow Characterisation in Pipe Flow Using Acoustic Methods	Hugh Rice (PDRA) University of Leeds
11:00	Morning Break, Coffee/Tea/Biscuits, Posters	
11:30	Study of Glass Degradation in a Simulated Crack	Chinnam Krishna (PDRA) Imperial College London
11:50	Enhanced Shear Microfiltration	Keith Schou (PhD) Loughborough University
12:10	Novel Ion Exchange Materials	Evin Chen (PDRA) University of Birmingham
12:30	Lunch, Coffee/Tea/Juice, Posters	
<b>Theme 4 – Structural Integrity</b>		
13:30	Structural Integrity - A Nuclear Licensed Site Perspective	John Riding ( <i>Session Chair</i> ) Sellafield Ltd.
13:50	In situ Monitoring and Characterisation of the Radioactive Sludge in the Legacy Ponds and Silos at Sellafield	Olusola Ayoola (PhD) University of Manchester

14:10	Novel Nanoparticle Cement for Crack Sealing and Water Transport	Riccardo Maddalena (PhD) University of Strathclyde
14:30	Afternoon Break, Coffee/Tea/Biscuits, Posters	
15:00	Use of Colloidal Silica Ground Barriers in Decommissioning	Matteo Pedrotti (PDRA) University of Strathclyde
15:20	NDA PhD Student Awards  Closing Remarks	 Rick Short NDA Michael Fairweather University of Leeds
15:40	End of Day	

Shaded name = eligible for the £250 prize for best oral presentation given by a **DISTINCTIVE PhD** student.

**All presentations will be made available to download from our consortium website:**

**<http://distinctiveconsortium.org/category/events/1st-annual-meeting/>**

# Posters

The following posters will be presented throughout the event:

Poster Number	Researcher	Poster Title	Leading Institution
1	James Edward Darnbrough	Thin Film Investigation of Spent Nuclear Fuel	Bristol
2	Sophie Rennie	Corrosion of Nuclear Fuel: Radiolysis Driven Dissolution at the UO <sub>2</sub> /Water Interface	Bristol
3	Elizabeth Howett	The Behaviour of Used Nuclear Fuel in Wet Storage	Lancaster
4	James Goode	Transitioning of Spent AGR Fuel from Wet to Dry Storage	Leeds
5	Oliver Preedy	The Retardation of Uranium by Nirex Reference Vault Backfill (NRVB)	Loughborough
6	Chiara Barcellini	Grain Boundary Damage Mechanisms in Strained AGR Cladding Under Irradiation	Manchester
7	Andrea Paulillo	A Life Cycle Approach as a Decision Tool for Nuclear Waste Management and Plant Decommissioning	UCL
8	Rashed Sarwar	Real-time Fast Neutron Plutonium Assay for Plutonium Storage and Ageing Applications	Lancaster
9	Dominic Laventine	Crystal Microbalance Investigation of the Interaction of Water with Plutonium Oxide Analogues	Lancaster
10	Sophie Sutherland-Harper	Contaminating Ceria with Chloride - An Analysis by X-Ray Diffraction and X-Ray Photoelectron Spectroscopy	Manchester
11	Shi-Kuan Sun	CaUTi <sub>2</sub> O <sub>7</sub> Ceramics for Actinide Disposition	Sheffield
12	Stephanie Thornber	Optimisation of Zirconolite Actinide Glass-Ceramics Consolidated by Hot Isostatic Pressing	Sheffield
13	Bengt Tegner	Towards Water Adsorption on Actinide Oxide Surfaces	UCL
14	Joseph Wellington	Computational Studies of Water Adsorption on UO <sub>2</sub> and PuO <sub>2</sub>	UCL
15	Ryan George	New Materials for Caesium and Strontium Waste Removal: Synthesis of Phosphate Ion-exchangers	Birmingham
16	George Day	Synthesis of Barium Doped Cs <sub>2</sub> TiNb <sub>6</sub> O <sub>18</sub> - A New Cs-Waste Form	Birmingham
17	Evin (Tzu-Yu) Chen	Novel Ion Exchanger Materials	Birmingham
18	Kate Wyness	Applications of Raman Spectroscopy for Nuclear Waste Characterisation	Bristol
19	Chinnam Rama Krishna	Study of Glass Degradation in a Simulated Crack	Imperial
20	Dimitri Pletser	Immobilisation Process for Contaminated Zeolitic Ion	Imperial

		Exchangers From Fukushima	
21	Charles Hutchison	Durability Study of a Glass Composite Material for Intermediate Level Waste Disposal	Imperial
22	Eleonora Cali	Nanoscale Investigation and Control of Radionuclides in Waste Management	Imperial
23	Olivia Lynes	Ab initio Molecular Dynamics Simulations of Strontium Hydrates	Lancaster
24	Michael Johnson	Gas Retention and Release from Nuclear Legacy Waste	Leeds
25	Hugh Rice	In-line Rheometry and Flow Characterisation of Dense Slurries in Pipe Flow Using Acoustic Methods	Leeds
26	Andre Botha	Quartz Crystal Microbalance as a Method to Characterise Sludge Rheology	Leeds
27	Keith Schou	Shear Enhanced Micro-Filtration Through Filter Oscillation	Loughborough
28	Laura Mayne	Characterisation of Silica Modified Nanoparticles Using Tunable Resistive Pulse Sensing for Metal Sequestration	Loughborough
29	Mel O'Leary	Irradiation of Sludge Mimics	Queens University Belfast
30	Conrad Johnston	Determination of Hydrogen Production from Legacy Fuel Storage Pond Sludges Through Molecular Modelling	Queens University Belfast
31	Luke Boast	Thermal Treatment of Plutonium Contaminated Material (PCM) Waste	Sheffield
32	Toby Lord	The Impact of Recycled Concrete Fines on the Engineering Performance of Cementitious Infill	Leeds
33	Olusola Ayoola	In situ Monitoring and Characterisation of the Radioactive Sludge in the Legacy Ponds and Silos at Sellafield	Manchester
34	Riccardo Maddalena	Novel Nanoparticle Cement for Crack Sealing	Strathclyde
35	Matteo Pedrotti	Use of Colloidal Silica Ground Barriers in Decommissioning	Strathclyde
36	Christopher Wong	An Electro-chemical Model and Experimental Validation of Silica Gelling	Strathclyde

Shaded name = eligible for the £250 prize for best poster presentation given by a **DISTINCTIVE PhD** student.

## Attendee List

First Name	Second Name	Organisation
Ian	Adsley	Nuvia Ltd.
Sean	Amos	AWE plc
Mike	Angus	National Nuclear Laboratory
Olusola	Ayoola	University of Manchester
Chiara	Barcellini	University of Manchester
Simon	Biggs	University of Queensland
Luke	Boast	University of Sheffield
Gary	Bolton	National Nuclear Laboratory
Johannes	Botha	University of Leeds
Colin	Boxall	Lancaster University
Jon	Brooking	Atkins
Gunnar	Buckau	European Commission
Ed	Butcher	National Nuclear Laboratory
Eleonora	Cali	Imperial College London
Tzu-Yu (Evin)	Chen	University of Birmingham
Warren	Cook	acQuire Technology Solutions
Claire	Corkhill	University of Sheffield
Fred	Currell	Queen's University Belfast
James	Darnbrough	University of Bristol
George	Day	University of Birmingham
John	Day	University of Bristol
Carlos	De La Fontaine	Nuclear Technologies
Peter	Dore	Jacobs
Michael	Edmondson	National Nuclear Laboratory
Grainne	El Mountassir	University of Strathclyde
Nick	Evans	Loughborough University
Michael	Fairweather	University of Leeds
Danny	Fox	NDA
Ryan	George	University of Birmingham
Steve	Graham	National Nuclear Laboratory
David	Hambley	National Nuclear Laboratory
Andrea	Hamilton	University of Strathclyde
Bruce	Hanson	University of Leeds
David	Harbottle	University of Leeds
Mike	Harrison	National Nuclear Laboratory
Marika	Hietala	University of Sheffield
Joanne	Hill	Amec Foster Wheeler
Jeff	Hobbs	Sellafield Ltd.
Elizabeth	Howett	Lancaster University
Joseph	Hriljac	University of Birmingham
Karl	Hughes	Cavendish Nuclear
Richard	Hunter	LLW Repository Ltd.

Tim	Hunter	University of Leeds
Charlie	Hutchison	Imperial College London
Neil	Hyatt	University of Sheffield
Enrique	Jimenez-melero	University of Manchester
Conrad	Johnston	Queen's University Belfast
Carwyn	Jones	Nuclear Technologies
Malcolm	Joyce	Lancaster University
Laurie	Judd	NuVision Engineering
Nik	Kaltsoyannis	University College London
Debbie	Keighley	Sellafield Ltd.
Simon	Kellet	Sellafield Ltd.
Jorge	Kohanoff	Queen's University Belfast
Chinnam	Krishna	Imperial College London
Dominic	Laventine	Lancaster University
Barry	Lennox	University of Manchester
Paola	Lettieri	University College London
Toby	Lord	University of Leeds
Rebecca	Lunn	University of Strathclyde
Olivia	Lynes	Lancaster University
Graham	Mackay	National Nuclear Laboratory
Riccardo	Maddalena	University of Strathclyde
Ewan	Maddrell	National Nuclear Laboratory
Kevin	Malone	MMI Engineering Ltd.
James	Marra	Savannah River National Laboratory
Laura	Mayne	Loughborough University
Eric	McFarland	University of Queensland
Derrick	Njobuenwu	University of Leeds
Mel	O'Leary	Queen's University Belfast
Peter	Orr	Environment Agency
Robin	Orr	National Nuclear Laboratory
Scott	Owens	National Nuclear Laboratory
Cristiano	Padovani	Radioactive Waste Management, NDA
Steve	Palethorpe	National Nuclear Laboratory
Andrea	Paulillo	University College London
Jeff	Peakall	University of Leeds
Matteo	Pedrotti	University of Strathclyde
Ian	Pegg	Catholic University of America
Simon	Pimblott	University of Manchester
Dimitri	Pletser	Imperial College London
Oliver	Preedy	Loughborough University
John	Provis	University of Sheffield
Geoff	Randall	Sellafield Ltd.
David	Read	Loughborough University
Mark	Read	University of Birmingham
Sophie	Rennie	University of Bristol
Joanna	Renshaw	University of Strathclyde

Dominic	Rhodes	National Nuclear Laboratory
Hugh	Rice	University of Leeds
John	Riding	Sellafield Ltd.
Rodrigo	Rimando	U.S. Department of Energy
Mary	Ryan	Imperial College London
Rashed	Sarwar	Lancaster University
Keith	Schou	Loughborough University
Tom	Scott	University of Bristol
Rick	Short	NDA
Howard	Sims	National Nuclear Laboratory
Neil	Smart	Sellafield Ltd.
Ross	Springell	University of Bristol
Jon	Squire	Sellafield Ltd.
Rob	Stephen	Sellafield Ltd.
Rustam	Stolkin	University of Birmingham
Shi-Kuan	Sun	University of Sheffield
Sophie	Sutherland-Harper	University of Manchester
Bengt	Tegner	University College London
Martyn	Thomas	AWE plc
Stephanie	Thornber	University of Sheffield
Divyesh	Trivedi	National Nuclear Laboratory
Luc	Vandeperre	Imperial College London
John	Vienna	Pacific Northwest National Laboratory
Abby	Ward	University of Leeds
Deborah	Ward	NDA
Joseph	Wellington	University College London
Chris	Wilding	Wilding Consultants Limited
Christopher	Wong	University of Strathclyde
Kate	Wyness	University of Bristol
James	Young	University of Leeds

# Project Summaries

For reference - full A4 copies can be downloaded from our consortium website:

<http://distinctiveconsortium.org/category/events/1st-annual-meeting/>

# Master Project List

Theme	Title	Leading Institution	Researcher	Researcher Type
1	An investigation of wastefrom evolution during wet-recovery and drying of SNF	Bristol	James Edward Darnbrough/Leila Costelle	PDRA
1	UO <sub>2</sub> surface reactivity and alteration – a fundamental study of photocatalytic and structural effects related to long term storage of SNF.	Bristol	Sophie Rennie	PhD
1	Options for Exotic Carbide Fuels	Imperial	Claudia Gasparrini	PhD
1	The Behaviour of Used Nuclear Fuel in Wet Storage	Lancaster	Elizabeth Howett	PhD
1	Determination of optimum drying conditions for AGR fuels	Leeds	James Goode	PhD
1	Use of TRLFS of investigate dissolution rates	Loughborough	Oliver Preedy	PDRA
1	Grain boundary damage mechanisms in strained AGR cladding under irradiation	Manchester	Chiara Barcellini	PhD
1	A Life Cycle Approach as a decision tool for nuclear waste management and decommissioning of existing and future plants	UCL	Andrea Paulillo	PhD
2	Computational modelling of PuO <sub>2</sub> ageing and fuel residues	Birmingham	-	PhD
2	In-situ characterisation of heavily-contaminated plutonium finishing environments	Lancaster	-	PhD
2	Real-time fast neutron plutonium assay for plutonium storage and ageing applications.	Lancaster	Rashed Sarwar	PhD
2	Understanding the Interfacial Interactions of Plutonium Dioxide with Water	Lancaster	Dominic Laventine	PDRA
2	Understanding surface species and interactions between adsorbed chloride and water on stored PuO <sub>2</sub>	Manchester	Sophie Sutherland-Harper	PhD
2	Understanding the Interfacial Interactions of Plutonium Dioxide with Water	Manchester	-	PDRA
2	Ceramic materials for actinide disposition	Sheffield	Shi-Kuan Sun	PDRA
2	Current glass-ceramic formulations for Pu disposition	Sheffield	Stephanie Thornber	PhD
2	Understanding actinide sorption and binding to cement materials for radioactive waste management	Sheffield	-	PhD
2	Modelling the surface chemistry of PuO <sub>2</sub> at the molecular level	UCL	Bengt Tegner	PDRA
2	The interaction of water with PuO <sub>2</sub> surfaces	UCL	Joseph Wellington	PhD
3	New Ion Exchange Materials for Effluent clean-up	Birmingham	Ryan George	PhD
3	Novel Ceramic Wasteforms for Cs and Sr Encapsulation	Birmingham	George Day	PhD
3	Novel Ion Exchange Materials	Birmingham	Evin (Tzu-Yu) Chen	PDRA
3	Corrosion of uranium in water and hydrogen	Bristol	Antonis Banos	PhD
3	Development of Raman Spectroscopy techniques for the remote analysis of nuclear wastes in storage.	Bristol	Kate Wyness	PhD

3	The evolution of grouted waste forms containing uranium	Bristol	Haris Paraskevoulakos	PhD
3	Durability of Heterogeneous ILW Glass/Ceramic Wasteforms from Complex Wastestreams.	Imperial	Chinnam Rama Krishna	PDRA
3	Glass Composite Materials for Fukushima ILW Immobilisation	Imperial	Dimitri Pletser	PhD
3	Glass Composite Materials for Sellafield LP&S ILW Immobilisation	Imperial	Charles Hutchison	PhD
3	Magnetic Nanoparticles for Waste Separation or Sequestration	Imperial	Eleonora Cali	PhD
3	Computational simulations of storage pond sludge disturbance	Lancaster	Olivia Lynes	PhD
3	Characterisation of flocculated waste suspensions with acoustic backscatter	Leeds	-	PhD
3	Gas Hold-Up in Sludges	Leeds	Michael Johnson	PhD
3	Measurement and Modelling of Sludge Mobilisation and Transport	Leeds	Hugh Rice	PDRA
3	The development of characterisation techniques for intermediate level waste sludges	Leeds	Johannes Botha	PhD
3	Enhanced shear micro- and ultra-filtration without recycle pumping	Loughborough	Keith Schou	PhD
3	One step extraction and quantification of radionuclides using superparamagnetic bead and nanopore technologies	Loughborough	Laura Mayne	PhD
3	Irradiated sludges - Experimental	Queens University Belfast	Mel O'Leary	PhD
3	Irradiated sludges - Modelling	Queens University Belfast	Conrad Johnston	PhD
3	Thermal treatment of PCM and ILW	Sheffield	Luke Boast	PhD
4	Production of real-time segmented as-built CAD models for the planning and execution of remote and human intervention tasks	Birmingham	-	PhD
4	The Impact of Recycled Concrete Fines on the Engineering Performance of Cementitious Infill	Leeds	Toby Lord	PhD
4	Autonomous systems for nuclear decommissioning in extreme radiation environments	Manchester	Olusola Ayoola	PhD
4	Crack sealing and water transport	Strathclyde	Riccardo Maddalena	PhD
4	In-situ ground contaminant containment (Physical barrier)	Strathclyde	Matteo Pedrotti	PDRA
4	In-situ ground contaminant containment (Physical barrier)	Strathclyde	Christopher Wong	PhD
4	Monitoring of moisture and chloride in contaminated storage structures	Strathclyde	-	PhD
4	Nano-cracking of cement phases: reactivity and dissolution	Strathclyde	-	PhD

# An Investigation of Wasteform Evolution During Wet-recovery and Drying of SNF

J.E. Darnbrough\*, L. Costelle, S. Rennie, R.S. Springell

\*Correspondence: j.e.darnbrough@bristol.ac.uk

HH Wills Laboratory, University of Bristol, Bristol, BS8 1TL, UK.

## Abstract

Through the production of ideal samples through DC magnetron sputtering the complexity of SNF will be given a bottom-up approach. Initial work has looked at single crystal UO<sub>2</sub> this will be expanded into looking at U/UO<sub>2</sub> interfaces. These interfaces will be investigated in various environments to observe the corrosion process in a controlled and deconvolutable way.

## Introduction

Waste products from the nuclear industry currently feature prominently in the mind of the public, given the recent news coverage of the proposed underground waste storage facility in Cumbria [1]. In fact, the long-term solution to the storage of spent fuel stores, particularly legacy fuels, has still to be found. One of the greatest problems facing any permanent underground disposal of legacy waste is the need for repackaging. Due to prolonged exposure to wet conditions, there is a considerable chance that this waste has formed a number of hazardous compounds, in particular the uranium hydride, UH<sub>3</sub> [2]. Since UH<sub>3</sub> forms as a powder, and in such form is pyrophoric, it is of paramount importance that an understanding of this mechanism is developed so that a safe disposal route can be planned. Observation of additional corrosion routes are also key, for developing a clear picture of SNF.

The primary significant questions that we will attempt to answer are: Does the hydride form as a layer under the oxide? What is the solubility limit? Where, under the oxide does the hydride initiate and in what quantity? Can we inhibit this formation? What is the natural corrosion route?

## Methodology

We will approach these tasks with a combination of experiment and theory. We undertake the synthesis and characterisation of idealised U/UO<sub>2</sub> interfaces, using DC magnetron sputtering of thin films in a

dedicated actinide deposition system [3]. These will be characterised using x-ray reflectivity and high angle diffraction and compared to natively grown oxide to give credence to this route of interface production. These model buried interfaces will be exposed to carefully controlled hydrogen, deuterium and water vapour (18O labelled) using a sealed cell in active laboratory gas rigs at Bristol. Secondary ion mass spectrometry (SIMS) will then be used to map the depth profile of metal, oxygen and hydrogen species. There may also be the potential to carry out neutron scattering investigations of these systems, using the ISIS or ILL international facilities.

The experiments will be complemented by a set of calculations of the model thin films and interfaces of UO<sub>2</sub>, largely using the general lattice utility (GULP) program. We will examine energies, geometry, diffusion, segregation and hydrogen location and mobility.

## Future Work

Given the success of this work a continuation will be made to enhance the complexity further to consider the effect of fission products (simulated through doping while growing samples or post-growth implantation) and radiation damage (conducted at Dalton Cumbria Facility, UK (light ions) and Ganil, France (heavy ions)).

## **Acknowledgements**

The authors recognise the support of the Distinctive grant for funds and Gerry Lander for intellectual input.

## **References**

- [1] BBC News Cumbria, 30 January 2013
- [2] A surface science study of the initial stages of hydrogen corrosion on uranium metal and the role played by grain microstructure, C. P. Jones et al., *Solid State Ionics* 231,81(2013)
- [3] Elemental engineering: Epitaxial uranium thin films, R. Springell et al., *Phys. Rev. B* 78, 193403 (2008)

# Corrosion Behaviour of Spent Nuclear Fuel

L. Costelle<sup>1</sup>, S. Rennie<sup>1</sup>, J. E. Darnbrough<sup>1</sup>, R. Burrows<sup>2</sup>, G. H. Lander<sup>3</sup> and R. Springell<sup>1</sup>

\*Correspondence: Leila.costelle@bristol.ac.uk

<sup>1</sup>Interface Analysis Centre, University of Bristol, Bristol BS2 8BS, United Kingdom

<sup>2</sup>National Nuclear Laboratory, 102B Stonehouse Park, Sperry Way, Stonehouse, Gloucester GL10 3UT, United Kingdom

<sup>3</sup>European Commission, Joint Research Centre, Institute for Transuranium Elements, Postfach 2340, D-76125 Karlsruhe, Germany

## Abstract

In the present project, we synthesise thin film samples of uranium dioxide-based materials and expose their surfaces to a range of chemical conditions and radiation fields in order to closely mimic the environments expected to be found at the surface of spent nuclear fuel. We use a range of techniques in order to probe the dynamic changes to the fuel's structural integrity and to measure the dissolution products. The arising experimental results will be used as important parametric input for calculations of the likely long-term degradation of Spent Nuclear Fuels in variety of potential storage and disposal scenarios.

## Introduction

Operational nuclear power plants are generating high level nuclear waste (HLW), increasing globally, by around 12,000 tons each year [1]. Managing this long-lived HLW presents many challenges, as its safe storage is necessary for several hundred thousand years. Despite the progress that has been made in developing containment facilities for nuclear waste, eventual failure of storage containers could lead to the release of radionuclides into the environment. This process occurs when the surface of waste fuel becomes exposed to ground water under conditions which lead to the degradation of the fuel matrix.

Presently, uranium dioxide (UO<sub>2</sub>), as spent nuclear fuel (SNF) accounts for the majority of HLW generated by modern society [2]. While UO<sub>2</sub> is essentially insoluble in water, interaction with radiolytic oxidants (H<sub>2</sub>O<sub>2</sub> and OH•) can result in the degradation of the UO<sub>2</sub> matrix, releasing radionuclides into the environment. This occurs primarily by the oxidation of the UO<sub>2</sub> surface to generate readily soluble U<sup>6+</sup> ions [3]. Although there have been many studies into the corrosion of spent fuel surfaces, the majority of this work has been conducted on bulk materials which contain a great deal of complexity [3-5], meaning experimental variables are difficult to refine [6].

As a first step we have set out to simplify the experimental system by synthesizing high quality single crystal thin films, in order to effectively model the impact of corrosion upon a single grain of UO<sub>2</sub>. This is

of great importance as we currently rely on calculations of these processes to predict the mid- and long-term effects of our nuclear waste containment strategies. Complexity is then added to the system by adding structural distortions introduced by controlled irradiation damage.

## Methodology Details

### Sample synthesis

Single-crystal thin films of UO<sub>2</sub> are grown in a dedicated dc magnetron sputtering facility at the University of Bristol under UHV conditions. Substrate heating is used to elevate the growth temperature to 1000°C, providing thermal energy to improve the crystalline quality, monitored using in-situ reflection high-energy electron-diffraction (RHEED).

### Characterisation

Samples are characterised using x-ray reflectivity (XRR) and high angle x-ray diffraction (XRD), which are particularly well-suited to probing the fine details of surfaces or buried interfaces, as well as synchrotron measurements at the I07 beamline, Diamond Light Source in UK. The synchrotron experiments allow probing of the surface structure of the UO<sub>2</sub>-based samples expected in an aqueous environment, whilst simultaneously providing the radiation fields similar to those expected at the surface of SNF.

The surface structure of the films is characterised with a suite of electron microscope (SEM and TEM).

## Results and Discussion

### Radiolysis driven dissolution of $\text{UO}_2$

$\text{UO}_2$  films were exposed to water, while simultaneously being illuminated by a high intensity x-ray beam at a synchrotron source, in order to study the oxidative dissolution of  $\text{UO}_2$  in water.

This technique was shown to effectively provide the radiation fields required to split the water into highly oxidising radiolytic products, and to probe the structure of the surface as it is modified by the dissolution process [7]. A finite element calculation of the highly oxidising hydrogen peroxide product suggests that a more complex surface interaction than simple reaction with  $\text{H}_2\text{O}_2$  is responsible for significant corrosion at the interface of water and  $\text{UO}_2$  [8] and this could impact on models of long-term storage of spent nuclear fuel.

### Future Work

#### Effects of radiation damage and chemical heterogeneity on the corrosion behaviour of uranium

Structural distortions in  $\text{UO}_2$  thin films will be introduced by controlled irradiation damage at GANIL in France, and chemical heterogeneity by doping the films with fission product simulants ("SIMFUEL") during synthesis. A variety of electrochemical cells will be constructed in order to perform laboratory-based experiments and to replicate scenarios of wet, moist and dry conditions in storage and the combination of these environments with other variables such as pH and the particular make-up of likely groundwaters in a geological repository [3,4].

#### Localized corrosion behaviour of uranium based materials

We are now working on the design of uranium microelectrodes for the study of localised corrosion. Conventional macro-electrodes are not suited for the study of these mechanisms as they tend to dilute the responses evident in the localised processes. However, the use of microelectrodes will enable to isolate the effect and investigate it without the parallel response of a surface undergoing an entirely different reaction. This is very relevant to pitting corrosion, which involves localised chemistries and very high current densities often on extremely small fractions of the surface while the entire remaining surface may be passive.

## References

[1] World Nuclear Association, Radioactive Wastes - Myths and Realities, Available at: <http://www.world-nuclear.org/info/inf103.html>

[2] S. Sunder, G. D. Boyer and N. H. Miller, Journal of Nuclear Materials, 175, (1990)163-169

[3] D. W. Shoesmith, Journal of Nuclear Materials, 282, (2000) 1-31

[4] S. Sunder et al., Corrosion Science, 32, (1991) 373-386

[5] M. E. Broczkowski, J. J. Noel and D. W. Shoesmith, Journal of Nuclear Materials, 346, (2005) 16-23

[6] A. Seibert et al., Journal of Nuclear Reports, 419, (2011) 112-121

[7] D. W. Shoesmith, Nuclear Waste Management Organization (2007).

[8] Springell et. al. Faraday Discuss. Accepted Manuscript (2015). DOI: 10.1039/C4FD00254G

## Radiation Driven Reactions at the Surface of Uranium Dioxide

S. Rennie\*<sup>1</sup>, J. E Darnbrough<sup>1</sup>, L. Costelle<sup>1</sup>, C. A Stitt<sup>1</sup>, E. Cocklin<sup>2</sup>, C. A. Lucas<sup>2</sup>, R. Burrows<sup>3</sup>, H. E. Sims<sup>4</sup>, D. Wermeille<sup>5</sup>, J. Rawle<sup>6</sup>, C. Nicklin<sup>6</sup>, W. J. Nuttall<sup>7</sup>, G. C. Allen<sup>1</sup>, D. Geeson<sup>9</sup>, J. Glascott<sup>9</sup>, T. B. Scott<sup>1</sup>, and G. H. Lander<sup>8</sup>, R. S. Springell<sup>1</sup>

\*Email: Sophie.rennie@bristol.ac.uk

<sup>1</sup> Interface Analysis Centre, University of Bristol (Bristol BS2 8BS, UK)

<sup>2</sup> Department of Physics, University of Liverpool (Liverpool L69 7ZE, UK)

<sup>3</sup> National Nuclear Laboratory (102B Stonehouse Park, Sperry Way, Stonehouse, Gloucester GL10 3UT, UK)

<sup>4</sup> National Nuclear Laboratory, (Harwell Science and Innovation Campus, Oxfordshire OX11 0QT, UK)

<sup>5</sup> XMaS, European Synchrotron Radiation Facility (BP220, F-38043 Grenoble Cedex 09, France)

<sup>6</sup> Diamond Light Source (Harwell Science and Innovation Campus, Harwell OX11 0DE, UK)

<sup>7</sup> Department of Engineering and Innovation, The Open University (Venables Building, Milton Keynes MK7 6AA, UK)

<sup>8</sup> European Commission, JRC, Institute for Transuranium Elements (Postfach 2340, D-76125 Karlsruhe, Germany)

<sup>9</sup> Atomic Weapons Establishment (Aldermaston, Reading, Berkshire RG7 4PR, UK)

### Abstract

In order to ensure resilient, long-term storage for nuclear material it is critical to have a thorough understanding of the reactions occurring at the surface of stored uranium oxides. This project aims to explore this topic in further detail; in particular two subsets of radiation induced reactions occurring at the surface of uranium oxides will be studied: *dissolution* and *photocatalysis*. Progress has been made in investigating the photocatalytic potential of uranium oxides for the application of gas remediation. A photocatalysis gas rig has been developed, and planned future work investigating the efficacy of uranium oxides for the remediation of CO<sub>2</sub> has been outlined. Initial dissolution experiments have utilised x-ray diffraction to probe the radiolytic corrosion of uranium dioxide. Single crystal thin films of UO<sub>2</sub> were exposed to an intense x-ray beam at a synchrotron source in the presence of water, in order to simultaneously provide the radiation fields required to split the water into highly oxidising radiolytic products, and to probe the crystal structure of the UO<sub>2</sub> film. By modelling the electron density, surface roughness and layer thickness, the observed reflectivity and diffraction profiles have been reproduced, enabling changes to be detected in oxide composition at the Angstrom level. A finite element calculation of hydrogen peroxide diffusion suggests that a more complex surface interaction than a simple reaction with H<sub>2</sub>O<sub>2</sub> is responsible for an enhancement in the corrosion rate directly at the interface of water and UO<sub>2</sub>, and this may impact on models of long-term storage of spent nuclear fuel.

### Introduction

With the ever increasing demand for energy and the need for a more sustainable future, providing improved energy solutions has become a pressing challenge for nations across the world [1]. With nuclear power presenting a reliable, readily available, carbon-free solution, many countries have chosen to invest heavily in nuclear technology, resulting in high level waste (HLW) increasing globally, by around 12,000 tonnes each year [2]. With uranium oxides comprising the vast majority of HLW generated by modern society, it is critical that a safe and efficient storage strategy is developed for these materials. Despite the recent advancement in HLW containment systems, eventual failure will expose the surface of nuclear material to reactive environments, which may lead to degradation and corrosion of the fuel surface, releasing harmful radionuclides in to the environment [3]. It is therefore crucial that we acquire a fundamental understanding of the reactions occurring within a failed storage environment in order to develop accurate, long term

corrosion models, ensuring the future security of nuclear waste.

In particular this project will focus on two subsets of radiation induced reactions that can occur at the surface of uranium oxide within the storage

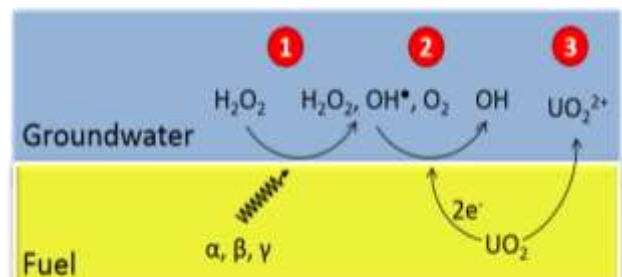


**Figure 1:** Oxidative dissolution of UO<sub>2</sub> via radiolysis of groundwater in a failed geological disposal facility. 1) Radiolytic production of oxidants via interaction of groundwater with residual radiation fields. 2) Cathodic reduction of oxidants. 3) Anodic oxidation and dissolution of the UO<sub>2</sub> fuel.

environment: *dissolution* and *photocatalysis*.

**Oxidative dissolution**

Previous studies suggest that within a failed nuclear storage container, the corrosion of  $UO_2$  is primarily driven by oxidative dissolution [4]. This is where the surface of  $UO_2$  is oxidised to give the readily soluble  $U^{6+}$  ions, resulting in the dissolution of the fuel matrix [4]. While the groundwater present within a failed storage container does not comprise the oxidation products ( $H_2O_2$ ,  $OH^\bullet$ ) required to drive this reaction, they are instead generated via water radiolysis, initiated by residual radiation fields of the stored fuel [5-6], Fig. 1.

The focus of this research will therefore be to investigate the impact of oxidative dissolution on the surface of uranium oxides. The key aim is to expose uranium oxide samples to a simulated failed storage environment and monitor the changes in surface morphology using synchrotron and lab based x-ray diffraction techniques.

**Photocatalysis**

Aside from groundwater, uranium oxide surfaces can interact with other species present within storage environments. Photocatalysis is one such mechanism, through which  $UO_2$  can react with gaseous species, altering the storage environment composition.

As semiconducting materials with band gaps of the order 2 eV, uranium oxides have significant potential as photocatalysts, operational in the visible region [7]. As shown in Fig. 2 for  $U_3O_8$ , illuminating uranium oxides with EM radiation can cause an electron in the valence band to be promoted to the conduction band, creating an electron hole pair [8-9]. This electron-hole pair has the potential to interact with adsorbed species to form highly reactive free radical species. It is believed that these photocatalytically generated, reactive oxygen species, are able to facilitate gas remediation via a series of complex reaction pathways [8].

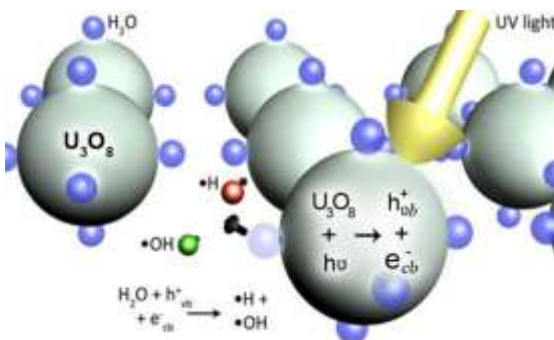


**Figure 2:** Illuminating a uranium oxide e.g.  $U_3O_8$  with EM radiation can cause an electron in the valence band to be promoted to the conduction band, creating an electron hole pair. This electron-hole pair then has the potential to interact with adsorbed species to form highly reactive free radical species.

Understanding the role of uranium oxides in gas

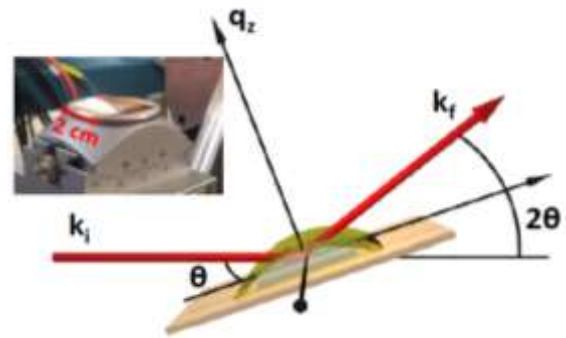


**Figure 3:** Schematic of the experimental set-up used at the Diamond Light Source, where  $k_i$  and  $k_f$  are the incident and exit wavevectors,  $\theta$  the angle of incidence with respect to the detector  $2\theta$  and  $q_z$  the wavevector momentum transfer. The thin layer surface tension cell hold a fixed volume of water over the sample during x-ray irradiation. The insert shows a photograph of the cell.

remediation is of significant importance to the nuclear community, as alterations in the gas composition of the storage environment may impact upon corrosion behaviour thus influencing long-term storage predictions.

This research, will therefore investigate the efficacy of uranium oxides for gas remediation, examining the effect of stoichiometry, crystallite size and radiation wavelength on the composition of gaseous environments.

**Methodology Details**

**Oxidative Dissolution Experiments**

To investigate the effect of oxidative dissolution on the surface morphology of uranium dioxide, a series of synchrotron x-ray diffraction experiments have been conducted at both BM28, ESRF and I07, Diamond Light Source beamlines. The samples used in these experiments were single crystal  $UO_2$  thin films, grown at the University of Bristol via reactive DC magnetron sputtering.

To simulate the oxidising environment required for oxidative dissolution to occur within a failed geological disposal facility, a layer of milliQ water was maintained across the film surface using a thin layer surface tension cell, Fig 3. The film, entirely covered by a layer of milliQ water, was then exposed to a 17.116keV x-ray beam in order to radiolyse the water and produce the oxidation products ( $H_2O_2$ ,  $OH^\bullet$ ) required for the dissolution process to occur.

X-ray Reflectivity (XRR) and high angle x-ray diffraction were then used to determine the change in surface morphology of the thin films on exposure to milliQ

water radiolysed by a 17.116 keV x-ray beam for a series of exposure times.

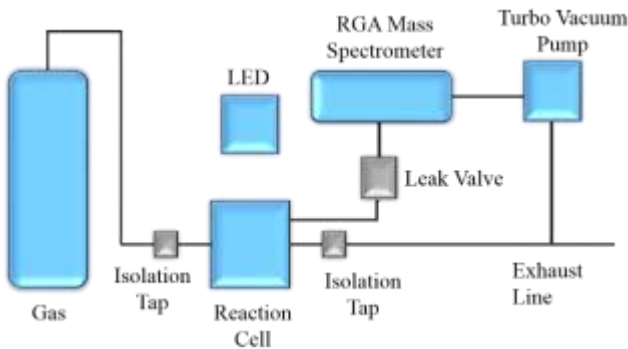


**Figure 4:** A photocatalysis gas rig has been designed such that uranium oxide samples are illuminated with a 40W UV LED, while exposed to a fixed volume of reactant gas. A residual gas analyser (RGA) will then be used to monitor the gas composition while the sample is illuminated.

### Photocatalysis Experiments

To investigate the potential for uranium oxides to act as photocatalysts in the remediation of harmful atmospheric gases, a photocatalysis gas rig has been designed, Fig. 4. Uranium oxide samples will be housed within a stainless steel reaction vessel, fitted with a UV transmitting window. This cell will then be connected to a residual gas analysis (RGA) mass spectrometer and associated pumping system via a sapphire leak valve, such that gaseous species in the reaction vessel can be sampled without any significant volume loss.

Using this gas rig setup, samples will be illuminated with a UV LED, while exposed to a fixed volume of

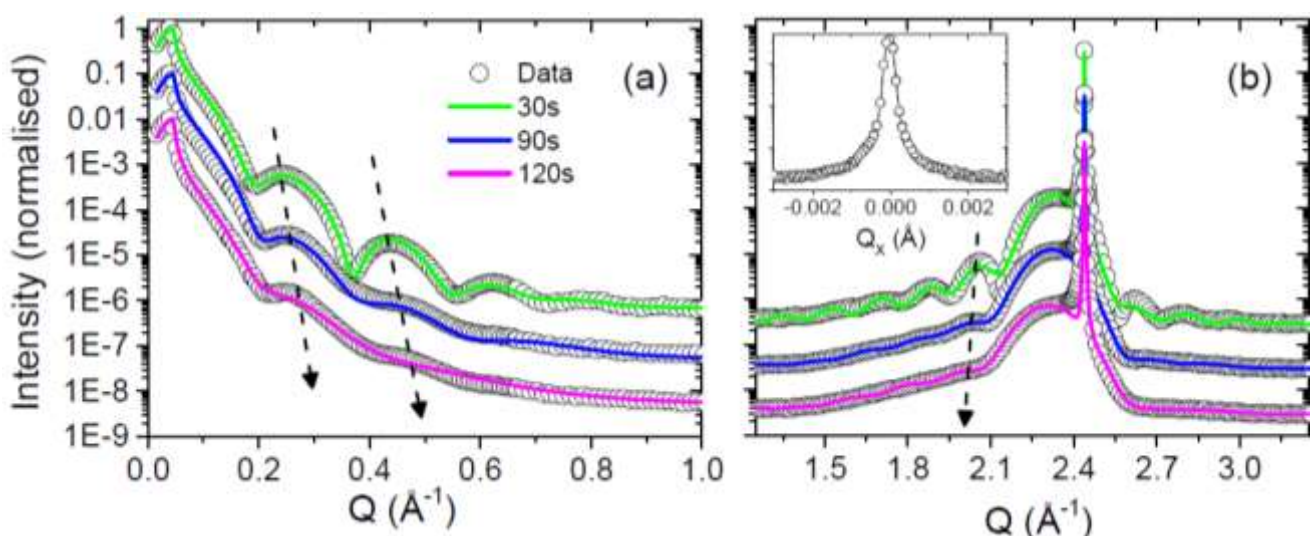
reactant gas, during which time the RGA will continuously monitor the gas composition. Analysis of RGA spectra combined with x-ray photoelectron spectroscopy (XPS) measurements of the sample surface, will enable the photocatalytic efficiency and gas remediation reaction pathways to be identified.

Currently the gas rig is under development, however once completed, initial experiments will focus on uranium oxide samples illuminated in the presence of  $\text{CO}_2$ . Key goals will be to identify the dominant parameters effecting photocatalytic efficiency for the application of  $\text{CO}_2$  remediation; variables to be examined will include: oxide stoichiometry, radiation wavelength and crystallite size.

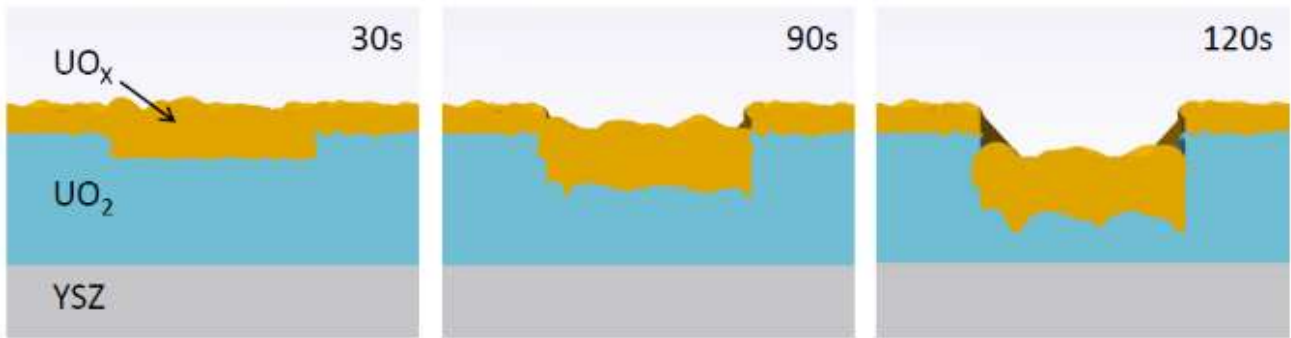
## Results and Discussion

### Oxidative Dissolution

The data presented here is from a single-crystal [001]- $\text{UO}_2$  film on yttria-stabilised zirconia (YSZ), with nominal thickness of  $40 \text{ \AA}$ , taken on the I07 beamline at the Diamond Light Source, UK. The beam energy was monochromated to 17.116 keV, and focussed in the vertical and horizontal directions to give an approximate beam size at the sample position of  $200 \mu\text{m} \times 200 \mu\text{m}$ . Once the thin layer surface tension cell had been filled with milliQ water, the surface was exposed at an incident angle of  $0.5^\circ$ , to give a footprint of  $200 \mu\text{m} \times 2 \text{ cm}$ , covering the whole length of the sample. This process was repeated for a series of exposure times, after which X-ray Reflectivity (XRR) and high angle x-ray diffraction were used to probe changes in the roughness, electron density, crystallinity and dissolution as a function of exposure time.



**Figure 5:** Panel (a) shows x-ray reflectivity and panel (b) shows high angle diffraction data, measured at exposure times of 30 s, 90 s and 120 s, the experimental data are represented by the open black circles and the fitted calculations by the solid green, blue and magenta lines, respectively. The insert of panel (b) shows the rocking curve of the (002) Bragg peak for the 30 s exposure. The dashed black arrows indicate an increase in fringe separation as a function of exposure time, which suggests a concomitant loss of material.



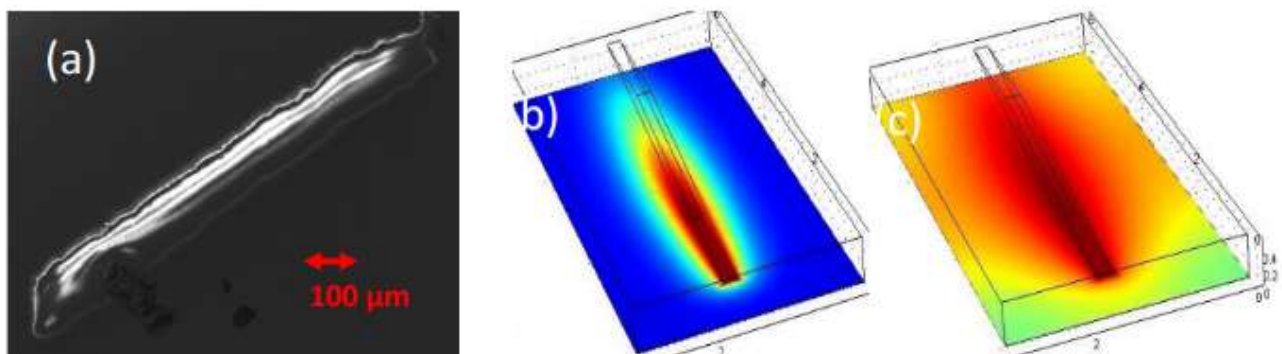
**Figure 6:** Pictorial representation of the increase in roughness and UOX thickness, and the amount of dissolution as the surface undergoes corrosion.

Figure 5 shows the XRR (panel (a)) and high resolution diffraction (panel (b)) from the single-crystal [001]- $\text{UO}_2$  thin film. Data are presented for three exposure times, 30 s (green), 90 s (blue) and 120 s (magenta), where the data are shown as open black circles and fitted calculations are represented by solid lines. The XRR data was fitted using the Parratt recursion method [10], using the GENX computer program. These fitted calculations are based on a structural model of the  $\text{UO}_2$  film that consists of a layer of crystalline  $\text{UO}_2$  with the standard bulk density and a surface layer of reduced electron density, labelled  $\text{UO}_x$ . Roughnesses for each of the interfaces were also computed. Table 1 summarises the fitting parameters and Fig. 6 shows a pictorial representation of the corrosion region at each of the 30 s, 90 s and 120 s exposures.

It is clear from Fig. 6 that the effect of radiolytically driven dissolution of the  $\text{UO}_2$  surface has been observed experimentally. In addition to these results, the quantity of radiolysis product has been calculated from first principles. In the first instance, the same assumption is made as in the vast majority of the literature, that the most dominant oxidising product is hydrogen peroxide [3, 11]. Based on the experimental

Exposure time (s)	$t_{\text{UO}_2}$	$\sigma_{\text{UO}_2}$	$t_{\text{UO}_x}$	$\sigma_{\text{UO}_x}$
0	34	3	10	6
30	27.5	2.5	16	9
90	21	7.6	20	11.5
120	13.5	11	22	13

**Table 1:** Parameters used in the fitted calculations to model the experimental reflectivity and high angle diffraction data. All values are in  $\text{\AA}$ , where  $t_{\text{UO}_2}$  is the thickness of the  $\text{UO}_2$  and  $\sigma_{\text{UO}_2}$  is the root mean squared roughness,  $t_{\text{UO}_x}$  and  $\sigma_{\text{UO}_x}$  are the thicknesses and roughnesses of the top layer of complex oxide, respectively.



**Figure 7:** Panel (a) shows an SEM image of a corroded  $\text{UO}_2$  single-crystal thin film, measured at the  $\text{UO}_2$  Bragg peak position for 500 s (an incident angle of about  $7^\circ$ ) with  $100\mu\text{m}$  vertical and horizontal slit settings. Panels (b) and (c) are images representing radiolysis product concentrations close to the beam footprint after 500 s, as calculated using finite element modeling, based on diffusion from the beam volume into the bulk liquid for short and long-lived species, respectively, with the latter being representative of  $\text{H}_2\text{O}_2$ .

conditions, it is expected that an equilibrium concentration in the region of  $1 \times 10^{-4}$  M of hydrogen peroxide will be generated. The question then arises - is the  $\text{H}_2\text{O}_2$  alone, enough to drive the changes that we are observing in our experiment? Figure 7 may provide a clue. Panel (a) is a scanning electron microscope image of the sample that has been exposed to the beam, this area is heavily corroded and so is not as conductive as the surrounding  $\text{UO}_2$  film; what is observed is the resultant charging of the corroded region. In particular it is noted that the width of the corrosion track is  $200\mu\text{m}$ , precisely the slit settings used in the experiment. However, over the duration of the experiment, one might imagine that due to diffusion of the  $\text{H}_2\text{O}_2$  species there would be a far wider area of corroded material. This is demonstrated in panels (b) and (c) of Fig. 7, where a finite element model has been used to represent two different diffusion profiles, (i) a short-lived species, confined to the radiolysis volume within the beam path, or one produced only at the sample surface and (ii) a long-lived species (such as  $\text{H}_2\text{O}_2$ ) subject to diffusive transport through the water layer. It is clear that a long-lived species subject to a bulk diffusion cannot be solely responsible. This suggests that the corrosion, which is restricted to the beam footprint, is driven by interactions at the surface.

There are several candidate propositions that may explain this interesting corrosion profile. One suggestion is a photocatalytic effect that can further enhance the formation of reactive oxygen species. This theory was tested by measuring the rate of corrosion at a range of x-ray energies spanning the uranium L3 absorption edge. Crossing through this edge enhances the number of electrons in the valence band, and thus would increase the oxidant species produced via photocatalysis. However, on passing through the U L3 edge, no statistically significant increase in the corrosion rate was observed, indicating that in this case a photocatalytic process is not responsible.

It is currently unclear as to why we observe this surface enhanced corrosion, another proposition that has yet to be tested experimentally is a significant concentration of short-lived oxidising species, such as OH radicals. Due to the extremely short-lived nature of such species, diffusion outside of the beam footprint would prove unlikely.

## Conclusions and Future Work

### Oxidative Dissolution

The experiments conducted so far have demonstrated that significant oxidation and further, dissolution of a  $\text{UO}_2$  surface can be induced using an intense beam of x-rays, mimicking the radiation fields found at the surface of spent nuclear fuel. Both the x-rays and the water interface are essential ingredients for these

changes. Synchrotron diffraction techniques have been used to measure variations in the electron density, surface roughness and rate of dissolution of a radiolysis driven corrosion front in a nuclear fuel material at the Angstrom length-scale, allowing a structural model to be generated, that details the change in surface composition over a series of exposure times. This work has been published in Faraday Discussions on Corrosion 2015 [15].

Future work will involve further investigation into the precise mechanism that is responsible for the observed corrosion, which from initial calculations seems unlikely to be due to hydrogen peroxide alone and may include a more complex surface effect. This could have significant consequences for previous research that has predominantly relied on this assumption to simulate the conditions driven by radiation fields [3, 11].

### Photocatalysis

Progress has been made in the development of a photocatalysis gas rig to investigate the efficacy of uranium oxides for the remediation of  $\text{CO}_2$ . Future work will focus on examining the effect of stoichiometry, crystallite size and radiation wavelength on the composition of gaseous environments.

### Acknowledgements

The authors wish to thank Paul Thompson and Laura Glaubes for their assistance in the first experiments on this project at the XMaS beamline BM28, ESRF. Sophie Rennie would like to thank the AWE and EPSRC for providing the PhD funding that supports this research. The authors would also like to thank the EPSRC for funding the DISTINCTIVE consortium grant on nuclear waste.

### References

- [1] U. Strandberg and M. Andren, Journal of Risk Research 12 (2009) 879-895.
- [2] World Nuclear Association, Available at: <http://www.worldnuclear.org/info/inf103.html> [Accessed: January 2013].
- [3] D. W. Shoesmith, Journal of Nuclear Materials 282 (2000) 1-31.
- [4] D. W. Shoesmith, Nuclear Waste Management Organization, (2007).
- [5] O. Roth, PhD Thesis, University of Stockholm (2008).
- [6] M. G. Bailey, L. H. Johnson and D. W. Shoesmith, Corrosion Science 25 (1985) 233-238.
- [7] P. W. Winter, Journal of Nuclear Materials 161 (1989) 38-43.

[8] O. Carp, C.L. Huisman, A. Reller, Progress in Solid State Chemistry 32 (2004) 33177.

[9] J.A. Herrera Melin et. al., Chemosphere 41 (2000) 323327.

[10] L. G. Parratt, Phys. Rev., 1954, 95, 359.

[11] S. Sunder, N. H. Miller and D. W. Shoesmith, Corrosion Science, 2004, 46, 1095–1111.

[12] R. S. Springell et al., Faraday Discussions (2015)  
DOI: 10.1039/C4FD00254G.

# Oxidation of Carbides Including Carbide Nuclear Fuels

C. Gasparri<sup>1</sup>, D. Coppersthaite<sup>2</sup>, T. B. Scott<sup>3</sup> and W.E. Lee<sup>4</sup>

\*c.gasparri14@imperial.ac.uk

<sup>1</sup>Centre for Nuclear Engineering, Imperial College London, UK

<sup>2</sup>National Nuclear Laboratory, Springfields, UK

<sup>3</sup>University of Bristol, Bristol, UK

<sup>4</sup>Centre for Nuclear Engineering, Imperial College London, UK

## Abstract

Despite the importance of the understanding of oxidation in uranium carbide fuels as a reprocessing step, this material is not readily available for experimental work. To understand the oxidation mechanism of carbide fuels, baseline work is being performed at Imperial College on an inert carbide material, zirconium carbide (ZrC). Oxidation experiments have been performed for the evaluation of the kinetic of the reaction. Investigations with SEM and FIB-SIMS on samples cross sections have shown the role of the interface between the carbide and the oxide in the development of the reaction. The mechanism of oxidation evaluated for zirconium carbide will be then used for comparison and understanding of the oxidation mechanism of uranium carbide based fuels.

## Introduction

Zirconium Carbide is a candidate ceramic for use in high temperature applications in fuel reactors because of its suitable properties including high hardness, high melting point, which exceeds 3500°C, and high thermal conductivity. ZrC has potential uses as an inert matrix fuel or as a structural component in the tri-structural isotropic-coated fuels (TRISO) particles<sup>1</sup>. It has also been used in the past with uranium carbide and carbon for the production of high temperature mixed carbide fuels<sup>2</sup>.

Oxidation experiments performed in a chamber lift furnace and with Thermal Gravimetric Analysis (TGA) is being carried out to evaluate the kinetics of oxidation of ZrC. Preliminary investigations on the mechanism of the oxidation have been performed by surface and cross section analysis by Scanning Electron Microscope (SEM), whilst characterization of the interface was performed by Transmission Electron Microscopy (TEM) and Focused Ion Beam – Secondary Ion Mass Spectrometry (FIB-SIMS) analysis. The mechanism of oxidation evaluated for zirconium carbide will be then used for comparison and understanding of the oxidation mechanism of depleted uranium carbide which will be examined experimentally using facilities at the NNL (National Nuclear Laboratory). In addition, understanding of the mechanism of oxidation of mixed fuels, will be analyzed again using a surrogate material, mixed cerium – uranium carbide, which will be produced in collaboration with Bristol University.

## Methodology Details

Dense zirconium carbide (ZrC) pellets were produced by hot pressing commercial ZrC powder (H. C. Starck, 90% < 8µm with 0.2% < Hf < 2%, average particle size between 3 – 5 µm) in a vacuum hot press furnace (FCT Systeme, GmbH, Germany) at 2000 °C in inert atmosphere. The starting material, commercial ZrC, has been analyzed by SEM, Energy Dispersive X-ray spectroscopy (EDX). Carbon and oxygen contents were measured by CO/CO<sub>2</sub> contents detected with an Infra Red Analyser after combustion. The disc shaped specimen (4cm diameter and 1cm height) produced by hot pressing was machined into specimens of known dimensions (cubes with 1cm side) via electrical discharge machining method (EDM). Thermal treatments were performed in a chamber lift furnace and with TGA in an air atmosphere. The temperature range investigated was 973 K – 1473 K and heating time was maintained for up to 6 hours, quenching after 0 – 15 – 30 – 60 – 120 – 240 minutes. Monitoring and post-oxidation characterization were performed using XRD, SEM+EDX, TEM and FIB – SIMS. The use of High Temperature Xray Diffraction (HT – XRD) on the ZrC powder revealed the zirconia polymorphic transitions that develop in the temperature range used during oxidation experiments.

## Results and Discussion

The oxide layer growth of ZrC assumes a particular shape, as reported for other carbides of the group IV and VI transition metals<sup>3</sup>, the so called Maltese cross.

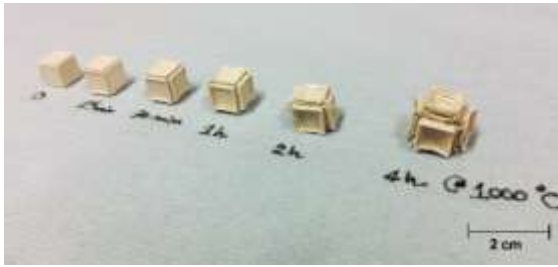


Fig 1. ZrC specimens after oxidation at 1000 °C at different times

Cross sections of oxidised pellets were analysed using FIB-SIMS to investigate the properties of the oxide structure. Four unique regions were observed via FIB milling: ZrC, an interfacial region, dense ZrO<sub>2</sub> and a cracked ZrO<sub>2</sub> region. Chemical analysis performed via SIMS and EDX of each region has showed that there is a rapid diffusion of material through the interface.

### Conclusions and Future Work

The presence of an interface region where the oxidation reactions occur has been observed and characterization is ongoing. Further investigations on the interface will be performed to get a full understanding of the mechanism of reaction of ZrC into ZrO<sub>2</sub>. The tracking of isotopic species (eg the use of Oxygen -18 in oxidation experiments) will give information on the mechanism of reaction.

The techniques used for the analysis of the oxidation of ZrC will be repeated at NNL for the oxidation experiments of depleted UC. The understanding of the mechanism of oxidation of ZrC and the oxidation experiments that will be performed on UC will give invaluable information for the industrial treatment of carbide spent fuels. The understanding of the oxidation of a mixed carbide fuel (U,Ce)C will give a better understanding on the oxidation as reprocessing step of future mixed carbide fuels.

### Acknowledgements

We thank Dr. Richard Chater for his help and support.

### References

1. Minato, K., Ogawa, T., Fukuda, K., Nabielek, H., Sekino, H., Nozawa, Y. & Takahashi, I. Fission Product Release From ZrC-Coated Fuel Particles During Postirradiation Heating at 1600 C. *J. Nucl. Mater.* **224**, 85–92 (1995).
2. Panda, B., Shah, S. & Hickman, R. R. Solid solution carbides are the key fuels for future

nuclear thermal propulsion. *NASA Technical Report Reports Server (NTRS)* (2005).

3. Silvestroni, L. & Sciti, D. Sintering Behavior, Microstructure, and Mechanical Properties: A Comparison among Pressureless Sintered Ultra-Refractory Carbides. *Adv. Mater. Sci. Eng.* **2010**, 1–11 (2010).

# The Behaviour of Used Nuclear Fuel in Wet Storage

Elizabeth Howett\*<sup>1</sup> and Colin Boxall<sup>1</sup>

\*Correspondence: e.howett@lancaster.ac.uk

<sup>1</sup> Lancaster University

## Abstract

The project aims to investigate the behaviour of spent nuclear fuel in interim storage, specifically AGR fuel in storage ponds at Sellafield. Corrosion behaviour will be studied in order to assess the validity of extended storage periods. Studies will be carried out on UO<sub>2</sub>, SIMFUEL and AGR cladding samples separately and in binary systems. Once these initial experiments have been completed, analogous experiments will be carried out on real spent AGR fuel.

## Introduction

The UK's AGR SNF is currently reprocessed at THORP. This is scheduled to close within 5 years. Future arisings will be sent to a GDF (geological disposal facility) however this is not due to open until c. 2075. Between THORP closing and the GDF opening, AGR SNF will be held in interim wet storage in buffered ponds at Sellafield. Current storage periods are typically less than 10 years, although this may extend to as long as 100 years after THORP closes.

AGR cladding can be breached due to stress corrosion cracking or damaged during dismantling. The former may be at least in-part facilitated by the steel cladding becoming sensitised to corrosion processes due to its in-reactor irradiation history. If the cladding is breached, the fuel itself can also become exposed. Evolution of both the steel & UO<sub>2</sub> surfaces upon consequent exposure to pond water can be considered as corrosion processes and so conveniently studied by electrochemical methods.

## Methodology Details

Using novel AGR SIMFUELS prepared especially for the NDA/EPSCRC funded UK SFR (Spent Fuel Research) Group, preliminary electrochemical studies on coupled SIMFUEL-20/25/Nb samples in pond buffer have been conducted and it was found that they exhibit open circuit potentials at which UO<sub>2</sub> oxidation may also occur. This suggests that both cladding and pellets of breached AGR SNF fuel pins can corrode during wet storage.

Therefore, using materials provided by the SFR Group, the following will be studied:

- (i) the corrosion behaviour of UO<sub>2</sub>, AGR SIMFUEL & 20/25/Nb in pond water chemistries;
- (ii) and recognising the limitations associated with SIMFUELS being simulant materials, we will use materials provided by NNL to study real exposed fuel under similar conditions.

The latter, specifically targeted at progressing PIE work on irradiated fuel in hot cells at Windscale, will allow for both study of corrosion reactions of real spent fuel under pond chemistry conditions and an assessment of how representative extant SIMFUEL samples are of real spent fuel behaviour.

In the first instance, open circuit, cyclic & linear sweep voltammetry and impedance spectroscopy studies will be conducted on separate UO<sub>2</sub>, SIMFUEL and 20/25/Nb samples as a function of [Fe<sup>2+</sup>], [Ni(II)], [CrO<sub>4</sub><sup>2-</sup>], temperature, burn-up (in SIMFUEL studies) and PH<sub>2</sub> & [H<sub>2</sub>O<sub>2</sub>], the latter to mimic radiolysis of water. Experiments on binary systems (UO<sub>2</sub>-20/25/Nb and SIMFUEL-20/25/Nb) will follow in order that coupling of fuel pellet & cladding corrosion / transformation processes may be studied. Finally, having developed appropriate experimental protocols using non-active simulants, analogous experiments on real irradiated fuel will be conducted as described above with particular emphasis on studying the effects of burn-up on electrochemical potential and therefore radionuclide release in wet storage environments.

# Transitioning of Spent AGR Fuel from Wet to Dry Storage

James Goode\*<sup>1</sup>, Bruce Hanson and David Harbottle

\*Correspondence: pmjbg@Leeds.ac.uk

<sup>1</sup>*School of Chemical and Process Engineering, University of Leeds, Leeds, LS2 9JT*

## Abstract

UK strategy relating to the treatment of spent nuclear fuel (SNF) has recently changed from reprocessing as part of a closed fuel cycle to direct disposal into a geological disposal facility (GDF). Since a GDF is not expected to be available until 2075 interim storage of fuel will be required. The use of interim dry storage has been mooted however, little research has been carried out into the effects of drying stainless steel (SS) clad spent nuclear fuel and this PhD is intended to begin work in this area.

Preliminary work has been carried out on simulant aluminium clad fuels as part of an MSc project which has been used to evaluate some initial experimental methods, however going forward work will concentrate on SS clad fuels. The initial phase of this work will be the development of a method for producing and characterising samples representative of SNF that has been stored for 20 years in caustic conditions (Sellafield's current strategy).

## Introduction

The UK government has made the strategic decision to stop spent fuel reprocessing and adopt an open fuel cycle. Empirical evidence has shown that caustic dosing allows fuel to be safely wet stored for at least 25 years and the Thorp receipt and storage pond (TR&S) will be used for the this purpose until at least 2038. In the long term, fuel will need to be transferred to a geological disposal facility (GDF) however since this is not expected to be available until 2075[1] a decision will need to be made in the future as to how the fuel will be stored during the interim period of approximately 35 years.

Should continued storage in caustic conditions be shown to cause unacceptable levels of cladding degradation, then the fuel will need to be stored dry. Dry storage is being utilised in many countries for the storage of LWR and MTR fuels however little research has been carried out into the dry storage of fuels utilising stainless steel (SS) cladding such as AGR fuel. Consequently, considerable work will be required to ensure that a safety case can be made for such work, and the current PhD project intends to begin working in this area.

## Methodology Details

Aluminium samples were treated in several different ways prior to analysis (Table 1). TGA was carried out

by heating between 25°C and 500°C. Samples were assessed by SEM.

Since Post Storage Examination (PSE) of stored fuel has only just begun, there is currently no definite knowledge of the condition spent fuel will be upon removal. Consequently the initial stages of this work will be to create characterise representative samples of fuel cladding. This is to be done by recreating the various treatments and processes which AGR fuel will undergo during its life.

1. Complete fuel rods are annealed in hydrogen at 930°C for 1 hr to homogenise crystal structure following welding.
2. Fuel is irradiated in a reactor for ~5 years in temperature range 750-850°C.
3. Upon removal from reactor fuel is transferred to a storage pond containing caustic at pH 11.4.

Table 1. Aluminium sample treatments.

Sample Designation	Treatment
Control	Heated in vacuum oven to 300°C for 2 hrs at ~100mBarA.
OA	Open Air. An untreated sample kept in open air since manufacture.
1W	Sample soaked in water for one week.
PP	Pressurised Plate. Sample stored in pressure chamber for 5 weeks followed by a further 5 weeks at atmospheric pressure.
MFA	Sample was repeatedly vacuum dried and water soaked for ~20 hrs on a daily basis for 5 weeks.
MFC	As per MFA but corroded in 1.6% FeCl and 0.1% HCl.

These processes will be replicated as follows; An annealing process used by Millward et al.[2] in work on AGR fuel deposits will be used. This annealing process is carried out at the same temperature and time as real fuel assemblies however an inert argon cover gas will be used rather than a reducing hydrogen atmosphere.

The SS alloy used for real fuel cladding contains 20 wt% chromium, 25 wt% nickel with an additional 1% niobium to prevent sensitisation from the formation of chromium carbides, however sensitisation will still occur due to Radiation Induced Segregation (RIS). Simulant fuel samples will use the commercial AISI 310 alloy which consists of 25 wt% Cr and 20 wt% Ni. This does not contain niobium to prevent sensitisation so the samples will be held at 800°C in CO<sub>2</sub> to induce sensitisation which will mimic RIS.

While PSE of intact fuel has not been carried out, examination of failed fuel has shown failures have occurred due to intergranular corrosion (IGC). This will therefore be taken as a worst case scenario and several fuel samples will be subjected to conditions known to promote intergranular corrosion. For AISI 310 SS, ASTM standard A262 recommends 240 hrs in boiling nitric acid to induce IGC and such a method has been used by numerous authors[3]. The process can be accelerated with the addition of oxidising ions such as Cr(VI)[4] and this will be carried out.

The effects of long term pond storage will be accelerated with the use of high temperature and pressures in order to increase the kinetics of the reaction. Both corroded and uncorroded samples will be treated in such a manner.

The simulant fuel samples will be analysed by TGA/DSC/MS after each treatment (e.g. after annealing, sensitisation, corrosion etc). In previous work on simulated aluminium fuel the loss of water could be clearly seen by TGA. In this work TGA will be used primarily to simulate the drying that fuel will likely be subjected to when transitioned from wet to dry storage. Analysis by optical microscopy and SEM/EDX will be used to assess how the various treatments and the drying process changes the microstructure and general composition of the samples and how the drying process affects the surface oxide.

The process and conditions used to remove water may be critical to maintaining integrity after wet storage. The effects on the cladding will need to be investigated and it is hoped to use XPS to analyse the water content of any oxides formed.

## Results and Discussion

Analysis of aluminium clad fuel by TGA clearly show by way of mass loss and negative heatflow the dehydration of the aluminium oxide bayerite (Al<sub>2</sub>O<sub>3</sub>.3H<sub>2</sub>O) to boehmite (Al<sub>2</sub>O<sub>3</sub>.H<sub>2</sub>O) at around 250°C when long soaked or corroded samples (PP, MFC and MFA) are analysed. A similar mass loss and heatflow change is not observed for the control and short or non-soaked samples suggesting that for aluminium fuels the quantity of water that can be removed is related to the thickness of the oxide produced.

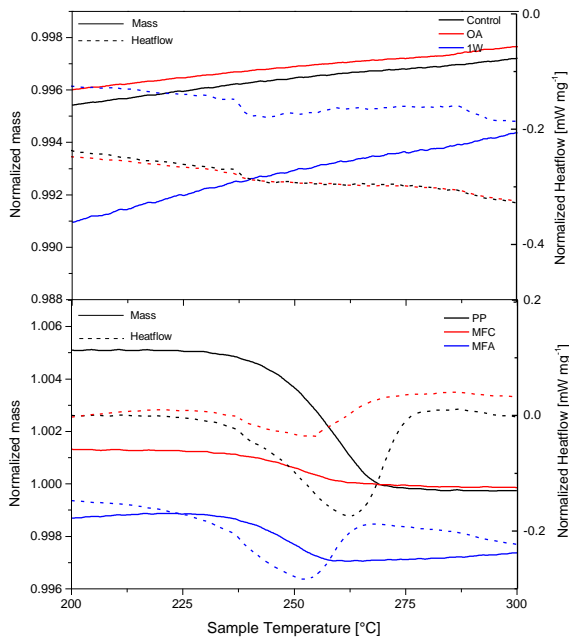


Figure 1. TGA curves for aluminium samples.

SEM images of samples before (Fig.2) and after (Fig.3) TGA show clear desiccation cracks in the oxide layer as result of the drying process which has the potential to reduce the mechanical strength of the fuel cladding.

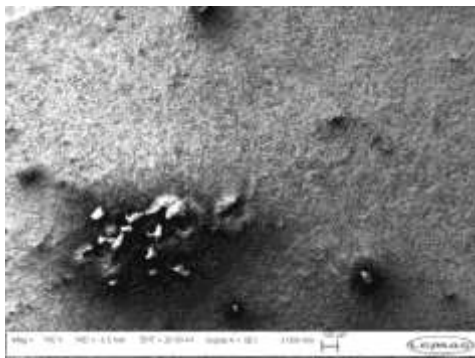


Figure 2. SEM image of PP sample pre TGA.

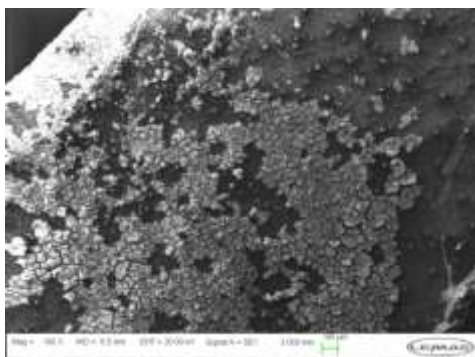


Figure 3. SEM image of PP sample post TGA showing desiccation cracks and oxide spallation.

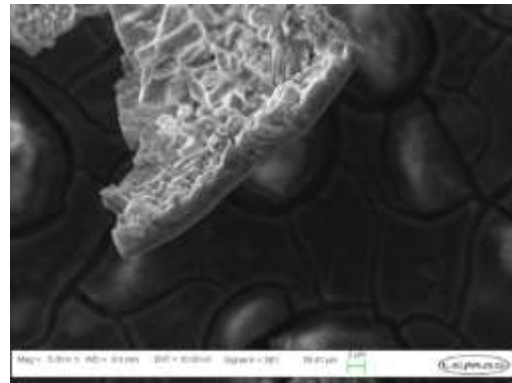


Figure 4. SEM image showing peeling oxide on PP sample post TGA.

Results for simulant AGR fuel are currently limited with only control samples having been analysed to date.

### Conclusions and Future Work

In the short term work will continue to complete the characterisation of simulant AGR fuel in the manner described. Upon completion, similar work is planned on samples of real cladding rather than the commercial alloy, and finally the analysis of irradiated fuel cladding samples obtained following PSE.

### Acknowledgements

I would like to thank the EPSRC Grant Number EP/L014041/1 and the DISTINCTIVE consortium for research funding.

### References

- 1 Kyffin, J. The technical case for interim Storage of AGR fuel and development of a programme of further work, in Manchester, IChemE, 9-11 April.
- 2 Millward, G.R., Evans, H.E., Aindow, M. and Mowforth, C.W. The influence of oxide layers on the initiation of carbon deposition on stainless steel. *Oxidation of Metals*. [Online]. 2001, **56**(3-4), pp. 231–250.
- 3 Jeng, J.Y., Quayle, B.E., Modern, P.J., Steen, W.M. and Bastow, B.D. Laser surface treatments to improve the intergranular corrosion resistance of 18/13/Nb and 304L in nitric acid. *Corrosion Science*. [Online]. 1993, **35**(5–8), pp. 1289–1296.
- 4 Ioka, I., Kato, C., Kiuchi, K. and Nakayama, J. Susceptibility of Intergranular Corrosion for Extra High Purity Austenitic Stainless Steel in Nitric Acid. [Online]. 2008, pp. 703–707.

# Time Resolved Laser Induced Fluorescence Spectroscopy of Uranium Compounds

O.Preedy \*<sup>1</sup>, C.Buck<sup>1</sup>, N.D.M Evans<sup>1</sup>, D.R.Worrall<sup>1</sup> and D.Read<sup>1</sup>

\*O.Preedy@lboro.ac.uk

<sup>1</sup>Loughborough University, Loughborough, Leicestershire, LE11 3TU, UK

## Abstract

The fluorescent properties of excited uranyl species was studied using a commercially available fluorimeter fitted with a 375 nm picosecond pulsed diode laser and time correlated single photon counting module. Spectral and temporal data was collected for both solid and liquid samples. The spectra collected showed characteristic uranyl emission bands with a limit of detection determined to be  $5 \times 10^{-5} \text{ mol dm}^{-3}$ . The lifetime data collected was consistent with the literature with all lifetimes in the order of microseconds.

## Introduction

Time Resolved Laser Fluorescence Spectroscopy (TRLFS) is a very useful technique for differentiating the chemical species of a fluorescent metal ion through analysis of characteristic excitation and emission spectra and decay (relaxation) lifetimes. The principal advantage over other spectroscopic techniques is the ability to determine in-situ metal speciation at environmentally relevant concentrations in solution and on ultra-thin surfaces[1].

Due to the spectral and temporal data being orthogonal to each other it is possible to differentiate the metal species by two discrete variables allowing speciation to be determined, which is difficult by any other laboratory based method[2].

The technique is becoming a widely used method for fundamental actinide & lanthanide studies. TRLFS is unique in being able to determine in-situ metal speciation at picomolar concentrations, which is essential when dealing with incipient corrosion of speciality metals or the alteration of ceramic and other materials used in the nuclear fuel cycle[3], [4].

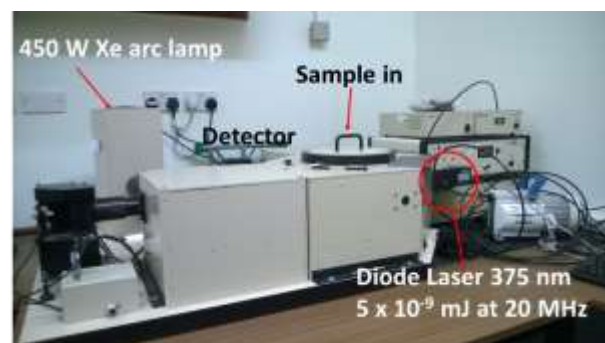
This project concerns the corrosion and dissolution rates of spent nuclear fuel (SNF) in water, using TRLFS to investigate the dissolution and corrosion rates of uranium fuels (U and UO<sub>2</sub>) are being investigated, with particular focus on the solid-solution interface.

The current work has focussed predominantly on accessing the capability and hence optimisation of the current instrumentation as well as generating a spectral library of uranium compounds.

## Methodology Details

### Instrumentation

The instrumentation used for all measurements was an Edinburgh instruments fluorescence lifetime



spectrometer (FLS900).

**Figure 1** Edinburgh instruments fluorescence lifetime spectrometer

There are two excitation sources available a picosecond pulsed diode laser with an excitation wavelength of 375 nm and a 450 W xenon arc lamp which allows a range of excitation wavelengths.

The FLS900 utilises a time-correlated single-photon counting (TCSPC) module for lifetimes between 10 ps – 50  $\mu\text{s}$  allowing both short and long lived species to be measured.

### Preparation of liquid samples

All liquid sample were prepared by dissolving sodium diuranate (Na<sub>2</sub>U<sub>2</sub>O<sub>7</sub>) in a perchlorate medium to ensure the absence of any complexing ligands. The sodium diuranate was prepared by dissolving uranyl nitrate (UO<sub>2</sub>(NO<sub>3</sub>)<sub>2</sub>) in deionised water and then precipitation

by addition of sodium hydroxide. The purity of the sample was determined by X-Ray diffraction.

**Preparation of solid samples**

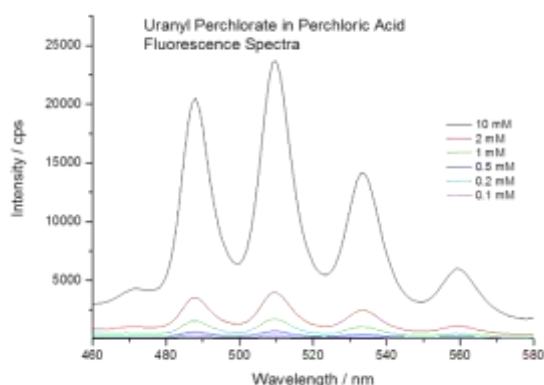
Powdered uranium compounds were homogenised and placed between two glass slides. A shallow sample well was created using adhesive plastic resulting in a window of approximately 2 cm<sup>2</sup>.

The samples were then mounted at a 45° angle to reduce the scattered light from the excitation source and placed into the spectrometer.

**Results and Discussion**

**Limit of detection**

The limit of detection for uranyl compounds was determined by collecting spectral data for uranyl species in perchloric acid at pH 2 to ensure that the uranyl ion (UO<sub>2</sub><sup>2+</sup>) would be the dominant species. The concentration range used for these measurements was between 10-0.1 mM, an overlay of the spectral data is



shown below in figure 2.

**Figure 2** Edinburgh instruments fluorescence lifetime spectrometer

The limit of detection was determined by using the intensity at the most intense peak (509 nm), shown in figure 3.

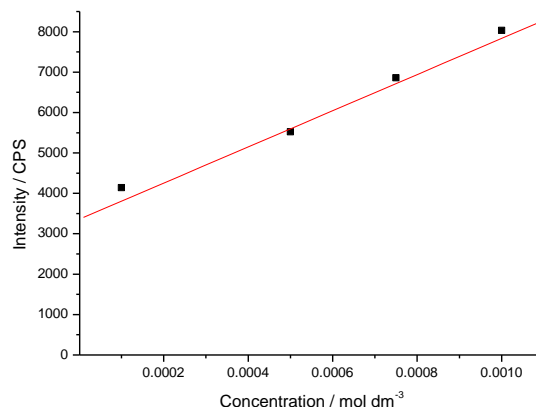
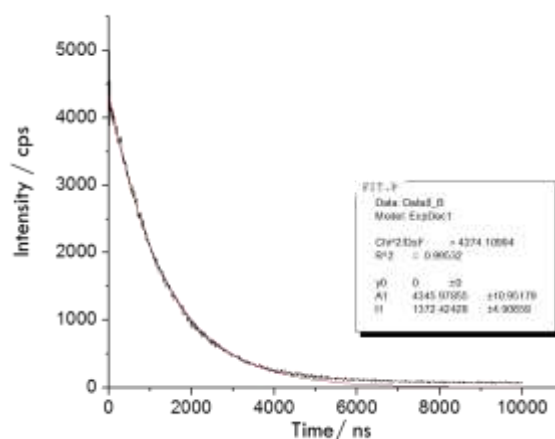


**Figure 3** Limit of detection for uranyl ion using fluorescence emission at 509 nm

The limit of detection was determined to be 5x10<sup>-5</sup> mol dm<sup>-3</sup>. This can be attributed to the low Molar absorptivity constant determined to be 9.05 molL<sup>-1</sup>cm<sup>-1</sup> and quantum efficiency of 3 %. This can potentially be improved by using an excitation source with greater peak energies. Another possible mechanism for increasing the limit of detection is collecting data at cryogenic temperatures, which will increase the absorption cross section and as a consequence lower the limit of detection.

**Fluorescence lifetime**

Fluorescence lifetime measurements were collected for the aqueous uranyl samples using the TCSPC



method. The lifetime data was

**Figure 4** Fluorescence lifetime measurement of excited uranyl complex

collected by counting single photons at the 509 nm emission peak, until an intensity of 5000 was achieved. The lifetimes of the excited uranyl species were determined to be relatively long lived 1.372 μs which is comparable with literature data.

### Spectral data for Solid samples

Spectral data was collected for three powdered uranyl species (uranyl acetate, uranyl nitrate and uranyl sulphate). The spectral overlay of the three compounds is shown below in figure four. The spectral data collected shows the sensitivity of the technique as by changing the ligand there are subtle differences in the emission spectra of the three samples. The most significant being the change in intensity and red shift of the uranyl sulphate.

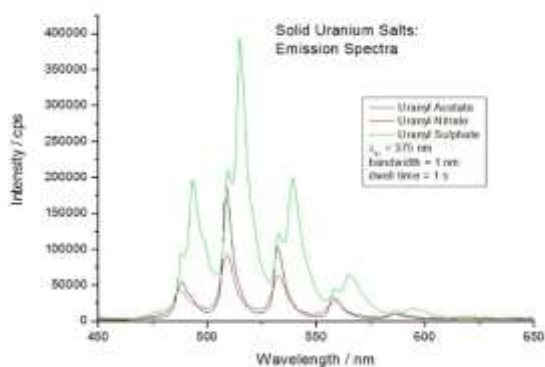


**Figure 5** Emission spectra for solid uranyl nitrate, uranyl acetate and uranyl sulphate.

### Conclusions and Future Work

Both spectral and temporal data were collected for a range of uranyl samples, both solid and liquid. The data collected was consistent with the literature, characteristic emission bands were observed as well as having lifetimes of the order of microseconds.

Future work will focus on improving the limit of detection, this can be done by changing the integration time allowing more signal to be collected. Another promising method is to collect the data at cryogenic temperatures.

Certified reference materials will be used to allow a library to be collated, which allow unknown samples to be identified more easily.

In addition to this a bespoke laser system is in the process of being commissioned focussing predominantly on uranium samples.

### Acknowledgements

The authors would like to thank the EPSRC for funding under grant EP/L014041/1. As well as all the members of the radiochemistry group at Loughborough for their valuable discussions.

### References

- [1] T. Reitz, A. Rossberg, A. Barkleit, R. Steudtner, S. Selenska-Pobell, and M. L. Merroun, "Spectroscopic study on uranyl carboxylate complexes formed at the surface layer of *Sulfolobus acidocaldarius*," *Dalton Trans.*, vol. 44, no. 6, pp. 2684–92, Feb. 2015.
- [2] C. Moulin and P. Decambox, "Uranium Speciation in Solution by Time-Resolved Laser-Induced Fluorescence," no. 28, pp. 348–353, 1995.
- [3] G. Geipel, T. Reich, V. Brendler, G. Bernhard, and H. Nitsche, "Laser and X-ray spectroscopic studies of uranium-calcite interface phenomena," vol. 248, pp. 408–411, 1997.
- [4] a Kowal-Fouchard, R. Drot, E. Simoni, and J. J. Ehrhardt, "Use of spectroscopic techniques for uranium(VI)/montmorillonite interaction modeling," *Environ. Sci. Technol.*, vol. 38, no. 5, pp. 1399–407, Mar. 2004.

# Grain Boundary Damage Mechanisms in Strained AGR Cladding under Irradiation

Chiara Barcellini<sup>1,2,\*</sup>, Enrique Jimenez-Melero<sup>1,2</sup>, Simon Pimblott<sup>1,3</sup>, and Simon Dumbill<sup>4</sup>

\*chiara.barcellini@postgrad.manchester.ac.uk

<sup>1</sup> Dalton Cumbrian Facility, Westlakes Science & Technology Park, University of Manchester, Moor Row, Cumbria, CA24 3HA, United Kingdom

<sup>2</sup> School of Materials, University of Manchester, Oxford Road, Manchester, M13 9PL, United Kingdom

<sup>3</sup> School of Chemistry, University of Manchester, Oxford Road, Manchester, M13 9PL, United Kingdom

<sup>4</sup> National Nuclear Laboratory, Central Laboratory, Sellafield, United Kingdom

## Abstract

The aim of this PhD project is to simulate the neutron damage in the AGR stainless steel cladding material using intense beams of protons and heavy ions of different energies and at relevant temperatures, therefore avoiding the problems related to the activation and handling of neutron-irradiated materials. Neutron bombardment damages the Nb-stabilised 20Cr/25Ni stainless steel claddings of Advanced Gas-cooled Reactors (AGRs) during their service life in the reactor core. This damage dose is of the order of a few tens of dpa and occurs while the cladding is at temperatures between 350°C and 700°C. The nano-micro scale changes in the structure of the claddings affect their mechanical integrity and their susceptibility to localised corrosion. Neutron irradiation, by spatially redistributing key alloying elements in the lattice, potentially causes local Cr depletion at grain boundaries, which can potentially make the material more sensitive to localised corrosion phenomena. The characterization of the ion-irradiated materials will be performed using various advanced analytical techniques, aimed to elucidate the principal radiation damage mechanisms operating at the grain boundaries and their local environment. We will link those mechanisms to the structural integrity and potential failure phenomena of AGR claddings. The fundamental understanding of these phenomena may lead to extend the lifetime of AGRs and to safely store the spent fuel in the cooling ponds.

## Introduction

Advanced Gas-cooled Reactors (AGRs) are second-generation gas-cooled reactors using graphite as moderator and CO<sub>2</sub> as coolant. The fuel is made up of slightly enriched UO<sub>2</sub> cylindrical pellets contained in austenitic stainless steel claddings. Thirty-six fuel pins surrounded by two concentric graphite sleeves form the fuel element, as can be seen in Figure 1.



**Figure 1** AGR fuel element showing the 36 fuel pins and the inner and outer graphite sleeve.

The fuel claddings are made of Nb-stabilised 20Cr/25Ni stainless steel and are provided with small transverse ribs on the outer surface to enhance the heat transfer. During manufacture, the claddings are compressed onto the fuel pellets in order to minimize the clearance gap between the pellet and the cladding. The remaining space is filled with Helium gas [1]. Due to the manufacturing process, certain parts of the stainless steel claddings retain a significant deformation. As a consequence, some areas of the structures may present localised stress even before the loading into the AGR core.

During the service inside the reactor, those claddings are constantly bombarded by a neutron flux at temperatures that may vary between 350°C and 700°C. This irradiation causes significant damages of the stainless steel structure (damage doses of the order of a few tens of dpa), due to the generation of additional vacancies and interstitial defects. This radiation-induced damage evolves during the time spent by the fuel in the reactor core giving rise to extended defects such as dislocation loops and channels, strain localisation and radiation induced segregation (RIS). These lattice defects can affect the mechanical

integrity of the cladding and potentially increase the susceptibility to localised corrosion.

After 3 or 4 years inside the reactor core the fuel becomes less efficient and therefore is removed. The refuelling machine transfers the hot irradiated fuel assembly to a decay store, where the fission products are allowed to decay while the assembly cools. In order to allow the decay heat to fall to an appropriate level, other storage steps will follow during which the AGR fuel spends a lot of time inside a water pond. Figure 2, for example, shows an internal view of the Sellafield pond, where the spent fuel is stored to allow further cool down before reprocessing. The storage in wet environment gives rise to serious corrosion problems. Therefore, the integrity of the fuel claddings needs to be guaranteed in order to avoid the release of radioactive materials inside the pond.



Figure 2 An internal view of Thorp recipient and storage in Sellafield.

Before extending the time scale of the AGRs cladding inside the reactors core, it is necessary to increase the knowledge and the mechanistic understanding of the effects of neutron irradiation at high temperatures on the Nb-stabilised 20Cr/25Ni stainless steel cladding. Knowing the consequences of radiation damage is of fundamental importance also for safe long-term storage in the wet storage ponds. Therefore, the main goal of this project is to elucidate the radiation damage mechanisms operating in Nb-stabilised 20Cr/25Ni stainless steel, and to link those atomic-scale mechanisms to the structural integrity and potential localised failure phenomena of AGR cladding in reactors and storage ponds conditions.

### Material Description

Nb-stabilised 20Cr/25Ni stainless steel is an austenitic stainless steel, where C is present in interstitial solid solution, while the other alloying elements (e.g. Cr, Ni and Nb) substitute Fe in the crystalline lattice. Cr is used to enhance the corrosion resistance of the alloy, since it tends to form a very thin protective oxide film; Ni is added to the alloy to decrease the temperature

above which the austenitic phase is stable, while Nb prevents the steel from becoming sensitized to intergranular attack [2].

Neutron bombardment causes damage to the crystal structure of metals and alloys. The generation of additional Frenkel pairs in a crystalline lattice due to neutron irradiation may cause physical changes of an essential permanent character. Both vacancies and interstitials move through the lattice at rates that depend on temperature. During the course of their migration, they can either annihilate or agglomerate with other lattice defects. In the first case, they may recombine or they can be trapped at sinks (e.g. dislocations, grain boundaries, etc.); in the second case, they can aggregate or cluster together to form interstitial/vacancy loops. Vacancy loops can collapse giving rise to dislocation loops, which would cause plastic instabilities and strain localisation near the grain boundaries [2]. This phenomenon has been studied extensively in 304 and 316 stainless steel series, but has not been considered as a major failure mechanism in AGR-type stainless steel.

Susceptibility to localised corrosion is enhanced in austenitic stainless steels subject to high neutron flux at relatively high temperatures. Current understanding of this phenomenon ascribes this increase to radiation-induced segregation (RIS). The irradiation at elevated temperatures causes a spatial redistribution of solutes and impurity elements in the material, leading to enrichment or depletion of alloying elements in regions near grain boundaries [3]. Such drastic changes at the grain boundaries can potentially alter the local properties of the material, and may induce susceptibility to processes that can degrade the integrity of the reactor component.

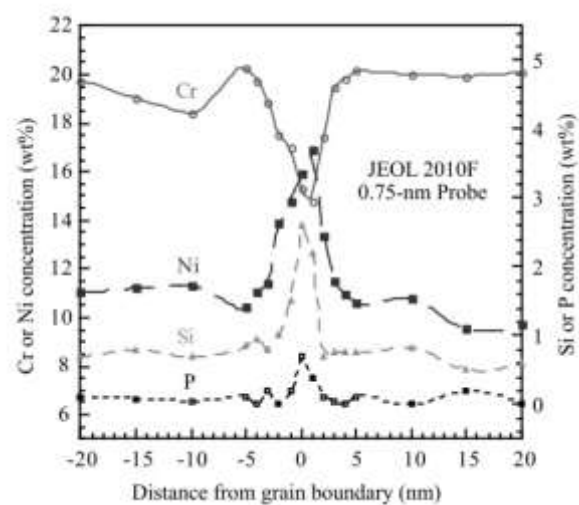


Figure 5 Radiation induced segregation of Cr, Ni, Si and P at the grain boundary of 300 series stainless steel irradiated in a light water reactor core up to several dpa at 300 °C [3].

As can be seen in Figure 5, Cr is depleted at the grain boundary in 300-series austenitic stainless steel, while the local content of Ni and Si is significantly enhanced. This has also been observed in Nb-stabilised 20Cr/25Ni stainless steel used for AGR claddings [4]. The local depletion of Cr may be the cause of the increased susceptibility to inter-granular corrosion, since Cr provides protection from corrosion by forming a thin, protective oxide film ( $\text{Cr}_2\text{O}_3$ ). However, the principal mechanism which causes the chemical depletion/segregation in AGR cladding materials at relevant reactor conditions is still largely unknown, and also how those localised structural alterations may lead to the (unpredicted) claddings failure. For these reasons, a detailed microscopic characterisation of the irradiated samples in the vicinity of the grain boundaries is of fundamental importance.

### Approach

This PhD project has just started in April 2015. It aims to elucidate the principal mechanisms of radiation damage in Nb-stabilised 20Cr/25Ni stainless steel at grain boundaries and their local environment, in order to link those atomic-scale mechanisms to potential localised failure phenomena. Since it seems that thermally sensitised Nb-stabilised 20Cr/25Ni stainless steel materials do not yield equivalent phenomena/microstructures as those expected in neutron-irradiated samples, it is necessary to irradiate the AGR-type stainless steel materials to systematically study the damage processes caused by neutron bombardment in the reactor. This project proposes to simulate the neutron irradiation using intense ion beams, in order to avoid high residual radioactivity in the irradiated material, which would then require specific transport/storage procedures and devoted active laboratories. The irradiated material will then be studied using advanced characterisation techniques. This project will be conducted at the Dalton Cambrian Facility (Figure 3), a state-of-the-art research base of The University of Manchester's Dalton Nuclear Institute.



Figure 3 Laboratory and office building of Dalton Cambrian Facility.

### Methodology

The study of the radiation damage on AGR cladding stainless steels will be approached using flat plates of this material outsourced via National Nuclear Laboratory (NNL). They will be

- irradiated with ions to simulate the reactor neutron bombardment;
- mechanically tested to study the evolution of their structure under loading;
- characterised with analytical electron microscopy to assess their damaged structures, and also with synchrotron X-ray diffraction (it is planned to apply for beam time at large scale synchrotron facilities);

Selected model alloys and AGR cladding materials will be irradiated with protons at relevant temperatures and total damage dose. The temperatures will be in the range between 350 °C to 500 °C, close to those reached inside the reactor core by the stainless steel claddings, while the proton energies will be close to 3 MeV and the total dose between 0.1 and 5 dpa. The ion irradiations under controlled conditions of temperature and radiation dose will be performed at the Dalton Cambrian Facility thanks to the 5 MV Pelletron accelerator (see Figure 4). This machine is able to supply up to 10 MeV protons and 15 MeV He ions, as well as a variety of partially stripped heavy ions. This ion accelerator is equipped with six beam lines allowing flexible experimental set-up, three of those beam lines being focused on materials damage.



Figure 4 Dalton Cambrian Facility's 5MV Pelletron housed in the accelerator hall.

After the irradiation, the characterisation will follow using electron microscopy and lab X-ray diffraction (XRD), mechanical testing, and X-ray synchrotron diffraction. In this stage it is important to develop experimental protocols to perform the proton irradiation at controlled conditions of temperature, total dose and dose rate, and to handle and transport the samples especially if they show residual activity after the irradiation. The obtained results will be

compared with existing data in the literature about neutron irradiated and thermally sensitised Nb-stabilised 20Cr/25Ni.

The evolution of their structures during loading will be studied using electron back-scattered diffraction (EBSD) and synchrotron X-ray diffraction. The first type of measurement is performed with a scanning electron microscope equipped with an EBSD detector, while the latter needs a synchrotron source. Both techniques can provide relatively high spatial resolution, but deeper volume of the material can be investigated with high-energy X-rays thanks to the high penetration depth. It is possible to go through more than 1 mm in steel with X-rays, while the EBSD signal comes from around 30 nm below the surface of the sample.

Equivalent proton irradiation experiments and sequential characterisation measurements will be performed on pre-strained samples in order to simulate the influence of the residual stress due to the manufacture of the AGR claddings. In order to achieve higher damage rates and total doses, up to 10-20 dpa, we intend to perform also sample irradiations with heavy ions. The irradiation will be then followed by the characterization of the samples. We will develop procedures to prepare and characterize the damage layer with a thickness of less than 2-3  $\mu\text{m}$ . As a conclusion of this 3.5 year work plan, initial corrosion tests are envisaged on selected irradiated samples as a guideline for future research aimed to assess localized corrosion phenomena during wet storage.

### Conclusions and Future Work

The study of radiation damage in stainless steel structures is of fundamental importance for the potential extension of AGR lifetime and for the safe storage of the spent fuel cladding in cooling ponds. Currently, our mechanistic understanding of the neutron damage on Nb-stabilised 20Cr/25Ni stainless steel claddings, used in AGRs, remains largely unknown. This PhD project, therefore, aims to deeply investigate these radiation damage processes, especially at grain boundaries and at their local environment. The main goal is to link those atomic-scale changes to the potential localised mechanical failure phenomena of the cladding material, such as inter-granular stress corrosion cracking. We also expect to provide advice on future paths to assess localised corrosion phenomena that may occur during the wet storage of the spent AGR fuel claddings. The obtained experimental results will be implemented into existing models of radiation damage, and compared with existing knowledge of AGR cladding performance in service and storage conditions.

### References

- [1] Carlo Lombardi, *Impianti Nucleari*, Polipress, 2009.
- [2] S. Glasstone, A. Sesonske, *Nuclear Reactor Engineering: Reactor Design Basics*, International Thompson Publishing, 1994.
- [3] G.S. Was, *Fundamentals of Radiation Material Science: Metals and Alloys*, Springer, 2007.
- [4] D.I.R. Norris, C. Baker, J.M. Titchmarsh, *Compositional profiles at grain boundaries in 20%Cr/25%Ni/Nb stainless steel*, Proc. Conf. on Radiation Induced Sensitisation of Stainless Steel, Berkely Nuclear Laboratory, UK, 1987.

# A Life Cycle Approach as a Decision Tool for Nuclear Waste Management

Andrea Paulillo<sup>\*1</sup>, Dr. Stephen Palethorpe<sup>2</sup>, Prof. Roland Clift<sup>3</sup> and Prof. Paola Lettieri<sup>1</sup>

\*Correspondence: andrea.paulillo.14@ucl.ac.uk

<sup>1</sup> Department of Chemical Engineering, University College London, Torrington Place, London, WC1E 7JE, United Kingdom

<sup>2</sup> National Nuclear Laboratory, Workington, Cumbria, CA14 3YQ, United Kingdom

<sup>3</sup> Centre for Environmental Strategy, The University of Surrey, Guildford, Surrey, GU2 7XH, United Kingdom

## Abstract

As world energy consumption is expected to grow and in light of Global Carbon Policy to reduce CO<sub>2</sub> emission, Nuclear Energy is going to play a bigger role. In the Nuclear Industrial Strategy document [1], nuclear energy is projected to contribute up to 40-50% of the UK energy mix, compared with nearly 20% today, in line with the Government's Carbon Plan to reduce CO<sub>2</sub> emissions by 80% by 2050. A Life Cycle Assessment (LCA) approach is proposed to evaluate environmental burdens of the nuclear industry and especially of nuclear waste management processes. LCA is a widely used methodology to assess environmental impacts of a product, process or activity. Whereas a set of indicators for the non-radiological component has been developed and standardised, little has been done with regards to the radiological component, especially to solid nuclear wastes. Between existing methodologies, a Risk-based approach seems to be the most promising for a future application in a LCA study.

## Introduction

In the modern industrial economy, energy production and use has the greatest impact on the environment of any human activity. Furthermore, as the United Nations (UN) estimates, world population is expected to increase up to eight billion by 2020 [2] and energy consumption to grow by 53% by 2040 [3]. Consequently there is an urgent need to develop sustainable strategies for energy supply, while minimising environmental impacts. In the 1987 report of the World Commission on Environment and Development, sustainable development was defined as "... development that meets the needs of the present without compromising the ability of future generations to meet their own needs". Within the goal of sustainability there are three main areas that are generally considered relevant in decision-making as practical constraints on human activities [4]: Environmental, Economic and Societal. Energy generation has links with all these areas, because energy services are essential for economic and social development. Therefore, as energy consumption is predicted to grow, its environmental impact will have to be controlled and alleviated in order to achieve sustainability goals. Nowadays, nuclear energy accounts for 24% of European and 11% of worldwide electricity supply [3] and its performance, based upon more than 10,000 reactors-years of experience world-wide is satisfactory, making nuclear energy as an

important component of electricity supply for many countries. Many argue that nuclear energy should play a bigger role in electricity supply because it has advantages in terms of global warming, cost stability and high capacity factors that make it compatible with the goals of sustainable development. However there are a number of problematic issues surrounding the development of nuclear power: e.g. the long-term management of radioactive wastes arising from electricity generation and the safety related issues associated with nuclear energy activities. Four different nuclear fuel cycle options are theoretically available, but only two are currently implemented; they differ in the way nuclear wastes are managed and eventually disposed. Both interim storage and open fuel cycle (or 'once through' cycle) disposes directly of nuclear spent fuel respectively in wet or dry storage within the nuclear power generation reactor and in geological disposal facility. Partially closed cycle (or single recycle) reprocesses spent nuclear fuel in order to recycle Uranium and Plutonium; whereas closed fuel cycle aims to a major separation and recycling: e.g. minor actinides. Wastes arising from nuclear plants are classified according to radioactivity and heat generation level in High Level Waste (HLW), Intermediate Level Waste (ILW) and Low Level Waste (LLW), each of them requires a different type of disposal. The UK has developed considerable expertise across the full nuclear fuel cycle over the past 60 years and adopted a partially closed nuclear fuel cycle. Its

power reactor fleet comprises of 14 AGR, 1 PWR and 1 Magnox reactor, which account for approximately 15% of the UK electricity generation. All UK nuclear spent fuel is reprocessed at Sellafield site by the THORP and Magnox fuel reprocessing plant. National geological disposal facility has not been yet located as it has to be approved through a long and thorough process by citizens. Thus currently, nuclear wastes are stored in interim and temporary storage at Sellafield site. Currently, the legacy ponds and silos at Sellafield are the biggest safety and security threat facing the UK, costing £70M/annum just to maintain their basic condition and prevent leakages. They represent 22% of all Sellafield site programmes, 35% of total site costs and 77% of major project costs during next 4 years and >90% of nuclear hazard potential.

It appears clear that nuclear waste management is a key aspect and driver for decision within the nuclear industry. A proposed tool to evaluate environmental impacts posed by and support the decision-making process within the nuclear power industry is the Life Cycle Assessment (LCA). Up until now, LCA application to the nuclear sector has been characterized by an independent and separate evaluation of radiological and non-radiological impacts. Treatments of those two fields have thus led to the evolution of two distinct cultures, whose aim was to control and reduce one impact without regard of the other. This approach results in well acknowledged reductions in one impact being coupled with unacknowledged increases in the other. For instance, the usual approach has been to reduce as much as possible the radiological impacts, thus causing major increases in the non-radiological impacts. However, the Environmental Optimum is defined as the minimum Environmental Impact resulting from the sum of radiological and non-radiological impacts.

## Methodology Details

### Life Cycle Assessment

Life Cycle Assessment (LCA) is a widespread technique used to evaluate environmental burdens associated with a product, process or activity by identifying and quantifying all energy and materials used and wastes released to the environment and to identify and evaluate opportunities to effect environmental improvements [5]. LCA belongs to a whole family of environmental assessment tools some more focused on physical metrics (ERA, EIA) other more focused on economic metrics (CBA), but differs from them in the way system boundaries are drawn. LCA encompasses the whole life cycle of a product, which extends from the extraction and processing of raw materials through manufacture, delivery and use to waste management; for this reason this approach is often termed as ‘cradle

to grave’ assessment. The LCA structure and methodology has been standardised [6] and applied from 1997 onwards. It is considered to be subdivided into four phases, shown schematically in Figure 1. Although the four phases proceed in sequence, the process is iterative in that earlier phases may be revisited in the light of the outcome of later phases.

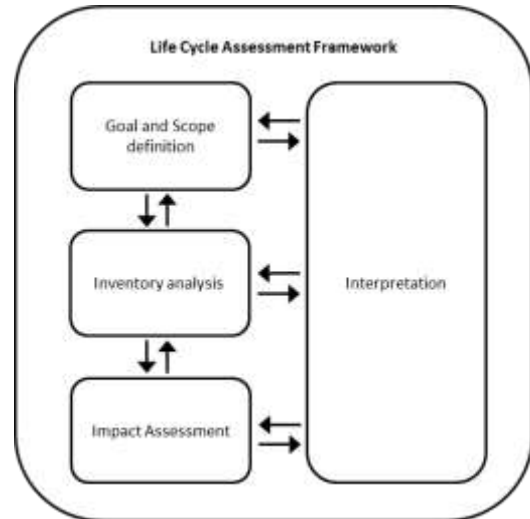


Figure 1 Phases in a Life Cycle Assessment (after ISO 144040 [6])

### Goal and Scope Definition

It is essential to define unambiguously the purpose or the intended application of the study and what decision is to be informed by the results. LCA may be applied to a single process in order to identify the stages in the life cycle with the greatest impact (*hotspot analysis*) or may be carried out to compare alternative ways of delivering some function. The basis for comparison is generally termed as *functional unit* whereas the scope of the study is expressed in terms of the *system boundary*.

### Inventory Analysis:

In this stage all emissions, wastes and use of resources, over the life cycle per functional unit are identified and quantified. The complete set of burdens per Functional Unit constitutes the *Inventory Table*. For multiple-output processes, it is necessary to find a rational basis for allocating the environmental burdens between different outputs. A set of recommendation for the allocation process is given by ISO 14041 [6], where system expansion [7] is considered as the best currently available approach.

### Impact Assessment:

The principal feature of the analysis or comparison is rarely clear from the inventory alone. According to ISO standard [6], the Life Cycle Impact Assessment is a phase aimed at understanding and evaluating the magnitude and significance of the environmental impacts of a product system. Once a set of impact categories significant to the specific system are

selected, the inventory data is assigned to the impact categories (*classification*) and then the potential contribution of each input and output to different impact categories is calculated (*characterization*).

**Interpretation:**

In this phase, the results of either the Data Inventory or the Impact Assessment or both are combined in line with the defined goal and scope of the study. The results are used to make recommendation for environmental improvements or as input to some form of decision process.

**On-going Work**

**Review: Radiological Impact Assessment**

In the routine operation of nuclear activities, environmental releases of radionuclide occur in the form of liquid and gaseous releases or arise over time from radioactive solid wastes. Although the non-radiological component of LCA has been extensively developed, a standardised framework is needed to deal with the radiological component, which is currently omitted within LCA. Hitherto, radiological burdens have only been identified in the Inventory stage of LCA and assessed in terms of Becquerels (which is the SI derived unit of radioactivity). Currently there are 6 published methodologies that aim to assess radiological impacts within LCA.

**Critical Volume Approach**

Critical Volume Approach is based on the Annual Limit of Intake (ALI), which is a quality standard designed to meet the basic limit for occupational exposure of a given radionuclide. It takes into account internal exposure (inhalation and ingestion) and also impacts of daughter products, but other factors, such as chemical toxicity, are ignored. Furthermore it does not consider the fate and exposure pathways of radionuclides through the environment but only accounts for the effects of internal exposure to direct emission.

**Site-Specific Approach - Critical Group Dose (CGD)**

Site-specific models can be used to assess the actual impact of a radionuclide released from a plant to individual humans within specific critical groups. The critical group is defined as the member(s) of the public most exposed to radiation due to activities carried out at a given site. The dose to members of a specific critical group is calculated as the average of the sums of effective doses as results of internal and external exposure during the year taking into account all relevant pathways. CGD impacts are calculated from the application of conversion factors, named *Dose Release Ratios*, which take into account local conditions.

**Damage Based Assessment**

A different approach based on the assessment of the human health damages related to the routine release of radioactive materials to the environment within the LCA has been proposed [8]. The fate and exposure analysis of radionuclides are taken from site-specific modelling of the French nuclear fuel cycle carried out by Dreicer et al. [9], from which exposure factors were derived. The result of the pathway analysis is the amount of radioactivity to which the population is exposed, which is then converted to an effective whole body and collective doses. From collective doses, health effects are estimated statistically by the use of Disability Adjusted Life Years (DALY) [10].

**Risk Based Assessment – Human Irradiation Category**

This approach [11] is able to assess quantitatively both the probability of an event and the probability of exposure. The risk of detrimental effect caused by radionuclides is taken to represent the contribution to the Human Irradiation Category. Furthermore, this approach divides solid waste and routine discharges into different sub-groups and quantifies the potential risk of detrimental effect posed by each of them. Individual risk is calculated as follows:

$$R = P E F \tag{1}$$

Where:

- R Annual risk of a detrimental health effect as a result of radiation exposure due to the waste emission ( $y^{-1}$ )
- P Probability that the individual will incur a dose; i.e. nature of discharge ( $y^{-1}$ )
- E The Effective or Committed Effective dose incurred (Sv)
- F Probability per unit dose of detrimental effect ( $Sv^{-1}$ )

The term probability is defined in terms of frequency of occurrence while risk is defined by the International Committee of Radiation Protection (ICRP) as the probability that a serious detrimental health effect will occur in a potentially exposed individual or their descendant. This definition of risk is only valid as an indicator for stochastic events at low doses; since for low values the average dose depends on a linear relationship between dose and response (usually fatal cancer is considered as the highest probability of occurrence).

**The Environmental Irradiation Category**

The Environmental Irradiation [11] approach may be used to assess radiological impact of radionuclides to the environment. This approach does not aim to evaluate the potential risk of detrimental effect since there are no established relationships for the effect of radionuclides on non-human biota. The potential

contribution of radionuclides is evaluated using Environmental Increments (EI) factors [12]. These represent the concentration that can be added to soil and water without causing detectable effects, which is based on the assumption that the biota are already exposed to radionuclides in the environment and therefore can tolerate some exposure.

**NDA – Safety and Environmental Detrimental Scores**

Safety and Environmental Detrimental (SED) score [13] has been developed within the NDA value framework tool kit [14] in order to express consistently the concerns generated by different facilities. SED score assesses the potential impact of the stored material being released in the environment, taking into account facilities conditions, typology and condition of contents, but it takes no account of the likelihood. It is based on the assumption that all the facility contents are released and they are released in their most dispersible form. In probabilistic risk assessment this event would be ranked as improbable and considered negligible.

**Conclusions, Discussions and Future Work**

Six existing methodologies to assess radiological impact of radionuclides have been reviewed. Critical Volume methodology appears to be an extremely limited and thus unsuitable approach since it fails to take into account the fate and exposure pathways of radionuclides through the environment and it only considers the effects of internal exposure to direct emission. Between the remainder methodologies Site-specific approach is the most realistic because it utilises ‘real’ and specific data to assess the actual impact of aerial and marine releases using advance impact-pathways models; however its applicability within LCA is somewhat limited because it requires an extremely comprehensive and specific amount of data and furthermore it cannot be applied to solid wastes, as their impact in terms of dose is negligible. The Damage Assessment approach is the only methodology that can assess and quantify detrimental effect to human beings. Furthermore, it is also a very realistic model, as it incorporates a significant quantity of site specific data [9], which on the other hands means that it can be applied only to European installations; and it doesn’t take into account health impacts of waste disposal. The Risk-based approach is the only methodology that can account for the radionuclide impacts associated with solid waste disposal, but in turn it is less accurate and more general than the two methodologies mentioned above. . On the other side, the Environmental Irradiation approach is the only published methodology that considers radiological impact to the environment; however its applicability is still limited since data for many radionuclides are still

missing. Finally, the SED score methodology evaluates the hazard posed by materials stored within different facilities across the NDA estate, providing useful information to support NDA’s corporate planning and prioritisation processes; but it takes no account for likelihood of an event.

Therefore, it is clear that hitherto the most appropriate methodology to properly evaluate the radiological impact of nuclear fuel cycles and waste management is the Risk-based approach, as it is able to assess radiological impacts of all waste forms and it is adequately general to be applied to different nuclear plants. Furthermore, data requirement for this methodology it is not excessively burdensome.

Along with a review of existing radiological impact assessment methodologies, a review of existing nuclear fuel cycle configurations is also being carried out. The aim of this work is to have a comprehensive perspective of nuclear energy and waste management worldwide approach. Future work comprises the identification of an open loop case scenario for a Life Cycle Assessment investigation.

**References**

- [1] Department for Business Innovation & Skills, “The UK ’ s Nuclear Future.”
- [2] United Nations: Department of Economic and Social Affairs, “World population prospects: The 2012 Revision,“ ESA/P/WP.228, 2013.
- [3] U.S. Energy Information Agency, “International Energy Outlook 2013.” p. 312, 2013.
- [4] M. O’Brien, A. Doig, and R. Clift, “Social and environmental life cycle assessment (SELCA),” *Int. J. Life Cycle Assess.*, vol. 1, no. 4, pp. 231–237, 1996.
- [5] J. Fava, R. Denison, B. Jones, M. A. Curran, B. Vigon, S. Selke, and J. Barnum, *A Technical Framework for Life-Cycle Assessment*. Washington: SETAC and SETAC Foundation for Environmental Education, 1991.
- [6] International Organisation for Standardisation, “Environmental Management - LifeCycle Assessment - Principles and Framework, ISO 14040; Goal and Scope Definition and Life Cycle Inventory Analysis, ISO 14041; Life Cycle Impact Assessment, ISO 14042; and Life Cycle Interpretation, ISO 14043.” ISO, Geneva.
- [7] A. M. Tillman, T. Ekvall, H. Baumann, and T. Rydberg, “Choice of system boundaries in life cycle assessment,“ *Doktorsavhandlingar vid Chalmers Tek. Hogsk.*, vol. 2, no. 1365, pp. 21–29, 1998.
- [8] R. Frischknecht and A. Braunschweig, “Human health damages due to ionising radiation in life cycle impact

assessment," *Environ. Impact Assess. Rev.*, vol. 20, pp. 159–189, 2000.

- [9] M. Dreicer, P. Tort, and P. Manen, "ExternE Externalities of Energy, Vol. 5, Nuclear," Luxembourg, 1995.
- [10] C. J. L. Murray and A. D. Lopez, "Alternative projections of mortality and disability by cause 1990-2020: Global Burden of Disease Study," *Lancet*, vol. 349, no. 9064, pp. 1498–1504, 1997.
- [11] B. Solberg-Johansen, "Environmental Life Cycle Assessment of the Nuclear Fuel Cycle," University of Surrey, 1998.
- [12] B. D. Amiro, "Protection of the environment from nuclear fuel waste radionuclides: a framework using environmental increments," *Sci. Total Environ.*, vol. 128, pp. 157–189, 1993.
- [13] M. Wareing, "ICEM2009-16399," in *Proceedings of 12th International Conference on Environmental Remediation and Radioactive Waste Management/Nuclear Decommissioning*, 2009, pp. 1–9.
- [14] Nuclear Decommissioning Authority, "NDA Prioritisation – Calculation Of Safety And Environmental Detriment Scores Doc No EGPR02 NDA Prioritisation," 2011.

# Real-time Fast Neutron Plutonium Assay for Plutonium Storage and Ageing Applications

R. Sarwar\*<sup>1</sup>, M. J. Joyce<sup>1</sup>, and C. H. Zimmerman<sup>2</sup>

\*Correspondence: r.sarwar@lancaster.ac.uk

<sup>1</sup>Engineering Department (Lancaster University, Lancaster, UK LA1 4YR)

<sup>2</sup>The Central Laboratory (The UK National Nuclear Laboratory, Sellafield, Cumbria, UK CA20 1PG)

## Abstract

The studentship supported by the National Nuclear Laboratory on this topic is part of the EPSRC DISTINCTIVE consortium along with Lancaster University with the aim of (i) identifying the multiplicity distribution of a sample in real-time using liquid scintillation detectors to discriminate between different isotopes and (ii) exploiting ( $\alpha$ , n) reactions to identify the uncorrelated events from the correlated neutrons. This report aims to outline the timeline of the project and summarize the progress made in the first quarter of the studentship.

## Introduction

Nuclear safeguards is the discipline that ensures that civilian nuclear installations are not being misused to pursue weapons and that associated materials are not diverted to illegal usage. The well-established techniques for verifying this includes containment, surveillance using cameras, passive/active radiation monitors (non-destructive analysis), material sampling (destructive analysis), etc.

The most important aspect of nuclear materials safeguard is to ensure that both irradiated and non-irradiated nuclear fuel are not being unlawfully tampered with during the nuclear fuel cycle. To identify tampering, several non-destructive techniques can be employed including: (i) reconstruction of the spatial distribution of various isotopes with gamma tomography methods, (ii) Fork Detector with a fission chamber [1], (iii) Neutron Underwater Coincidence Counters (UWCC) using <sup>3</sup>He [2], (iv) the Cherenkov viewing device [3], etc. Each method has its benefits, but individual limitations too, like the enrichment requirements for Fork Detector fission chamber, limited availability of <sup>3</sup>He for UWCC [4], etc.

Development of advanced fuel cycle material, such as mixed-oxides (MOX) fuel leads to further ineffectiveness of existing safeguard techniques. For example, safeguard techniques like gamma-ray spectroscopy are made complicated by the presence of different actinides and long-lived fission products in MOX fuel leading to multiple gamma emission, particularly from <sup>137</sup>Cs (662 keV gamma-ray emission) thereby overwhelming the response of almost all gamma detection systems. At the same time, neutron

based techniques using <sup>3</sup>He detectors are made complex by (i) presence of multiple actinides in the MOX fuel acting like neutron sources having signatures comparable to plutonium, (ii) loss of information regarding the initial energy of the neutron as moderation of incident neutrons is typically required for these techniques and (iii) the increased likelihood of accidental coincidence counts due to long gate width of <sup>3</sup>He detectors, typically in the order of microseconds [5]. Additionally, <sup>3</sup>He is becoming increasingly scarce since it is a radioactive material with a short half-life and is produced as a by-product of the production of nuclear weapons.

A solution to the above mentioned difficulties could be achieved by using liquid scintillation detectors (LSD) [6] for fast neutron multiplicity analysis. In these types of detectors, the incident radiation excites the electrons of the atoms in the detector's active region, sending them to a higher energy state. Excited atoms then return to the ground state by releasing energy, in some cases as a photon of light, which is then detected using a photomultiplier tube. These detectors are sensitive to both fast neutrons and gamma-radiation. Furthermore, they hold several advantages over the detectors mentioned in the earlier paragraph. Firstly, they can be used for the detection of fast neutrons without moderation leading to retention of incident energy of the detected neutrons. Secondly, they have extremely short gate time (three orders of magnitude lower than <sup>3</sup>He detectors), allowing reduced accidental coincidences and thus being able to detect high order of multiplicity. Last but not least, being sensitive to both gamma and neutron radiation allows a system using these detectors to determine other parameters

about the test environment by utilizing both photon and neutron multiplicities.

### Aim of the studentship

The studentship supported by the National Nuclear Laboratory on this topic is part of the EPSRC DISTINCTIVE consortium along with Lancaster University. The proposal is to focus on plutonium assay and isotopics in high-background environments and on the assessment of ageing via the separation of Pu-240 and Am-241-induced neutron signatures. The hypotheses behind these activities are as follows:

1. Can plutonium (Pu-240) be discerned from curium (Cm-244) in the field on the basis of differences in their fast neutron fission multiplicity distributions?
2. Can the relative difference between uncorrelated, 'singles' neutrons derived from ( $\alpha$ , n) reactions and correlated neutron emissions from plutonium (Pu-240) be exploited to infer plutonium ageing?

### Review of project

The activities completed during the first quarter primarily include a literature review in the specific areas of research. Additionally, simulations using MCNP6<sup>1</sup> and MCNPX-PoliMi were carried out to better the understanding of the physics involved in the work.

In the nine months to follow the submission of this summary, it is advisable to be resident at Sellafield for one week in order to meet with NNL experts, the facilities of relevance to this work-package of the DISTINCTIVE consortium and to observe and understand the current techniques and challenges for plutonium assay. However, the focus of the period will be on learning the experimental techniques central to the project. This will be done primarily at Lancaster. Since the move to the new departmental building has now been completed, this step can start soon. The equipment central to this activity will derive from the ADRIANA set up, as part of the National Nuclear Users' Facility. Key analytical goals in this period will be to: i) determine the uncertainty between singles events and coincident events and ii) obtain a multiplicity distribution for Cf-252. The completion of this activity will coincide with the end of year 1 and the university probationary report requirement, these measurements being the content of that.

Year 2 will focus on the engineering design of field-deployable detection systems for high-field plutonium assay amidst curium contamination and plutonium

ageing. Routine interaction with NNL experts will be necessary to ensure the system designs are compatible with use in the NNL laboratory and, if possible, with in-field measurements at Sellafield. It is anticipated that some of the equipment used in the systems will derive from the ADIRANA instrumentation already in place at Lancaster, with the focus being on the number of detectors, transportability, prevention of accidental contamination and real-time data analysis.

Year 3 will be dedicated to obtaining in-field plutonium data in the UK, either at NNL or Sellafield facilities. This schedule has been planned with the foresight that this activity will take significant preparation, especially if we are to emulate 'real' plutonium storage challenges associated with contamination fields and ageing. The output from this will be high-quality peer-reviewed papers reporting fast neutron based separation of plutonium and curium, and fast neutron based ageing of plutonium for the first time. Discussions will be ongoing as to the deployment of these techniques against UK decommissioning challenges.

### Progress in first quarter

Over the last three months, literature review of the physics and engineering concepts required for the project has been undertaken. Some of the topics that were particularly significant include: gamma & neutron radiation and its interaction with matter, neutron detection and multiplicity techniques, curium in spent fuel, etc [7]-[14]. Additionally, some simulations were conducted in MCNP6 and DRAGON<sup>2</sup> to understand changes in isotopic composition following different fuel irradiation histories and cooling times.

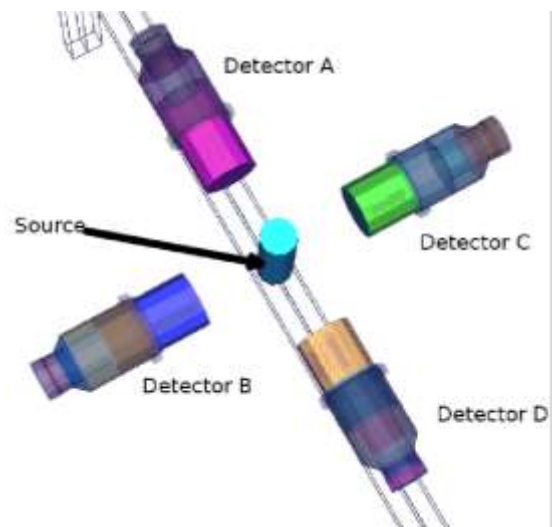


Figure 1 MCNP model

<sup>1</sup> Developed by Los Alamos National Laboratory, it is a general-purpose Monte Carlo N-Particle code that can be used for neutron, photon, electron, or coupled neutron/photon/electron transport.

<sup>2</sup> Developed by POLYTECHNIQUE MONTRÉAL, it is a collection of models which can simulate the neutron behaviour of a unit cell or a fuel assembly in a nuclear reactor.

In order to simulate the expected detector response, a set of detailed models of possible experimental setup was implemented in both MCNP6 and MCNPX-PoliMi. Figure 1 shows one such possibility.

Unfortunately, neither of the two transport codes is able to process energy and multiplicity response for a liquids scintillation system in the manner needed that allows neutron cross-talk between detectors. To do this, special C++ Classes were written to parse the PTRAC (and the DUMN1/DUMN4 from MCNPX-PoliMi) files from MCNP6/MCNPX-PoliMi output files and process the information as per requirement. This allowed collection of energy response for individual detector as well as neutron (and gamma) multiplicities while preserving information about neutron (and gamma) crosstalk<sup>3</sup> between detectors (i.e. the tool is able to identify and remove crosstalk). Additionally the program is also able to process data in both time-related<sup>4</sup> and fission-related<sup>5</sup> manner while taking into consideration user defined cut-off energy to ensure a detector response close to practical expectation<sup>6</sup>.

Using this tool, research is being conducted into quantifying the severity of neutron crosstalk between detectors<sup>7</sup>.

## Conclusions and Future Work

The project has started off well. The major research undertaking during the period has been the literature review and MCNP simulation. Till date the project is moving forward according to plan and progressing as expected.

Listed below are some of the plans for the upcoming six months:

1. *Finalisation of the cross-talk investigation:* initial simulations have been completed. There is however a matter of investigating the results in depth and possibly conducting

further experiments to better understand the findings.

2. Build a *shift register* using a De2-115 which will allow the acquisition of real time data from liquid scintillation detection system with the aim of carrying out multiplicity and time-of-flight analysis.
3. *Multiplicity distribution of Cf-252:* determination of the multiplicity distribution of Cf-252 and the uncertainties of experiments using liquid scintillation detector.
4. *Uncertainty analysis:* determination of the uncertainties in experiments collecting single and coincidence events using liquid scintillation detector.

## References

- [1] P. M. Rinard, G. E. Bosler, Safeguarding LWR spent fuel with the fork detector.
- [2] G. Eccleston, H. O. Menlove, M. C. B. M. Abhold, J. Pecos, The underwater coincidence counter UWCC for plutonium measurements in mixed-oxide fuels, Nuclear Materials Management: 39th Annual Meeting Proceedings, Naples, Florida.
- [3] E. Attas, J. Chen, G. Young, "A cherenkov viewing device for used-fuel verification ", Nuclear Instruments and Methods in Physics Research Section A: Accelerators, Spectrometers, Detectors and Associated Equipment 299 (1–3) (1990) 88 – 93.
- [4] A. J. Keller, An increasingly rare isotope, Stanford University, 2011.
- [5] D. L. Chichester, et al., Mpsact fast neutron multiplicity system design concepts, Los Alamos National Laboratory, Report INL/EXT-12-27619
- [6] M. Joyce, M. Aspinall, F. Cave, A. Laviertes, Real-time, digital pulse-shape discrimination in non-hazardous fast liquid scintillation detectors: Prospects for safety and security, Nuclear Science, IEEE Transactions on 59 (4) (2012) 1245–1251.
- [7] Reilly, N. Ensslin, H. S. Jr. (Eds.), Passive Nondestructive Assay of Nuclear Material, Los Alamos National Laboratory Report, Report LA-UR-90-732, Washington, DC 20555, 1991.
- [8] G. Choppin, J.-O. Liljenzin, J. Rydberg, C. Ekberg, in: Radiochemistry and Nuclear Chemistry (Fourth Edition), fourth edition, Academic Press, Oxford, 2013.
- [9] A. Enqvist, C. C. Lawrence, B. M. Wiegner, S. A. Pozzi, T. N. Massey, Neutron light output response and resolution functions in ej-309 liquid scintillation detectors, Nuclear Instruments and Methods in Physics Research Section A: Accelerators, Spectrometers, Detectors and Associated Equipment 715 (0) (2013) 79 – 86.
- [10] M. Joyce, K. Gamage, M. Aspinall, F. Cave, A. Laviertes, Real-time, fast neutron coincidence assay of plutonium with a 4-channel multiplexed analyzer and organic scintillators, Nuclear Science, IEEE Transactions on 61 (3) (2014) 1340–1348.
- [11] J. M. Verbeke, C. Haggmann, D. Wright, Simulation of neutron and gamma ray emission from fission and photo fission, Lawrence Livermore National Laboratory, UCRL-AR-228518, 2014.
- [12] N. Ensslin, W. C. Harker, M. S. Krick, D. G. Langner, M. M. Pickrell, J. E. Stewart, Application guide to neutron multiplicity counting, Los Alamos National Laboratory Report, LA-13422-M.
- [13] P. Chard, S. Croft, I. Hutchinson, Compensating for curium in wastes measured by neutron assay systems, Proceedings of the 31st ESARDA Symposium on Safeguards & Nuclear Material Management, France, May 1997.
- [14] J. G. Richard, Analysis of the neutron source term of a spent fuel assembly, Thesis, University of Florida, 2010 (unpublished).

<sup>3</sup> A single neutron is scattered between two detectors where these consecutive events are interpreted as a coincidence of two correlated neutrons.

<sup>4</sup> Detection is made based on detector window: number of particle detected within a user-specified gate width following an event-generated trigger. In this case, it is possible for a particle to be scattered between two detectors and being registered as two different singles if the two events fall in two different detector window.

<sup>5</sup> Detection is made based on the number of neutron detected per fission event, ignoring detection window altogether.

<sup>6</sup> This algorithm considers the amount of energy deposited in the active region of each detector rather than looking for number of particles passing through them.

<sup>7</sup> This algorithm considers the amount of energy deposited in the active region of each detectors as well as the amount of energy deposited by each particle in different detectors. A crosstalk is only considered if the multiplicity order for a given detector window changes had there been no scattered events.

# The Behaviour of Used Nuclear Fuel in Wet Storage

D. M. Laventine\*<sup>1</sup>, C. Boxall<sup>1</sup>, R. Taylor<sup>2</sup> and D. Woodhead<sup>2</sup>

\*Correspondence: d.laventine@lancaster.ac.uk

<sup>1</sup> University of Lancaster, Lancaster, LA1 4YR, UK

<sup>2</sup> Central laboratory, B170, National Nuclear Laboratory, Sellafield, CA20 1PG, UK

## Abstract

We have developed a method which enables direct gravimetric measurement of water adsorption onto CeO<sub>2</sub> thin films. Porous CeO<sub>2</sub> films were fabricated from a surfactant based precursor solution. The absorption of water onto the CeO<sub>2</sub> coating at different relative humidities was studied in a closed reactor. Quartz Crystal Microbalance (QCM) gravimetry was used as a signal transducer, as changes in crystal resonant frequency due to absorbed mass are directly and linearly related to mass changes occurring at the crystal surface.

## Introduction

The product of approximately 50 year's civil nuclear fuel reprocessing, about 100 tonnes of Pu are stored at the UK Sellafield site alone. With minor differences, the storage system is very similar to the US approach (DOE standard: stabilization, packaging, and storage of plutonium-bearing materials, DOE-STD-3013-2012, Washington, D.C., 2012). Specifically, the general form of this Pu is as calcined plutonium dioxide (PuO<sub>2</sub>) powder usually contained within a series of nested stainless steel cans with the outer can welded to maintain storage integrity, although the characteristics of UK PuO<sub>2</sub>, predominantly derived from the Magnox and THORP reprocessing plants, are somewhat different from US PuO<sub>2</sub>. Current UK plans are to store in cans long term for several decades with the UK Nuclear Decommissioning Authority (NDA) estimating UK Pu stocks will remain in storage for at least 30-50 years, and possibly until 2120.[1] Whilst PuO<sub>2</sub> is also produced from reprocessing operations in e.g. France, storage times are generally much shorter before incorporation into MOX fuel. Thus, the UK situation is unique in relation to PuO<sub>2</sub> characteristics, expected duration of storage and amount stored.

Under certain circumstances, Pu stores have been observed to cause gas generation within the can and consequent pressurisation of the storage package. This comprises one of the most serious fault scenarios that must be considered in the safety cases for long term

PuO<sub>2</sub> storage and avoided in practice. Whilst empirically or phenomenologically derived criteria are used to maintain safe storage conditions, the fundamental mechanisms that lead to pressurisation are poorly understood, although samples withdrawn from can headspaces indicate that the gas is oxygen deficient with a high hydrogen content. 5 main routes to gas production have been suggested:

- Helium accumulation from alpha decay;
- Decomposition of polyethylene packing material;
- Steam produced from adsorbed water during self-heating of cans;
- Radiolysis of adsorbed water;
- Generation of H<sub>2</sub> by chemical reaction of PuO<sub>2</sub> with H<sub>2</sub>O, also producing a postulated PuO<sub>2+x</sub>.

## Methodology

Water adsorption on PuO<sub>2</sub> has previously been investigated by measuring headspace pressure, as a function of temperature within a closed system containing a fixed quantity of PuO<sub>2</sub> in the presence of varying amounts of deliberately added water [2].

This involves making a number of assumptions relating to the pressure-volume-temperature behaviour of the headspace of the closed system, usually based on the behaviour of an ideal gas, in order to estimate the mass of water adsorbed at the PuO<sub>2</sub> surface. Assuming ideality at high temperatures and pressures is

problematic and, at best, only gives an indirect measurement of water adsorption on PuO<sub>2</sub>. Water adsorption on PuO<sub>2</sub> has also been investigated as a function of relative humidity at 25°C [2]. These studies, however, were not carried out at the high temperatures that can exist within a THORP derived plutonium dioxide storage containers, with Pu238 having a high thermal output of 560 W/kg. Thus, there currently exists a gap in the knowledge regarding the exact mass of water which adsorbs on PuO<sub>2</sub> powders in the closed, heated conditions within a PuO<sub>2</sub> storage container.

Ceria (CeO<sub>2</sub>) is widely used as a non-radioactive PuO<sub>2</sub> surrogate due to its oxidation state, ionic radius and fluorite crystal structure. We have proposed to deposit thin films of ceria onto piezo-active crystals and use QCM methodology to directly measure any mass changes under a range of temperatures and humidities. The mass changes, combined with accurate measurements of surface area, can then be used to calculate the amount of water adsorbed onto the ceria surface and the thermodynamic requirements for its desorption [3].

Thin films of ceria have previously been deposited onto quartz wafers through spin-coating a precursor cerium salt aqueous solution followed by calcination. Scanning electron microscopy was used to determine the thickness and roughness of the layers produced. The coated crystals were mounted within the pressure vessel using a custom made crystal holder which exposed both faces of the crystal to the pressurized environment of the vessel, so preventing breakage. The holder had a maximum operating temperature of 200 °C and was constructed of PTFE.

The change in mass resulting from deposition or desorption of water onto or from the metal oxide coating could then be directly measured by Quartz Crystal Microbalance (QCM) methodology. This is a well-established gravimetric device that measures the change in resonant frequency of a piezo-electrically active crystal as mass is added or removed from the surface. The linear relationship between frequency shift and mass change on the crystal surface is described by the Sauerbrey Equation.

## Results and Discussion

Measurement of the mass changes using the above methods was performed in a sealed pressure reactor,

allowing control of the temperature, pressure and humidity. A number of studies were undertaken that allowed the adsorption of water to be measured under a variety of real-world applicable conditions.

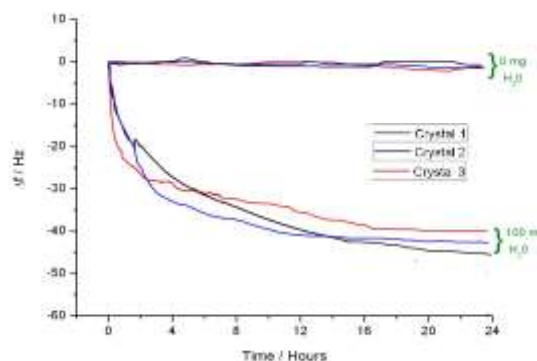


**Figure 1** Graph showing the reduction in frequency of a CeO<sub>2</sub> coated (40 nm thick) quartz crystal due to adsorption of water.

The crystals employed in the initial ceria model studies were SiO<sub>2</sub> quartz, and evince a cubic temperature-frequency relationship. The current goal of the project is to repeat this work using GaPO<sub>4</sub> crystals, which have a linear temperature-frequency correlation, allowing more accurate measurement of the frequency (and hence mass) changes.

## Conclusions and Future Work

Subsequent to this optimisation and validation of the initial results, the experimental set up will be transferred to the National Nuclear Laboratories at Sellafield. These facilities will allow the use of radioactive plutonium oxide and investigation of its interactions with water.

## Acknowledgements

This work was funded by the UK's National Nuclear Laboratory, the EPSRC and further supported by the Lloyd's Register Foundation (LRF), a UK registered charity.

## References

- [1] Gilchrist, P., *Plutonium Strategy: Current Position Paper*. Nuclear Decommissioning Authority, 2011.
- [2] J. M. Haschke, T.E. Ricketts, J. Alloy Compd., 252, 148-156, 1996.
- [3] C Lu, O. Lewis, J. Appl. Phys., 43, 4835, 1972.

# Studying the Effects of Chloride Contamination on the Surface of Plutonium Dioxide

Sophie Sutherland-Harper\*<sup>1</sup>, Jeff Hobbs<sup>2</sup>, Simon Pimblott<sup>1</sup>, Robin Taylor<sup>1,3</sup>, and Carolyn Pearce<sup>1</sup>

\*sophie.sutherland-harper@postgrad.manchester.ac.uk

<sup>1</sup>*School of Chemistry and Dalton Nuclear Institute, University of Manchester*

<sup>2</sup>*Sellafield Ltd., Cumbria*

<sup>3</sup>*National Nuclear Laboratory, Sellafield, Cumbria*

## Abstract

A quantity of plutonium dioxide powders in storage at the Sellafield site in Cumbria has become contaminated with chloride ions from the degradation of polyvinyl chloride (PVC) within the package, along with moisture from the atmosphere; chloride and water are thus adsorbed to the surface of PuO<sub>2</sub>. This 'high chloride' PuO<sub>2</sub> must be dried prior to repackaging in welded cans for safe, long term storage. Therefore an interfacial study of water- and Cl<sup>-</sup>-contaminated PuO<sub>2</sub> is essential to understand its properties and develop a treatment process. Due to difficulties in working with plutonium, using analogues is important to optimise analytical techniques and to provide more complete predictions of the probable behaviour of PuO<sub>2</sub> in advance of plutonium-active experiments. This review summarises the techniques which will be employed to study PuO<sub>2</sub> and includes initial data obtained using X-Ray Diffraction and X-Ray Photoelectron Spectroscopy for analysis of Cl<sup>-</sup>-contaminated ceria (CeO<sub>2</sub>) as an analogue.

## Introduction

There are currently over 100 tonnes of PuO<sub>2</sub> stored at the Sellafield site in Cumbria as the product of reprocessing spent fuel from nuclear reactors. During some of the early reprocessing operations between 1970 and 1975, powder production was placed into a packaging system consisting of a screw top aluminium inner container, inside 2 layers of PVC and placed into an aluminium screw top outer container. The PVC has degraded due to the radiation emitted by the PuO<sub>2</sub> and contaminated around 5 tonnes of the PuO<sub>2</sub> with chloride from the evolved HCl as well as adsorbed moisture from the atmosphere. The leading option for plutonium disposition in the U.K. is to re-use the PuO<sub>2</sub> as a mixed-oxide fuel for new-build nuclear reactors, but it must be stored safely and securely in the meantime. Repacking this material for interim storage in welded cans in the new Sellafield Products and Residue Store is planned but this requires meeting specific conditions for acceptance (C.F.A.); most notably the material must be dried to meet a low loss on heating (L.O.H.) condition. Therefore understanding how the material will behave when dried in a retreatment plant as well as how Cl<sup>-</sup>-contaminated PuO<sub>2</sub> evolves over time is necessary. Past experiments have revealed a recalcitrant fraction of Cl<sup>-</sup> within PuO<sub>2</sub> that cannot be leached out under the conditions studied. It is ideal for PuO<sub>2</sub> to have an oxidation state of 4+, which is insoluble in water, so it will not leach as

much as +5 or +6 in groundwater. PuO<sub>2</sub> is both toxic and radiotoxic, so using non-toxic analogues with the same oxidation state and similar properties to PuO<sub>2</sub>, such as CeO<sub>2</sub> or ZrO<sub>2</sub>, is beneficial as it avoids dangerous and expensive laboratory work.<sup>1</sup> Investigations on these analogues should provide an insight into the expected behaviour of contaminated PuO<sub>2</sub>, particularly with respect to physical effects, despite the fact that plutonium will have radiological effects, which cerium does not, and a different affinity for various oxidation states in solid form (Pu (IV) exists in solid form and Pu (III) in liquid, whereas Ce (III) and (IV) both exist in the solid phase, so both oxidation states could be seen). Techniques which will be used to analyse the surface of water- and Cl<sup>-</sup>-contaminated PuO<sub>2</sub> and its analogues are reviewed here, as well as some initial X-Ray Diffraction and X-Ray Photoelectron Spectroscopy data which have been collected for Cl<sup>-</sup>-contaminated CeO<sub>2</sub>.

## Experimental Methods

### Sample preparation

CeO<sub>2</sub> microparticles and nanoparticles were prepared by oxalate precipitation at 25 °C and calcined at 900 °C and 500 °C respectively in order to establish how Cl<sup>-</sup> is adsorbed to particles of low specific surface area (low SSA) and high specific surface area (high SSA). After exposing CeO<sub>2</sub> to a Cl<sup>-</sup> atmosphere by placing the samples in glass vials within HCl solution for 7 days, the

samples were heat treated at 500 and 900 °C. Analyses were carried out on low SSA and high SSA as-synthesised, Cl<sup>-</sup> contaminated and heat treated samples.

### Transmission/Scanning Electron Microscopy-Energy Dispersive X-Ray Analysis (TEM/SEM-EDX)

TEM and SEM will provide images of the surface of the materials to determine particle size and distribution, and how the particles agglomerate. EDX will analyse the chemical composition of the samples, both qualitatively and quantitatively, to determine the extent of Cl<sup>-</sup>-contamination.<sup>2,3 and 4</sup>

### X-Ray Diffraction (XRD)

XRD will identify the crystalline phases and cell parameters in the average bulk materials-it does not provide surface detail. It can also provide information about particle sizes from the width of the peaks.<sup>5</sup> PuO<sub>2</sub> and CeO<sub>2</sub> have Fm3m face-centred cubic phases, so CeO<sub>2</sub> should prove to be an appropriate surrogate when measuring XRD patterns.<sup>6</sup>

### X-Ray Photoelectron Spectroscopy (XPS)

XPS will determine the chemical composition of samples and provide further information about bonding on the surface, as each element has specific orbital energies which correspond to specific binding energies of the electrons; the bonding environment of an atom will affect these binding energies, so an understanding of the surface species can be developed.<sup>7</sup>

### Thermogravimetric Analysis (TGA)

TGA measures how the mass of the sample changes with temperature from 25 °C up to 1,000 °C, confirming which molecules are present and a quantitative value of their content. It can be carried out in a variety of atmospheres (e.g. air, N<sub>2</sub> and He) as well as under vacuum, so any reactions with air and other gases can be analysed. It can also be used to assess the purity of the sample and to determine the volatility of the sample using calculated evaporation rates.<sup>8</sup>

### X-Ray Absorption Spectroscopy (XAS)

XAS analyses the oxidation state and average coordination environment for a specific atom within a sample. Core electrons absorb X-Rays at an energy above their binding energy and hence are excited from their shell. The ejected electrons then interact with surrounding atoms, emitting energy as waves, which are detected as a function of energy. X-Ray Absorption Near Edge Structure (XANES) measures the absorption spectrum between the atom and its nearest neighbour and X-Ray Absorption Fine Structure (XAFS) measures the absorption spectrum of atoms at larger interatomic

distances; both combine into XAS. It is a diagnostic technique, as different oxidation states and surrounding atoms produce unique absorption spectra.<sup>9</sup>

## Results and Discussion

### XRD

XRD was carried out on each of the samples to examine how contaminating CeO<sub>2</sub> with Cl<sup>-</sup> affects the purity of the Fm3m cubic phase.

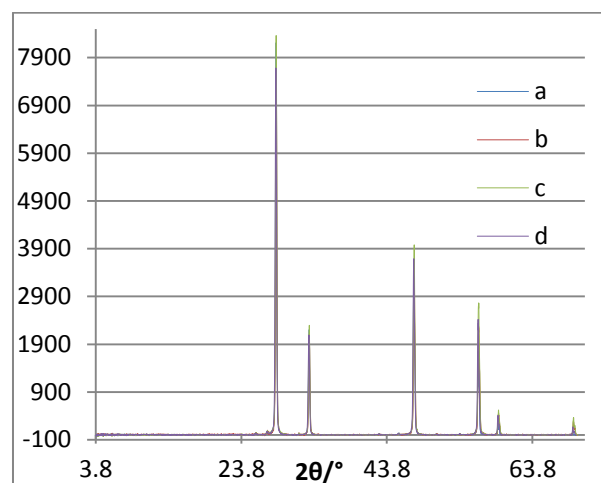


**Figure 1** XRD patterns of Cl<sup>-</sup>-contaminated CeO<sub>2</sub> microparticles (a=CeO<sub>2</sub>, b=Cl<sup>-</sup>-contaminated CeO<sub>2</sub>, c=Cl<sup>-</sup>-contaminated CeO<sub>2</sub> with calcination afterwards at 500 °C and d=Cl<sup>-</sup>-contaminated CeO<sub>2</sub> with calcination afterwards at 900 °C).

The XRD pattern of the uncontaminated and Cl<sup>-</sup>-contaminated CeO<sub>2</sub> microparticles (Fig. 1) show that Cl<sup>-</sup> does not affect the purity of the cubic phase,. Also, the full width half maximum (FWHM) of the peaks confirms that microparticles have been synthesised. Heat treatment results in only slight changes in the peak position and peak width as demonstrated by the 111 peak (Fig. 2) .

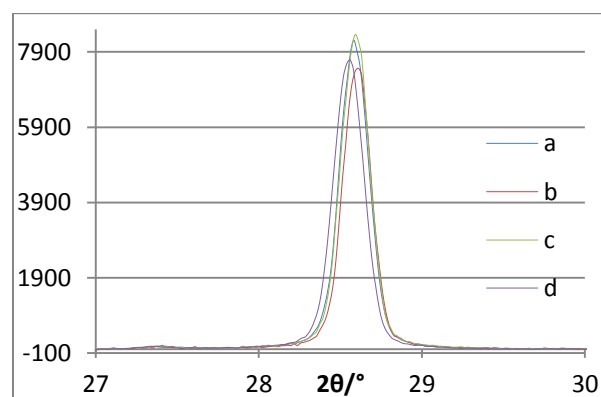


**Figure 2** XRD patterns of Cl<sup>-</sup>-contaminated CeO<sub>2</sub> microparticles for the 111 peak at 2θ ≈ 28.5 ° (a=CeO<sub>2</sub>, b=Cl<sup>-</sup>-contaminated CeO<sub>2</sub>, c=Cl<sup>-</sup>-contaminated CeO<sub>2</sub> with calcination afterwards at 500 °C and d=Cl<sup>-</sup>-contaminated CeO<sub>2</sub> with calcination afterwards at 900 °C).

The nanoparticles have much broader peaks and lower intensities than the microparticles due to their smaller size (Fig. 3). This confirms that CeO<sub>2</sub> particles of nanometre size were synthesised with the same cubic Fm3m phase as the microparticles.

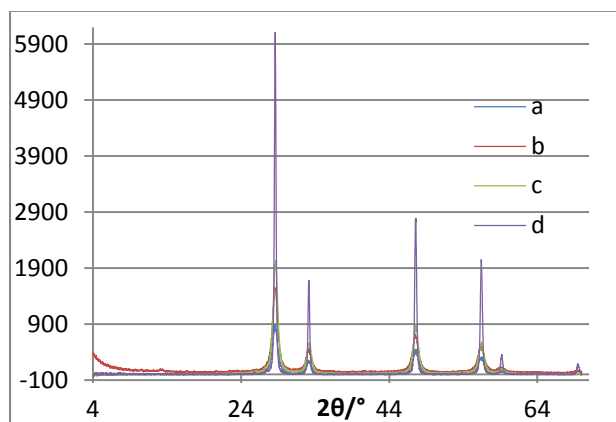


**Figure 3** XRD patterns of Cl<sup>-</sup>-contaminated CeO<sub>2</sub> nanoparticles (a=CeO<sub>2</sub>, b=Cl<sup>-</sup>-contaminated CeO<sub>2</sub>, c=Cl<sup>-</sup>-contaminated CeO<sub>2</sub> with calcination afterwards at 500 °C and d=Cl<sup>-</sup>-contaminated CeO<sub>2</sub> with calcination afterwards at 900 °C).

Unlike the microparticles, there is more of a variation between the broadened XRD peaks of the different nanoparticle samples (Fig. 4). Especially noticeable is the narrowing and increasing intensity of the peak corresponding to Cl<sup>-</sup>-contaminated CeO<sub>2</sub> after heating to 900 °C (Fig. 4d) compared to that heated at 500 °C (Fig. 4c). This is because the nanoparticles were only heated to 500 °C in the first calcination, so heating at a higher temperature resulted in particle aggregation to form particles with larger crystallite sizes.

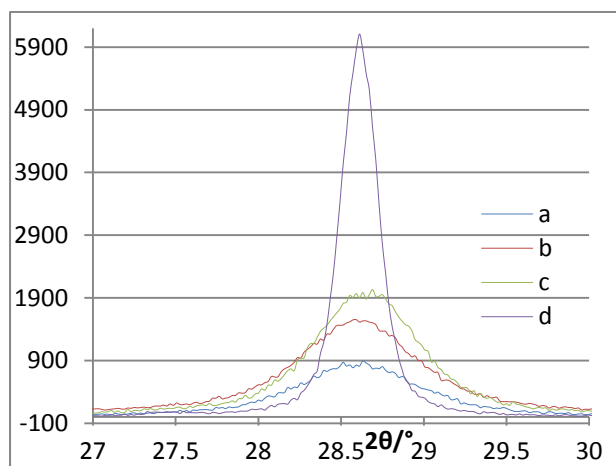


**Figure 4** XRD patterns of Cl<sup>-</sup>-contaminated CeO<sub>2</sub> nanoparticles at the main peak of 2θ ≈ 28.6 ° (a=CeO<sub>2</sub>, b=Cl<sup>-</sup>-contaminated CeO<sub>2</sub>, c=Cl<sup>-</sup>-contaminated CeO<sub>2</sub> with calcination afterwards at 500 °C and d=Cl<sup>-</sup>-contaminated CeO<sub>2</sub> with calcination afterwards at 900 °C).

## XPS

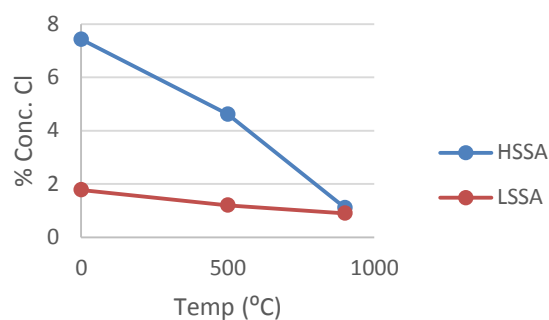


**Figure 5** XPS spectra of the Cl 2s shell Cl<sup>-</sup>-contaminated CeO<sub>2</sub> nanoparticles (HSSA) and microparticles (LSSA) heated to different temperatures.

XPS analysis shows that the CeO<sub>2</sub> nanoparticles are able to adsorb more Cl<sup>-</sup> than the microparticles, as they have a higher surface area (Fig. 5). As the particles are heated, a greater percentage of Cl<sup>-</sup> is removed from the nanoparticles, which are sintered even further to become more like the microparticles. However not all the Cl<sup>-</sup> is removed by this method, confirming earlier predictions and results.

## Conclusions and Future Work

A broad range of analytical techniques have been set out in order to provide a fully comprehensive and conclusive surface structure for water- and Cl<sup>-</sup>-contaminated PuO<sub>2</sub> and will be put into practice in the near future.

Cl<sup>-</sup>-contamination and heat treatment of CeO<sub>2</sub> does not appear to have a significant effect on the structure as the XRD peaks for the cubic Fm3m phase remain constant. However, heat treating the contaminated CeO<sub>2</sub> microparticles and nanoparticles above 500 °C does significantly affect the particle size, suggesting physical entrapment as a potential mechanism of stabilisation for the recalcitrant Cl<sup>-</sup>. XPS data suggest that heating to 900 °C has little effect on the Cl<sup>-</sup> concentration associated with the microparticles.

XPS confirms that more Cl<sup>-</sup> can be adsorbed to high SSA particles of ceria than low SSA ones and can be removed by heat treatment, but not totally. It also shows how similar the nano and microparticles become after being sintered at the same temperature.

Further XPS and XRD measurements of CeO<sub>2</sub> will be undertaken, in addition to TEM/SEM studies to determine how the structure changes with temperature and time, and to give an understanding of how the non-leachable fraction of Cl<sup>-</sup> remains trapped in the structure.

## Acknowledgements

Dr. Mark Sarsfield (National Nuclear Laboratory) for providing the samples and Mr. Mark Engelhard (Pacific Northwest National Laboratory) for the XPS analysis.

## References

- 1 C. Campbell, C. Gregson, R. Orr, H. Sims, R. Taylor and K. Webb, *NNL, National Nuclear Laboratory, Sellafield*, 2014, **12869**, 1–68.
- 2 D. Williams and C. Carter, *Transmission Electron Microscope*, 1996.
- 3 J. Atteberry, 2009, <http://science.howstuffworks.com/scanning-electron>.
- 4 B. Hafner, *Energy Dispersive Spectroscopy on the SEM : A Primer*, .
- 5 Philips Innovation Services, 2013. <http://www.innovationservices.philips.com/sites/default/files/materials-analysis-xrd.pdf>
- 6 D. Hudry, C. Apostolidis, O. Walter, A. Janßen, D. Manara, C. Griveau, E. Colineau, T. Vitova, T. Prüßmann, D. Wang, C. Kübel and D. Meyer, *Chemistry-A European Journal*, 2014, **20**, 10431–10438.
- 7 Seal Laboratories, . <http://www.seallabs.com/how-xps-works.html>
- 8 Anderson Materials Evaluation Inc., 2015. <http://www.andersonmaterials.com/tga.html>
- 9 M. Newville, *Fundamentals of XAFS*, 2004, 1-43.

## CaUTi<sub>2</sub>O<sub>7</sub> Ceramics for Actinide Disposition

Shikuan Sun, Martin Stennett and Neil Hyatt

\*Correspondence: shikuan.sun@sheffield.ac.uk

*Immobilisation Science Laboratory, Department of Materials Science and Engineering, The University of Sheffield,  
(Mappin Street, Sheffield S1 3JD, United Kingdom)*

### Abstract

Betafite pyrochlore, prototypically CaUTi<sub>2</sub>O<sub>7</sub>, is a potential host phase for actinide disposition in ceramic and glass-ceramic wasteforms. Processing – micro-structure - property relations were investigated, targeting nominal compositions A - Ca<sub>0.96</sub>U<sub>0.482</sub>Zr<sub>0.177</sub>Ti<sub>2.203</sub>O<sub>7</sub> and B - Ca<sub>0.872</sub>U<sub>0.669</sub>Zr<sub>0.161</sub>Ti<sub>2.01</sub>O<sub>7</sub>, with and without Ni or Fe buffer additions (10 wt%) to control uranium oxidation state. Ceramics of near theoretical density (>95%) were prepared by solid state reaction between CaTiO<sub>3</sub>, TiO<sub>2</sub>, ZrO<sub>2</sub> and U<sub>3</sub>O<sub>8</sub>, under 1 bar N<sub>2</sub>. Rietveld analysis of powder X-ray diffraction data, quantitative analysis of back-scattered electron microscopy data, and U L<sub>3</sub> edge XANES investigation revealed: Composition A, comprised 85% of the betafite phase, with an average U oxidation state of 4.3+; whereas Composition B, comprised 90% of the betafite phase with an average oxidation state of 4.4+. Addition of a Ni buffer had little effect on the phase assemblage but addition of the Fe buffer lead to the formation of an iron rich ulvospinel phase, Fe<sub>2</sub>TiO<sub>4</sub>; the U oxidation state remained unchanged at ca. 4.4+. This work is significant in demonstrating the synthesis of betafite pyrochlores in high yield at relatively low temperature (>85% at 1320°C) compared to previous studies (<<75% at 1450°C).

# Optimisation of Processing Parameters for the Consolidation of Actinide Glass-ceramic Wasteforms by Hot Isostatic Pressing

Stephanie Thornber\*<sup>1</sup>, Ewan Maddrell<sup>2</sup>, Martin Stennett<sup>1</sup>, Paul Heath<sup>1</sup> and Neil Hyatt<sup>1</sup>.

\*Correspondence: sthornber1@sheffield.ac.uk

<sup>1</sup> University of Sheffield, Immobilisation Science Laboratory, Department of Materials Science & Engineering, Sheffield, UK

<sup>2</sup> National Nuclear Laboratory, Sellafield, Seascale, Cumbria, CA20 1PG, UK

## Abstract

Hot Isostatic Pressing is a consolidation technique proposed to process glass-ceramic wasteforms for Pu-residue immobilisation. A matrix of samples were analysed by SEM and XRD to optimise pre-HIP calcination and bake out parameters and thus produce high density wasteforms suitable for long-term storage and disposal. Results show that the crystalline phases formed are conformed by glass phase composition, and that a high temperature calcination or bake out step is required to achieve high density HIP materials.

## Introduction

Glass-ceramics are an attractive matrix for Pu immobilisation as they can incorporate higher waste loadings than glass wasteforms, whilst maintaining an ease of processing. Excellent immobilisation of Pu is reported and these wasteforms have lower dissolution rates than their vitrified equivalents.<sup>3</sup> Glass-ceramics act as a double barrier system to prevent radionuclide release by partitioning actinides into the crystalline phase (ceramic) and retaining the remaining miscellaneous material in the amorphous matrix (glass).

Zirconolite, CaZrTi<sub>2</sub>O<sub>7</sub> is a ceramic phase that readily accepts actinides and rare earth elements into its structure and, unlike a range of other ceramic materials, exhibits excellent durability even when subjected to high radiation doses and amorphisation.<sup>4</sup> Therefore, this project studies the development of high fraction zirconolite glass-ceramics consolidated by Hot Isostatic Pressing for the long-term immobilisation of Pu-residues. In recent literature, it was reported that the crystalline phase assemblage changed as a function of the glass phase composition.<sup>5</sup> The sample matrix discussed here was developed to investigate experimental parameters to improve the HIP process, thus the samples were batched as a worst case scenario where very little/no zirconolite was expected to form due to a reduced Al concentration.

Hot Isostatic Pressing (HIPing) applies high temperature and pressure simultaneously to a workpiece to produce bodies of near 100% theoretical density. Originally developed for the diffusion bonding of fuel element assemblies in nuclear reactors, HIPing

now has applications for many different industries and materials including aerospace and defence, metals and ceramics.<sup>1</sup> It also holds multiple advantages as a consolidation technique for nuclear wasteforms. The minimal porosity in the final product reduces the wasteform source term by providing fewer pores and cracks for the release of the homogeneously incorporated radionuclides. Similarly, the use of high pressures allows samples to be processed at lower temperatures resulting in a finer grain structure, thus increasing the strength and durability of the glass-ceramic wasteform.<sup>2</sup> The raw matrix constituents and waste are homogeneously mixed, contained and processed in a stainless steel canister. There are minimal off-gases produced throughout the whole HIP process and the final product is hermetically sealed ready for long-term storage with the primary and secondary containment barriers (the glass-ceramic wasteform and steel canister, respectively) already supplied.

Typically, canisters undergo an evacuation and bake out step before sealing to remove any volatiles that would inhibit densification. The packed can is first evacuated before the temperature is increased. The vacuum pressure reduces due to the release of volatiles at the elevated temperature. Once the vacuum returns to its original pressure the canister is crimped and sealed.

This report discusses a sample matrix which investigated the effect of calcining raw materials in a furnace before they are packed into the HIP can as opposed to the in-can bake out. It is envisaged this will increase sample through-put without compromising product quality.

## Methodology Details

The powders were batched to a 70/30 wt. % ratio of glass to ceramic with the target glass phase being Na<sub>2</sub>Al<sub>0.5</sub>B<sub>1.5</sub>Si<sub>6</sub>O<sub>16</sub>. The batches were then packed and sealed into the stainless steel HIP cans (approximately 36x38mm (h x d)) followed by a calcination or bake out step, which took place either before being packed into the canister or during the evacuation of the canister. The heat treatments taken by each sample are described in Table 1. Samples were HIPed at 1250 °C, 100 MPa with a 4 hr dwell. The processed canisters were opened using a Buehler abrasimet 250 saw with a HH ferrous blade. Samples were polished and carbon coated for analysis using an Hitachi TM3030 analytical scanning electron microscope (SEM) at a 15 kV accelerating voltage and a working distance of 8 mm. Samples were ground and sieved to 106 µm for X-ray diffraction (XRD) by using a Bruker D2 PHASER desktop diffractometer between 10 ° < 2θ < 70°. The raw powders also underwent thermogravimetric and differential thermal analysis (TG/DTA) using a PerkinElmer STA 8000 TGA/DTA instrument, with 20 mg of sample in a platinum crucible at a heating rate of 10 °C/min to 1250 °C in an argon atmosphere.

**Table 1.** Heat treatments undergone by each sample during the canning process. Calcinations were done in a crucible in a general furnace and the bake outs took place in the HIP can during evacuation.

Sample	Heat Treatment	
	Calcine (°C)	Bake out (°C)
A	0	300 °C
B	0	600 °C
C	600 °C	300 °C
D	600 °C	0

## Results and Discussion

Compositions previously investigated by the authors highlighted the difference between samples that had undergone a low temperature bake out (300 °C) and a high temperature bake out (600 °C), with the latter proving of superior quality in terms of densification. Figure 1 shows the incomplete compaction and porosity obtained when using the low bake out temperature compared to the high bake out temperature. In the latter, porosity was eliminated producing a dense, uniform glass-ceramic sample. This implies that decomposition of a reagent material occurred during the HIP cycle, liberating gas which remained trapped in the sealed HIP can. Preparing a large number of samples via the high temperature bake out would severely limit sample throughput, as each could take up to 20 hrs to reach vacuum pressure. Hence this investigation aimed to optimise the bake

out step, and hence improve product quality and throughput.

### Raw Material

Thermogravimetric analysis (TG) and XRD were conducted on the raw batched powder before and after a 600 °C calcination. XRD data did not show any significant difference in the phase assemblage of materials after calcination at 600 °C. A mass loss between 200 °C and 600 °C was observed in the TG data for the uncalcined material but was not observed for the calcined material (data not shown). This agrees with the hypothesis that a gas was liberated inside the sealed HIP can between 300 °C and 600 °C resulting in porous products. It is hypothesised that the observed mass change may be water loss from hygroscopic reagents such as borax, Na<sub>2</sub>B<sub>4</sub>O<sub>7</sub>, the decahydrate of which is reported to lose the last 2 moles of water at a temperature of ca. 600 °C.<sup>6</sup>

### HIPed material

SEM analysis of samples A-D (Table 1, Figure 2) showed microstructures with large zirconium-rich crystals and a smaller titanium-rich phase distributed in a glass matrix. As expected, sample A had a high level of porosity (as visible by eye) and sample B showed no evident porosity.

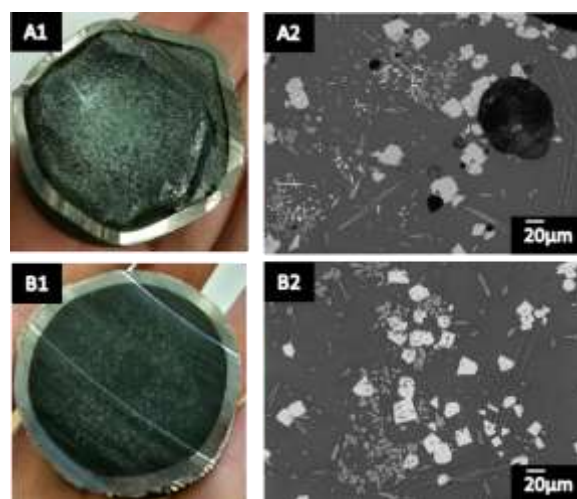


**Figure 1.** A1) Photograph of low temperature bake out sample, A2) BSE micrograph showing microstructure and porosity. B1) Photograph of high temperature bake out sample, B2) BSE micrograph showing a similar microstructure and no visible porosity.

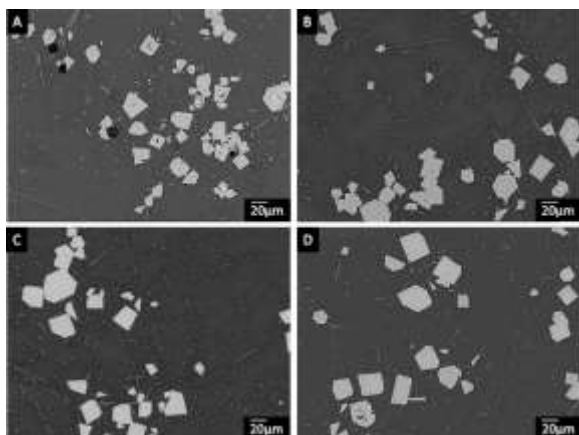


**Figure 2.** SEM images comparing the microstructures of glass-ceramic samples A-D.

The microstructure and spatially resolved composition of the calcined samples C and D are indistinguishable from those of samples not subject to calcination at 600 °C (A & B). Sample A, subjected to only a 300 °C bake-out, shows evidence of entrained porosity however, samples C and D have no visible porosity, which implies the addition of a calcination step was broadly similar to increasing the bake out temperature, removing volatiles without affecting the final product (Figure 2). XRD data (Figure 3) for each sample showed the same phase assemblage for all samples. The only variation between the XRD patterns related to a minor secondary TiO<sub>2</sub> phase, brookite. The three major reflections associated with brookite (TiO<sub>2</sub> pdf-card 00-015-0875) were observed in all samples, however the reflection intensity was significantly reduced in samples C and D. Zircon (ZrSiO<sub>4</sub>; pdf-card 01-071-0991) was the major crystalline phase formed for all samples and rutile (TiO<sub>2</sub>; pdf-card 01-078-4188) was also observed.

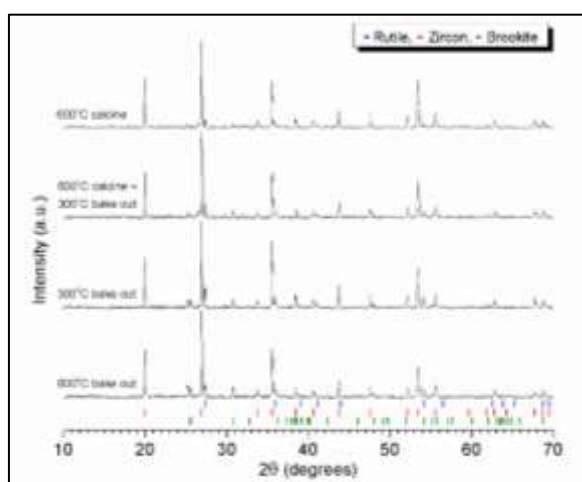


**Figure 3.** XRD plot with pdf-cards identifying phases present in each sample.

## Conclusions and Future Work

A matrix of samples were fabricated to compare the effects of pre-HIP processing options to optimise wasteform quality. Results have shown that no major differences in the phase assemblage or microstructure were realised between the high temperature bake out and calcined samples. Further analysis of the behaviour of borax will be performed using TG/mass spectrometry to determine if water is indeed liberated at 300-600 °C.

Future experiments will seek to optimise the formulation of glass-ceramics and understand the stability of the crystalline phases formed and will be processed via a calcination plus low temperature bake out route to ensure full densification and to maintain an efficient throughput of samples.

## Acknowledgements

The authors would like to thank the National Nuclear Laboratory and Nuclear Decommissioning Authority for sponsorship of the project.

## References

- 1 M.H. Bocanegra-Bernal, "Review Hot Isostatic Pressing (HIP) technology and its applications to metals and ceramics," *J. Mater. Sci.*, **39** 6399–6420 (n.d.).
- 2 E.R. Vance, M.W.A. Stewart, and S.A. Moricca, "Progress at ANSTO on SYNROC," *J. Aust. Ceram. Soc.*, **50** [1] 38–48 (2014).
- 3 P.W. McMillan, *Glass-ceramics*, 2d ed. Academic Press, London ; New York, 1979.
- 4 Lumpkin et al., "Alpha-recoil damage in zirconolite (CaZrTi<sub>2</sub>O<sub>7</sub>)," *J. Mater. Res.*, **1** [4] 564– (1986).
- 5 E. Maddrell, S. Thornber, and N. Hyatt, "The influence of glass composition on crystalline phase stability in glass-ceramic wasteforms," *J. Nucl. Mater.*, (2014).
- 6 Ahmet Ekmekyapar, Ahmet Baysar, and Asim Kunkul, "Dehydration Kinetics of Tincal and Borax by Thermal Analysis," *Ind. Eng. Chem. Res.*, **36** 3487–3490 (n.d.).

# Computational Studies of Water Adsorption on UO<sub>2</sub> and PuO<sub>2</sub>

J. Wellington\*<sup>1</sup>, A. Kerridge<sup>2</sup>, and N. Kaltsoyannis\*<sup>1</sup>

\*Correspondence: joseph.wellington@ucl.ac.uk  
n.kaltsoyannis@ucl.ac.uk

<sup>1</sup>Department of Chemistry, University College London, 20 Gordon Street, London WC1H 0AJ, UK

<sup>2</sup>Department of Chemistry, Lancaster University, Bailrigg, Lancaster LA1 4YP, UK

## Abstract

Density functional theory (DFT) and the periodic electrostatic embedded cluster method (PEECM) are used to study AnO<sub>2</sub> bulk and surfaces (An = U, Np, Pu). The electronic structure of AnO<sub>2</sub> clusters representing the bulk was investigated by looking at the projected density of states (PDOS). With the use of a hybrid DFT functional the composition of the valence and conduction bands agrees well with experiment. Water adsorption was then investigated on the (111) and (110) surfaces of UO<sub>2</sub> and PuO<sub>2</sub> with 1 to 4 water molecules adsorbing on the cluster dissociatively or molecularly. Water adsorption on the (110) surface is stronger than on the (111) surface. A mixture of molecular and dissociative adsorption is found to be most favourable on the (111) surface whilst dissociative adsorption is seen to be most favourable on the (110) surface.

## Introduction

Of the world's c. 250 tonnes of separated plutonium, more than 100 tonnes are stored at Sellafield in the UK as PuO<sub>2</sub> powder in sealed steel cans. Under certain circumstances, gas generation may occur in these cans, with consequent pressurization. Five routes to gas production have been suggested; (i) helium accumulation from a decay (ii) decomposition of polymeric packing material (iii) steam produced by H<sub>2</sub>O desorption from hygroscopic PuO<sub>2</sub> due to self-heating (iv) radiolysis of adsorbed water and (v) generation of H<sub>2</sub> by chemical reaction of PuO<sub>2</sub> with H<sub>2</sub>O, producing a postulated PuO<sub>2+x</sub> phase. The last three mechanisms, all involving PuO<sub>2</sub>/H<sub>2</sub>O interactions, are complex, interconnected and poorly understood.

Actinide compounds such as the actinide dioxide systems investigated in this study are known as strongly correlated materials. Such materials are usually compounds containing first row transition metals, lanthanides or actinides where the valence d or f orbitals are compact and spatially localised, leading to weak overlap, in the case of actinide oxides, with neighbouring oxygen ions. DFT within the local density approximation (LDA) or generalised gradient approximation (GGA) poorly describes these systems; in the case of the actinide dioxides such approaches predict metallic behaviour. Alternative methods within DFT have been employed in order to obtain the insulating character of these systems; one of these is the hybrid DFT approach, which is used here.

Experimental studies of water adsorption on PuO<sub>2</sub> surfaces have shown that water adsorbs via a multi-step process with initial strong chemisorption due to dissociation of water, forming a hydroxylated surface, followed by successive layers of H<sub>2</sub>O physisorbed above the hydroxylated layer<sup>1</sup>.

Theoretical studies comparing water adsorption between the UO<sub>2</sub> and PuO<sub>2</sub> surfaces have found water adsorption to be more favourable on the UO<sub>2</sub> surface than the PuO<sub>2</sub> surface<sup>2,3</sup>, however these studies only considered the water molecules adsorbing dissociatively. Comparing the (111) and (110) surfaces theoretical studies have predicted adsorption of water to be stronger on the (110) than the (111) surface, whether the adsorption is molecular<sup>4</sup> or dissociative.<sup>2,4</sup> Comparing dissociative and molecular adsorption recent studies have predicted fully dissociative adsorption to be stronger than fully molecular, however a mixture of dissociatively and molecularly adsorbed water was seen to be the most stable structure on UO<sub>2</sub>.<sup>4</sup> For PuO<sub>2</sub> dissociative adsorption has been predicted to be more stable than molecular adsorption on the (110) surface.<sup>5,6</sup>

In this study we employ the periodic electrostatic embedded cluster method (PEECM), where a portion of the surface is described quantum mechanically and the rest of the system is approximated by point charges. We examine the electronic structure of AnO<sub>2</sub> (An = U, Np, Pu) as well as the adsorption of water on the (111) and (110) surfaces of UO<sub>2</sub> and PuO<sub>2</sub>. Both experimental and theoretical studies of water adsorption on UO<sub>2</sub> are more abundant than on PuO<sub>2</sub>,

therefore our inclusion of UO<sub>2</sub> in this study allows us to compare the results obtained here with previous studies.

To the best of our knowledge the PEECM has never been applied to AnO<sub>2</sub>, and it was our hope that it could provide useful additional insight. The PEECM offers certain advantages over more traditional periodic boundary condition approaches; not only can all of the analysis tools of molecular quantum chemistry be applied, but it is relatively straightforward to employ hybrid DFT.

## Computational Details

All calculations were performed with the TURBOMOLE6.5<sup>7</sup> program. The PBE (GGA) and PBE0 (hybrid-GGA) exchange-correlation functionals were used for single-point, benchmarking calculations of bulk actinide oxide systems; as we show, PBE0 performs well here and hence it was used for all surface calculations.

### PEECM

All calculations were performed using the PEECM<sup>8</sup>. In this approach, the system is split into three regions; an inner explicit cluster region, which is treated quantum mechanically as described above, the outer embedding region, consisting of point charges and an intermediate embedding region, consisting of negative point charges and ECPs (Figure 1).

The infinite outer embedding region recreates the Madelung potential of the bulk system; formal charges were used for the ions in this region, +4 for actinide ions and -2 for oxygen ions. The ECPs used in the intermediate embedding region were the Ce CRENBL ECPs, employed in order to avoid overpolarization of the electron density in the explicit cluster, whilst -2 charges again represented the oxygen ions. The Ce CRENBL ECP, which corresponds to a +4 charge when used without any basis functions, was used since no actinide ECPs corresponding to a +4 charge were available. The 8-coordinate Ce(IV) ionic radius, 0.97 Å, is very similar to that of U(IV), 1.00 Å, Np(IV), 0.98 Å and Pu(IV) 0.96 Å.

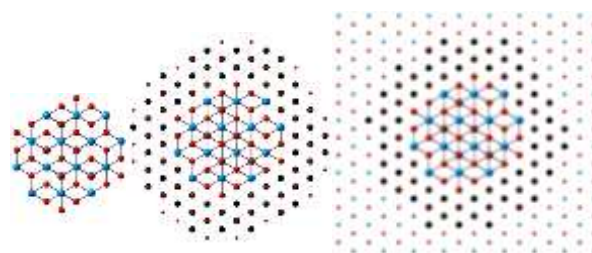


**Figure 1** Embedding of quantum mechanical (QM) cluster in PEECM scheme. Left, QM cluster, actinide ions in blue oxygen ions in red. Middle, QM cluster embedded in intermediate region of ECPs (black) and -2 point charges (small red), representing actinide and oxygen ions respectively. Right, QM cluster and intermediate region embedded in infinite array of +4 (small blue) and -2 (small red) point charges representing the actinide and oxygen ions respectively.

## Results and Discussion

### Electronic Structure of Bulk UO<sub>2</sub>, NpO<sub>2</sub> and PuO<sub>2</sub>

The electronic structure of An<sub>16</sub>O<sub>32</sub> clusters representing bulk AnO<sub>2</sub> was calculated with the PBE0 functional. PDOS plots were produced by the Mulliken partitioning of orbitals into their s, p, d and f contributions.

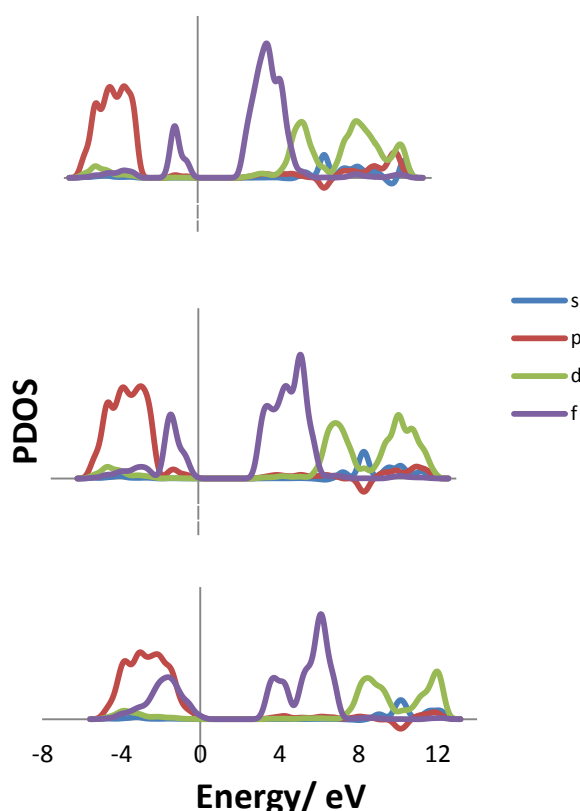


**Figure 2** PDOS of An<sub>16</sub>O<sub>32</sub> clusters representing the bulk. From top to bottom UO<sub>2</sub>, NpO<sub>2</sub> and PuO<sub>2</sub>.

It can be seen from Figure 2 that each AnO<sub>2</sub> cluster is predicted to be an insulator. From the decomposition of the states into their s, p, d and f contributions it can be seen that both UO<sub>2</sub> and NpO<sub>2</sub> have both valence

and conduction orbitals of f character. They are hence both predicted to be Mott-Hubbard insulators, with an f-f transition. It can be seen, however, that the occupied f orbitals in NpO<sub>2</sub> are more stabilized than in UO<sub>2</sub>, being closer to the valence oxygen p orbitals.

PuO<sub>2</sub> has more stable occupied 5f orbitals than uranium and neptunium, with energies comparable with the highest O 2p valence orbitals. Thus PuO<sub>2</sub> is not a Mott insulator, as there is a significant portion of oxygen 2p valence orbitals in the transition. PuO<sub>2</sub> is better described as an LMCT system, in agreement with experiment.

### Water Adsorption on UO<sub>2</sub> and PuO<sub>2</sub> (111) Surface

Water can adsorb onto AnO<sub>2</sub> surfaces in two ways: molecularly, where the water molecule remains intact on adsorption, or dissociatively, where an O-H bond is broken. Molecular adsorption on the (111) surface occurs with an oxygen adsorbing above an actinide ion and two hydrogen atoms pointing towards two surface oxygen atoms. Dissociative adsorption forms two hydroxyl groups: a hydroxide, formed from a hydrogen of the water molecule binding to a surface oxygen, and a second in which a OH group of water adsorbs above an actinide ion. These adsorptions are shown in Figure 3.

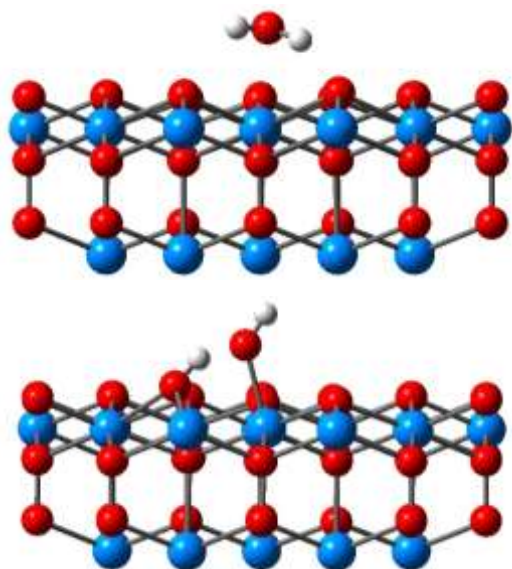


**Figure 3** U<sub>15</sub>O<sub>38</sub> cluster of the (111) surface with water adsorbing molecularly (top) and dissociatively (bottom). Uranium atoms shown in blue, oxygen atoms in red and hydrogen atoms in white.

The energies for molecular and dissociative adsorption on the (111) surfaces of UO<sub>2</sub> and PuO<sub>2</sub> are shown in Table 1.

For one water molecule, dissociative adsorption is more stable than molecular on the UO<sub>2</sub> surface but the reverse for PuO<sub>2</sub>. The hydrogen of the hydroxyl containing a surface oxygen points towards the adsorbed hydroxyl (Figure 3), with a distance of 1.63 Å

for UO<sub>2</sub>; hence there is a hydrogen bond between the two hydroxyl species.

Adsorption is stronger on the UO<sub>2</sub> surface than PuO<sub>2</sub>, except for one water adsorbing molecularly where both have an adsorption energy of -1.05 eV, agreeing with previous theoretical studies finding water adsorption to be stronger on UO<sub>2</sub> than PuO<sub>2</sub>.<sup>2,3</sup>

With increasing numbers of adsorbed water molecules, a mixture of molecular and dissociative adsorption now becomes favourable, with small energy differences between different configurations. This agrees with recent theoretical studies which find neither a fully hydroxylated surface nor one covered in molecular water, but a mixture of the two.<sup>4</sup>

Number of water molecules	Type of adsorption	Adsorption energy/ eV	
		UO <sub>2</sub>	PuO <sub>2</sub>
1	1m	-1.05	-1.05
	1d	-1.08	-0.99
2	2m	-	-1.04
	1m,1d	-1.19	-1.12
	2d	-1.02	-1.01
3	3m	-1.07	-1.04
	2m,1d	-1.14	-1.08
	1m,2d	-1.12	-1.06
	3d	-0.99	-0.91
4	4m	-	-1.09
	3m,1d	-1.17	-1.10
	2m,2d	-1.19	-1.09
	1m,3d	-1.09	-1.04
	4d	-	-0.89

**Table 1** Adsorption energies of water molecules on the U<sub>15</sub>O<sub>38</sub> cluster of the (111) surface of UO<sub>2</sub> and PuO<sub>2</sub>. Adsorption energies shown for 1 to 4 water molecules adsorbing with differing amounts of molecular and dissociative adsorption, m refers to a water adsorbing molecularly and d for one adsorbing dissociatively. No energy is given for two water molecules adsorbing molecularly (2m) or four waters adsorbing molecularly (4m) or dissociatively (4d) on UO<sub>2</sub> (111), as these configurations relaxed to adsorptions of one molecular, one dissociative (1m,1d), three molecular one dissociative (3m,1d) and one molecular three dissociative (1m,3d) respectively.

### Water Adsorption on UO<sub>2</sub> and PuO<sub>2</sub> (110) Surface

As with the (111), there are two types of adsorption on the (110) surface, molecular and dissociative. Molecular adsorption occurs with the hydrogen atoms tilted towards the surface, the oxygen atom is now not directly above the actinide ion (Figure 4). Dissociative adsorption again forms two hydroxides, the adsorbed hydroxide has its oxygen above the actinide ion and its hydrogen tilted towards a surface oxygen, whilst the surface hydroxide has its hydrogen angled towards another surface oxygen ion. (Figure 4).

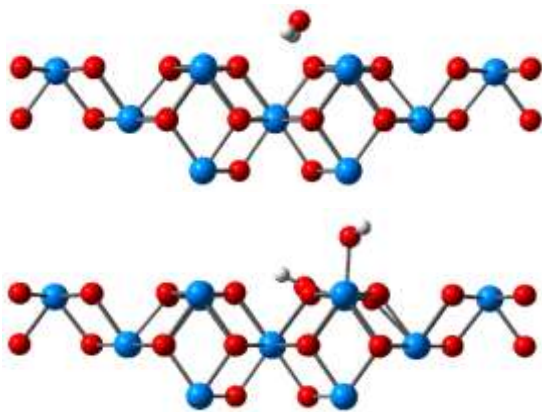


**Figure 4** U<sub>25</sub>O<sub>50</sub> cluster of the (110) surface with water adsorbing molecularly (top) and dissociatively (bottom). Uranium atoms shown in blue, oxygen atoms in red and hydrogen atoms in white.

The energies for molecular and dissociative adsorption on the (110) surfaces of UO<sub>2</sub> and PuO<sub>2</sub> are shown in Table 2.

Number of water molecules	Type of adsorption	Adsorption energy/ eV	
		UO <sub>2</sub>	PuO <sub>2</sub>
1	1m	-1.46	-1.61
	1d	-1.90	-1.89
2	2m	-1.50	-1.65
	1m,1d	-1.72	-1.79
	2d	-1.89	-1.91
3	3m	-1.48	-1.61
	2m,1d	-1.61	-1.70
	1m,2d	-1.67	-1.77
	3d	-1.81	-1.79
4	4m	-1.51	-1.60
	3m,1d	-1.55	-1.68
	2m,2d	-1.69	-1.72
	1m,3d	-1.73	-1.74
	4d	-1.77	-1.74

**Table 2** Adsorption energies of water molecules on the U<sub>25</sub>O<sub>50</sub> cluster of the (110) surface of UO<sub>2</sub> and PuO<sub>2</sub>. Adsorption energies shown for 1 to 4 water molecules adsorbing with differing amounts of molecular and dissociative adsorption, m refers to a water adsorbing molecularly and d for one adsorbing dissociatively.

Adsorption of water on the (110) surface is energetically more favourable than on the (111), by up to 0.61 eV for molecular adsorption and 0.90 eV for dissociative adsorption. This agrees with other theoretical studies which have compared water adsorption between the (111) and (110) surfaces.<sup>2,4</sup>

On the (110) surface dissociative adsorption is more favourable than molecular by 0.44 eV and 0.28 eV for UO<sub>2</sub> and PuO<sub>2</sub> respectively. This trend is seen with increasing number of water molecules adsorbing; dissociative adsorption is always the most favourable configuration. This suggests that a (110) surface covered in water would form a fully hydroxylated first layer. This is what is seen experimentally for PuO<sub>2</sub>.<sup>1</sup>

however this is experimental procedure is not performed on a single surface crystal of (110).

## Conclusions and Future Work

The results have shown that the PEECM is able to reproduce the correct electronic structure of the AnO<sub>2</sub> systems. The PEECM was then used to investigate water adsorption on UO<sub>2</sub> and PuO<sub>2</sub>. The results show that adsorption is much stronger on the (110) surface, that there is little difference between molecular and dissociative adsorption on the (111) surface but a larger difference on the (110) surface where dissociative adsorption is seen to be more favourable.

Experimentally a first layer of water is seen to adsorb strongly to PuO<sub>2</sub> surfaces and then to have weaker reversible adsorption on successive layers. To our knowledge no theoretical studies go beyond a single monolayer of water on PuO<sub>2</sub> surfaces, therefore we are currently extending our model to explore multiple layers of water on the surface.

## Acknowledgements

We are grateful to the National Nuclear Laboratory and UCL for financial support for a PhD studentship to JW. We also thank UCL for computing resources via the Research Computing “Legion” cluster (Legion@UCL) and associated services, and also the “Iridis” facility of the e-Infrastructure South Consortium’s Centre for Innovation. We are also grateful to Dr Scott Owens of the National Nuclear Laboratory for helpful discussions.

## References

- [1] J. M. Haschke and T. E. Ricketts, *Journal of Alloys and Compounds*, 1997, **252**, 148–156.
- [2] Z. Rák, R. C. Ewing, and U. Becker, *Surface Science*, 2013, **608**, 180–187.
- [3] J. C. Boettger and A. K. Ray, *International Journal of Quantum Chemistry*, 2002, **90**, 1470–1477.
- [4] T. Bo, J.-H. Lan, Y.-L. Zhao, Y.-J. Zhang, C.-H. He, Z.-F. Chai, and W.-Q. Shi, *Journal of Nuclear Materials*, 2014, **454**, 446–454.
- [5] G. Jomard, F. Bottin, and G. Geneste, *Journal of Nuclear Materials*, 2014, **451**, 28–34.
- [6] X. Wu and A. Ray, *Physical Review B*, 2002, **65**, 085403.
- [7] R. Ahlrichs, M. Bär, M. Häser, H. Horn, and C. Kölmel, *Chemical Physics Letters*, 1989, **162**, 165–169.
- [8] A. M. Burow, M. Sierka, J. Döbler, and J. Sauer, *Journal of Chemical Physics*, 2009, **130**, 174710.

# New materials for caesium and strontium waste removal: Synthesis of phosphate ion-exchangers.

R.George\*<sup>1</sup> and Dr J.A.Hriljac<sup>1</sup>

\*Correspondence: RXG034@bham.ac.uk

<sup>1</sup>School of Chemistry, University of Birmingham, Edgbaston, Birmingham, UK B15 2TT.

## Abstract

The synthesis of new materials for ion exchange and subsequent disposal of radionuclides will be explored in this work; the concept being the formation of novel open framework rare earth based materials with high selectivity for caesium and strontium that can be thermally transformed into dense phosphates. Preliminary work shows that the synthesis of such materials is hindered by the formation of stable REPO<sub>4</sub> (RE=rare earth) phases at varying conditions and batch compositions. The result of the hydrothermal synthesis of these materials varies between amorphous to highly crystalline REPO<sub>4</sub> materials which are not porous and as a result are not applicable for ion exchange.

## Introduction

The synthesis of novel ion exchange materials for uses in nuclear waste management and environmental remediation is a key area of research. Much effort is being placed in designing materials with high selectivity and ion exchange capacity, especially in relation to caesium and strontium. The established methodology for the removal of these radionuclides in the UK involves the use of a natural zeolite material clinoptilolite[1]. These porous natural or synthetic zeolite materials have been widely investigated and have resulted in a wide range of zeotype and open framework materials.

The aim of this work is to synthesize novel open framework or layered rare earth phosphate materials, with compositions that can be transformed to ceramics that contain xenotime and monazite type phases. These minerals contain varying amounts of radioactive elements naturally, mainly uranium and thorium. The result of this is that these minerals are exposed to radiation over a long period of time [2]. For this reason they were suggested as candidates for immobilizing nuclear waste. This is because they can be converted into high density ceramic phases by exposure to high temperature and pressure treatment. It is hoped that open framework RE phosphates could be synthesized for ion exchange and converted into dense ceramics for disposal.

Open framework rare earth materials have been synthesized before. The Rocha group have synthesized rare earth silicate materials, designated as AV-1 and AV-5. These materials were synthesized

hydrothermally, with the general formula Na<sub>4</sub>K<sub>2</sub>RE<sub>2</sub>Si<sub>16</sub>O<sub>38</sub>.10H<sub>2</sub>O, where RE is either yttrium or cerium. These microporous materials consist of REO<sub>6</sub> octahedra, sodium octahedra and silicon tetrahedra. This forms a double sheet structure with large channels in which the potassium cations are located [3-4].

It is hoped that similar phosphate materials can be synthesized which allow for the encapsulation of caesium and strontium. This could be done via a hydrothermal route as demonstrated by the Rocha group.

## Methodology Details

### Synthesis of materials

Varying amounts of cerium nitrate (Sigma), yttrium nitrate (Sigma), and tetraethylammonium hydroxide (Alfa Aesar) were dissolved in deionized water. To the stirring mixture phosphoric acid was added dropwise with constant stirring. This produced a gel which was further stirred for 1 hour to homogenise the mixture.

The resulting mixture was then transferred to a 45ml Teflon liner and placed in a Parr autoclave at temperatures ranging from 100 to 200°C. The autoclave was then heated for 1 to 7 days. The resulting white solids were then washed in deionized water and dried overnight at 60°C.

### Characterisation of materials

The synthesized compounds were analysed using Powder X-ray diffraction (XRD) on a Bruker D8 Advance using a Cu K $\alpha$  source at room temperature. Phase

matching was performed using the EVA software from known databases.

## Results and Discussion

Powder XRD of the various samples, with varying batch composition and conditions, unfortunately did not result in the formation of any open framework materials. XRD data showed that the main phase formed was  $\text{YPO}_4$ , this varied from being largely amorphous to highly crystalline in nature (Figure 1).

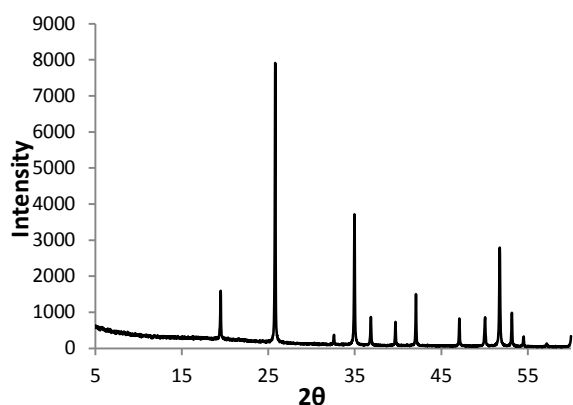


Figure 1: Powder XRD pattern of  $\text{YPO}_4$  synthesized hydrothermally.

This shows that  $\text{YPO}_4$  is the most stable product that this system can form and as a result prevents the formation of any other phases. Variation of the water content of the initial gel and by using an excess of tetraethylammonium hydroxide and phosphoric acid had no outcome on the final material synthesized.

A similar approach was applied to the synthesis of open framework cerium materials; this was again done at varying batch compositions and conditions. The results were very similar to that of the yttrium based materials, with the only product being  $\text{CePO}_4$ . It became apparent that these RE phosphates can be synthesized hydrothermally relatively easily; the result of this is that it may be difficult to access any other phases.

The variation of structure directing agents in both cases had no effect on the final product formed, it was hoped that by using tetraethylammonium hydroxide instead of ethylenediamine that we could form products with large pores however this was not the case.

The open framework RE silicates synthesized by the Rocha group are structurally similar to materials found in nature. Natural RE phosphates are much more dense materials and this is the hurdle that may need to be overcome in order to progress with the concept of open framework phosphate materials.

## Conclusions and Future Work

Preliminary work shows that the synthesis of open framework yttrium phosphate materials is hampered by the formation of  $\text{YPO}_4$ . Variation of conditions and batch compositions makes very little difference to the final product. Future work in this area will focus on finding conditions in which  $\text{YPO}_4$  does not form, in the hope that preventing  $\text{YPO}_4$  formation may allow for the formation of a different phase. This also applies for the cerium system, where a similar approach will be required.

Another potential research area focuses on zirconium phosphates, once again trying to synthesize them as open framework or layered materials hydrothermally. This could be done by using various structure directing agents, initial work will focus on the use of tetraethylammonium hydroxide. The intention will be to form a TEA derivative of the layered  $\alpha$ -zirconium phosphate, then remove the template. These layered materials may then be able to encapsulate caesium and strontium.

The final area of research focuses on the synthesis of aluminophosphate materials which have a non 1:1 Al:P ratio. These materials will have negative frameworks and once again may have possible application in ion exchanging caesium and strontium.

## Acknowledgements

The authors would like to thank the school of chemistry and the ESPRC for the funding provided. We would also like to thank advantage west midlands for providing the equipment required to carry out the experiments.

## References

- [1] A.Dyer, A.Chimedtsogzol, L.Campbell and C.Williams, *Micropor.Mesopo. Mat*, 2006, **95**, 172-175.
- [2] M.R.Rafiuddin, E.Mueller, A.P.Grosvenor, *J.Phys. Chem.C*, 2014, **110**, 18000-18009.
- [3] J.Rocha, P.Ferreira, Z.Lin, P.Brandao, A.Ferreira and J.D.Pedrosa de Jesus, *Chem.Commun*, 1997, 2103-2104
- [4] J.Rocha, P.Ferreira, L.D.Carlos and A.Ferreira, *Angew.Chem.Int.Ed*, 2000, **39**, 3276-3279.

# Synthesis of Barium Doped Cs<sub>2</sub>TiNb<sub>6</sub>O<sub>18</sub> - A New Cs-waste Form

G.Day\*<sup>1</sup>, T.Chen<sup>1</sup>, and J.A. Hriljac<sup>1</sup>

\*Email: gxd988@bham.ac.uk

<sup>1</sup> University of Birmingham, Birmingham, UK

## Abstract

Cs<sub>2</sub>TiNb<sub>6</sub>O<sub>18</sub> has the potential to be an excellent waste form for the immobilisation of radioactive caesium. A previous study revealed that Cs<sub>2</sub>TiNb<sub>6</sub>O<sub>18</sub> is the major Cs-containing phase produced when Cs-loaded IONSIV, a commercial ion exchanger, is hot isostatically pressed (HIPed).<sup>1</sup> Cs<sub>2</sub>TiNb<sub>6</sub>O<sub>18</sub> demonstrates excellent chemical durability which compared well to the Cs containing phase hollandite in SYNROC.<sup>2</sup>

## Introduction

<sup>137</sup>Cs is one of the primary heat generating radio nuclides in nuclear waste. It is a strong beta-gamma emitter with a half life of approximately 30 years.<sup>3,4</sup> It is often the radionuclide accidentally released into the biosphere on account of its high environmental mobility.<sup>5-7</sup>

Crystalline Silicotitanate (CST) with a formula Na<sub>2</sub>Ti<sub>2</sub>O<sub>3</sub>(SiO<sub>4</sub>)·2H<sub>2</sub>O, is an inorganic ion exchanger which was developed by the Sandia National Laboratory and Texas A&M University.<sup>4,8,9</sup> CST demonstrates tremendous properties, possessing excellent selectivity for Cs over a wide pH range, excellent radiation stability and importantly, is compatible with final waste forms making it a great candidate for radioactive Cs clean-up.<sup>4,5,9,10</sup> It is well known that varying the composition in CST by doping Nb<sup>(V)</sup> for Ti<sup>(IV)</sup> enhances the exchange capabilities for Cs.<sup>1,5</sup> Universal Oil Products (UOP) and Sandia in a joint collaboration commercialised this product labelled as IE-911, an engineered form of Niobium doped CST.

A recent study demonstrated that Cs-loaded IE-911 could be immobilised into a suitable waste form through hot isostatic pressing (HIPing).<sup>1,6</sup> HIPing is suitable for immobilising a variety of nuclear wastes into dense robust crystalline waste forms ideal for final disposal.<sup>6</sup> The major Cs waste form produced from HIPing was identified as Cs<sub>2</sub>TiNb<sub>6</sub>O<sub>18</sub>. This phase demonstrated exceptional leach rates which compared well to other ceramic Cs waste forms such as hollandite.<sup>1</sup> Hollandite is a well studied Cs waste form which is a major component of SYNROC.<sup>11,12</sup> It is known that hollandite, formula (Ba,Cs)<sub>x</sub>Al<sub>2x</sub>Ti<sub>8-2x</sub>O<sub>16</sub>, is chemically durable and reported to be able to retain the transmutation products of <sup>137</sup>Cs (**figure 1**).<sup>2,11-17</sup> The release of a β<sup>-</sup> particle in the transmutation process is able to simultaneously reduce Ti<sup>(IV)</sup> to Ti<sup>(III)</sup> meaning Ba can be retained in the hollandite

structure.<sup>17</sup> It is not yet known how Cs<sub>2</sub>TiNb<sub>6</sub>O<sub>18</sub> will respond to the transmutation of <sup>137</sup>Cs<sup>+</sup> to <sup>137</sup>Ba<sup>2+</sup>.

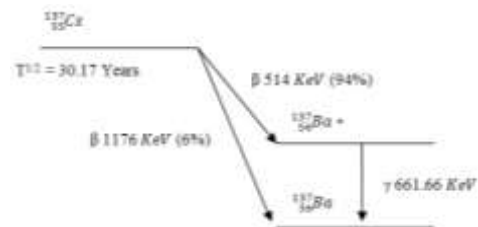


**Figure 1.** Transmutation of <sup>137</sup>Cs Adapted from reference<sup>18</sup>

It was envisaged a similar process that occurs in hollandite could also take place in Cs<sub>2</sub>TiNb<sub>6</sub>O<sub>18</sub>. In this scenario the β<sup>-</sup> particle could reduce either the Nb<sup>(V)</sup> or Ti<sup>(IV)</sup> to balance the overall charge giving **formulas 1.1** and **1.2**. Proof of barium substitution could therefore provide decent evidence to suggest that Cs<sub>2</sub>TiNb<sub>6</sub>O<sub>18</sub> is able to retain Ba and be a suitable final waste form for Cs immobilisation.

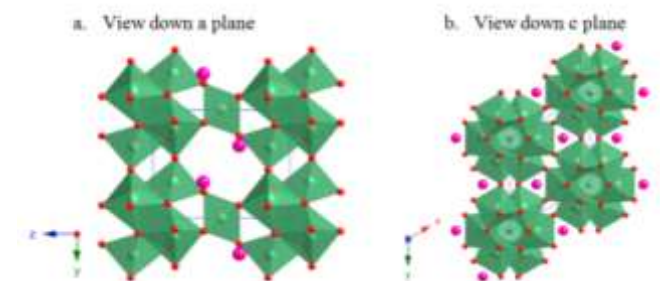
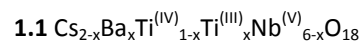


**Figure 2.** Crystal Structure of Cs<sub>2</sub>TiNb<sub>6</sub>O<sub>18</sub>. Sourced from Desgardin et al<sup>19</sup>

## Methodology Details

### Preparation of Materials

Samples were synthesised using both sol gel and solid state techniques based on those outlined by Balmer et al<sup>20</sup>. and Desgardin et al<sup>19</sup>.

### Characterisation of materials

X-ray diffraction (XRD) experiments were carried out on a Bruker D8 Diffractometer in transmission mode using a Cu  $\alpha_1$  1.5406 X-ray source. Wavelength dispersive X-ray fluorescence spectroscopy was carried out using a Bruker S8 Tiger (WDXRF).

## Results and Discussion

The results discussed here are related to Ba doped samples where the charge compensation is achieved through doping excess Ti<sup>(IV)</sup> for Nb<sup>(V)</sup> giving the formula  $Cs_{2-x}Ba_xTi_{1+x}Nb_{6-x}O_{18}$ . Although not necessarily realistic these samples provided a decent starting point in order to confirm Ba doping in the phase of interest.

Elemental analysis was carried out using X-ray fluorescence spectroscopy. Samples were prepared into fusion beads by heating to 1050°C dissolved in appropriate flux. The results shown in **table 1** within a decent error agree with the expected increase in Ba concentration with increased Ba doping. Following this further analysis was then carried out in order to identify whether Ba had actually incorporated into the desired phase.

**Table 1** XRF  $Cs_{2-x}Ba_xTi_{1+x}Nb_{6-x}O_{18}$

Sample/x	Expected Ba/ wt%	XRF Ba/ wt%
0.05	0.60	0.53(3)
0.10	1.19	1.13(4)
0.15	1.79	1.77(4)

XRD analysis of  $Cs_2TiNb_6O_{18}$  confirmed that it crystallises in the trigonal structure (structure shown in **figure 2**), with the space group  $P\bar{3}m1$ . It was thought that Ba substitution would occur directly on the Cs site and therefore not change the symmetry of the system. Initial XRD results shown in **figure 3** suggested that the symmetry of the system had not been changed and therefore Ba potentially had been incorporated into the structure.

On closer inspection of the XRD patterns, some additional impurity peaks to what was expected were found. These impurities were able to be identified as  $BaTiNb_4O_{13}$ ,  $BaTi_3Nb_4O_{17}$  and  $Ti_2Nb_{10}O_{29}$ . GSAS analysis enabled a rough estimate of the impurity phases which is summarised in **table 2**.

**Table 2** GSAS analysis Weight fractions  $Cs_{2-x}Ba_xTi_{1+x}Nb_{6-x}O_{18}$

Phase	x=0.05	x=0.10	x=0.15
$Cs_2TiNb_6O_{18}$	95.11(2)	91.52(5)	88.19(5)
$BaTi_3Nb_4O_{17}$	2.2(3)	1.1(5)	4.9(3)
$BaTiNb_4O_{13}$	0	3.9(5)	4.7(3)
$Ti_2Nb_{10}O_{29}$	2.7(4)	3.5(8)	2.2(5)
Total Ba %	0.35	0.88	1.62
Expected Ba %	0.60	1.19	1.79

$Cs_{2-x}Ba_xTi_{1+x}Nb_{6-x}O_{18}$  (x= 0, 0.05, 0.10 and 0.15)

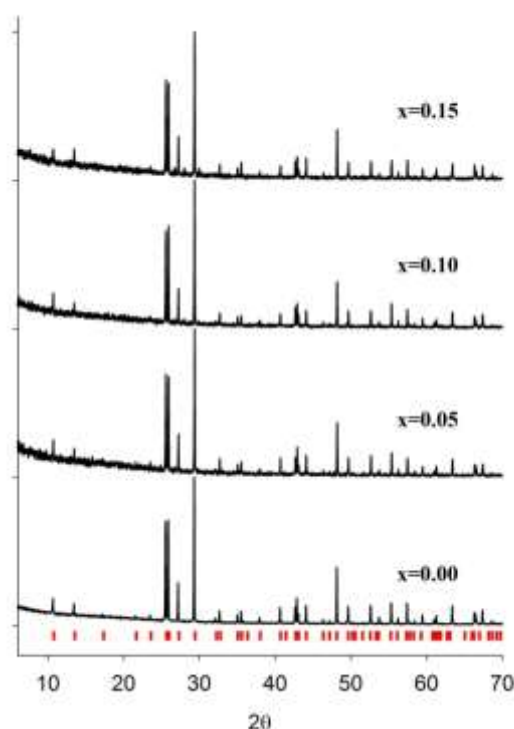


**Figure 3.** X-ray diffraction (5-70°)  $Cs_{2-x}Ba_xTi_{1+x}Nb_{6-x}O_{18}$  (x=0.00, 0.05, 0.10 and 0.15)

The weight fractions of phases calculated in **table 2** suggest that there may be a small amount of Ba doping in the  $Cs_2TiNb_6O_{18}$  phase. The stoichiometric amount of Ba initially reacted and that suggested by XRF is consistently higher than the level of Ba impurities calculated using GSAS. In order to further probe this lower Ba doping samples were synthesised and results will be presented.

## Conclusions and Future Work

So far in this study it is difficult to conclude to what level of Ba can incorporate in the  $Cs_2TiNb_6O_{18}$  phase if at all. The identification of impurities particularly at higher levels of Ba doping did hint that the Ba cation may not be suitable for the crystallographic Cs site which may be down to cation size. However the XRF results coupled with Rietveld

analysis seem to suggest some sort of solubility limit is being reached which is yet to be confirmed.

Further work on these materials will involve addition techniques that may yield more information regarding the location and presence of Ba in the sample. TEM/WDX analysis is planned to better determine the location of Ba in the sample. Wavelength dispersive x-ray spectroscopy should help distinguish the similar emission lines of Ba and Ti.

### Acknowledgements

Thank you to the School of Chemistry, University of Birmingham for funding and equipment and also advantage west midlands. Acknowledgements to Dr. J.A.Hriljac and Dr. Tzu-Yu Chen for their invaluable assistance in this work.

### References

1. T.-Y. Chen, J. . Hriljac, A. . Gandy, M. . Stennett, N. C. Hyatt, and E. . Maddrell, in *Scientific Basis for Nuclear Waste Management XXXVI, MRS Symp*, 2013, pp. 67–72.
2. A. Ringwood, *Miner. Mag.*, 1985, **49**, 159–176.
3. M. S. Denton and M. J. Manos, in *Phoenix, AZ Conference Proceedings WM2009*, 2009, pp. 1–8.
4. B. Yu, J. Chen, and C. Song, *J. Mater. Sci. Technology*, 2002, **18**, 206 – 210.
5. V. Luca, J. Hanna, M. Smith, M. James, D. Mithchell, and J. Bartlett, *Microporous Mesoporous Mater.*, 2002, **55**, 1–13.
6. E. Maddrell, *Chem. Eng. Res. Des.*, 2013, **91**, 735–741.
7. A. M. El-Kamash, *J. Hazard. Mater.*, 2008, **151**, 432–445.
8. National-Research-Council, in *Alternatives for High-Level Waste Salt Processing at the Savannah River Site*, National Academies Press, Washington DC, 2000, pp. 55–65.
9. R. G. Anthony, R. G. Dosch, D. Gu, and C. V. Philip, *Ind. Eng. Chem. Res.*, 1994, **33**, 2702–2705.
10. A. Clearfield, L. Bortun, and A. Bortun, *React. Funct. Polym.*, 2000, **43**, 85–95.
11. A. Y. Leinekugel-le-Cocq-Errien, P. Deniard, S. Jobic, E. Gautier, M. Evain, V. Aubin, and F. Bart, *J. Solid State Chem.*, 2007, **180**, 322–330.
12. A. Y. Leinekugel-le-Cocq, P. Deniard, S. Jobic, R. Cerny, F. Bart, and H. Emerich, *J. Solid State Chem.*, 2006, **179**, 3196–3208.
13. I. Donald, B. Metacalfe, and R. Taylor, *J. Mater. Sci.*, 1997, **32**, 5851–5887.
14. S. Stefanovsky, S. Yuditsev, R. Giere, and G. Lumpkin, *Energy, Waste Environ. a Geochemical Perspective*, 2004, **236**, 37–63.
15. L. M. Wang, J. Chen, and R. C. Ewing, *Curr. Opin. Solid State Mater. Sci.*, 2004, **8**, 405–418.
16. A. E. Ringwood, S. E. Kesson, N. G. Ware, W. Hibberson, and A. Major, *Nature*, 1979, **278**, 219–223.
17. L. Bursill, *J. Solid State Chem.*, 1987, **69**, 355–359.
18. J. Namiesnik and P. Szefer, *Analytical Measurements in Aquatic Environments (Google eBook)*, CRC Press, 2010.
19. G. Desgardin, C. Robert, D. Groult, and B. Raveau, *J. Solid State Chem.*, 1977, **22**, 101–111.
20. M. Lou Balmer, Y. Su, H. Xu, E. Bitten, D. McCready, and A. Navrotsky, *J. Am. Ceram. Soc.*, 2001, **84**, 153–160.

# Novel Ion Exchanger Materials

T. Chen\*<sup>1</sup> and J.A. Hriljac<sup>1</sup>

\*Correspondence: t.chen.3@bham.ac.uk

<sup>1</sup> University of Birmingham

(School of Chemistry, the University of Birmingham, Edgbaston, Birmingham, UK. B15 2TT)

## Abstract

Zirconium silicate - petarasite (AV-3) and tin silicates - umbite (AV-6) and kostylevite (AV-7) - were hydrothermally prepared and their ion exchange properties towards Sr were studied. The products were characterised using XRD, Rietveld refinement, XRF, and SEM/EDX. Batch experiments were carried out to study the uptake of Sr and to estimate the distribution coefficients ( $K_d$ ) for the above synthesised silicates from non-radioactive and radioactive <sup>85</sup>Sr solutions. Partially protonated forms of the minerals were also prepared by ion exchange with acetic acid, and the structures and Sr uptake were also studied and compared.

## Introduction

Inorganic ion exchangers typically show better selectivity, greater resistance to radiation damage, chemical oxidation and thermal degradation over organic ion exchangers due to their highly crystalline framework structure. Natural zeolite materials have been extensively studied for applications in nuclear waste treatment, however their use is limited because of the dissolution of Si and Al from the framework at low pH conditions and a lack of easy conversion routes to dense wastefoms for geological disposal. They also suffer from variable properties due to natural variation in composition. The development of novel synthetic inorganic materials as ion exchangers for the selective separation of cations, especially for Cs and Sr, is therefore of importance.

Silicate chemistry presents a wide range of structural units extending from [SiO<sub>4</sub>] tetrahedra to three dimensional structures. The extended 3D framework structure offers the ability to tune the selectivity based on the size of the cavities and channels. In general, the ion exchange characteristics of these and similar tunnel-type structures depend upon the tunnel sizes, which mediate the accessibility of the ions into the tunnel and the strength of cations bonding to the framework oxygen bonds. Many aluminosilicates, synthetic or natural[1], layered or porous titanosilicates[2] or zirconosilicates[3], such as CST (Na<sub>2</sub>Ti<sub>2</sub>SiO<sub>7</sub>·2H<sub>2</sub>O)[4, 5], ETS-10[6] and Zr-umbite[7, 8] were successfully used as cationic exchangers. We have been exploring potential candidates in those families for radionuclide cleanup.

A zirconosilicate possessing the structure of the mineral petarasite with the formula Na<sub>5</sub>Zr<sub>2</sub>Si<sub>6</sub>O<sub>18</sub>(Cl,OH)·2H<sub>2</sub>O (AV-3) was studied. The

framework of petarasite is composed of corner-sharing, six-membered silicate rings linked by [ZrO<sub>6</sub>] octahedra, as shown as Figure 1. The phase can be thermally transformed to a dense phase wadeite[9], which is considered as a potential ceramic wasteform. However, its ion exchange properties are not fully understood and more studies are required.

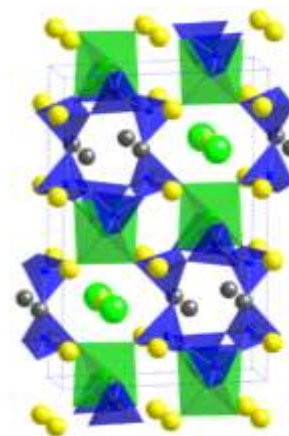
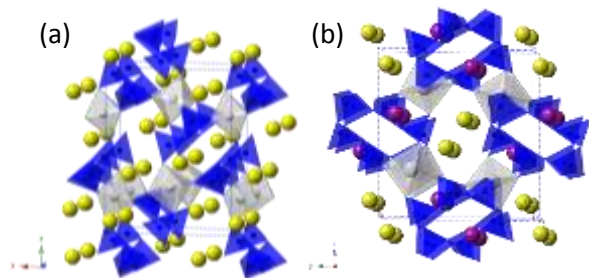


Figure 1 Polyhedral representations of the petarasite (AV-3)

Stannosilicates possessing framework structures built of [SnO<sub>6</sub>] octahedra and [SiO<sub>4</sub>] tetrahedra have been raising considerable interest. The chemical compositions of umbite (K<sub>2</sub>SnSi<sub>3</sub>O<sub>9</sub>·H<sub>2</sub>O) and kostylevite [(Na,K)<sub>2</sub>SnSi<sub>3</sub>O<sub>9</sub>·H<sub>2</sub>O] are very similar, and their microporous frameworks are very similar way[10, 11]. Umbite, the orthorhombic form, is a long-chain polysilicate whereas kostylevite, the monoclinic form, is a cyclohexasilicate (Figure 2). It is reported that umbite and kostylevite exhibit a clear structural relationship but however show different affinities for different alkali cations. This fact is related to the difference in flexibility of both umbite- and

kostylevite-type structures and their capacity to adapt to counterion dimensions. [11]



**Figure 2** Polyhedral representations of the (a) Sn-umbite and (b) Sn-kostylevite structures

To improve the ion exchange properties, protonated Sn-umbite and Sn-kostylevite were prepared. This modification provides several advantages. For example, the exchange process is often accelerated when the microporous material is in a H-form. Furthermore, the application of this material may require it to be emerged in a caustic solution, and having a protonated microporous framework will serve to decrease the pH of the overall solution. [8]

The aim of this work is to evaluate the ability of microporous stannosilicates (Sn-umbite and Sn-kostylevite) and zirconosilicate (synthetic petarasite), to uptake  $\text{Sr}^{2+}$  from aqueous solutions, assessing their potential for  $\text{Sr}^{2+}$  decontamination. The structural differences and their ion-exchange behaviour especially for Sr under “non-standard” conditions such as acidic solutions or the presence of complexants from decontamination processes were studied.

## Methodology Details

### Synthesis and Characterisations

Typical syntheses of AV-3, Sn-umbite, and Sn-kostylevite were carried out in Teflon-lined autoclaves under hydrothermal conditions, according to the methods reported by Lin et al. [12], Navascues et al. [13] and Lin et al. [10], respectively. Proton-form materials were made by shaking the as-synthesised materials in 0.5 M acetic acid at a volume to mass ratio of 100 mL:1 g for 24 h. The solid was filtered off, washed with an excess of distilled water and dried in air at 70 °C.

The powder X-ray patterns of the crystals were collected using X-ray diffraction analysis (Bruker D8 diffractometer  $\text{Cu-K}\alpha$  radiation), and Rietveld refinements of the structures were performed using GSAS. The elemental compositions were determined using XRF (Bruker S8 Tiger) and the morphologies were observed in SEM (Philips XL30 ESEM-FEG).

### Ion Exchange Studies

The Sr uptake was tested by shaking the materials in 0.1 M  $\text{Sr}(\text{NO}_3)_2$  solution under batch conditions at V:m = 100:1 (mL:g) for 24 hr at room temperature. The white powder was washed first with water and dried at 50 °C. The Sr content into the material was evaluated using XRF.

## Results and Discussion

### (1) Synthesis and characterisation

These three materials were successfully synthesised via hydrothermal route from 1 to 7 days at 200–230 °C. The unit cell parameters are summarised in Table 1.

**Table 1** Unit Cell Parameters for the synthetic phases

	Petarasite (AV-3)	Sn-umbite (AV-6)	Sn-kostylevite (AV-7)
Crystal system	Monoclinic	Orthorhombic	Monoclinic
Space group	$P2_1/m$	$P2_12_12_1$	$P2_1/c$
<i>a</i>	10.771 Å	10.080 Å	6.466 Å
<i>b</i>	14.505 Å	13.141 Å	11.545 Å
<i>c</i>	6.575 Å	7.146 Å	12.93 Å
$\beta$	113.214°		105.040°

SEM micrographs (Figure 3) show that Sn-umbite and Sn-kostylevite exhibit very different crystal morphologies. Umbite appears as spherical particles with diameters of 2–3  $\mu\text{m}$ . The spherical aggregates are made up of a variety of sheet crystals in rosette form. Kostylevite crystals exhibit generally bigger particles with diameter of  $\sim 10 \mu\text{m}$  and the crystals consist of “rods” extending from the centre of nucleation.

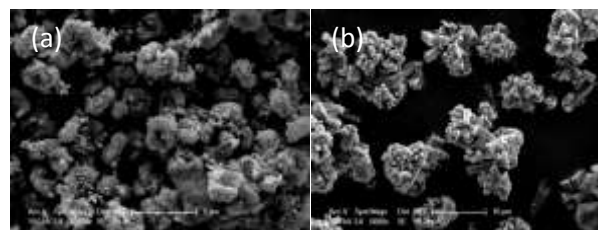


**Figure 3** SEM images of (a) Sn-umbite and (b) Sn-kostylevite structures

### (2) Sr exchange tests

The relative chemical compositions normalised to Sn before and after ion exchange are listed in Tables 2 and Table 3. For Sn-umbite, Sr was detected after ion exchange and the K content reduces, suggesting the ion exchange process has replaced some  $\text{K}^+$  with  $\text{Sr}^{2+}$ .

**Table 2** Sr uptake in Sn-umbite (XRF, loose powder)

	Sn-umbite		Sr-Sn-umbite	
	wt.%	at. (to Sn)	wt.%	at. (to Sn)
<b>Sn</b>	23.20%	1	19.59%	1
<b>K</b>	15.10%	1.98	12.08%	1.87
<b>Si</b>	10.48%	1.91	8.63%	1.86
<b>Sr</b>	-	-	2.64%	<b>0.18</b>

For Sn-kostylevite, however, even though Sr was observed after ion exchange, the relative ratio of elements does not correspond to the expected formula. This may be because there are more light elements such as Na, which are poorly determined using XRF. Furthermore, it is difficult to eliminate the matrix effect by analysing fusion beads because Sn and Si are troublesome elements in fused bead preparation.[14]

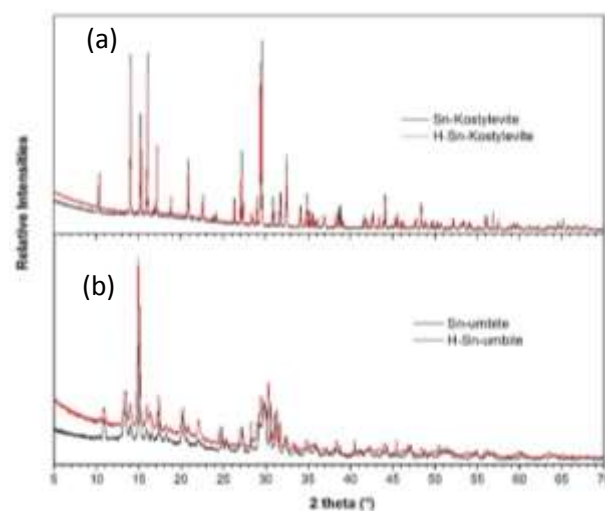
**Table 3** Sr uptake in Sn-kostylevite (XRF, loose powder)

	Sn-kostylevite		Sr-Sn-kostylevite	
	wt.%	at. (to Sn)	Wt.%	at. (to Sn)
<b>Sn</b>	34.24%	1	22.32%	1
<b>K</b>	14.45%	1.28	13.19%	1.79
<b>Si</b>	14.15%	1.75	11.57%	2.19
<b>Na</b>	2.79%	0.42	1.54%	0.36
<b>Sr</b>	-	-	2.90%	<b>0.18</b>

### (3) Protonated form

Attempts to make the protonated forms of the minerals umbite and kostylevite were made by treatment of Sn-umbite and Sn-kostylevite with acetic acid. The XRD patterns, Figure 4, suggest no significant changes in the structure.

Fewox and Clearfield found in Zr-umbite ( $K_2ZrSi_3O_9 \cdot H_2O$ ) that upon conversion to the protonated form, the unit cell volume decreased by approximately  $40 \text{ \AA}^3$ , and the space group changed from  $P2_12_12_1$  to  $P2_1/c$ . [15] However, only a slight decrease ( $\sim 5 \text{ \AA}^3$ ) in the unit cell is observed in Sn-umbite. More detailed structure determination is underway to support whether the H-form of umbite changes space group after ion exchange.

**Figure 4** XRD patterns of K-form and H-form (a) Sn-kostylevite and (b) Sn-umbite

## Conclusions and Future Work

### Conclusions

Microporous zirconium silicate petarasite (AV-3), tin silicates umbite (AV-6) and kostylevite (AV-7), and their partially protonated phases were synthesised. The differences in crystal structure, especially for umbite and kostylevite, and their effect on the incorporation of Sr cation into the phases were studied. XRF preliminary results suggest that those silicates possess the abilities of Sr uptake, however, their capacity and selectivity towards Sr required further improvement.

### Future Work

- (1) The ion exchange studies in this work were carried out using a relatively high Sr concentration without any competing cations present. Future work will focus on studies with more realistic simulated conditions, such as low concentration of Sr, a large amount of  $Na^+$  as competing cation, and various pH conditions.
- (2) Due to the inaccuracy of Sr quantitation in XRF arising from the matrix effect, a better quantitative route has to be developed. Ion exchange experiments involving radioactive  $^{85}Sr$  can be designed and performed, thus a more sensitive measurement of Sr content by detecting the gamma radioactivity from the ion exchanger and the residual solution can be achieved.
- (3) Protonated materials are beneficial for the future studies in mechanism of Sr exchange. Due to the insignificant contribution of hydrogen to the powder XRD pattern, any change observed in the calculated Fourier difference maps may be attributed to the cation exchanged into the

structure.[8] Although the protonated materials have not been proved successfully made, more active conditions such as reflux, acid exchanged in a microwave or autoclaves will be performed.

- (4) More potential ion exchange materials will be explored. In addition, atomistic simulation to predict ion exchange sites, framework response to exchange, and potential migration pathways during exchange will be performed in order to assist mechanistic understanding and materials performance optimisation.

### Acknowledgements

We gratefully acknowledge the EPSRC DISTINCTIVE grant for the financial support, and the Advantage West Midlands for the facilities. S Savva for the help with syntheses and ion exchange studies is much acknowledged.

### References

- [1] Dyer, A., et al., *Uptake of caesium and strontium radioisotopes by natural zeolites from Mongolia*. Microporous and Mesoporous Materials, 2006. **95**(1-3): p. 172-175.
- [2] Al-Attar, L., A. Dyer, and R. Harjula, *Uptake of radionuclides on microporous and layered ion exchange materials*. Journal of Materials Chemistry, 2003. **13**(12): p. 2963-2968.
- [3] Chukanov, N., et al., *Kinetics of cation exchange on hetero-framework microporous titano- and zirconosilicates*. Russian Journal of Physical Chemistry B, Focus on Physics, 2011. **5**(2): p. 278-283.
- [4] Poojary, D.M., R.A. Cahill, and A. Clearfield, *Synthesis, crystal-structures, and ion-exchange properties of a novel porous titanosilicate*. Chemistry of Materials, 1994. **6**(12): p. 2364-2368.
- [5] Luca, V., et al., *Nb-substitution and Cs+ ion-exchange in the titanosilicate sitinakite*. Microporous and Mesoporous Materials, 2002. **55**(1): p. 1-13.
- [6] Al-Attar, L., et al., *Purification of nuclear wastes by novel inorganic ion exchangers*. Journal of Materials Chemistry, 2003. **13**(12): p. 2969-2974.
- [7] Clearfield, A., et al., *On the selectivity regulation of K<sub>2</sub>ZrSi<sub>3</sub>O<sub>9</sub>·H<sub>2</sub>O-type ion exchangers*. Journal of Molecular Structure, 1998. **470**(1-2): p. 207-213.
- [8] Fewox, C.S., A. Clearfield, and A.J. Celestian, *In Situ X-ray Diffraction Study of Cesium Exchange in Synthetic Umbite*. Inorganic Chemistry, 2011. **50**(8): p. 3596-3604.
- [9] Xu, H., et al., *Crystal-chemical and energetic systematics of wadeite-type phases A<sub>2</sub>BSi<sub>3</sub>O<sub>9</sub> (A = K, Cs; B = Si, Ti, Zr)* Physics and Chemistry of Minerals, 2005. **32**(5): p. 426-435.
- [10] Lin, Z., et al., *Synthesis and structure of a novel microporous framework stannosilicate*. Journal of Materials Chemistry, 2000. **10**(6): p. 1353-1356.
- [11] Pertierra, P., et al., *Thermal behavior of K<sub>2</sub>MSi<sub>3</sub>O<sub>9</sub> center dot H<sub>2</sub>O with the structure of umbite (M = Sn) and kostylevite (M = Pb) minerals*. Thermochemica Acta, 2004. **423**(1-2): p. 113-119.
- [12] Lin, Z., et al., *Synthesis and structural characterization of microporous framework zirconium silicates*. Journal of Physical Chemistry B, 1999. **103**(6): p. 957-963.
- [13] Navascues, N., et al., *Reconstruction of umbite framework variants by atomistic simulations using XRD and sorption data*. Chemical Engineering and Processing, 2008. **47**(7): p. 1139-1149.
- [14] Bennett, H. and G.J. Oliver, *XRF analysis of ceramics, minerals, and allied materials*. 1992, Chichester, England; New York: Wiley.
- [15] Fewox, C.S. and A. Clearfield, *Synthesis and characterization of protonated zirconium trisilicate and its exchange phases with strontium*. Journal of Physical Chemistry A, 2008. **112**(12): p. 2589-2597.

# The Corrosion of Uranium in the Presence of Water Vapour and Hydrogen

A. Banos\*<sup>1</sup> and T. Scott<sup>1</sup>

\*Correspondence: Antonis.Banos@bristol.ac.uk

<sup>1</sup> University of Bristol, Bristol BS8 1TL, UK

## Introduction

The following text and attached diagram is an overview of the body of work which is planned to form the thesis of Antonis Banos. Currently this is an outline draft, and the work may be subject to change through the course of his studies. In this regard this document should not be viewed as a final thesis structure, rather a road map of experiments that have been highlighted as academically interesting and industrially relevant.

## Literature Review

An extensive literature review of current knowledge of uranium corrosion (rates, mechanisms, controlling influences) will be performed, with a specific focus on the corrosion in water and hydrogen. This body of work will be used to form the introductory chapters for the arising PhD thesis. A great deal of this work has been already undertaken by Antonis, and it is hoped that in the coming months this will be published as a review paper in an international journal.

## Gas Control Rig Experiments

These will form a large part of the PhD research activities. They will be used to determine the rates of reaction, kinetics and mechanisms for uranium corrosion in different environmental systems including nominally dry through to full immersed conditions. This will be achieved through the use of isotopically labelled gases and water to react with samples, using RGA mass spectrometry to monitor the evolving head-space gas chemistry. The arising samples will subsequently be analysed with secondary ion mass spectrometry (SIMS) and other surface analysis techniques to examine the arising corrosion products (thickness, morphology, composition, locations etc). For a detailed list of experiments please see the attached diagram. It is through these isotopic scenarios that full reaction kinetics and mechanisms for the U, H<sub>2</sub>O, H<sub>2</sub> reaction will be determined across a range of pressures and temperatures. Reactions exploring the reaction of U and H<sub>2</sub>O in a sealed inert environment (i.e. U with H<sub>2</sub>O with a cover gas of argon) will be also examined.

## TGA-DSC Experiments

To supplement the rig experiments, we will combine this work with thermo-gravimetric analysis (TGA) and differential scanning calorimetry (DSC), which will provide an alternative means of extracting corrosion rate data (for TGA) and also the specific heat (DSC) of certain reactions e.g. the oxidation of UH<sub>3</sub> in air. TGA experiments will be performed in a glovebox, in a precisely controlled atmosphere (N<sub>2</sub> or Ar) whilst the DSC measurements will be made using a 'bomb calorimeter' developed as part of the CoE for Uranium and Reactive metals and engineered to attach directly to the gas rig system. This will allow us to measure the specific heat of hydride formation at different temperatures and pressures – yielding possible benefits for determining differences between the formation of alpha and beta hydride.

## Visual Cell Experiments

Hydride formation in a visual cell will examine the nature of hydride initiation. Experiments will use metal coupons held within a sealed cell with a glass window. Using a high resolution camera, the formation of hydride nucleation/growth sites (e.g. number density, nucleation rate etc) will be determined for a range of samples prepared in a different manner, including mechanical polishing, electropolishing and nitric acid pickling. This will be used to determine if there is a tangible benefit to performing different surface treatments in order to alter the nature and onset of the hydride formation. We will examine hydriding under both wet and dry conditions.

## Stress Effects on Hydride Formation

In conjunction with visual cell experiments, the effects of localised stress within the metal will be examined in relation to the rate of corrosion (i.e. is it accelerated and if so, what is its proportionality in relation to the induced stress?). Principally this will be examined by the induction of stress within the uranium metal by forming a weld within the sample. Stress will be characterised using EBSD and within the visual cell

apparatus, the samples will be corroded in H<sub>2</sub>. This set of work will characterise, for the first time, the effect of stress on the rates of uranium corrosion. If time permits, we will also seek to make use of linear tensile-test and 3-point bend stages (available within the IAC) to strain uranium samples whilst subjecting them to corrosion.

### **Experiments at the Diamond Light Source**

Although the direct benefits of the Diamond experiments will be of more advantage to other students at the IAC, Antonis will be involved with the Diamond Light Source experiments in order to gain training and experience with Synchrotron experiments. We will apply for further beam time at DLS and ESRF, specifically to address the unresolved question of strain versus corrosion rate.

### **Corrosion Probe Experiments**

A further aspect of the project will be tied to the activities of Dr Robert Burrows (NNL) and the research being performed as part of a Knowledge Transfer Secondment (KTS) project to develop uranium probes for measuring the rates of corrosion in ponds and other storage environs. This work will potentially yield in-situ and directly relevant information for the rate of uranium corrosion at Sellafield site.

# Applications of Raman Spectroscopy for Nuclear Waste Characterisation

K.E. Wyness\*, J.C.C.Day<sup>1</sup>.

\*Correspondence: kw14747@bristol.ac.uk

(University of Bristol, H H Wills Physics Laboratory)

## Abstract

Here we show the potential and possibilities of performing stand-off Raman spectroscopy with the test subject of the polymer PTFE. Development of this technique could have promising applications for corroded Magnox sludge analysis. As it currently stands, many of the UK storage pond facilities from the start of the nuclear industry, have had little maintenance due to the high levels of radiation emitted. Therefore categorising the contents is important issue and needs to be completed. Contamination of equipment is the key factor when acquiring data, as the reliability of apparatus could be inconsistent with radiation damage. This is what led to the thought of utilising long distance Raman in-situ, with it being both non-invasive and non-destructive, strong attributes when dealing with high risk areas. Stand-off Raman here was measured to <3m and showed strong enough potential to increase in distance significantly. Efforts were made to simulate the ponds environment of great depths of water.

## Introduction

Nuclear decommissioning goes to extreme length to avoid human contact with the processed waste; here in the UK we have numerous fuel storage ponds dating back to the very start of the nuclear industry. However these established facilities contain huge quantities spent MAGNOX fuel, but with improper care certain ponds have run into difficulties, as the storage capabilities for the legacy ponds are now under investigation of what is chemically in them [1]. The legacy ponds are of particular interest due to the complex topography it now has. Knocked over skips have lead to fuel mixing amongst biological matter found from flourishing algae blooms and the debris has caused it to become problematical chemically speaking: Ultimate it needs to resolved.

Raman Spectroscopy is a powerful technique for detection of the vibrational modes in organic and inorganic materials. Each chemical compound has its own unique fingerprint, which corresponds with different wavelengths (called Raman shift) against arbitrary intensity counts. Stand-off Raman here was measured to a few metres however other literature shows larger distances are very much a possibility [2]. There has been much discussion on the potential of stand-off Raman through recent literature, with such applications for astronomy use, art preservation and even bomb disposal [3]. It is an incredibly useful for in-situ when attempting to classify foreign substances;

especially when dealing with radioactivity. Regular Raman spectroscopy would involve long fibre optic cabling for this kind of analysis with a probe attachment. However the concern is causing damage to the equipment from radiation exposure, very much the motive to investigate stand-off.

The use of PTFE as test subject was understandable for its clearly defined peaks intensities. An investigation performed by Koenig and Boerio [4] shows clear Raman shift at multiple intensities. 8 in total, with them being at 291, 383, 575, 595, 729, 1215, 1295 & 1379.(units of  $cm^{-1}$ ), with typically  $729cm^{-1}$  being the most noticeable. Although you can intensify these peaks by altering the temperature, all experimentation was performed at room temperature to stay true to the conditions of the ponds, as there would not be any extreme flux of temperature present.

*The overall proposal is to construct a safe and functional method for data sampling of the ponds bed through Raman spectroscopy. This report shows the initial experiments conducted.*

Figure 1 : Schematic Drawing of optical component box

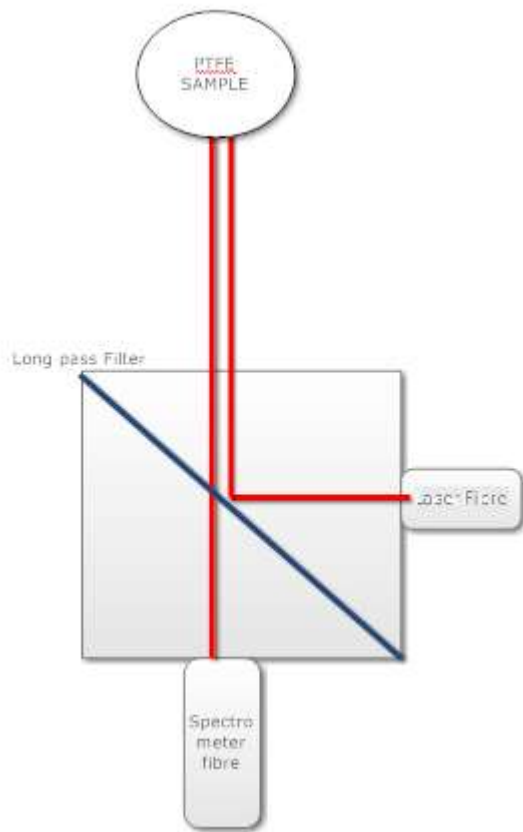


Figure 2 : schematic drawing of acrylic tube set up.

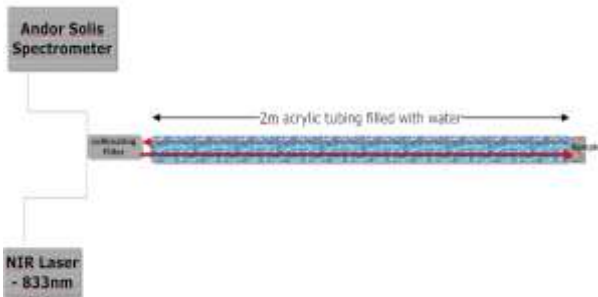


Figure 3: 100µm fibre in use for open air stand-off.

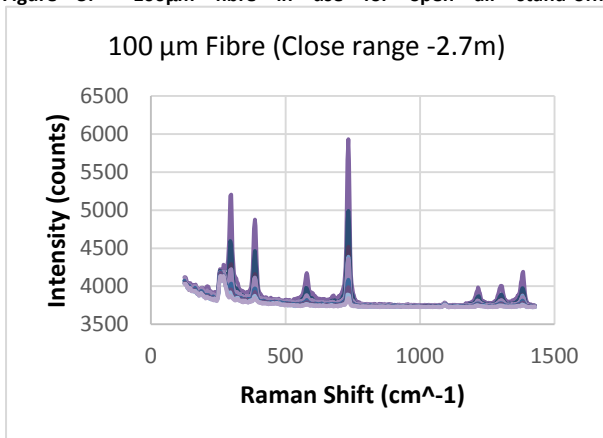


Figure 4: 62µm fibre in use for open air stand-off.

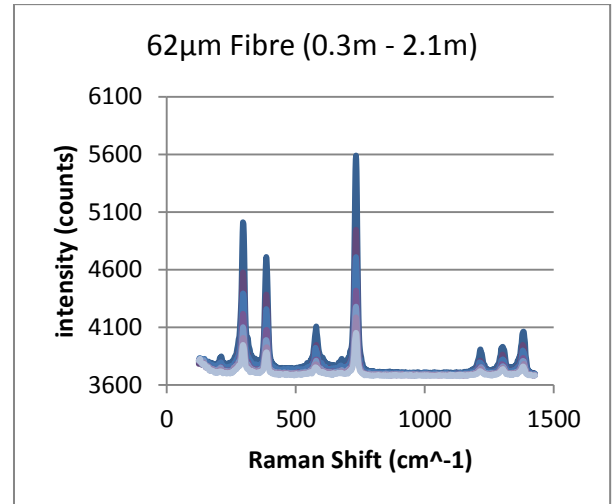


Figure 5: Results of 5 acquisitions of PTFE through acrylic tube.

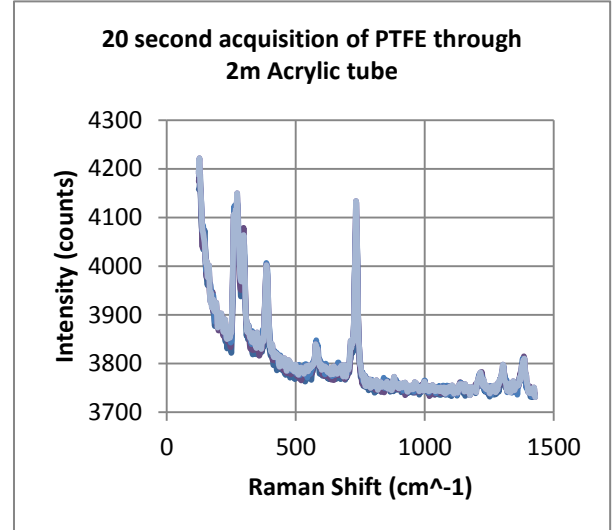


Figure 6: results of 2 acquisitions of PTFE underwater.

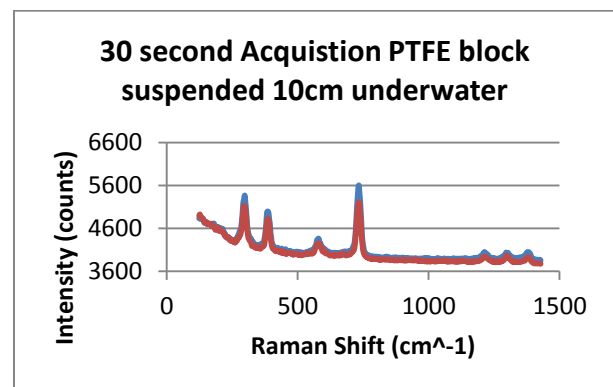


Table 1: list of equipment

Equipment	Type
Laser	NIR 833nm
Spectrometer	Andor Solis
Test subject	PTFE sheet

## Methodology Details

### *Performing Stand-off in open air*

The laser and spectrometer fibres are brought together into one optical component box. There is one long pass filter at 45° to the laser and spectrometer fibres (see figure 1), which allows only the wavelength of the laser to pass through, and then the returned Raman signal to get to the spectrometer. The PTFE sample was initially placed directly in front of the light path to gain a maximum intensity reading, This set a starting point at what traditionally you might expect when using a microscope (NB: a Plano-convex lens in front of the laser was adjusted to optimise the lasers focal point). Next the PTFE was placed at a distance of 30cm (increasing by 30cm increments) away from the laser, using a fluorescence card to keep track of the lasers focal point (NB: limitations to the experimental space meant a maximum distance of 2.7m was achieved and no more). The experiment was repeated 3 times to ensure true accuracy with readings, with it also (NB: the 833nm NIR laser used needed a short warming up period for a consistence output power)

The initial experiment a laser fibre width of 100µm was used. This was then switch to a 62µm width to test for a change in signal intensity, with the entire experiment being repeated with no variable changes.

### *Acrylic Tube feedback*

The next stage of the experiment was to perform stand-off Raman through a distance of water. To allow this in a laboratory situation, a water filled acrylic tube of 64mm inner diameter was used to simulate the depths of the storage ponds Sellafield have, however in-situ the ponds are 30m wide. This is difficult to simulate such a large space of water within laboratory conditions, therefore a tube is used. However the tube itself has to be tested to see if any background signal is present, therefore it can be taken into account when performing such experiments. From calculations of the Rayleigh length, the laser beam waist would take 45m before it would increase by a factor of  $\sqrt{2}$ , therefore a 2m tube would affect the beam waist by a mere 1%. This was evidence enough to understand the beam could pass through the tube and not disperse enough to pick up any signal from the material. PTFE was now placed at the bottom of the tube, and the laser aligned. 5 repeats of 20 second acquisitions were performed to ensure consistency.

## Results and Discussion

### *Stand-off in open air*

Stand-off Raman proved fairly successful. Adjustment of a Plano convex lens placed in front of the laser output established a stronger Raman signal. This

focused the beam at an arbitrary distance away from the point source, allowing the beam to have a focal point at long ranges. The drop off rate was fairly slow , initially from the closest point to 30cm saw a huge loss, however continued to lose only a fraction of counts per increment. At 2.7m away the results were still very distinguishable of PTFE. Intensity of the 291 peak rose significantly as the 729 peak dropped away, but clear spectra of PTFE was being detected.

NB: Initial thoughts on changing the Fibre size from 100µm to 62µm was that the laser power could be concentrated to a smaller focal point, therefore intensifying its interaction.

### *62µm fibre*

This part of the experiment again showed promise. Initially having a smaller fibre increased the count rate when compared directly with the 100µm fibre. However when the sample is taken at the greater distances, the fibre size made negligible impact on the intensity counts. Taking each individual peak the drop off rate did change with each peak – in some cases the 62 fibre performed better, but on the contra, with the 729 peak it actually performed worse. From comparing them the improvement is small but could be valuable.

### *Stand-off through acrylic tube*

The acrylic tube was now placed in between the PTFE sample and the laser beam. With the tube being 2 metres in length, the component box holding both the laser and spectrometer fibre optics now needed more accuracy to ensure the light reached the test subject. We also let the acquisition time remain as 20 second to improve the signal/noise ratio. An improvement was made to the spectra's intensities (taken from previous results). This was tested by removing the tube from the experiment and just measuring the PTFE through open air. This showed the spectra to return to lower intensity as shown from the first set of experiments, showing the returned light could be more detectable than without the tube there. Ultimately no interference was present from the acrylic as discussed previously; the tube had a large enough diameter to avoid interaction.

### *Stand-off through water*

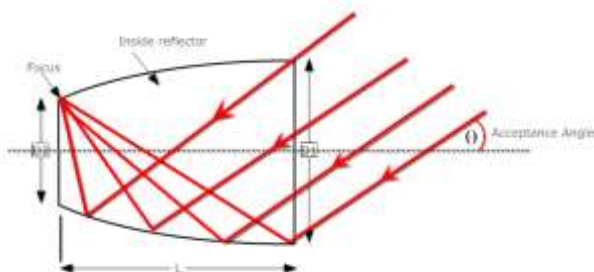
So far limited work has been done with the tube filled with water due to lack of response. The PTFE sample was initially suspended in the top of tube at 10cm and at then at 25cm. This demonstrated some signal back but the water clearly impacted on the lasers contact with the sample. The PTFE was then dropped into the tube at its full depth of 2m, however it could then not be detected from the spectrometer from several adjustments of the laser. The laser is only visible with a thermal imaging camera when passing through water

due to the dispersion of the light. Without one this makes it near impossible to correctly align the laser when dealing with a depth of 2m. Therefore a camera is necessary to aid this step of the process.

### Conclusions and Future Work

PTFE provides a bias interruption of what stand-off Raman is capable of. The intensity of peaks from magnesium hydroxide (main compound found in MAGNOX fuel storage) has lower energy vibrational modes which results in less intense peaks. This could lead to further investigation into laser power, since NIR is at the lower energy range of laser's capabilities. It is also well understood that increasing the lasers power (going to either the visible or UV range), means higher Raman signal. When testing the tube out for signal, it become very clear some of the light previously not reaching the collection fibre, now was. This was the tube allowing total internal reflection within the inner surface and consequently intensifying the signal when taking measurements. Due to the acrylic providing a surface for the return signal to ricochet off and not be lost in open air, the acceptance angle of the small collection fibre was now increased. The signal gain was significant enough to be implemented in the design of the real probe. An application of this already exists, with it being a "light cone" (compound parabolic concentrator, CPC), which allows to extend the acceptance angle for the collection fibre.

Figure 7: diagram of CPC.



This could be vital when attempting to detect weak Raman signals. As discussed before, Magnesium hydroxide has weaker peaks, so will definitely be implemented in the future. With respects to the water based testing, it provided an unclear outcome of whether stand-off through water was possible. There is clear evidence that it weakens the spectra, but needs further investigation. A method where the PTFE can be lowered into the tube at a steady rate will be the next step to figure out the limitations to this, and whether it has any application for nuclear waste characterisation.

### Acknowledgements

I would like to thank Dr John Day for all his advice and words of encouragement.

### References

- [1] Gregson C.R. et al. , Combined electron microscopy and vibrational spectroscopy study of corroded magnox sludge from a legacy spent fuel storage pond. *Journal of nuclear materials*
- [2] Sharma S.K (2007), New trends in telescopic Raman spectroscopic instrumentation. *Spectrochimica Acta Part A*. (1) 1008-1022
- [3] Hobro A.J Lendl B. (2009) Stand-off Raman spectroscopy . *Trends in Analytical chemistry*. 28 (11), 1235-1242
- [4] Koenig J.L Boerio F. J. (1969). Raman scattering and band assignments in polytetrafluoroethylene. *The Journal of Chemical Physics*. 50 (1), 2823-2829.

# Assessment of the Behaviour of Metallic Uranium During Encapsulated Product Evolution

Haris Paraskevoulakos\*<sup>1</sup>, T.B Scott<sup>1</sup>

\*Email address: cp13846@bristol.ac.uk

<sup>1</sup>Interface Analysis Centre (School of Physics, University of Bristol, Bristol BS8 1TL, UK)

## Abstract

Intermediate level wastes (ILW) are stored in stainless steel canisters, encapsulated in grout. A fraction of these have become a major concern for the UK nuclear community, as significant bulging around the circumference of the canisters have been observed. Distortion is ascribed to voluminous and flammable corrosion products forming on uranium metal, e.g. uranium hydride. Thus potential oxygen influx caused by fracturing of canisters will threaten their suitability for waste disposal, potentially causing release of the encapsulated radioactive material or even radioactive fire. The association of the uranium corrosion mechanisms with the mechanical degradation of the encapsulants (stainless steel and grout), is this project's targets.

## Introduction

The safe long term containment of radioactive waste is an essential goal for the UK nuclear community. Within the UK radioactive waste inventory, metallic uranium fuel and its associated Magnox cladding are key 'reactive' materials requiring long term containment. Currently, this intermediate level waste (ILW) is encapsulated in cementitious materials and stored in stainless steel canisters [1]. However, even when encapsulated, the waste can potentially corrode to produce uranium oxide and uranium hydride that cause severe volumetric expansion, mechanical distortion or even failure of the encapsulated system. The behaviour of the whole encapsulated system is thoroughly investigated through this project using different techniques such as Finite Element (FE) modelling, high energy X-Ray computed tomography (XRT) and diffraction (XRD), enabling us to study the structural integrity of the system as well as characterizing the arising corrosion products.

## Methodology Details

Finite element (FE) modelling can prove to be a useful predictive tool in terms of determining the strain state within the grout bulk and the surrounding stainless steel and consequently investigating grout and steel deterioration. Initially, simple 2D axisymmetric models have been employed. Reasonable assumptions regarding the properties of uranium, grout and steel were adopted. The corrosion – induced volumetric expansion was simulated using displacement load path. The grout softening behaviour is also taken into account while an elastic-perfectly plastic model dominating steel yielding is incorporated enabling as to detect potential yielding. The latter could be a sign of

the drum's severe deterioration but not a failure indication due to steel's post yielding hardening behaviour. According to the constitutive model adopted to describe the behaviour of the grout, there are two failure modes: tensile cracking and compressive crushing. Tensile cracking initiation, surface cracking, crushing initiation and steel's yielding initiation are the critical stages of an analysis to define material degradation. However, the axisymmetric models are an idealised case where the rod is practically a metal ring inside the grout bulk. A 3D model with one embedded metal bar could be more representative. Figure 1 shows the crack pattern resulting from both tensile and compressive damage at the moment of steel's yielding.

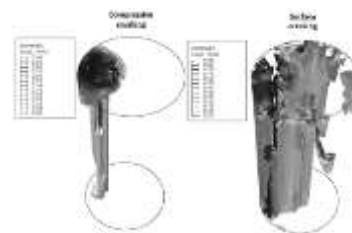


**Figure 1.** Grout's crack network due to both tensile and compressive damage at the moment of yielding initiation (3Dmodel).

The validity of the proposed models should be ensured from experimental work. Miniaturised uranium – grout – steel systems are employed in order to verify the findings raised from the FE analyses by conducting accelerated corrosion tests using a specifically designed reaction cell, a high magnification camera set up and a gas control provoke a uranium – hydrogen reaction (Fig 2).



**Figure 2.** Experimental set up employed to conduct uranium accelerated corrosion tests

## Results and Discussion

A parametric investigation has already been performed to identify the effect of the uranium location on the system's degradation based on the FE results. The metal's volume expansion was calculated, converted into corrosion percentage and associated with the different modes of cracking behaviour. Table 1 illustrates the values of corrosion percentage at different stages of material degradation. The parameter X indicates the horizontal distance between the uranium rod and the steel surface.

	Crack initiation	Surface cracking	Compressive crushing	Steel Yielding
X=8	0.010	0.714		13.265
X=4	0.009	0.484	0.923	4.274
X=2	0.009	0.341	1.382	2.829
X=1	0.013	0.192	1.755	2.163

The corrosion percentage when the steel starts yielding is reduced as the distance between uranium and steel becomes smaller. Also, surface cracking occurs at lower levels of corrosion as the grout cover is reduced.

## Conclusions and Future Work

The FE results show a reasonable trend if observed from a qualitative perspective. The models where the uranium is located closer to the stainless steel surface show more rapid deterioration levels. More specifically, surface cracking and steel yielding occurs at lower corrosion percentage. This is reasonable, since the pressure from corrosion products' evolution is exerted to a reduced amount of grout's volume so the steel needs to accommodate the arising strains. This causes the steel to deform excessively more rapidly. Besides, grout cracking takes place almost immediately after an almost negligible volume expansion allowing the cracks to propagate rapidly. This is due to the relatively limited grout's tension strength. Basically, this could imply that the grout within the drum is fully degraded from the very initial stages of corrosion. More parameters such as uranium orientation,

uranium shape and distribution as well as grout properties will be investigated in terms of affecting material's deterioration, as part from a parametric study using the newly created and more realistic 3D models. Besides, accelerated corrosion experiments will be performed in order to measure the reaction rates and correlate the corrosion percentage with the modes of cracking failure. Also, ILW mini drums with acrylic instead of steel will be implemented in order to visualize the crack network formation. Moreover, X-Ray Powder Diffraction (XRPD) and X-Ray Tomography (XRT) will be performed in similar systems after deliberately corroding them in situ, in Diamond Light Source [2]. Corrosion products' characterisation, mechanisms of internal cracking and corrosion mechanisms will be revealed through this work. All the experimental work will be also used to validate the proposed FE models.

## Acknowledgements

National Nuclear Laboratory (NNL)

National Decommissioning Authority (NDA)

Camilla Stitt (Interface Analysis Centre)

## References

- [1] G.A. Fairhall, J.D. Palmer, The encapsulation of Magnox swarf in grout in the United Kingdom, *Cem. Concr. Res.* 22 (1992) 293–298
- [2] C.A. Stitt, M. Hart, N.J. Harker, K.R. Hallam, J. MacFarlane, A. Banos, C. Paraskevoulakos, E. Butcher, C. Padovani, T.B. Scott, Nuclear waste viewed in a new light; a synchrotron study of uranium encapsulated in grout, *J.Haz. Mater.* 285 (2015) 221–227

# Study of Glass Degradation in a Simulated Crack

Chinnam Rama Krishna\*<sup>1</sup> and Bill Lee<sup>1</sup>

\*Correspondence: r.chinnam@imperial.ac.uk

<sup>1</sup> Department of Materials, Imperial College London, London SW7 2AZ, UK

## Abstract

A method to simulate degradation behaviour of glass in a crack was tested by placing two slides of international simple (IS) glass on each other in distilled water for 3 weeks at 90°C. Observations at the interface of glass slides revealed growth of gel layer on the bottom glass slide and cracks in the top glass slide. This study revealed the presence of a complex glass degradation behaviour in cracks which is absent on surface degradation of glass.

## Introduction

Vitrified nuclear waste canisters disposed in repositories are vulnerable to physical and chemical changes over time. The chemical change is by ion exchange between Glass Composite Material (GCM) and water/mineral rich solutions. The physical change is by fracture of GCM increasing the total surface area participating in ion exchange. The ion exchange changes the pH of surrounding solution leading to increasing glass dissolution rates. The degradation behaviour of glass in the fractured surface is less understood because of the complexity involved in controlling the conditions. Access to greater surface area and low water volume could accelerate degradation. Therefore, it is important to understand this subject in more detail to assess the long term degradation of vitrified intermediate level waste (ILW).

## Methodology Details

IS glass of 1cm x 1cm x 1mm was cut using a diamond saw blade and grinded using 4000 SiC paper until the glass surface is clear of scratches. Two such slides were carefully placed on each other in distilled water and left for 3 weeks at 90°C in Perfluoroalkoxy (PFA) vessel. Observations were made using optical microscope, SEM and EDX mapping.

## Results and Conclusions

Under SEM, the surface of the polished glass (upper surface of upper slide) exposed to

surrounding water formed a gel layer. Observations at the interface revealed a gel layer that was formed on the bottom glass slide and cracks growing into the top glass slide. Further observation revealed that bottom slide with gel layer has formed pits round in shape while the top slide surface exhibited cracks growing into the glass with gel layer formed in to them. The cracks growing into glass slide could be an effect of stress corrosion cracking initiated by the surface roughness and capillary forces. Initial experiments thus found that glass degradation in a crack is complex and different than that is observed on the surface of glass. The cracks growing into the upper glass slide could be used to model the long term degradation behaviour of vitrified ILW.

## Future Work

The studies (experiments and characterization) on simulated cracks will continue by varying parameters such as surface roughness, thickness of glass, load on glass slides, temperature and water volume. Similar experiments are planned on active wastes with the help of Distinctive Active Fund at NNL. The data obtained from these experiments will be used to model long term stability of vitrified ILW using Finite Element Modelling.

## Acknowledgements

Funding from EPSRC and support of DISTINCTIVE consortium members is acknowledged.

# Immobilisation Process for Contaminated Zeolitic Ion Exchangers from Fukushima

D. Plester<sup>1</sup> and W.E. Lee<sup>\*1</sup>

\*Correspondence: w.e.lee@imperial.ac.uk

<sup>1</sup> *Centre for Nuclear Engineering, Imperial College London*

## Abstract

The remediation of the Fukushima site in Japan has generated large volumes of contaminated zeolitic ion exchangers. These zeolitic adsorbents are currently stored on site but need to be immobilised in a solid wasteform before being permanently disposed of. The majority of the radionuclides in these adsorbents are Cs and Sr with relatively short half-lives so that the level of long-term performance of the wasteform is not as demanding as for usual High Level Waste immobilisation matrices. To preclude volatilising Cs and Sr species, a maximum immobilisation processing temperature of 600 °C is necessary. The requirement of developing low temperature processing conditions appropriate for treating nuclear waste using vitreous matrices has led to challenges in the design of a suitable process and durable wasteform. To accommodate these challenges a glass composite wasteform composed of a low melting temperature lead borosilicate glass frit sintered with a simulant waste zeolitic ion exchanger has been developed. The produced wasteforms have been submitted to mechanical testing to ascertain whether they would be suitable for handling in an industrial setting. Future work will include MCC-type leach testing of the produced wasteform to test chemical durability. Preliminary results notably show that producing a robust composite wasteform is possible at 550 °C, surpassing the initial requirement.

# Glass Composite Materials for Nuclear Waste Disposal

C. Hutchinson\*<sup>1</sup>

\*Correspondence: charles.hutchison08@imperial.ac.uk

<sup>1</sup> *Imperial College London, London, SW7 2AZ, UK*

## Abstract

The final resting place of nuclear waste is general thought to be several kilometers underground, with many layers of protection. The most crucial of these is the waste matrix itself, and currently this means a waste form comprised of glass. Although glass has many benefits, such as corrosion resistance, radiation resistance, and a capacity to store a large variety of elements into its structure, problems do exist. One such example is the limitation imposed that no crystallization can occur in the final glass, an event which is considered to harm the durability. This puts severe restrictions on the amount of certain elements that can be placed in the waste. Rather than have one glass to suit all wastes, it is necessary to have several waste forms-choose the right waste form for the right waste and to this end, Glass Composite materials are being studied.

Glass composite materials (GCM's) are described as having both a crystalline and amorphous component, either of which can be the primary phase. These are currently being investigated to immobilize all categories of nuclear waste due to their flexibility; their properties can be tailored by altering the composition and manufacturing method.

The plan for my PhD is to create a standard of characterization techniques to allow determination of various phases and glasses in GCM's both before and after leach studies, of varying conditions. This will allow tracking of how crystalline components affect the durability and ultimately whether these materials should be further considered and researched as a nuclear waste material.

# Nanoscale Investigation and Control of Radionuclides in Waste Management

E. Cali\*<sup>1</sup>

\*Correspondence: e.cali14@imperial.ac.uk

<sup>1</sup>Imperial College London, London, SW7 2AZ, UK

## Introduction

The rapid development of industry and associated production of toxic waste, especially heavy metals, leads to a great interest in creating and upgrading new materials to remove this pollutants from the environment <sup>1</sup>.

The environmental challenges into waste disposal are sensing, measuring, quantifying the contaminants that are in the groundwater and to separate those contaminants. For this reason, treatment of contaminated water to remove soluble metals and radionuclides has been and continues to be a technical challenge due to the very low concentrations established by current regulations.

In recent years nanotechnologies have reached much development that has the potential to be used also in this field. Nanoparticles offer advantages as nanosensors in rapid and high-throughput detection methods, since the small size of these NPs gives them large surface-to-volume ratios.

Magnetic nanoparticles are of great interest for researchers from a wide range of disciplines. In particular, the use of magnetite nanoparticles as adsorbents in water treatments provides a convenient approach for separating and removing contaminants by applying external magnetic fields.

In most of their applications, the particles perform best when the size of the NP is below a critical value, which is usually around 10-20 nm. In this case, if the temperature is above the so-called blocking

## Goals of the Project

The aim of the project is, therefore, threefold: to synthesise superparamagnetic Fe<sub>3</sub>O<sub>4</sub> nanoparticles via a thermal decomposition method; to replace the hydrophobic ligand with an hydrophilic one, in order to establish a water stable system; and to monitor and sequester environmentally heavy pollutants, via specific or non-specific ligand agents, thereby tuning the magnetic properties for sensitive detection.

temperature, the nanoparticles show a superparamagnetic behaviour, and the magnetisation of nanoparticles can be easily flipped, with the energy required for flipping the magnetisation being Room Temperature. The system behaves like a superparamagnet: there is now a giant moment inside each particle instead of atomic moments. Each nanoparticle is still a permanent magnet because of spontaneous magnetisation within the particle, but the magnetisation of each single particle is fluctuating rapidly subject to thermal agitation, resulting in zero net macroscopic magnetisation for a collection of particles.

An example of this kind of material is magnetite, a common magnetic iron oxide that has a cubic inverse spinel structure. Magnetite nanoparticles can be produced via coprecipitation of ferrous and ferric ions by a base in an aqueous solution, method which, despite simple and convenient, leads to systems that are not stable under ambient condition; or via thermal decomposition of organic iron precursor in the presence of hydrophobic ligands<sup>2</sup>. Superparamagnetic nano crystals with smaller and tunable sizes can be obtained via this method, nanoparticles which are stable in various hydrophobic solvents. However, water-soluble NPs are more desirable for their application in water treatment, and this feature can be easily obtained through a ligand exchange modification, which doesn't affect the characteristics of the nanoparticles and leads to perfectly water dispersible systems

Technologies based on the utilisation of magnetite nanoparticles for the removal of contaminants from wastewater are highly effective, efficient and economically viable, however, there are some fundamental requirements for their application, since Fe<sub>3</sub>O<sub>4</sub> nanoparticles need to be stable and capable of the contaminants removal, and not to aggregate in groundwater systems. In addition, ideally, they can be regenerated and reused for more than one cycle. In

order to achieve these aims, selectivity and sensibility are strongly relevant characteristics.

## Yearly PhD Plan

### First year

Will focus on synthesising the NPs via a thermal decomposition method, using iron (III) acetylacetonate as the organic precursor in the presence of 1,2-hexadecanediol, oleylamine and oleic acid in phenol ether<sup>3</sup>.

The synthesis of the hydrophobic magnetite nanoparticles will be followed by a ligand-exchange reaction involving  $\text{NaH}_2\text{PO}_4$  and  $\text{K}_2\text{HPO}_4$  in order to obtain a water dispersible system<sup>4</sup>, such that it can be further applied. The phosphate groups on the nanoparticles' surface will also provide the ligand that will be used to make different radionuclides and heavy metals absorb, by starting from uranium, as it has been observed that the phosphate group has a strong tendency to form complexes with uranyl ions<sup>5</sup>. In order to verify the adsorptive capacity of the system, absorption and desorption tests will be undertaken.

Characterisation tests will be applied on bare magnetite nanoparticles, in particular TEM (Transmission Electron Microscopy) and HR-TEM will be used to determine the size of the nanoparticles, DLS (Dynamic Light Scattering) will be used to verify the dispersibility of bare magnetite NPs and of phosphate-functionalised magnetite NPs in hexane (the first) and in water (the second). Zeta-potential technique will also be adopted to determine the surface charge of the functionalised particles. ICP-OAS will determine the quantity of bare NPs in the suspension samples to enable accurate control of sorption experiments.

The superparamagnetism of either bare and functionalised particles will be tested using the SQUID magnetometer, which can measure extremely subtle magnetic fields.

In order to quantify the amount of phosphate groups on NPs surfaces, a titration method will be utilised.

### Second year

Will focus on tuning the magnetism of the superparamagnetic nanoparticles and eventually changing the ligand in order to achieve the best performing system for absorbing Pb, Sr, and other heavy metals.

In addition to all the characterisation techniques listed, the effect of the solution

pH, which is one of the most crucial parameters for the sorption of metal ions, will be evaluated. The effect

of contact time between  $\text{Fe}_3\text{O}_4$  NPs and the contaminants will also be determined, and, in order to evaluate the selectivity of the phosphate capped system for the metal and radionuclide ions, co-existing ions will be added into the reaction system at the optimal conditions.

Desorption studies will also be carried in order to test the feasibility of regeneration and reuse the adsorbents.

### Third year

will see the combination of the system of superparamagnetic magnetite NPs with nanopores. This will be done in collaboration with Loughborough University (Laura Mayne, a PhD student also on the EPSRC DISTINCTIVE programme will work to develop the nanopores), and will take advantage of the change in the local resistance measured, and hence change in conductivity, when a physical object moves through the pores. If uranium is attached to a ligand, its mobility through the nanopores should be different, hence, using a magnetite core structure with a silica coating and a ligand to which uranium is attached will lead to better direction and better encapsulation and sensing capability<sup>1</sup>.

## References

- (1) Fialova, D.; Kremplova, M.; Melichar, L.; Kopel, P.; Hynek, D.; Adam, V.; Kizek, R.; *Materials* **2014**, *7*, 2242-2256, "Interaction of Heavy Metal Ions with Carbon and Iron Based Particles"
- (2) An-Hui Lu, A.H.; Salabas, E. L.; Schüth, F.; *Angew. Chem. Int. Ed.* **2007**, *46*, 1222 – 1244, "Magnetic Nanoparticles: Synthesis, Protection, Functionalization and Application"
- (3) Sun, S.; Zeng, H.; *Jacs Communications* **2002**, "Size-controlled Synthesis of Magnetite Nanoparticles"
- (4) Xue Yi, L.; Yan, T.; GuangLu, G.; *SCIENCE CHINA Physics, Mechanics and Astronomy* **2011**, "Preparation and zeta-potential characterization of highly dispersible phosphate — functionalized magnetite nanoparticles"
- (5) Yu, X.F.; Liu, Y.H.; Zhou, Z.W.; Xiong, G.X.; Cao, X.H.; Li, M.; Zhang, Z.B.; *J Radioanal Nucl Chem* **2014**, "Adsorptive removal of U(VI) from aqueous solution by hydrothermal carbon spheres with phosphate group"

# ***Ab initio* Molecular Dynamics Simulations of Strontium Hydrates**

O.Lynes\*, and A.Kerridge\*

\*Correspondence: o.lynes@lancaster.ac.uk , a.kerridge@lancaster.ac.uk

Lancaster University, Bailrigg, Lancaster. LA1 4YW

## **Abstract**

Across the UK are 35 sites producing radioactive waste, and the 2013 Nuclear Waste Inventory put the levels of waste at 4.4 million m<sup>3</sup> according to the Nuclear Decommission Authority. External waste ponds and silos dating back to the 1950s have been used to hold spent uranium fuel rods, along with the associated magnesium alloy cladding (Magneox). Over time the corrosion of the Magnox cladding into the mineral brucite, as well as variation in external conditions, have led to a fine particulate sludge forming in the legacy ponds, which is thought to be comprised of the aquo and hydroxide complexes of the radionuclide <sup>238</sup>U and two of its fission products, <sup>90</sup>Sr and <sup>137</sup>Cs, as well as external debris.

This study details *ab initio* molecular dynamics calculations which have been performed on strontium octahydrates, using the TURBOMOLE FROG module. Various parameters for *ab initio* MD calculations have been tested for optimal performance. These are the first stages into an investigation of the interactions of the strontium radionuclides found in storage ponds, and initial results show a preference for the 7-coordinated strontium octahydrates, in agreement with previous literature. Further investigation into both the smaller strontium hydrates and larger double shell systems is ongoing.

## **Introduction**

High and intermediate level nuclear waste, such as spent uranium fuel rods and their magnesium-aluminium alloy cladding (Magneox), are held in storage ponds at the Sellafield site in North West England<sup>1</sup>. These uncovered ponds are filled with water, which shields the surrounding environment from radioactivity, as well as aiding the cooling of the spent fuel rods. The magnox cladding used in early gas-cooled nuclear reactors has, over time, corroded to produce the mineral brucite, Mg(OH)<sub>2</sub>, which has a highly adsorbent hydroxyl-terminated reactive surface. The removal of heavy metals from water using brucite has been studied and an adsorption capacity 10-15 times higher than that of zeolites was found.<sup>1</sup> The corrosion of the cladding has produced a layer of particulate sludge in the storage ponds which is likely to contain not only brucite, but also uranium and its fission products.<sup>1</sup> Due to the open air nature of the storage ponds there are also likely to be carbonate species, as well as a build-up of organic matter.<sup>1</sup>

Over several decades a build-up of decay products has developed in the storage ponds. The radionuclides currently present in greatest quantity in the storage ponds are thought to be <sup>238</sup>U and two of its fission products, <sup>90</sup>Sr and <sup>137</sup>Cs, as well as much smaller amounts of <sup>235</sup>U and trace <sup>232</sup>U and <sup>236</sup>U.<sup>2</sup> Storage ponds

are alkali dosed in the pH range of 10-12 to limit the further dissolution of the cladding and as a result the ions present exist in highly basic aqueous environments as aquo and more often, hydrated hydroxide complexes of UO<sub>2</sub><sup>+</sup>, Sr<sup>+</sup> and Cs<sup>+</sup>.<sup>1,3</sup> Variation outside of this pH range, combined with the length of time the storage ponds have been in use has produced a higher level of sludge build up than was initially expected.<sup>4</sup>

This project builds on previous work performed on the micro solvation of strontium, and initially uses the molecular dynamics methodology to investigate the interactions of strontium, caesium and uranium with water and hydroxide. Following these molecular dynamics studies attention will be focussed on investigations of the interaction of strontium hydrated hydroxides with the reactive surface of brucite. Understanding the interactions of these radionuclides with the mineral surface is key for the development of strategies for the continued storage and eventual disposal of nuclear waste.

## **Methodology Details**

Initially the project uses *ab initio* molecular dynamics (AIMD), a technique which uses density functional theory (DFT) to model the electronic structure of molecules from first principles.<sup>5</sup>

DFT is a computational method of obtaining an approximate solution to the Schrödinger equation for a many-electron system.<sup>6</sup> It is one of the most routinely applied computational investigative techniques and is instrumental for understanding the electronic, structural and vibrational properties of large molecular systems.<sup>7</sup> DFT also provides a method by which to calculate the thermodynamic properties of a compound.<sup>6</sup>

AIMD performs DFT calculations “on the fly”, electronic structure calculations are performed as the trajectory of the system is generated.<sup>5</sup> This provides a huge amount of data about a system, and allows for the visualisation of quantum chemical events e.g. bond formation and proton transfer. These calculations will be performed so as to provide initial data on how the radionuclides discussed above interact with water, hydroxide and the reactive brucite surface.

All quantum mechanical calculations have been carried out using TURBOMOLE Version 6.6. The Generalised Gradient Approximation exchange-correlation functional BP-86 and a def-SV(P) basis set were chosen for the initial calculations to minimise computational cost.<sup>9</sup>

AIMD calculations were performed using the FROG module of this code. Total simulation time is divided into time steps of equal duration. At each time step the energy and gradient of the system are calculated using the leapfrog Verlet algorithm.<sup>10</sup> A Nosé-Hoover thermostat was used to maintain the temperature of the system. Temperature is fixed using the kinetic energy of the atoms in the system, and was chosen to be 298.15 K for all simulations presented.

## Results and Discussion

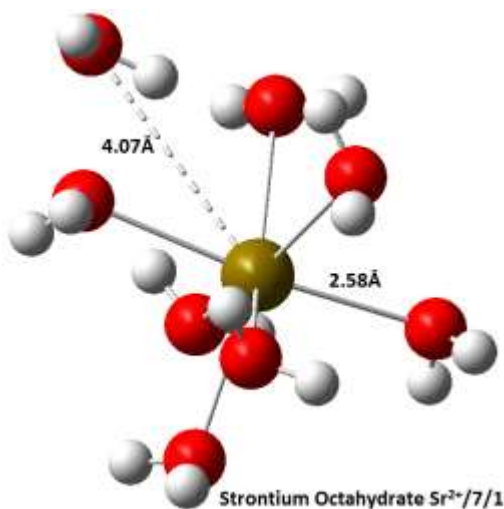


**Figure 1:** Ball and stick representation of the hepta co-ordinated Strontium Octahydrate

Initial DFT calculations were carried out on strontium hydrates,  $\text{Sr}_n\text{H}_2\text{O}$  where  $n=1-8$ , in order to ensure previous computational results could be reproduced.<sup>11</sup> This was to provide test structures for initial AIMD calculations and the checking of the methodology used.

There are several key factors to consider when performing any AIMD calculation. The time step, the initial velocity, the relaxation parameter and the total number of steps for the simulation. It is important to verify that the simulation describes the chemical system correctly. Comparing computed values to experimental results will indicate the quality of various aspects of the model system.

The choice of time step is crucial in AIMD calculations. A time step which is too large can cause atoms to move too far in each step leading to a failure to simulate the trajectory correctly. A too small time step will make it necessary to perform more steps, thus taking longer to run the simulation. As a general rule, the time step should be no longer than 10% of the shortest vibrational period in the system being studied. For the strontium hydrates this gives a suggested time step of tenths of a femtosecond.

Initial AIMD calculations were carried out on a  $\text{Sr}^{2+}/7/1\text{H}_2\text{O}$  (**Fig. 1**) molecule in TURBOMOLE. The structure in **Fig 1**. has 7 waters in the first solvation shell with an average starting bond length of 2.58 Å, and a single water in the second solvation shell with a distance of 4.07 Å between the strontium ion and the water in the second solvation shell.

The simulation parameters were set at an initial temperature of 500 K, 240 a.u. initial relaxation parameter and an 80 a.u. time step. The simulation was allowed to run for 6000 time steps a total time of 11.61 ps, to allow the system to equilibrate.

At ~4500 time steps the system is considered to be in equilibrium. The *ab initio* simulations calculate kinetic energy, potential energy and temperature as a function of time step (**Fig.2**). For the purposes of these simulations equilibrium is considered to be reached when the temperature variation has settled into a constant range. In this case the equilibrium range is between ~250-350K.

When the trajectory was examined a preference for a 7 coordinate structure was observed (**Fig.3**). For the period between 1000 and 4000 time steps the strontium is 6 coordinated, but by the time the equilibrium phase is reached at ~4500 time steps the strontium is 7 coordinated again. This result is in agreement with a previous DFT study which found that Strontium ions coordinated by 7 waters in the first solvation shell, along with a single water in the second solvation shell. are the most stable.<sup>12</sup>

Further AIMD calculations were performed with a reduced time step of 40 a.u. which corresponds to 0.9 fs or  $1/10^{\text{th}}$  of the O-H bond vibrational frequency which is the shortest present in the system. After a simulation of 7000 time steps a total time of 13.55 ps as shown in **Fig. 4** there is no clear equilibrium has been reached.

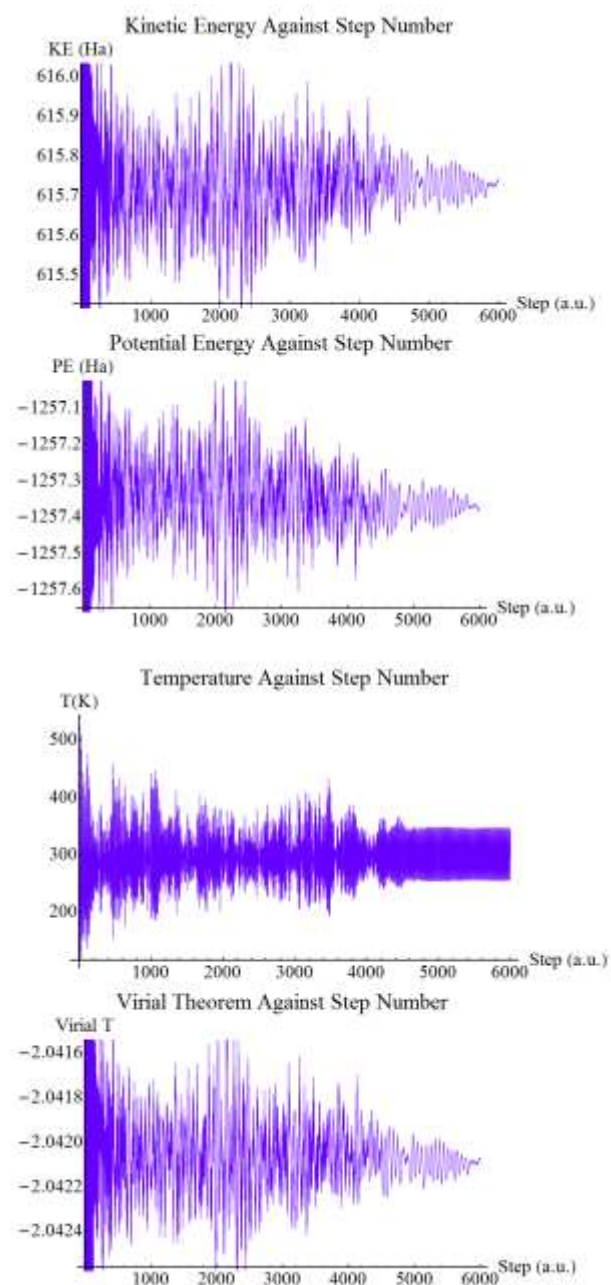


**Figure 2:** Calculated values of kinetic energy, potential energy, temperature and virial theorem against step number.

The relaxation parameter for the system as a whole in an AIMD simulation should be between 2 and 10 times the time step. Simulations were repeated, varying the total system relaxation parameter between 80 a.u.

and 400 a.u., however no clear equilibrium was found for any of these relaxation values.

This lack of equilibrium range could be attributed to a number of factors, there is a second relaxation parameter to consider for the Nosè-Hoover thermostat may have to be adjusted so that a constant temperature can be maintained. Another reason is that there are simply not enough time steps to reach equilibrium with the shorter time step. Alternatively it may be that there are not enough atoms in the systems for equilibrium to be meaningful.

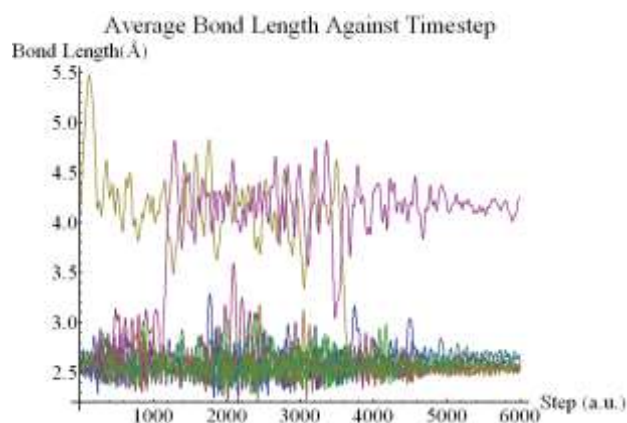


**Figure 3:** Calculated Sr-O Separations as a function of step number. The first solvation shell waters are in the 2.5 Å range and the second solvation shell waters are in the 4-4.5 Å range.

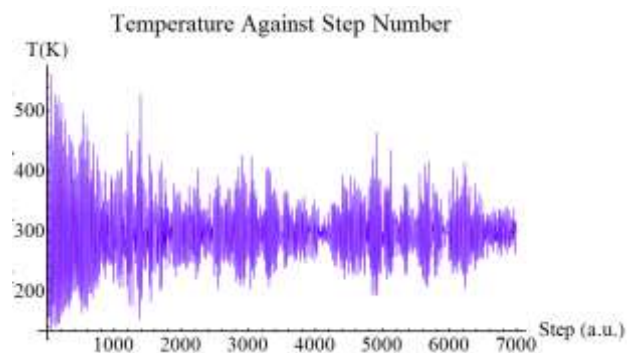


**Figure 4:** Temperature as a function of time step.

The next stage in the project forms part of an on-going collaboration with Nik Kaltsoyannis at UCL and builds upon work that has previously been performed in this area.<sup>9,10</sup> The structures of two hydrated strontium hydroxide complexes, shown in Fig. 5 and Fig. 6, have been provided by our collaborators. The di-hydroxide structure has been shown to be the more stable of the two conformers, with both hydroxide groups in the first solvation shell of the complex.

The existence of the second structure, with one hydroxide group in the first solvation shell and one hydroxide group in the second solvation shell, indicates that proton transfer may be occurring between the

two shells. These structures were taken as starting points for AIMD calculations in order to investigate if proton transfer events could be identified. Initial simulations suggest that proton transfer is possible and, apparently, probable, however this is preliminary data and work is ongoing.

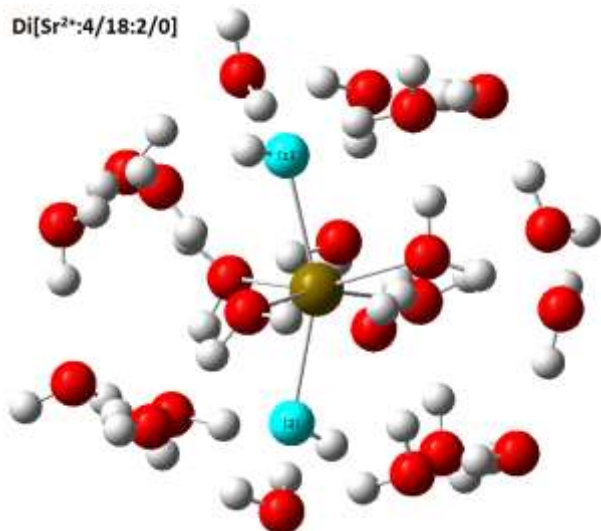


**Figure 5:** Hydrated strontium hydroxide di structure, the oxygen's labelled [1] and [2] indicate the hydroxide functional groups.

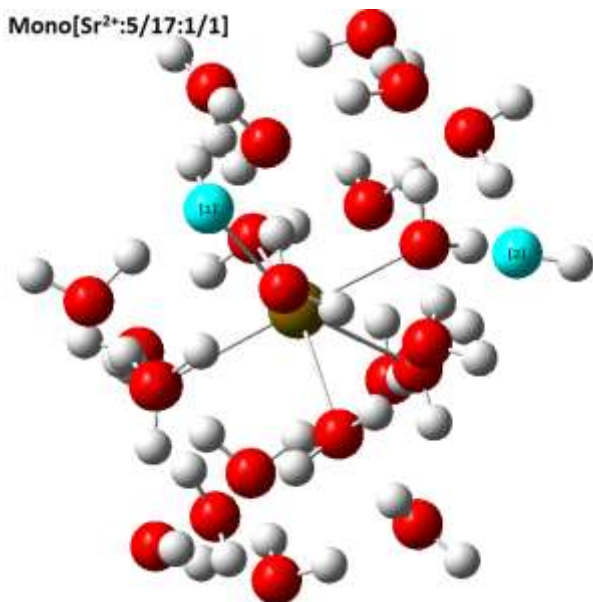


**Figure 6:** Hydrated strontium hydroxide mono structure. The oxygen's labelled [1] and [2] indicate the hydroxide functional groups.

## Conclusions and Future Work

We have begun the process of using molecular dynamics to model strontium ions in water, both as small single shell structures and as larger strontium double shell complexes, building upon the work of our

collaborators at UCL. The next stages of our research include refining the *ab initio* MD process to achieve a constant equilibrium at an appropriate time step and simulation length.

Going forwards the interactions of other radionuclide ions such as <sup>137</sup>Cs and <sup>238</sup>U will be examined with *ab initio* molecular dynamics. We then plan to model the interactions of the radionuclides known to be present in the storage ponds with the reactive surface of brucite.

## Acknowledgements

Jonathan Austin and Scott Owens the industrial supervisors for the project.

The DISTINCTIVE consortium for providing research funding for EPSRC grant: EP/L014041/1

Mike Pacey and Lancaster University for access to their High End Computing HPC facility machine which allowed me to complete the majority of this research.

To Eszter Makkos and Nik Kaltsoyannis at UCL for providing the optimised structures of the Hydrated Strontium Hydroxide Complexes for the next stage of research.

The authors would like to acknowledge the use of the EPSRC UK National Service for Computational Chemistry Software (NSCCS) at Imperial College London in carrying out this work.

## References

- 1 S. a. Parry, L. O'Brien, A. S. Fellerman, C. J. Eaves, N. B. Milestone, N. D. Bryan and F. R. Livens, *Energy Environ. Sci.*, 2011, **4**, 1457.
- 2 S. Wallace, S. Shaw, K. Morris and J. Small, *Appl. Geochemistry*, 2012, 1–17.
- 3 J. D. Farr, M. P. Neu, R. K. Schulze and B. D. Honeyman, *J. Alloys Compd.*, 2007, **444-445**, 533–539.
- 4 G. R. Bochkarev and G. I. Pushkareva, *J. Min. Sci.*, 2009, **45**, 104–109.
- 5 M. P. Allen, 2004, **23**.
- 6 M. Orio, D. a Pantazis and F. Neese, *Photosynth. Res.*, 2009, **102**, 443–53.
- 7 G. Sun, J. Kürti, P. Rajczyk and M. Kertesz, *J. Mol. ...*, 2003, **624**, 37–45.
- 8 K. Capelle, *arXiv Prepr. condmat/0211443*, 2006, **36**, 1318–1343.
- 9 R. Ahlrichs, M. Bär, M. Häser, H. Horn and C. Kölmel, *Chem. Phys. Lett.*, 1989, **162**.
- 10 N. York, 2001.
- 11 A. Kerridge and N. Kaltsoyannis, *Dalton Trans.*, 2011, **40**, 11066–9.
- 12 A. Kerridge and N. Kaltsoyannis, *Chem. A Eur. J.*, 2011, **17**, 5060–7.

# Gas Retention and Release from Nuclear Legacy Waste

Mike Johnson<sup>1\*</sup>, Simon Biggs<sup>2</sup>, Jeff Peakall<sup>1</sup>, Mike Fairweather<sup>1</sup>, David Harbottle<sup>1</sup>, Tim Hunter<sup>1</sup>

<sup>1</sup> School of Chemical and Process Engineering, University of Leeds, Leeds, UK, LS2 9JT

<sup>2</sup> Faculty of Engineering, Architecture and Information Technology, University of Queensland, Brisbane Qld 4072, Australia

\*corresponding author: pm12mcj@leeds.ac.uk

## Abstract

A laboratory scale experiment is presented to analyse gas retention in nuclear legacy waste. Retention of flammable gases in legacy waste, formed during long-term underwater storage of Magnox clad fuel and cladding swarf waste, has caused concern ahead of the proposed decommissioning activities at the Magnox Swarf Storage Silos and First Generation Magnox Storage Pond. This gas retention and release behaviour must be characterised in order to justify a storage and disposal route. Evidence suggests that large voidages of up to 41 % are feasible within a realistic magnesium hydroxide test material. This would test the storage capacity of the new SPP1 facility at Sellafield and would place new, low strength sludge wastes at risk for buoyant gas release events.

## Introduction

Decommissioning of the Magnox Swarf Storage Silos (MSSS) and First Generation Magnox Storage Pond (FGMSP) are priority activities for the Sellafield site.[1] Long term underwater storage of Magnox clad fuel has allowed the magnesium/aluminium alloy in the cladding to corrode, with precipitation products consolidating into a legacy waste of corroded Magnox sludge (CMS).[2, 3] Concerns have arisen regarding the episodic release of flammable gases retained within the sludge, formed by a combination of the corrosion reactions and by radiolysis of the pond and silo liquors.

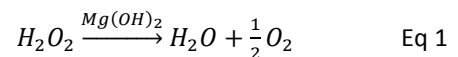
Flammable gas generation presents no safety risk when it is released steadily from the consolidated sludge layer as ventilation of the MSSS prevents the headspace approaching the lower flammability limit. However, significant retention of gas within the consolidated waste layer can lead to large periodic gas release events (GREs)[4] either through disturbance of the waste or through rising buoyant regions of waste. Large GREs have been observed at some of the Single (SST) and Double (DST) Shell Tanks at Hanford, Washington leading to potentially flammable ratios of hydrogen and nitrous oxide in the tank ullage.[5]

Research on kaolinite test materials for Hanford sludge waste indicates that the extent of gas retention in the bed is greatly dependent on yield stress.[6] A threshold strength is required to prevent bubbles rising, largely unhindered, through the bed. Conversely, stable, self-supporting channels can form within strong, highly consolidated beds. These channels and cracks enable continuous gas release from the bed thereby mitigating large periodic releases.[7] Current understanding suggests a compromise strength in the order of 10s of Pascals is likely to have the greatest capacity for high risk void fractions greater than 40%.

A robust safety case is required to mitigate the risks associated with GREs and this safety case is compounded by economic drivers to limit waste swell due to entrained gas. Increases in waste volume due to sludge swell could significantly increase the expense of transporting sludge from the MSSS to the processing plant and greatly reduce the working volume of intermediate storage facilities such as the Sellafield Sludge Packaging Plant (SPP1), which is due to receive diluted sludge from the FGMSP.

## Methodology Details

Versamag magnesium hydroxide (Martin Marietta Magnesia Specialties LLC, USA) and water are prepared into a sludge using an overhead stirrer. A litre of sludge is pumped to a 5" acrylic column with a gas tight lid using a peristaltic pump. A 4 ml volume of 35 % v/v hydrogen peroxide (Merck Chemicals, Germany) was injected into the flow on route to the test column. Over the course of around 8 hrs, the hydrogen peroxide, H<sub>2</sub>O<sub>2</sub>, decomposes according to equation 1, generating 500±20 ml oxygen.



Some oxygen is trapped by the bed causing the bed to swell, while the total volume of gas generated displaced an equivalent volume of water from an adjacent upturned measuring cylinder suspended in a water bath. The bed height in the test cylinder and the meniscus level in the gas collection cylinder were monitored at 8 minute intervals until gas generation ceased. The ratio of the instantaneous bed height to the initial bed height provides the bed swell and hence the void fraction can be deduced.



Figure 1: Bed swell due to gas retention in 8 Pa Mg(OH)<sub>2</sub> sludge

Experiments were performed across a range of sludge yield stresses which were characterised using the ‘vane method’ with a Brookfield Viscometer.

**Results and Discussion**

Three images of the experimental apparatus are shown in Figure 1, demonstrating the bed growth and displaced gas volumes at 0, 3 and 8 hrs for an 8 Pa yield stress bed. A typical profile of void fraction and gas volume with time in Figure 2 demonstrates bed growth to a maximum voidage,  $\nu$ , of 38 % before a small reduction in bed volume.

During this period 480 ml of gas was evolved. The small decrease in the collected gas volume after 5-6 hrs reflects the sensitivity of the gas volume to atmospheric temperature and pressure. This, in part, could account for the reduction in bed volume after 4 hrs rather than a series of GREs.

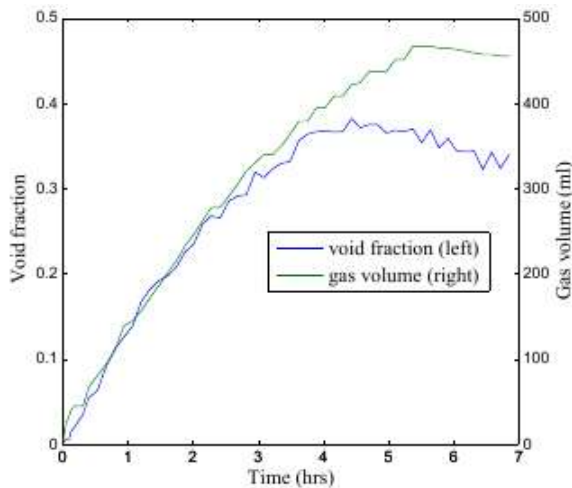


Figure 2: Void fraction profile in 8 Pa Mg(OH)<sub>2</sub> sludge

This methodology was repeated for beds in the concentration range of 28-45 % w/w, corresponding to yield stresses of 4-264 Pa. The yield stress,  $\tau$ , correlation with weight fraction of Mg(OH)<sub>2</sub>,  $\omega$ , is given by equation 2.

$$\tau = 2.84 \times 10^5 \omega^{8.7} \quad \text{Eq 2}$$

The maximum void fraction for each system is shown as a function of yield stress in Figure 3.

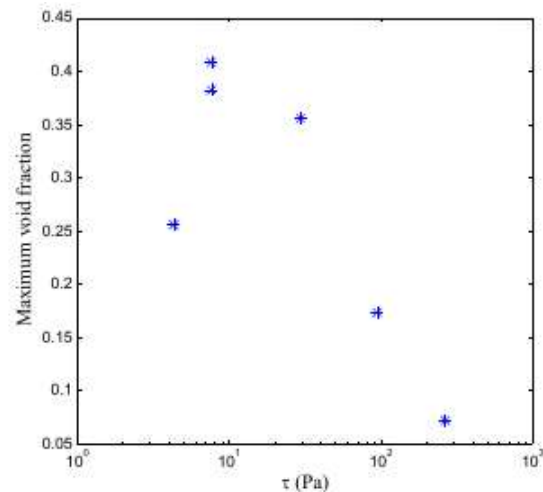


Figure 3: Maximum void fraction as a function of waste yield stress

Figure 3 shows peak void fractions of 0.38 and 0.41 in two beds of 8 Pa yield stress, demonstrating respectable repeatability in the methodology. A lower yield stress bed of 4 Pa lacked the strength to retain very large void fractions greater than 0.25. Above 30 Pa, the capacity of settled beds to retain gas pockets declined markedly. This mirrors the discussion of Van Kessel and Van Kesteren 2002[7], which proposed a continuous gas release mechanism through stable channels in high yield stress beds. However, this phenomenon is conventionally associated with beds of yield stress in the order of kilopascals rather than sludge of 94-264 Pa.

One principal difference between this methodology and those reported in the literature[6,7] is the absence of a supernatant layer of water above the settled bed. At laboratory scale a supernatant layer will not contribute measurably to the hydrostatic load on the bed. However, if the bulk density of the bed falls below that of water, the supernatant could promote buoyant

releases. In addition, a convective layer of water can help to erode channels formed in the bed as gas is released, promoting further continuous gas release by the Van Kessel mechanism. Consequently the addition of a supernatant layer is likely to reduce the bed void fraction, rather than augment it.

### Conclusions and Future Work

Significant gas retention up to 41 % voidage has been observed in laboratory scale gas hold up tests in magnesium hydroxide. Peak gas retention occurred at relatively low strength beds of around 8 Pa yield stress. Such strengths are likely in the young beds formed from the transfer of diluted sludge from the FGMSP to SPP1.

Above 30 Pa, a sharp decline in gas retention can be attributed to the steady release of gas through stable channels, as proposed by Van Kessel and Van Kesteren 2002[7], although magnesium hydroxide sludge appears to promote this release mechanism from a much lower yield stress than previously discussed.

Future work will aim to characterise the mechanisms of gas retention and release at a more fundamental level. The impact of particle wettability on gas retention through 'direct bubble attachment' will be considered. X-ray tomography will be used to visualise trapped voids within the bed and a novel ultrasonic approach will be investigated for the non-invasive identification of void locations using acoustic backscattering.

### Acknowledgements

Many thanks to Sellafield Ltd. for funding this work. In particular we wish to thank Geoff Randall at Sellafield for his contribution to the project.

### References

- [1] G. McCracken and M. Eilbeck. Clean up progress on high hazard facilities at Sellafield: Magnox Swarf Storage Silos. In ANS Topical Meeting on Decommissioning, Decontamination, and Reutilization 2005, pages 161–167, 2005.
- [2] R. Burrows, S. Harris, and N.P.C. Stevens. Corrosion electrochemistry of fuel element materials in pond storage conditions. *Chemical Engineering Research and Design*, 83 (7A): 887–892, 2005.
- [3] C.R. Gregson, D.T. Goddard, M.J. Sarsfield, and R.J. Taylor. Combined electron microscopy and vibrational spectroscopy study of corroded Magnox sludge from a legacy spent nuclear fuel storage pond. *Journal of Nuclear Materials*, 412(1):145–156, 2011.
- [4] Paul D Whitney, Perry A Meyer, and NE Miller. Flammable gas data evaluation. progress report. Technical report, Pacific Northwest Lab., Richland, WA (United States). Funding organisation: USDOE Assistant Secretary for Nuclear Energy, Washington, DC (United States), 1996.
- [5] R.T. Allemann. Physical mechanisms contributing to the episodic gas release from hanford tank 241-sy-101. In *High Level Radioactive Waste Management 92*, Las Vegas, Apr 1992.
- [6] P.A. Gauglitz, W.C. Buchmiller, S.G. Probert, A.T. Owen, and F.J. Brockman. Strong-sludge gas retention and release mechanisms in clay simulants, 2012.
- [7] T. Van Kessel and W. G. M. Van Kesteren. Gas production and transport in artificial sludge depots. *Waste Management*, 22(1):19–28, 2002.

# In-line Rheometry and Flow Characterisation of Dense Slurries in Pipe Flow Using Acoustic Methods

H.P. Rice<sup>\*1</sup>, D. Harbottle<sup>1</sup>, T.N. Hunter<sup>1</sup>, J. Peakall<sup>2</sup> and M. Fairweather<sup>1</sup>

\*Correspondence: h.p.rice@leeds.ac.uk

<sup>1</sup>School of Chemical and Process Engineering (University of Leeds, Leeds LS2 9JT, UK)

<sup>2</sup>School of Earth and Environment (University of Leeds, Leeds LS2 9JT, UK)

## Abstract

The UK's civil nuclear waste inventory is large, diverse and requires processing and disposal but characterisation of nuclear waste slurries during storage, resuspension and hydraulic transport is made difficult by poor accessibility, radioactivity and chemical hazards. The aim of this study is to develop a suite of safe, accurate, versatile and cost-effective acoustic methods for rapid monitoring and characterisation of high-concentration nuclear waste-analogue slurries, based on existing expertise at the University of Leeds. Several proposed methods are outlined – in-line pipe rheometry, time-domain velocimetry and multi-frequency concentration measurement - and initial proof-of-concept results will be presented. A new flow loop laboratory is being commissioned in which these methods will be combined with other, established methods – particle image velocimetry and determination of bed depth and deposition velocity – to investigate horizontal, inclined and vertical flow of suspensions of relevance to nuclear waste decommissioning and disposal.

## Introduction

The sludges, slurries and suspensions that comprise a proportion of the UK's nuclear waste inventory have a wide range of properties – in terms of particle size, density, concentration, chemistry and radioactivity – and so the methods that are used to characterise them must be versatile and simple to deploy. Following on from expertise developed at the University of Leeds, a number of acoustic methods are proposed for use in nuclear waste characterisation and flow measurement, and preliminary results will be presented.

## Methodology Details

### In-line rheometry

The viscosity,  $\eta$ , of a fluid can be measured in tube or pipe flow as a function of radial distance from the centreline,  $r$ , as follows:

$$\eta(r) = \frac{\tau(r)}{\dot{\gamma}(r)}$$

where  $\tau(r)$  and  $\dot{\gamma}(r)$  are the local shear stress and shear rate, respectively, and are defined below:

$$\tau(r) = \frac{\Delta P r}{2L},$$

$$\dot{\gamma}(r) = \frac{dU(r)}{dr},$$

where  $\Delta P$  is the pressure drop over a measurement distance  $L$ , and  $U$  is the local mean axial flow velocity. This method has been shown to give accurate results when compared with conventional off-line viscometry, as shown in Figure 1 [1].

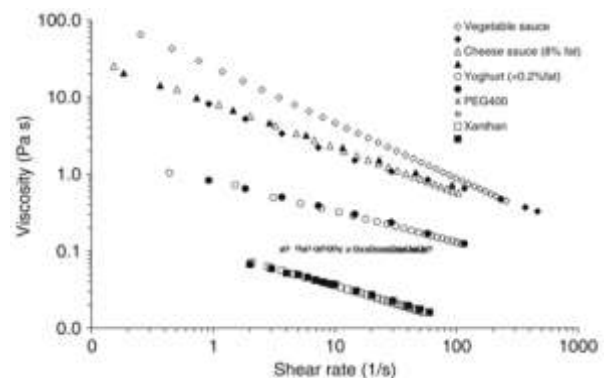


**Figure 1** In-line pipe rheometry for various substances compared to conventional off-line results [1].

This method can be used in situ and non-intrusively, and avoids the need for potentially costly, dangerous off-line measurement of viscosity.

### Time-domain velocimetry

Ultrasonic Doppler velocimetry (UDV) is commonly used for flow rate measurement in a range of industries. However, although less well known, time-domain velocimetry has great potential in nuclear applications as it suffers less from near-wall artefacts

and is computationally very simple to implement. An illustration of the method is shown in Figure 2 [2]. Two parallel transducers (emitter-receivers in the present study) are separated by a known distance; as suspended particles pass by in laminar, unidirectional flow, the time series of the voltage received by each transducer are compared via a cross-correlation algorithm to yield the time delay between them, and therefore the flow velocity, since the spatial separation is known.

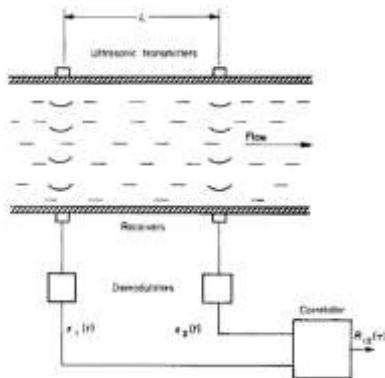


**Figure 2** Diagram of time-domain velocimetry method with separate emitters and receivers [2];  $x_1$  and  $x_2$  are signals from transducers 1 and 2,  $R_{12}$  is correlation function.

### Multi-frequency instrumentation

The acoustic dual-frequency method allows particle concentration profiles to be computed in a flow from the echo signals at two or more frequencies, and an example is shown in Figure 3. The method requires that the acoustic scattering properties of the suspended particles be known, and a method for measuring them for arbitrary particle types was presented recently [3].

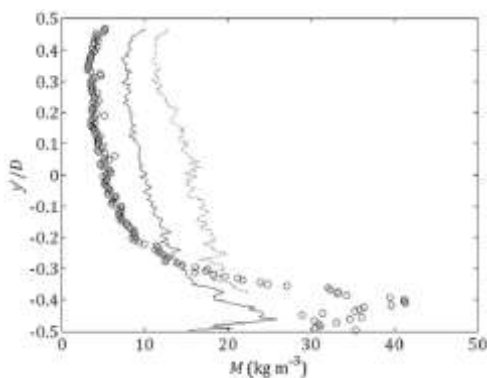


**Figure 3** Example of particle concentration profile in pipe flow [3] computed using acoustic dual-frequency method;  $M$  is concentration,  $y/D$  is normalised distance from pipe centreline. Solid species is glass spheres, mean diameter  $77 \mu\text{m}$ , nominal concentration  $M_w = 24.7 \text{ kg m}^{-3}$ .

The method has potential in nuclear applications as it can be used to visualise the degree of segregation/settling in a flow, and can be combined with bed depth and critical deposition velocity

measurements to identify the flow regime (fully suspended, flow with a bed, plug flow, etc.) in optically opaque flows.

## Results and Discussion

The following results will be presented:

1. Initial in-line pipe rheometry results using the Doppler velocimetry/pressure-drop method from a pipe flow loop (internal diameter  $D = 42.6 \text{ mm}$ ) will be presented. Water, glycerol-water and xanthan-water suspensions mixtures were chosen as the test fluids because (a) water and glycerol-water are Newtonian and have viscosities that can be predicted accurately, for validation; (b) xanthan-water exhibits more complex, non-Newtonian behaviour and so allows testing of the effectiveness of various models to fit the measured velocity profiles. Results will be compared to conventional, off-line viscometry measurements.

2. In order to test the time-domain velocimetry method, measurements of particle velocity were taken in an unmixed column of water with two parallel transducers. Non-spherical plastic particles, which were known to scatter strongly, were allowed to settle vertically under gravity. This configuration was chosen as the settling velocity can be accurately predicted and therefore compared directly to measured values.

3. A new acoustic instrument, capable of receiving data over 16 channels simultaneously, each over a range of frequencies, has been designed and commissioned at the University of Leeds. The acoustic properties of spherical glass particles of known physical and acoustic properties were measured in a custom-built mixing vessel over a range of insonication frequencies. For validation of the instrument, the results were then compared against values measured previously using a commercial instrument [1].

4. In addition, details and images of the new flow loop laboratory will be presented.

## Conclusions and Future Work

Once completed, the new flow loop laboratory will allow for thorough characterisation of suspensions and slurries with arbitrary concentrations and physical properties with the acoustic methods discussed above, in horizontal, vertical and inclined configurations over a range of flow diameters. In addition, a variety of other acoustic methods will be available, all of which have been used extensively at the University of Leeds – dual-frequency concentration measurement and determination of bed depth and critical deposition velocity – in addition to laser-based particle image velocimetry (PIV) and pumped sampling for validation.

## Acknowledgements

The authors thank David Cowell, Gareth Keevil and Robert Thomas for their advice and technical assistance.

## References

[1] Wiklund J (2007), Chem. Eng. Sci. 62 (16) 4277-4293.

[2] Jacobson SA, Denbigh PN and Naudé DEH (1985), Ultrasonics 23 (3) 128-132.

[3] Rice HP, Fairweather M, Hunter TN, Mahmoud B, Biggs SR and Peakall J (2014), J. Acoust. Soc. Am. 136 (1) 156-169.

# Quartz Crystal Microbalance as a Method to Characterise Sludge Rheology

J.A. Botha\*<sup>1</sup>, T.N. Hunter<sup>1</sup>, S. Biggs<sup>1,2</sup>, G.A. Mackay<sup>3</sup>, R. Cowley<sup>5</sup>, S.E. Woodbury<sup>4</sup>, and D.Harbottle<sup>1</sup>

\*Correspondence: pm10jab@leeds.ac.uk

<sup>1</sup>*School of Chemical and Process Engineering, University of Leeds, UK*

<sup>2</sup>*The University of Queensland, Brisbane, Qld 4072, Australia*

<sup>3</sup>*NNL Workington Laboratory, Cumbria, UK*

<sup>4</sup>*NNL Central Laboratory, Sellafield, Cumbria, UK*

<sup>5</sup>*Sellafield Analytical Services, Cumbria, UK*

## Abstract

A new method to measure the yield stress of concentrated particle suspensions has been investigated. Quartz crystal microbalance (QCM) is a high frequency (5MHz) resonator which undergoes a frequency and resistance shift when submerged in a fluid or particle suspension. The sample used throughout the study was magnesium hydroxide (Versamag A + B) prepared at different particle concentrations and aged for increasing length of time. The yield stress of the Versamag A suspensions was measured using rotational viscometry and shown to be an exponential function of the particle concentration, ranging from ~ 0 Pa at 30 wt% up to ~ 580 Pa at 50 wt%. The air-to-sample frequency shift of the QCM sensor was shown to increase from – 950 Hz at 30 wt% to – 570 Hz at 50 wt%. At the same time the sensor resistance changed from 340 Ohm to 650 Ohm as the particle concentration of the suspension was increased. While the general trend in sensor frequency response is linear, the resistance response appears more sensitive, demonstrating an exponential change with increasing particle concentration.

The second series of experiments considered the yield stress aging of two Versamag samples with different MgO contents; Versamag A = 2.7 vol% and Versamag B = 0.4 vol%. The higher content of MgO in Versamag A provided a catalyst to age and increase the sample yield stress over time. Measured using a rotational viscometer the yield stress for 30 wt% slurry increased from ~ 0 Pa to ~ 70 Pa over 1 day. While a higher particle concentration slurry (40 wt%) increased from ~60 Pa to 610 Pa over the same length of time. For equivalent concentrations of Versamag B the yield stress did not increase over the 1 day aging. Equivalent data collected using the QCM showed that the frequency increased by 401 Hz and 130 Hz for Versamag A and B, respectively. For the same samples the resistance was measured to increase 525 Ohm (Versamag A) and 127 Ohm (Versamag B).

In all experiments the sensitivity of the QCM to measure changes in suspension rheology has been demonstrated. The potential for QCM to be used as a dip-probe rheometer for application in the nuclear industry is part of this ongoing research.

# Enhanced Shear Microfiltration

K. Schou\*, M.D. Dragosavac, R.G. Holdich<sup>1</sup>

\*Correspondence: K.Schou@Lboro.ac.uk

<sup>1</sup>Affiliation (Loughborough University, Epinal Way, Loughborough LE11 3TU, United Kingdom, UK)

## Abstract

This project investigates the application of enhancing the microfiltration and ultrafiltration flux rate through directed membrane surface shear. This is achieved by oscillating the filters either vertically or azimuthally, or by oscillating the fluid. Preliminary results indicate that a large increase in flux is indeed possible by increasing shear, however this increase in flux may come at a cost of loss of particle retention. This project is in its early stages as such this document will look at what will be investigated rather than results and conclusions.

## Introduction

Microfiltration is used in many industries, including in the treatment of nuclear effluent. Currently crossflow filters are employed to filter suspensions. In order to receive reasonable flux across the membrane the crossflow filtration requires constant recirculation of the suspension. By replacing the recirculating pump with directed shear at the membrane surface it may be possible to reduce energy usage and increase flux [1][2][3][4].

The application of shear enhancement on filtration has been reported to increase flux as high as 18x the pseudo steady state filtration amount [2]. A significant amount of research has already been done in this field, [5][6]. There are industrially available units (V-SEP)[6][7], but there is scope for further work.

This enhancement in pseudo steady state flux can be very large, prompting interest in the usage of shear enhanced filtration. In the papers currently reviewed though there is no mention of the cost to particle retention and little analysis of energy usage.

The purpose of this project is to determine the specific mechanism behind the flux increase, to study the controlled shear at the surface of a filtering membrane and obtain a theoretical understanding of a compact, but efficient, filtering system.

A range of polymer and non-polymer filters will be tested, starting with the slotted pore membrane.

The goal is to replace the current crossflow filtration methods, which require constant recycling of the suspension in order to obtain reasonable fluxes, with a more efficient filtration method.

## Key research questions

The following are the main questions which this project aims to answer.

- Is it the effect of localised shear which creates the increase in flux? If so, then is the method by which the shear is applied irrelevant?
- What are the specific advantages of oscillating, or pulsed flow?
- What are the key parameters for optimisation (e.g. flux, power efficiency, particle retention)?
- How can the filters be scaled up (i.e. sized)?
- How do filter coatings effect filtration?
- What are the potential problems of using this technology?
- What is the effect of frequency and amplitude on flux (apart from shear)?
- How easy would a filter be to clean?
- Does the localised shear damage the suspension, creating a more difficult to filter suspension?

## Methodology

### Initial Setup

A simple filtration setup (Fig 1) was tested. For the initial work, this was a filter (5 µm, slotted membrane, supplied by Micropore Technologies Ltd), which had been submerged into a beaker filled with the suspension (1% w/w calcium carbonate). The filter had a negative pressure applied, through a peristaltic pump (RS 440-515). The trans-membrane pressure (TMP) was read off a gauge (-1 barg to 0 barg), and the flowrate was calculated by reading the increase in weight measured on a balance (Ohaus TP4KD) of fluid out.

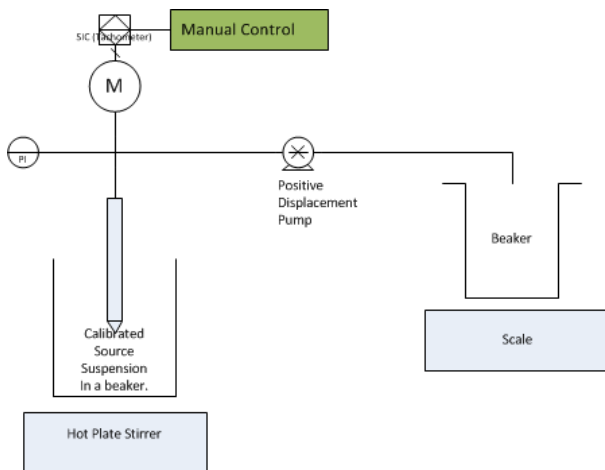


Figure 1 Simple experimental setup

The motor was controlled via a variable power supply. Attached to the motor is one of 2 gear boxes. One provides vertical oscillation, the other azimuthal.

From this simple setup a major consideration which is not discussed in the literature was found. The filtration flux indeed did increase, but so did the turbidity of the filtrate. Hence increasing shear at the surface of the membranes disrupted the 'secondary' membrane and particle retention capacity diminished.

### Enhanced Setup

The experimental setup was improved to give greater accuracy of readings, and to include light absorbance, flowrate, pressure, acceleration, see Fig 2.

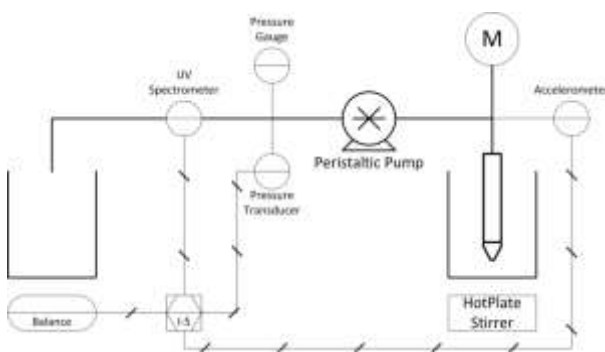


Figure 2 More thorough experimental setup

Using this system it becomes possible to monitor the light absorbance as well as the specific shear being applied and gives much more accurate control of the motor speed.

The particle size distribution and concentration are determined with a couple of pieces of analytical equipment:

The NANOSIGHT is an optical method of determining particle size distribution and concentration. It records a video of laser tracked particles, and knowing the temperature, the Brownian motion provides particle size data. A Horiba particle size distribution analyser was also used to determine the particle size distribution of the filtrate. These two techniques are able to give a good indication of both the effect of the increased shear on the filtrate efficiency and which particles sizes are most affected.

This simple but effective system allows for a significant amount of variance in testing towards the first goal of determining if identical shear, applied in different ways to the membrane surface shows a change in the flux.

### The membrane

The membrane now being used is a slotted pore filter with slots 7-8 microns wide. The slots help to prevent blockage while still retaining filtration capability [8][9]

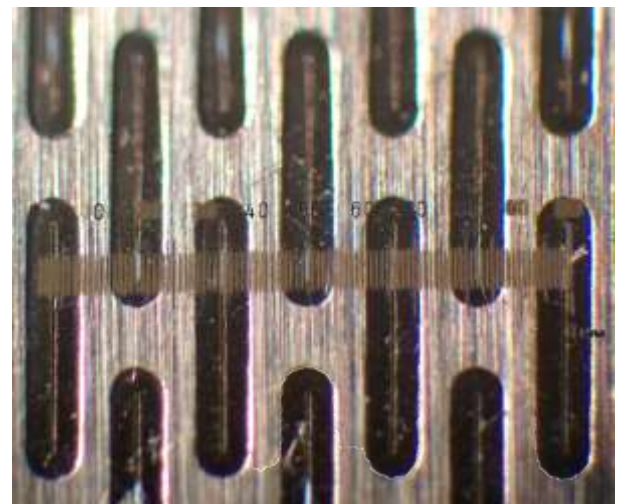


Figure 3 The membrane under microscope.

The main advantage to using these filters with nuclear waste is their inherent ease of cleaning. Depth filters trap particles within their structure, becoming waste themselves. Ideally if slotted pore filters can be used they may become self-cleaning.

Calcium carbonate was used a suspension medium due to its fine particle size range, safety, availability & ease of cleaning.

## Results and Discussion

There are currently limited results from the available project time. This is due to the short period of time between the start of the project and presentation of this report, three months.

The preliminary results show that a dead end vertically oscillating filter will have increased flux in comparison to a dead end non-oscillating filter (Figures 4 & 5), in regions similar to that of a system with no particles at all, however the filtrate was not clear, and would contain particles which were intended to be filtered out.

In addition to the increased flux, the TMP dropped significantly for the oscillating system. This is believed to be due to the breakdown of the filter cake, and hence the filter particle retention.

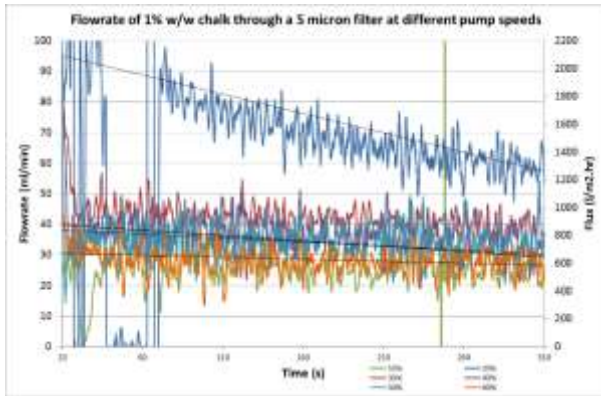


**Figure 4** Flux rates without enhanced shear over a range of pump speeds

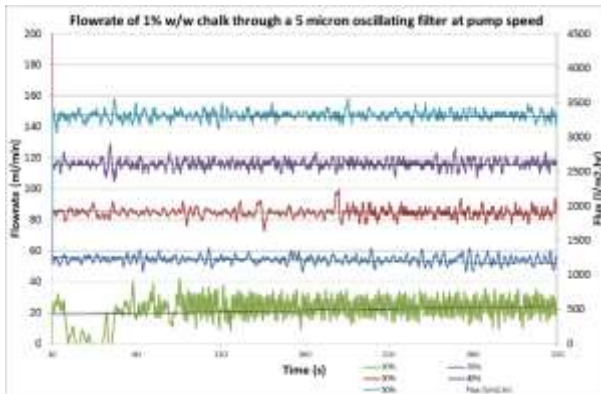


**Figure 5** Flux rates with enhanced shear over a range of pump speeds

Both vertical and azimuthal oscillation have been tested and showed different results. This is not an unambiguous comparison, however, as the motor that was used in the azimuthal system was significantly more powerful than the vertically oscillated system. However this does allow a glimpse at the extremes of shear.

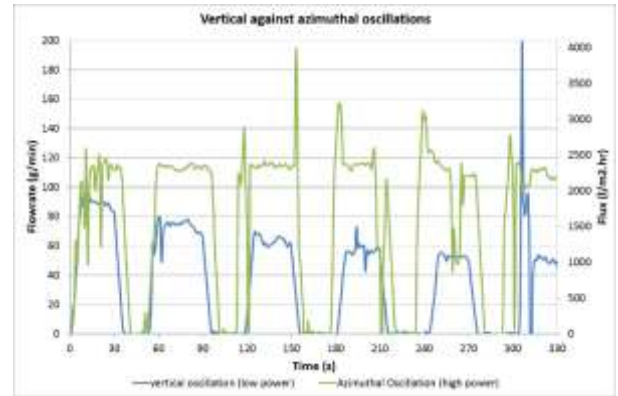


**Figure 6** A comparison between azimuthal oscillation at high shear and vertical oscillation at low shear

In the graph above, the apparent drops to zero flow are when samples were drawn off, therefore the balance saw no difference in mass. The trends of the tops of the graphs should be used as a guide.

These extremes of shear can be seen in the filter cake on the filter post filtration



**Figure 7** Filter cake formed with no shear (left), low shear (middle) and high shear (right)

With the filters shown in Fig 7, the short term filtration with no oscillation (left), low power vertical oscillation (middle) and high power azimuthal oscillation (right) show how the filter cake differs with the added shear. It is difficult to see from these images, however the cake on the low power vertical oscillation is smaller than the cake with no oscillation.

With the improved system, the UV spectrometer shows a significant step change in absorbance and hence particles between the oscillated and non-oscillated system.

## Conclusions and Future Work

At this time limited data has been collected, however the patterns already seen are that significant flux increases are indeed possible with oscillation (Figures 4 & 5).

Currently the large shear generated at the surface of the membranes causes a breakdown in filter cake (Figure 7) which while expected, can work against the filtration as the filter cake is a significant filtration media itself (i.e. secondary membrane).

A more thorough investigation into the effect of shear by oscillation type and magnitude on flux and particle retention will be investigated.

Further testing into how shear enhanced filtration is affected by using different filters, filter aids or surface coatings will also be investigated.

It may be beneficial to investigate the control rather than breakup the filter cake with shear, for both flux increase and particle retention.

The current testing has been done with calcium carbonate. More relevant alternatives, such as testing with ferric floc and magnesium hydroxide, will be used to determine how the theory relates to more appropriate materials.

How the enhanced shear at the membrane surface effects floccs and other shear sensitive materials also will be investigated. This will entail a careful analysis, and modelling, of the fluid flow near to the oscillating membrane surface.

## Acknowledgements

The authors would like to thank the project sponsor Sellafield Ltd through the DISTINCTIVE consortium and Loughborough University for making this project possible.

## References

- [1] M. Y. Jaffrin, "Dynamic shear-enhanced membrane filtration: A review of rotating disks, rotating membranes and vibrating systems," *J. Memb. Sci.*, vol. 324, no. 1–2, pp. 7–25, Oct. 2008.
- [2] F. Zamani, J. W. Chew, E. Akhondi, W. B. Krantz, and A. G. Fane, "Unsteady-state shear strategies to enhance mass-transfer for the implementation of ultrapermeable membranes in reverse osmosis: A review," *Desalination*, vol. 356, pp. 328–348, Jan. 2015.
- [3] H. G. Goma, S. Rao, and a. M. Al-Taweel, "Intensification of membrane microfiltration using oscillatory motion," *Sep. Purif. Technol.*, vol. 78, no. 3, pp. 336–344, Apr. 2011.
- [4] T. Li, A. W.-K. Law, M. Cetin, and a. G. Fane, "Fouling control of submerged hollow fibre membranes by vibrations," *J. Memb. Sci.*, vol. 427, pp. 230–239, Jan. 2013.
- [5] S. C. Low, H. H. Juan, and L. K. Siong, "A combined VSEP and membrane bioreactor system," *Desalination*, vol. 183, no. 1–3, pp. 353–362, Nov. 2005.
- [6] M. D. Petala and A. I. Zouboulis, "Vibratory shear enhanced processing membrane filtration applied for the removal of natural organic matter from surface waters," vol. 269, pp. 1–14, 2006.
- [7] M. Y. Jaffrin, L.-H. Ding, O. Akoum, and A. Brou, "A hydrodynamic comparison between rotating disk and vibratory dynamic filtration systems," *J. Memb. Sci.*, vol. 242, no. 1–2, pp. 155–167, Oct. 2004.
- [8] R. Holdich, S. Kosvintsev, I. Cumming, and S. Zhdanov, "Pore design and engineering for filters and membranes," *Philos. Trans. A. Math. Phys. Eng. Sci.*, vol. 364, no. 1838, pp. 161–74, Jan. 2006.
- [9] A. Bromley, "Slotted and circular pore surface microfiltration," Loughborough University, 2002.

# Modified Silica Nanoparticles for Metal Sequestration

L. J. Mayne\*<sup>1</sup>, S. Christie<sup>1</sup>, and M. Platt<sup>1</sup>

\*Correspondence: L.Mayne@lboro.ac.uk

<sup>1</sup>Department of Chemistry (Loughborough University, Loughborough, Leicestershire, LE11 3TU, England)

## Abstract

Tunable resistive pulse sensing allows the characterisation of silica nanoparticles for their size, charge and concentration. Silica nanoparticles are used as a support for (3-aminopropyl)triethoxysilane which will be used to extract metal ions from solution. The APTES- functionalised silica was used to extract copper from solution which was confirmed using ICP-OES.

## Introduction

Radioactive wastes are an inevitable part of the production of nuclear energy. Treatment of the waste effluents is an essential task in cleaning up the legacy nuclear sites due to the radionuclides polluting the environment which pose chemical and radiological toxicity threats to living organisms.<sup>1</sup> Heavy metals such as mercury and lead, belong to a group of toxic elements and many are a danger to human health even at low concentrations.<sup>2</sup> There are many techniques for removing metal contaminants from aqueous solutions; including chemical precipitation, ion and solvent exchange and adsorption. Superparamagnetic nanoparticles offer new opportunities for waste treatments. They offer a large surface area, high adsorption capacity and fast adsorption rate. Silica can be used to support ligands for surface modification of the particles, due to its stability. The superparamagnetic properties of the particles allow for easy separation from the bulk liquid as they are attracted to a magnetic field.

Tunable resistive pulse sensing (TRPS) is a sensing technique which is a useful tool in characterising nanoparticles. TRPS allows the size and concentration of a sample to be analysed simultaneously. TRPS benefits from the ability to tune the pore in real time to suit the analyte size which helps the characterisation of surface modified particles.<sup>3</sup> As well as size and concentration analysis, TRPS can also perform charge analysis of nanoparticles.<sup>4</sup> Zeta potential is the measurement of electrostatic interactions between charged particles.<sup>5</sup> Studying the zeta potential of nanoparticles allows the user to track changes on the surface on the nanoparticle.

TRPS has previously been used for the detection of biological analytes<sup>6</sup> however it has a large scope for

potential analytes. Here we extract copper from solution and will use TRPS to characterise silica nanoparticles.

## Tunable Resistive Pulse Sensing

### Theory

The resistive pulse sensor consists of two fluid cells with are separated by a pore membrane. The membranes are penetrated with a needle to create a conical pore.<sup>7</sup> The fluid cells are filled with a conducting electrolyte solution which when a voltage is applied a baseline current is obtained. A sample is added to the upper fluid cell, positioned above the pore, and when a particle traverses the pore a blockade event is observed. The blockade is created by the particle displacing a volume of electrolyte solution which increases the resistance in the circuit. This change in resistance temporarily lowers the current. The magnitude of the blockade is directly related to the particle size allowing size analysis. The frequency of the blockades,  $J$ , can be related to the sample concentration,  $C_s$ , as well as the particle velocity,  $v_p$ . The velocity term is the sum of the fluidic,  $v_f$ , electrophoretic,  $v_E$ , and electroosmotic,  $v_o$ , velocities. The contributions from diffusion are ignored due to the magnitude of other forces and end effects are not taken into account for the analysis.<sup>4</sup>  $v_p$ , can be written as;

$$v_p = \frac{Q}{\pi \left(\frac{D_S}{2}\right)^2} + \frac{\epsilon \zeta_{particle}}{\eta} E - \frac{\epsilon \zeta_{pore}}{\eta} E \quad (1)$$

Where

$$Q = \frac{3\pi D_S^3 \Delta P}{128\eta \left(\frac{L}{D_L - D_S}\right)} \quad (1a)$$

$\epsilon$  and  $\eta$  are the permittivity of the solution and kinematic viscosity respectively,  $\Delta P$  is the pressure

across the pore,  $\zeta_{\text{pore}}$  and  $\zeta_{\text{particle}}$  are the zeta potential of the channel surface and of the particle. The pulse frequency,  $J$ , is then related to both the velocity and sample concentration,  $C_s$ , via the equation;  $J = C_s \times v_p$ .

From the equation the velocity of a particle is related to its zeta potential. Zeta potential is a measure of the electrostatic interactions between charged surfaces and is defined as the potential between the stern layer and the diffuse layer.<sup>5</sup> The electrical potential at the solid surface of a particle cannot be directly measured, zeta potential is an adequate substitute.<sup>5</sup> The Smoluchowski approach defines zeta potential in equation (2), where  $\zeta$  is zeta potential,  $\eta$  is dynamic viscosity of the fluid,  $\mu$  is particle mobility and  $\epsilon$  is the dielectric current.

$$\zeta = \frac{\eta\mu}{\epsilon} \quad (2)$$

The particles zeta potential can be determined from its velocity taking into account the convective and electroosmotic forces and the electrophoretic mobility of the particle. Methods have been developed to determine the zeta potential of nanoparticles using TRPS.<sup>4,8</sup> By studying the zeta potential we can track changes on the nanoparticles surface. In this work we modify silica nanoparticles with APTES which will be used for metal sequestration.

## Methodology Details

### Silica Modification

Silica nanoparticles were modified with (3-aminopropyl)triethoxysilane (APTES).

### Copper Extraction

A 10ppm solution of Copper was prepared in deionised water from  $\text{CuCl}_2 \cdot 2\text{H}_2\text{O}$ . To this solution APTES-functionalised silica was added. This was repeated three times and each was left to incubate for 24 hours. After 24 hours a sample was filtered off and run on inductively coupled plasma - optical emission spectroscopy (ICP-OES).

## Results and Discussion

### Copper Extraction

Our initial studies focussed on the removal of copper, following, work done previously at Loughborough University. The copper solutions were incubated for 24 hours with the modified silica. The silica turned blue which was an indication that the copper was bound to the silica material. The results from the ICP-OES show a decrease in the concentration from the original concentration.

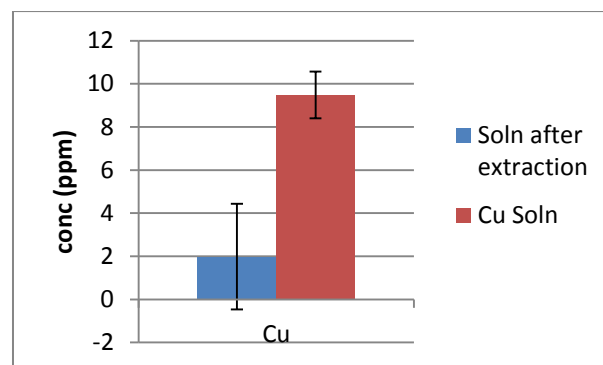


**Figure 1** A graph to show the concentration change in the copper solution following the addition of APTES- functionalised silica. The blue column shows the concentration of copper remaining in solution after a 24 hour incubation. The red column shows the initial concentration of the copper solution.

Figure 1 shows the change in concentration after the incubation period. The APTES-functionalised silica will have copper bound to it and can be analysed using TRPS.

## Conclusions and Future Work

We have demonstrated that nanoparticles modified with a ligand can extract copper from solution. TRPS will be used to characterise the nanoparticles before modification, after modification and when the copper is bound to the materials. By determining the zeta potential of the particles, changes on the surface can be tracked and used to determine that the metal has successfully been extracted.

## References

- Chen, Y. & Wang, J. Removal of radionuclide  $\text{Sr}^{2+}$  ions from aqueous solution using synthesized magnetic chitosan beads. *Nucl. Eng. Des.* **242**, 445–451 (2012).
- Radi, S., Toubi, Y., Bacquet, M., Degoutin, S. & Cazier, F. 1-(Pyridin-2-yl) Imine Functionalized Silica Gel: Synthesis, Characterization, and Preliminary Use in Metal Ion Extraction. *Sep. Sci. Technol.* **48**, 1349–1355 (2013).
- Roberts, G. S. *et al.* Tunable nano/micropores for particle detection and discrimination: scanning ion occlusion spectroscopy. *Small* **6**, 2653–8 (2010).
- Vogel, R., Anderson, W., Eldridge, J., Glossop, B. & Willmott, G. A variable pressure method for characterizing nanoparticle surface charge using pore sensors. *Anal. Chem.* **84**, 3125–31 (2012).
- Salg, S., Salgi, U. & Soyer, N. Streaming Potential Measurements of Polyethersulfone Ultrafiltration Membranes to Determine Salt Effects on Membrane Zeta Potential. **8**, 4073–4084 (2013).
- Blundell, E. L. C. J., Mayne, L. J., Billinge, E. R. & Platt, M. Emergence of tunable resistive pulse sensing as a biosensor. *Anal. Methods* **00**, 1–12 (2015).
- Sowbery, S. J., Broom, M. F. & Petersen, G. B. Dynamically resizable nanometre-scale apertures for molecular sensing. *Sensors Actuators B Chem.* **123**, 325–330 (2007).
- Somerville, J. a, Willmott, G. R., Eldridge, J., Griffiths, M. & McGrath, K. M. Size and charge characterisation of a submicrometre oil-in-water emulsion using resistive pulse sensing with tunable pores. *J. Colloid Interface Sci.* **394**, 243–51 (2013).

# Irradiated Sludges

M. O'Leary<sup>\*1</sup>, C. Johnston<sup>2</sup>, G. Tribello<sup>2</sup>, J. Kohanoff<sup>2</sup>, F. Currell<sup>1</sup>

\*Correspondence: moleary05@qub.ac.uk

<sup>1</sup> Centre for Plasma Physics (Queen's University Belfast, University Road, Belfast, BT9 1NN, UK)

<sup>2</sup> Atomistic Simulation Centre (Queen's University Belfast, University Road, Belfast, BT9 1NN, UK)

## Abstract

This project aims to identify production mechanisms of important radiolytic products, especially gaseous products for example molecular hydrogen gas, from Magnox sludges at Sellafield sites. We will use the Q14 irradiation platform, in Queen's University Belfast, to irradiate sludge mimics, and then take measurements of the type and amount of different end products, like hydrogen gas, produced by irradiation. These results will then be compared to the predictions of simulations made by the Atomistic Simulation Centre, also at Queen's University Belfast.

## Introduction

Sellafield site has one of the largest inventories of nuclear legacy waste in Europe. Sludge makes up a large amount of this waste, the Magnox Sludges are the most common form of sludge. Magnox sludge is the corroded nuclear fuel rod cladding from the early Magnox nuclear reactor; the cladding is made from alloy Magnox AL80[1], which is made mostly magnesium. Most of the sludge is in the Magnox Swarf Storage Silos. During the 1974 miner's strike, the Magnox Power plants, importantly Calder Hall located on the Sellafield site, had more fuel cycled, to make up for power lost from the coal burning plants. The buffer ponds at Calder Hall, where the fuel rods were stored before being moved for reprocessing, were overwhelmed by the increase in the amount of fuel used in such a short amount of time. The legacy of this is in the First Generation Storage Pond (seen in figure 1), the sludge in these ponds will soon be moved to the Sellafield Sludge Packaging Plant (SPP1, in Figure 2)[1]. The major safety issue in these sludges is the build up and retention of gases. Two main ways to produce gas are through radiolytic production of gases and through the corrosion of the fuel rod cladding. This project will investigate the ways that irradiating sludges affects gas produced in them.

In order to investigate the gases produced by the effects of irradiation on sludges: we will irradiate sludge mimics, and measure the quantity and types of gases produced. The irradiations will be done using Q14, a new irradiation platform at Queen's University Belfast (Figure 3). At the heart of Q14 is a mechatronic irradiation control apparatus, called MJOLNIR-2 that builds on the previously developed MJOLNIR; which was developed to be used as an end station for hanging drip irradiation experiments at the Diamond Light Source[2]. MJOLNIR-2 includes an integrated

broad band x-ray source, with the capability to do vertical and horizontal irradiations of samples. Primary application of Q14 will be in the domain of nano-medicine, irradiating various nano-particle solutions.



Figure 1 First Generation Storage Pond



Figure 2 SPP1, Under Construction

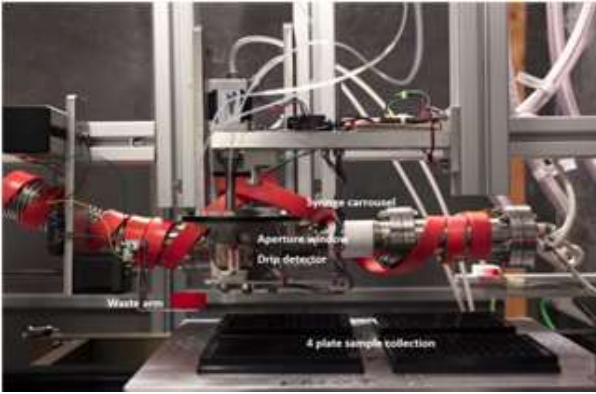


Figure 3 Inside Q14 (MJOLNIR-2)

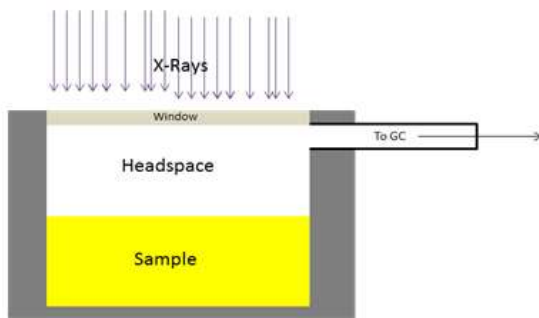


Figure 4 Sample Container Schematic Diagram

Element	Min (% w/w)	Max (% w/w)
Aluminium	0.7	0.9
Beryllium	0.002	0.03
Cadmium	-	0.0002
Calcium	-	0.008
Cerium(1)	-	0.02
Copper	-	0.01
Iron	-	0.006
Lead	-	0.005
Magnesium	base	base
Manganese	-	0.015
Neodymium(1)	-	0.02
Nickel	-	0.005
Silicon	-	0.01
Silver(1)	-	0.01
Thorium(1)+Uranium(1)	-	0.0001
Zinc	-	0.01
Zirconium	-	0.025

Table 1 Composition of Magnox AL80

### Methodology Details

The basic methodology, employed in this project, is to: irradiate sludge mimics; then after irradiation to measure the amount of a particular end product produced by irradiating the sample; then these results are compared to the predictions made by simulations, to validate physical reliability of the simulations or to investigate possible radiation induced mechanisms in the sludge.

Initial irradiation will be done on the newly developed Q14 irradiation platform. Q14 consists of MJOLNIR-2, its lead housing and a control station. MJOLNIR-2 has an inbuilt radiation source, an x-ray tube. The x-rays are produced by accelerating electrons at a truncated cylindrical piece copper, onto which pieces of other materials can be placed to produce different x-ray energy spectra. Below and to the side of the target there are beryllium windows, through which the x-rays are emitted.

The samples will be held in a sample container made out of stainless steel. The sample container will be a cylindrical chamber milled out of stainless steel. The top of the container will have a thin metal foil window through which will be x-ray-transparent, but also keep the container air tight. The side of the sample container will have gas fittings that allow for the removal and sampling of the headspace.

Before the irradiation of sludge mimics can begin the apparatus has to be calibrated, so that the results obtained can be properly interpreted. The aim will be to use chemicals that have well known G values, the amount of a particular end product produced by irradiation for an amount of energy absorbed by the medium. G value for molecular hydrogen from gamma irradiation is well known for water, across the full range of pH [3]. Sludge mimics that will be used will start out as a mixture of water with Magnesium Hydroxide at the pH of the ponds; then materials of increasing similarity to the sludge in the ponds will be added.

The measurement of the end products will involve the use of a variety of methods tailored for each specific end product. For gaseous end products use the gas chromatograph to measure the amount produced. With a thermal conductivity detector (TCD) the concentrations of the different chemicals in a gaseous sample can be measured. By sampling the headspace of the sample container, and then desiccating the headspace sample and then sending the headspace sample through the Gas Chromatograph, the amounts of different gaseous end products can be measured. The Hydrogen gas given off during irradiation can be directly measured by this method; and any gaseous products trapped in the sample can be measured by agitating the sample after taking a headspace sample and then repeating the above method.

For aqueous end products we will use a variety of colorimetric assays in solution. Trapping assays are particularly useful in that they remove the particular end product from solution while also producing a noticeable change, acting as a scavenger and an assay.

When, using methods outlined above, the amount of an end product produced is measured; then to get a

G-value for the end product one has to know how much energy was absorbed by the sample. Measuring the dose (energy absorbed per unit mass), dosimetry, is important to calculate how much energy was absorbed in the sample. For water many methods of dosimetry have been developed like the Fricke dosimeter, a chemical dosimeter that measures the production of Fe (III) from Fe (II) by irradiation<sup>[3]</sup>. But it will probable that other methods of dosimetry may have to be developed for sludge mimics, for example applying correction factors to the dose to water derived from Monte Carlo radiation Transport simulations.

### Discussion and Future Work

Comparison of the results to the predictions of the simulations will help to calibrate those simulations. The mechanisms can be further investigation using scavengers to remove certain intermediary species from solution; thus cutting off certain pathways that were predicted produce a particular end product, then by comparing the yield of that end product with and without the scavenger it will be possible to establish potential pathways for gas production, here using trapping assays will be useful because the amount of the intermediary species produced can also be measured.

Since Q14 was not designed to host experiments with long irradiations that may be necessary later in the project, and may not be capable of the high dose rates that will be needed to get a suitable stimulant of the sludge environment. Then for these longer irradiations and higher dose rates, we are considering the development of a new dedicated radiation source, for this project, will probably be necessary. A design that uses an x-ray source that can perform irradiations in from many angles on a sample is being considered, currently.

### Conclusions

This document outlines the proposed shape of this project over the next few years. The project will mainly look into the possible mechanisms for the production of gaseous end products from the irradiation of sludges, in particular the Magnox sludges. This will be done through the measurement of yields of a variety of end products produced in sludge mimics when they are irradiated; then comparing these results to the predictions of simulations.

### Acknowledgements

Thanks to the Mechanical workshop for their help in the construction of our experimental apparatus. Also thanks to Martyn Barnes, of Sellafield Ltd, our industrial supervisor. Thanks to Hannah Watson for the photo of Q14.

### References

- [1] <http://www.sellafieldsites.com>
- [2] C Polin et al. Rev. Sci. Instrum. **86** 035106 (2015)
- [3] JWT Spinks, RW Woods, *An Introduction to Radiation Chemistry*, John Wiley and Sons, New York, 1990

# Determination of Hydrogen Production from Legacy Fuel Storage Pond Sludges through Molecular Modelling

Conrad Johnston<sup>\*1</sup>, Gareth Tribello<sup>1</sup>, Jorge Kohanoff<sup>1</sup>, and Martyn Barnes<sup>2</sup>

\*Correspondence: cjohnston859@qub.ac.uk

<sup>1</sup>Atomistic Simulation Centre, Queen's University Belfast, Belfast, BT7 1NN, UK

<sup>2</sup>Sellafield Ltd, Birchwood Park Avenue, Warrington Cheshire WA3 6GR, UK

## Abstract

The First Generation Magnox Storage Pond (FGMSP) represents one of the highest priority targets for risk reduction at the Sellafield Site. This legacy pond has accumulated a deep layer of sludge over many years, formed primarily from corroding Magnox alloy, but also from windblown debris and decaying organic matter. This sludge is of complex and uncertain composition. Additionally it contains dissolved fission products where cladding has failed and split, or even fragments of spent fuel where cladding has corroded entirely. The production of methane and hydrogen gas complicates the future handling and storage of this sludge. The focus of the modelling project will be on the radiolytic route to hydrogen production through the study of a water-brucite-hydrocarbon system. By studying a simple model system we will develop an understanding of the underlying chemical reactions. Simulations will be carried out using both classical and quantum mechanical molecular dynamics

## Introduction

The sludges found in the First Generation Magnox Storage Pond are essentially the mineral brucite ( $\text{Mg}(\text{OH})_2$ ), formed as a corrosion product by reaction of the magnesium in the Magnox alloy with water over many years. The sludge also includes a complex cocktail of contaminants in the form of dissolved fission products and fragments of spent fuel from fuel elements where corrosion has led to cladding failure. Hydrogen gas is formed by the reaction of water with magnesium, by radiolysis of water, and speculatively by a thermal or a catalytic route. Reliable estimates for hydrogen generation are required to underpin the safety case and design for a future sludge processing plant. Presently, most of the hydrogen produced in the FGMSP can be attributed to the reaction of the magnesium-based Magnox alloy with water, with the radiolysis of water suspected to be a minor secondary route arising due to the high radiation flux from fission products dispersed throughout the sludge. Screening of the sludge as it is transferred to Sludge Packing Plant 1 will remove large solids, effectively removing the corrosion route for hydrogen production and leaving only the radiolysis route, and a postulated catalytic route.

This research will attempt to give quantitative estimates for hydrogen production through the use of multi-scale atomistic modelling. Colleagues will also be irradiating corroded Magnox sludge samples using the in-house x-ray platform.

## Methodology Details

The basis of the modelling project will be the study of a water-brucite-hydrocarbon system. By studying a simple model system we will develop an understanding of the underlying chemical reactions. Simulations will be carried out using both classical and quantum mechanical molecular dynamics using the CP2K package. In the beginning, a brucite bulk system will be modelled. Later, we will increase the complexity by including actinide species to better represent Magnox sludge. Initial work is being undertaken to select components required for the *ab initio* method that will be employed, such as different Density Functional Theory (DFT) functionals and basis sets, and to establish their suitability for the problem. The impacts of other factors affecting accuracy are being benchmarked also, such as cell size and real-space grid scaling. Following this testing, a geometry optimisation, followed by a molecular dynamics run at a representative temperature, will be carried out to relax the target brucite system. Next, replicating the method of Smyth and Kohanoff<sup>[1]</sup>, the effect of incident irradiation will be established by vertically attaching an electron to the system and observing where it localises. The free energy barrier to OH group cleavage will then be calculated. This additional electron is representative of the low energy electrons that occur in material following a radiation event. Later work will examine the effect of the interaction of water with the surface of the brucite, again looking at electron localisation and

free energy barriers to bond breaking. The effect of the surface on hydroxyl radical formation and stability is suspected to be important and so later studies will introduce these radicals with their conjugate hydrogen radicals. Other products known to form from bulk water irradiation will need to be examined, such as hydrated electrons, hydronium ions and oxygen radicals.<sup>[2,3,4]</sup> A catalytic route may exist for hydrogen production. It is hoped that suspect metal ions can be identified and the system modified to test the effects of these contaminants when they are embedded in the surface in contact with water.<sup>[5]</sup>

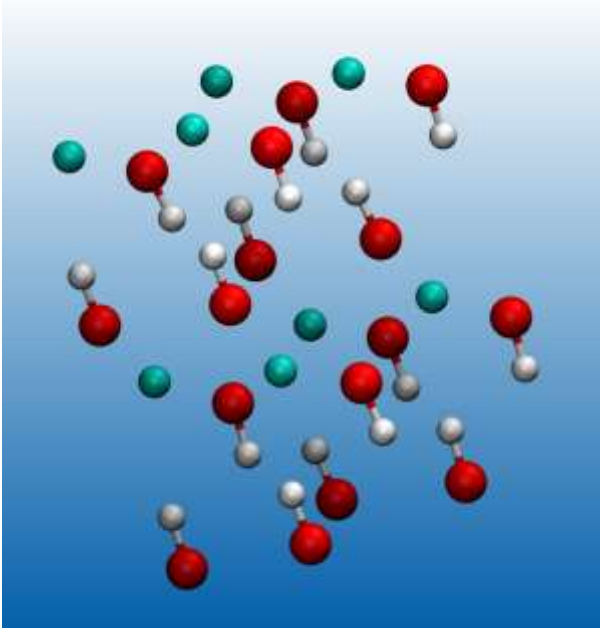


**Figure 1:** Structure of brucite mineral, depicting magnesium as turquoise, oxygen as red and hydrogen as white.

We will examine the rates for different decomposition pathways and will build up a library of likely chemical processes. We can use this information to examine the long term behavior of larger scale systems by inserting this information into a kinetic Monte Carlo program. More complex systems can be studied by examining how these basic processes are perturbed when metallic surfaces are present.

## Discussion

The problem of accounting for hydrogen generation in the absence of a corrosion pathway is complicated by the many routes that may contribute to the process. These processes need to be de-coupled from each other and considered independently.

Direct thermal decomposition of water only occurs at elevated temperatures, in the region of  $2000\text{ K}^{[6]}$ , which are infeasible in sludge. However, in the presence of a metallic surface where adsorption can occur, the barriers to water dissociation are reduced through a catalytic process. The low-temperature water-gas shift reaction is an interesting example of a

reaction involving the catalysed dissociation of water molecules<sup>[5]</sup>. In the reversible reaction scheme, CO oxidised by an oxygen atom, generated from the dissociation of water, forms  $\text{CO}_2$  and  $\text{H}_2$ . As the reaction is exothermic, it is favoured at low temperatures, typically around  $150\text{ }^\circ\text{C}$ . The kinetics at lower temperatures (sub  $100\text{ }^\circ\text{C}$ ) would be interesting to examine. It is conceivable that some of the metals that catalyse this process would be present in the sludge as contaminants through the decay of fission products from the spent Magnox fuel. The use of a reactor inventory code such as FISPIN would be necessary to quantify the likely composition of species in the sludge.

Modelling of temperatures in hotspots around fission product contaminants to be evaluated in the sludge could be performed, indicating if temperatures were high enough for a direct catalytic mechanism to occur.

If one considers a purely radiolytic route to hydrogen production, some surface effect still is likely to play a role. The production of hydrogen from plutonium dioxide surfaces can be considered a related problem. Sims, Webb, Brown, Morris and Taylor found that a recombination route reduced radiolysis yields of hydrogen from water adsorbed in monolayers closest to a plutonium dioxide surface, even below what would be expected from bulk water radiolysis<sup>[3]</sup>. An opposite result is reported for oxides of cesium and zirconium, where greatly elevated yields for monolayers nearest the surface were observed.<sup>[7]</sup> It is clear that adsorbed water behaves very differently than bulk water under radiolysis and needs close investigation.

The radiochemistry of water is a rich and complex subject. Many different reactions compete simultaneously, involving a range of species, including atoms, ions and radicals of H,  $\text{H}_2\text{O}$ ,  $\text{O}_2$ , OH,  $\text{H}_2\text{O}_2$  and aqueous electrons. Ershov and Gordeev identified 32 such reactions for their kinetic model.<sup>[4]</sup> The interactions between these species and a brucite surface will be a subject of particular interest over the course of this work.

## Conclusions and Future Work

The problem of hydrogen generation from corroded Magnox sludges is a rich subject with many factors affecting the underlying processes. These processes need to be identified at the most fundamental level before their interactions within the system can be explored.

Current work is attempting to quantify the free energy barriers to Mg-OH bond cleavage. The following work will apply this same approach to a brucite-water surface and the bond cleavage of adsorbed water molecules will also be evaluated. It is expected that the strong adsorption of water on to the surface of brucite will play a key role.

## Acknowledgments

consortium for providing a useful and stimulating network for discussion.

The authors thank the EPSRC for providing this studentship. Thanks goes to the DISTINCTIVE

## References

- [1] Smyth, M., Kohanoff, J., 2012. Excess electron interactions with solvated DNA nucleotides: Strand breaks possible at room temperature. *Journal of the American Chemical Society* 134, 9122–9125.
- [2] Hart, E.J., 1970. *The hydrated electron* / (by) Edwin J. Hart, Michael Anbar. Wiley-Interscience, Chichester
- [3] Sims, H.E., Webb, K.J., Brown, J., Morris, D., Taylor, R.J., 2013. Hydrogen yields from water on the surface of plutonium dioxide. *Journal of Nuclear Materials* 437, 359–364.
- [4] Ershov, B.G., Gordeev, A.V., 2008. A model for radiolysis of water and aqueous solutions of H<sub>2</sub>, H<sub>2</sub>O<sub>2</sub> and O<sub>2</sub>. *Radiation Physics and Chemistry* 77, 928–935.
- [5] Phatak, A.A., Delgass, W.N., Ribeiro, F.H., Schneider, W.F., 2009. Density Functional Theory Comparison of Water Dissociation Steps on Cu, Au, Ni, Pd, and Pt. *J. Phys. Chem. C* 113, 7269–7276.
- [6] Ohya, H., Yatabe, M., Aihara, M., Negishi, Y., Takeuchi, T., 2002. Feasibility of hydrogen production above 2500 K by direct thermal decomposition reaction in membrane reactor using solar energy. *International Journal of Hydrogen Energy* 27, 369–376.
- [7] LaVerne, J.A., Tandon, L., 2002. H<sub>2</sub> production in the radiolysis of water on CeO<sub>2</sub> and ZrO<sub>2</sub>. *Journal of Physical Chemistry B* 106, 380–386.  
doi:10.1021/jp013098s

# Thermal Treatment of Plutonium Contaminated Materials (PCM) Wastes

L.Boast\*<sup>1,2</sup>, R.J.Hand<sup>1</sup>, and N.C.Hyatt<sup>1</sup>

\*Correspondence: LBOAST1@sheffield.ac.uk

<sup>1</sup> Immobilisation Science Laboratory, Department of Materials Science and Engineering, the University of Sheffield

<sup>2</sup> Nuclear Decommissioning Authority, Westlakes Science and Technology Park, Cumbria, UK

## Abstract

Considering the high overall costs of waste disposal and the growing requirements for improved quality of the final waste form, the benefits offered by thermal processing become very significant. Key drivers for the application of thermal treatment processes include the reduced volume, improved passive safety, and superior long term stability, of the vitrified wasteform products. Currently a fundamental lack of scientific knowledge and understanding significantly hinders the uptake of thermal treatment processes for the immobilisation and disposal of plutonium contaminated material waste. The project will contribute to accelerating the acquisition of knowledge and experience required to support the NDA in deploying thermal technologies as a national asset for ILW treatment

## Introduction

PCM waste is a subcategory of intermediate level waste, which is generated as a result of the handling of plutonium during nuclear fuel processing and other related activities. PCM wastes accounts for 7 % of the UK ILW inventory [1]. The amount of PCM waste in the UK is estimated to be over 31000m<sup>3</sup>, with 70% of PCM waste stored at the Sellafield site [2]. The PCM waste, which can incorporate masonry, metal, organic or a mixture of each, are double bagged in heat sealed PVC linings before being stored in 200L mild steel drums. The heterogeneous nature of the waste material presents a considerable materials science and engineering challenge for PCM waste immobilisation. A process is already in place at the Sellafield site for the treatment of some categories of PCM waste, centred on the Waste Treatment Centre (WTC). The general method of the WTC is compression of the 200L drums containing the PCM waste, and the resulting crushed drums are grouted in cement and stored within 500L steel storage containers [3]. However there are significant concerns regarding the reliability of the supercompaction and subsequent grouting process to deliver a consistent wasteform suitable for long-term storage and eventual disposal [4].

Thermal treatment is the main alternative technology available for the treatment of PCM waste. Key drivers for the application of thermal treatment processes include the reduced volume, improved passive safety, and superior long term stability, of the vitrified wasteform products. These benefits are derived from oxidation of the metallic waste fraction, destruction of

organic components, and evaporation of entrained water, combined with simultaneous immobilisation of radioactive and chemotoxic elements within a glass or slag (i.e. a partially crystallised glass) material. Proof of concept studies by Sheffield and others, have demonstrated PCM compatibility with currently available thermal treatment technology platforms [5]. However a fundamental understanding of waste incorporation reactions and the impact of waste inventory on product quality remains to be established [6]. This generic understanding is clearly critical to successful technology deployment, irrespective of selected platform. To address such issues a fundamental understanding of waste incorporation and waste inventory on product quality needs to be established; signifying the aims of the project.

More specifically the aims of the project are to develop an understanding of waste / matrix interactions during thermal treatment of PCM wastes. The project will contribute to accelerating the acquisition of knowledge and experience required to support NDA in deploying thermal technologies as a national asset for ILW treatment.

## Methodology Details

Using Ce as a Pu surrogate laboratory scale experiments using simulant PCM drum mock ups of PVC waste, metal waste, mixed waste and masonry waste have been performed in order to understand the reactions and processes of waste digestion and incorporation during thermal treatment.

### Experimental Procedures

The compositions of the four PCM waste simulants are given in table 1. Fig 1-5 show mock up PCM drums.

**Table 1 Representative inactive PCM waste simulants**

Waste Type	PVC Waste	Metal Waste	Masonry Waste	Mixed Waste
Mild Steel (wt%)	44.44	20.00	30.00	30.00
PVC (wt%)	55.56	10.00	10.00	10.00
Metal items (wt%)	0	70.00	0	15.00
Masonry items (wt%)	0	0	60.00	40.00
Glass (wt%)	0	0	0	5.00
Total	100.00	100.00	100.00	100.00



Fig1: PVC waste Simulant



Fig2: Metal waste simulant



Fig3: Masonry waste simulant



Fig4: Mixed waste simulant



Fig5: Simulant waste with addition of glass frit at 1:1 wt ratio

The upper estimated  $\text{PuO}_2$  content of PCM wastes is the molar equivalent of 0.207 wt%  $\text{CeO}_2$ . All melts were doped with 1.043 wt%  $\text{CeO}_2$  as a  $\text{PuO}_2$  surrogate to allow for conservatism. In the case of PVC and metal wastes, no oxide materials were themselves available in the waste materials to immobilise the Pu/Ce

surrogate inventory therefore a glass frit (soda-lime-silica) was selected as an additive at a ratio of 1:1 (waste to additive) for all waste streams. Crucibles, containing simulant waste and additive, were placed in an electric muffle furnace and heated overnight at  $2^\circ\text{C min}$  to  $1100^\circ\text{C}$  for 8 h; crucibles were subsequently transferred to a gas-fired furnace, which had been preheated to  $1100 \pm 25^\circ\text{C}$ , then ramped to  $1560 \pm 10^\circ\text{C}$  over a period of 90 min. The preheat step was necessitated by the requirement to avoid thermal shock of the alumina crucibles. The crucibles were held at  $1560^\circ\text{C}$  for 4 hours before being removed and allowed to cool in air to room temperature.

### Results and Discussion

Melting behaviour shows no violent reactions between the waste simulant and glass additive. A substantial metallic fraction resulted for the vitrified metal type. PVC and masonry waste types were composed of 100% glass waste form. Glass in masonry and metallic feed exhibited little crystallinity. Glass derived from PVC and Mixed were partially crystalline throughout. Cl presented in the PVC was volatilised at high temperature



Fig6: Showing vitrified simulant PCM drum mock ups (a) PVC waste, (b) metal waste, (c) masonry waste, and (d) mixed waste

Component (wt%)	PVC	Masonry	Metal	Mix
$\text{SiO}_2$	37.93	54.85	69.87	54.23
$\text{MgO}$	0.86	0.86	1.17	0.93
$\text{Al}_2\text{O}_3$	16.51	11.70	7.6	9.29
$\text{CaO}$	5.46	7.07	7.43	6.9
$\text{Na}_2\text{O}$	6.02	6.81	7.72	6.53
$\text{Fe}_2\text{O}_3$	30.38	17.65	0.82	18.13
Other	2.2	1.25	3.98	3.08
Sum	99.31	99.53	98.59	99.09

Table 2 Composition of wastefrom components via XRF

XRF determined composition of major elements in the glass waste form is shown in table 2. The overriding difference in slag fraction composition is the  $Fe_2O_3$  content of the final oxide fraction of the wasteform. The higher  $Fe_2O_3$  content in the slag fraction of the PVC waste, compared to that derived from masonry and mixed waste types, is a consequence of the proportionately higher mild steel component. The slag resulting from the metal waste type, melted in a clay/graphite crucible, has a very low  $Fe_2O_3$  content consistent with partitioning of Fe into the substantial metal fraction under reducing conditions. Chemical analysis determined no measurable retention of Cl within the slag fraction of the wasteforms. It was therefore concluded that all Cl present in the PVC was volatilised by the high temperature treatment.

**Masonry Waste**

Powder XRD and SEM/EDS demonstrated the glass wasteform to be composed of a  $CaO-Fe_2O_3-Al_2O_3-SiO_2$  glass. Fig 7 shows an amorphous structure with no undissolved material within the glass matrix.

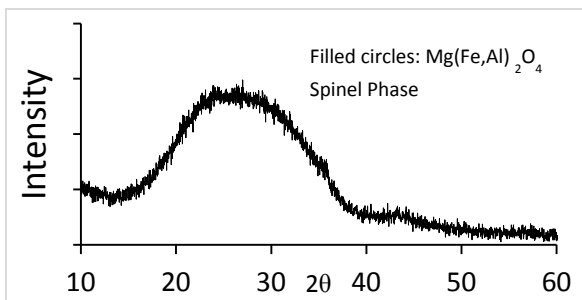


Fig7: X-ray powder diffraction pattern showing diffuse scattering corresponding to an amorphous component in the vitrified masonry waste stream.

**PVC Waste**

XRD pattern (Fig 8) showing identified reflections corresponding to spinel phase  $(Mg)(Fe,Al)_2O_4$  (Magnesioferrite). Diffuse scattering corresponding to the presence of an amorphous component in the form of  $CaO-Al_2O_3-SiO_2-Fe_2O_3$  glass. The SEM/EDS (Fig9) image shows dendritic crystal structure corresponding to the identified spinel phase

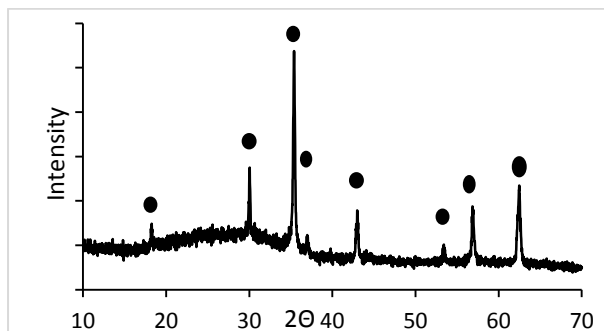


Fig8: X-ray powder diffraction pattern showing identified reflections corresponding  $(Mg,Fe)(Cr,Fe,Al)_2O_4$  (filled circles) phases, together with diffuse scattering corresponding to the presence of an amorphous component, in the slag produced by vitrification of PVC waste type.



Fig9: BSE image showing microstructure of slag produced by vitrification of PVC waste type. S corresponds to identified spinel phase

**Metal Waste**

XRD pattern (Fig10) showing diffuse scattering corresponding to an amorphous component in the form of  $CaO-Al_2O_3-SiO_2-Fe_2O_3$  glass. Graphite inclusions present.

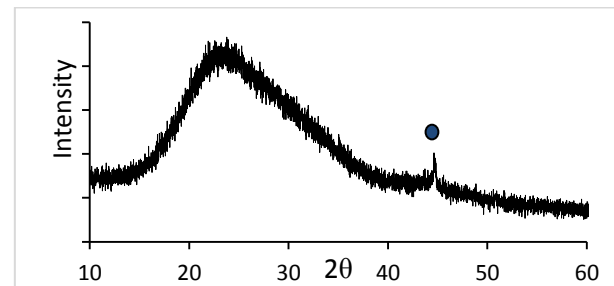


Fig10: X-ray powder diffraction pattern of the vitrified metal waste stream. Filled circle corresponds to graphite inclusions found within the glass matrix.

Using EDS maps to analysis the metallic phase, the microstructure shows an Fe-Si-Ni alloy.

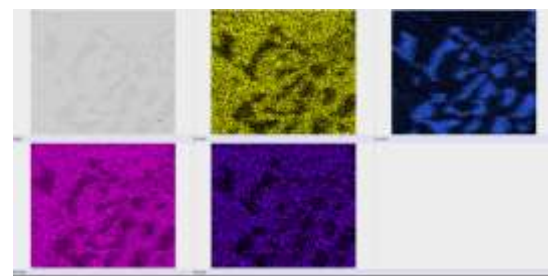


Fig11: EDS maps showing microstructure metal fraction produced by vitrification of metallic waste and partitioning of key elements.

**Mixed Waste**

XRD pattern (Fig12) showing identified reflections corresponding to crystalline  $Ca(Si,Al)_2O_6$  (diopside), and  $(Cr,Fe,Al)_2O_4$  (spinel) phases. Diffuse scattering corresponding to the presence of an amorphous component in the form of  $CaO-Fe_2O_3-Al_2O_3-SiO_2$  glass.

SEM image (Fig13) shows dendritic structure (spinel phase) and diopside crystal phase.

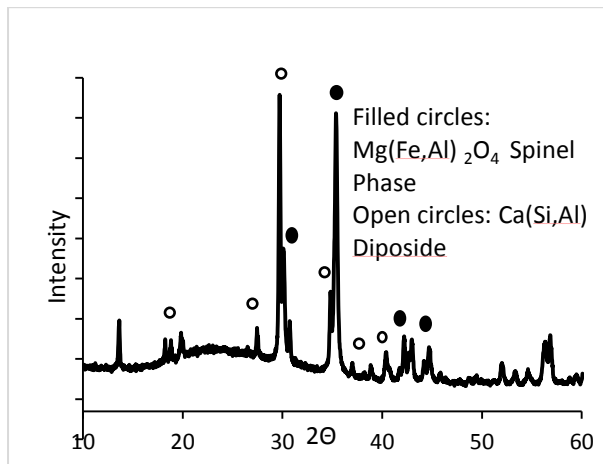


Fig12: X-ray powder diffraction pattern showing identified reflections corresponding  $(\text{Mg,Fe})(\text{Cr,Fe,Al})_2\text{O}_4$  (filled circles) phases and  $\text{Ca}(\text{Si,Al})_2\text{O}_6$  diopside (open circles), together with diffuse scattering corresponding to the presence of an amorphous component, in the slag produced by vitrification of mix waste type.

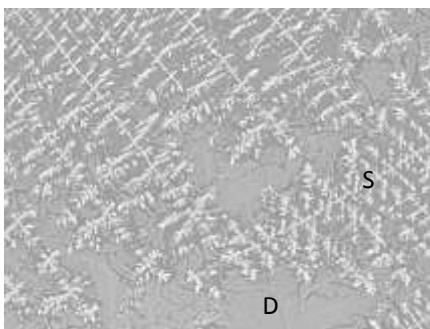


Fig13: BSE image showing microstructure of slag produced by vitrification of mix waste type. S corresponds to identified spinel phase and D to identified diopside phase

## Conclusions

$\text{PuO}_2$  ( $\text{CeO}_2$  surrogate) from the PCM is physically and chemically immobilised in the resulting materials, i.e. no residual  $\text{PuO}_2$  ( $\text{CeO}_2$ ) remains after processing. All of the analysis indicated that Ce was incorporated into the oxide phase in all samples. No residual waste remained following processing – Visual, XRD and SEM investigations lead to the conclusion that in all samples no unmelted waste or additives remained following processing. No adverse waste / matrix reactions occurred during or following processing.

## Future Work

### Long term Durability tests

Selection of optimised waste forms and develop an understanding of product stability with respect to generic ILW disposal concepts, through accelerated dissolution experiments

## Off Gas Waste form Emission

Time resolved investigation of the melting process through in situ characterisation of off gas chemistry and particle entrainment, and post mortem characterisation of the product phase assemblage, microstructure, and composition, supported by thermodynamic calculations where possible.

## Challenges Surrounding Treatment of High Metallic Waste Streams

It may be possible to treat the resulting metal phase as LLW or VLLW, if efficient and reproducible Pu partitioning into the slag phase can be achieved to the required threshold. This would require the slag and metal phases to be tapped separately from the melter (not yet demonstrated in an active context) or separated from the slag post processing (which is not desirable). The project will aim to address this issue.

## Acknowledgements

The project is sponsored by NDA i-case award student bursary

## References

- [1] "UKAEA's strategy for the decommissioning of its nuclear licensed sites", Health & Safety executive HM nuclear installations inspectorate, 2002, - <http://www.hse.gov.uk/nuclear/nuc20.pdf>
- [2] "Treatment of Plutonium Contaminated Materials at Sellafield", Stakeholder Consultation Briefing Note - <http://sellafieldsites.com/wp-content/uploads/2012/08/PCM-brochure-low-res.pdf>
- [3] "Plutonium Contaminated Materials (PCM) – A review of the status at Sellafield, Dounreay, Harwell and Aldermaston"- NuSAC (2005) P15 - <http://www.hse.gov.uk/aboutus/meetings/iacs/nusac/131005/p15.pdf>
- [4] "The management of higher activity radioactive waste on nuclear licensed sites" Joint guidance from the Office for Nuclear Regulation, the Environment Agency and the Scottish Environment Protection Agency to nuclear licensees – Nov (2011)
- [5] "Electricity Systems: Assessment of Future Challenges – Summary "-Department of Energy & Climate Change URN 12D/265 Aug (2012) - [https://www.gov.uk/government/uploads/system/uploads/attachment\\_data/file/48549/6098-electricity-system-assessment-future-chall.pdf](https://www.gov.uk/government/uploads/system/uploads/attachment_data/file/48549/6098-electricity-system-assessment-future-chall.pdf)
- [6] N.C. Hyatt and M. James, Nuclear Engineering International, Feb., 10-13, (2013)

# The Impact of Recycled Concrete Fines on the Engineering Performance of Cementitious Infill

T. Lord\*

\*Correspondence: cn10tl@leeds.ac.uk

## Abstract

Around 50% of the UK's classified nuclear waste is building waste including concrete, cement and rubble. While research has gone into ways to minimise the volume of this waste, little has examined recycling of the materials. This research is in very early stages of examining recycling options for contaminated concrete. Powdered mortars, mimicking scabbled waste concrete have been cast and ground, with tests undertaken to examine the reactivity of the material in terms of additional useable hydration. Initial results show possible hydration with further work required to discount the filler effect. Long term work includes examining the possibility of using the waste material as filler in low or intermediate waste encapsulation grouts.

## Introduction

Within the United Kingdom, a growing aspect of the nuclear industry is decommissioning work. A number of sites include power generation facilities either at, or coming towards, the end of their design life, as well as the Sellafield nuclear reprocessing site containing a number of old processing systems in addition to operational plants soon to be decommissioned.

Arising from the decommissioning are large quantities of building wastes, rubble and soil, accounting for over half of all classified waste [1]. In an effort to reduce the volume of concrete waste, part of the decommissioning work involves scabbling of the concrete; a process involving the removal of the outer, contaminated layer of concrete (usually the top 2-3cm) from the larger mass through laser or mechanical means, enabling the bulk of the concrete to be disposed of as low level or exempt waste.

The scabbled material produced is a fine granular material with a large particle size distribution, contaminated with a number of radionuclides that are either chemically bound to specific solid phases of the concrete or absorbed into the pore water of the material [2]. As a contaminated material the scabbled concrete is at present treated as a new Intermediate Level Waste (ILW) stream. The purpose of this project is to examine the nature of the scabbled material and examine options for possible re-use or recycling, primarily as a replacement material in existing cementitious encapsulation grouts.

Re-use and recycling of concrete has been taking place for a number of decades, in an attempt to reduce waste and carbon emissions arising from the construction industry [3]. Due to economic reasons however, little or no research has been conducted into the re-use of concrete fines as they are seen as detrimental and produced in insufficient quantities during processing. Within the nuclear industry however, disposal of material incurs a significant cost, and so recycling may be economically viable.

## Methodology Details

Initial research is focussed around examining reactivity of the scabbled material, to ascertain whether any latent hydration could occur if the material were recycled as opposed to direct disposal.

## Material Production

As requisitioning and handling of contaminated scabbled material would be extremely difficult, two reference mixes of mortar were cast. The mortars were based on mix designs for 50MPa concretes, emitting the coarse aggregate that is unlikely to be present in the outer scabbled layer. Mortar 1 (M1) is an ordinary portland cement (OPC) CEM1 mortar, with mortar 2 (M2) being a 20% PFA CEM1 mortar, with 20% of the cement replaced by Pulverised Fuel Ash. These mixes were chosen to be representative of the type of concrete that is likely to have been used on nuclear sites.

Following casting and curing, samples of each mortar were ground using a gyromill for varying periods of time. Following grinding, the fineness of the mortar powder was then matched to the fineness of the cement powder using Blaine testing. Quartz was also ground to match the fineness, for use as inert filler.

### Material Testing

With the initial aim of experimental testing to ascertain whether any reaction is occurring with the mortar powder, 3 series of tests were initiated. These include micro and macro scale testing.

Calorimetry tests were run on three samples; one containing only OPC, the second containing OPC and mortar filler and the third sample containing OPC and quartz filler. An inert filler is required to discount for any extra reaction caused solely by the filler effect, whereby the surfaces of the filler material provide nucleation sites for additional cement hydration and increase the amount of hydration per unit weight of cement [4].

Concurrent with the calorimetry testing were a series of chemical shrinkage tests, with the same three sample mixes over the same curing time of 28 days. Chemical shrinkage testing monitors the rate and amount of shrinkage of a sample during curing, which can be linked to the degree of hydration through the volume change brought about by the reaction of water and cementitious material [5].

The macro scale test carried out is a standardised compressive strength test on mortar cubes with 100mm dimensions [6]. M1, M2 and quartz fillers were used to replace the OPC at 10, 20 and 40% by weight in the mortar cubes. The strength at 1, 7 and 28 days was compared to a reference mix with zero replacement material.

### Results and Discussion

With calorimetry data, the degree of hydration can be directly linked to the overall heat evolution, or heat flow through the sample, as hydration is an exothermic reaction.

Figure 1 shows the normalized heat flow against time for a mortar 1 filler with different replacement values, per gram of cement in the mix. While the results are largely similar, it can be observed that a 40%

replacement has a slightly higher peak than other mixes, suggesting possible hydration.

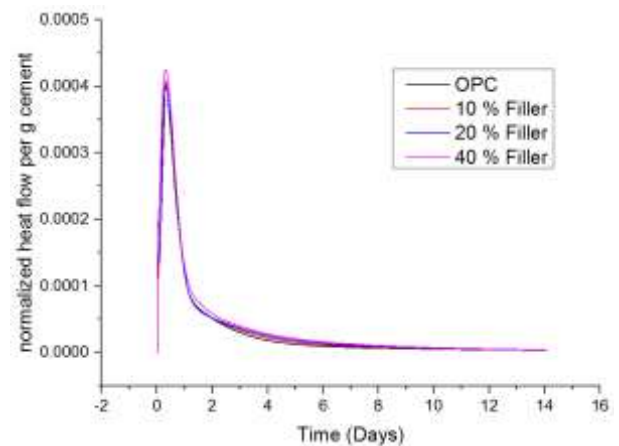


Figure 1 - M1 filler heat flow against time, normalized per gram of cement

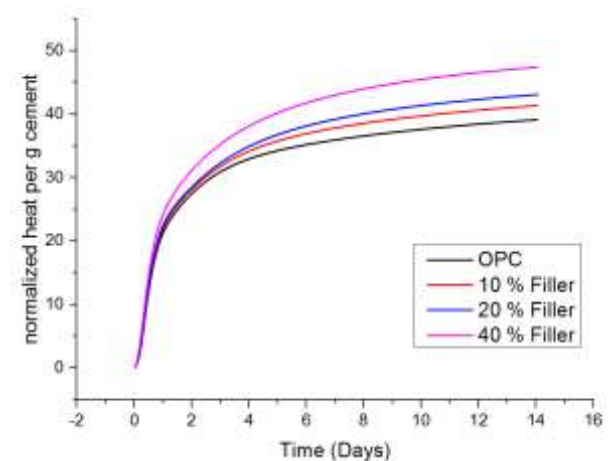


Figure 2 - M1 filler cumulative heat evolution against time, normalized per gram of cement

Figure 2 shows cumulative heat produced over the first 14 days of curing from the three mixes. From these results it is clear that a significant amount of increased heat from hydration is produced when increased amounts of filler are used.

While this increased hydration is likely to be from reaction of the filler material, it cannot fully be discounted and results need to be compared to that of the inert filler in order to discount the filler effect.

### Conclusions and Future Work

This research is still in very early stages, with much still to be carried out, initially in order to ascertain whether the scabbled material is reacting or is inert. From the first initial results increased heat of hydration per gram

of cement can be observed but this cannot yet be confirmed until further results are collected.

Near future work includes the collection of data from micro scale tests to ascertain increased hydration due to the filler effect, as well as concrete cube testing to compare compressive strengths and thus link filler content to the overall quality of the mortar.

Following the near future work, material analysis will be undertaken to examine the effects of replacement fillers on the microstructure of the mortar. SEM and TGA work will be carried out to examine individual phases within the cement matrix created by any reaction with the M1 and M2 fillers.

Long term work will examine effects of any observed reactions on the performance of cementitious infill, with the possibility of being incorporated in encapsulation grouts for low and intermediate level wastes, as part of a full recycling programme.

## Acknowledgements

I would like to thank in particular Leon Black for his supervision and my colleague Josh Hawthorne for his patience and direction. Thanks also to the civil engineering technicians and the Nuclear Group at Leeds University.

## References

- [1] Nuclear Decommissioning Authority, *2013 UK Radioactive Waste Inventory: Radioactive Waste Composition*. 2014: Moor Row, Cumbria.
- [2] Bath, A., G. Deissmann, and S. Jefferis. *Radioactive Contamination of Concrete: Uptake and Release of Radionuclides*. in *The 9th International Conference on Radioactive Waste Management and Environmental Remediation*. 2003. Oxford.
- [3] The Cement Sustainability Initiative, *Recycling Concrete*. 2009, World Business Council for Sustainable Development: Geneva.
- [4] Gutteridge, W.A. and J.A. Dalziel, *Filler Cement: The Effect of the Secondary Component on the Hydration of Portland Cement*. Cement and Concrete Research, 1990. **20**: p. 778-782.
- [5] Tazawa, E., S. Miyazawa, and T. Kasai, *Chemical Shrinkage and Autogeneous Shrinkage of Hydrating Cement Paste*. Cement and Concrete Research, 1995. **25**(2): p. 288-292.
- [6] The Concrete Centre, *National Structural Concrete Specification for Building Construction*. 2010, The Concrete Centre: Camberley, Surrey.

# In-Situ Monitoring and Characterisation of the Radioactive Sludge in the Legacy Ponds and Silos at Sellafield.

O. Ayoola\*<sup>1</sup>, B. Lennox<sup>1</sup>, and S. Watson<sup>1</sup>

\*Correspondence: olusola.ayoola@postgrad.manchester.ac.uk

<sup>1</sup>The University of Manchester, Dalton Cumbrian Facility, Cumbria, United Kingdom

## Abstract

The evacuation of the radioactive sludge from the legacy silos shall be effected by a series of excavation cycles using a mechanical equipment. The aim of this research is to develop a system that will scan every volume of sludge for the presence of gas pockets, metals and concrete materials in the region that is to be excavated. Also important is the development of a 3D density distribution and temperature characterisation map of the investigated volume. In this report, tomographic techniques which are of interest to this research are discussed on the basis of technical and environmental limitations with a view to justify the choice of a suitable technique to characterise a volume of radioactive sludge within the silo. Acoustic backscattering tomography is considered to be most suitable within the context of achieving system portability and in-depth penetration. A plan for the experimental validation of the proposed technique is presented.

## Introduction

The focus of this project is to develop a tomographic method that autonomously characterises radioactive sludge in legacy nuclear storage silos. In supporting nuclear decommissioning operations at Sellafield, this in-situ tomographic system would obtain sufficient information on the composition, temperature and potential hazards of a volume of sludge in the immediate area that is to be excavated.

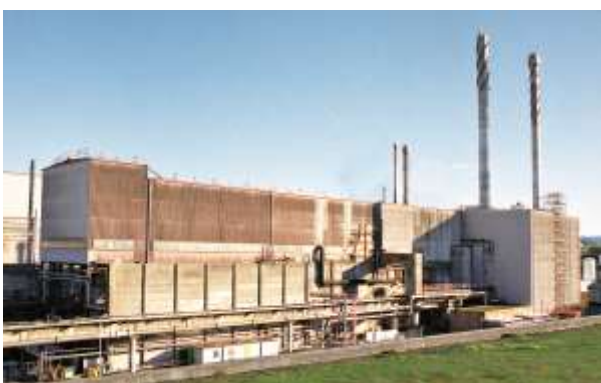


Figure 1: Magnox Swarf Storage Silos at Sellafield<sup>[1]</sup>

Figure 1 shows some legacy silo facilities at Sellafield. Each silo is a one metre thick concrete-steel reinforced enclosure, having a restricted service access of about one metre at the top. Retrieving sludge content from a silo is expected to involve the mechanical excavation using equipment deployed from the open access at the top. The silos contain water and magnesium sludge, but there is the need to scan thoroughly for the

presence of pockets of gases, metals and concrete amongst other objects that may require hazard control or additional logistics. To do this, a tomographic imaging system needs to be designed to characterise the top layer of sludge before retrieval begins. The imaging system is to be attached to this mechanical system thereby operating from only one side of the investigative volume. Figure 2 is not an exact depiction of the mechanical equipment to be used, but gives an idea of the environment to which the characterisation system will be deployed.

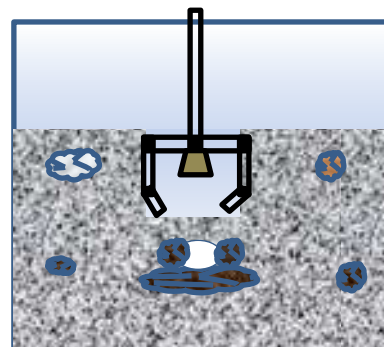


Figure 2: Schematic Diagram Showing the Area of Deployment

This Research aims to achieve a 3D characterisation and Identification of sludge content to a depth of >15 cm and with spatial resolution of 3 mm. As a result of the silos being encased in a one-metre thick concrete-steel reinforced wall, traditional non-invasive methods such as Electrical Impedance Tomography and

Ultrasonic Transmission-mode Tomography are not suitable.

## Methodology Details

### An Overview of Tomographic Techniques

Tomographic imaging involves obtaining information about an object from projections of transmitted energies when illuminated by an energy source whose beam could undergo reflection, diffraction or refraction<sup>[2]</sup>.

Tomographic methods can be generally classified into three types namely; transmission, reflection and emission tomography<sup>[3]</sup>. Transmission tomography involves positioning sensor systems around the investigated medium so as to illuminate from one side and receive the transmitted field on the other side for analysis after a successful penetration. This method is however only possible where the investigated medium can be encircled as is the case with Ultrasonic Transmission Tomography which was used in characterising velocity flow profile in a pond<sup>[13]</sup>. This can also be seen in the research on the use of Muon Tomography in characterising nuclear waste<sup>[4]</sup> and the use of Electrical Capacitance Tomography in solid concentration measurements<sup>[15]</sup>. In the event of restricted access around an object, reflection tomography becomes most suitable as would be discussed in the following sub-section. Alternatively, emission tomography relies on emitted fields from the investigated object for projection analysis; it may be passive or induced. This can be noted in the case of Single-Photon Emission Computed Tomography (SPECT), Positron Tomography and Scintigraphy.

### A Review of Alternative Techniques

#### 1. X-Ray Backscatter Tomography:

This method makes use of the Compton Scattering interaction between a material's free electrons and incident x-ray photons. In research conducted by Greenawald et al, 1996<sup>[5]</sup>, it was held that the number of x-ray photons scattered from a volume element within the investigated space is a function of the material's density. Also, information on the position of such density is obtained with the aid of collimated scanners. This was used to showcase the benefit of x-ray in the underwater environment. The technique was able to inspect large composite naval sonar domes underwater<sup>[5]</sup>.

However, the paper also noted the challenge of increasing attenuation effects with inhomogeneity and material thickness thereby limiting inspection depth to 10 cm<sup>[5]</sup> and as observed in the study on landmine

detection<sup>[14]</sup>. This is against the >15 cm depth required in this research.

#### 2. Vibrational Spectroscopy and LIDAR Systems

Techniques such as Raman Spectroscopy, Rayleigh, Near-Infrared Tomography, Laser Absorption amongst others make use of incident beam around the region of the visible light spectrum. Raman and Near-Infrared are referred to as vibrational spectroscopy. They provide an insight into molecular bonding activities within a compound as different intermolecular bonds have different vibrational energy levels which cause them to absorb and reflect certain wavelengths when illuminated. The intensity of the reflection is related to the concentration of chemical compositions in the material being tested.

In an underwater environment, optical Imaging will experience high light scattering and absorption<sup>[7]</sup>, thereby preventing significant penetration in an inhomogeneous volume. However, in a research conducted towards the detection and identification of underwater mines and submarines for military interest in the United States<sup>[8]</sup>, Light Detection and Ranging (LIDAR) was considered a viable solution. This involved transmitting short high-powered pulses of laser beam from an airborne transmitter into the water column, illuminating light-scatterers and returning backscattered light to an airborne receiver sensor comprising a PMT and an array of CCDs for analysis. The bulky gadget involvement may not fit into the area of deployment in this research.

#### 3. Ground Penetrating Radar Systems

Ground Penetrating Radar (GPR) technique is often used for detecting the presence of objects buried in opaque media ranging from underground utilities, archaeological matter, geophysical activities and buried landmines amongst others. It involves the transmission of radar signals of frequencies ranging from tens of MHz to some GHz<sup>[9]</sup> into the investigated volume and analysing the measured reflections. These transmitted signals get reflected when at boundaries of materials having dissimilar dielectric properties. The greater the difference between the dielectric properties, the clearer will be the reflections observed. Hence, an image which shows distinct boundaries will be produced. This concept is applied in detecting regions of subsurface water leakages from underground pipes as the leaked water creates a region of sharp dielectric contrast to the surrounding dry subsurface<sup>[10]</sup>. However, in a generally water logged environment, GPR is not suitable in distinguishing various components within such medium as it is known to develop significant errors as boundaries diminish in dielectric contrast<sup>[10]</sup>. This is even more significant where the medium comprises of

metallic sludge and foreign metals with relatively similar dielectric properties. Hence, it is not a suitable solution for this research.

#### 4. Magnetic Field Technology Systems

Magnetic field technology also known as Magnetic Induction Tomography works on the principle of electromagnetic induction. When an electromagnetic field is created by allowing current to flow in a coil, it is expected that there would be an induced current (acting as a flux receiver) on a similar coil or conductor brought in proximity to this already induced field (acting as a flux transmitter). The presence of any metallic substance nearby would cause interference to the existing electromagnetic field thereby affecting the value of this induced current as can be observed. This technology is a major industrial tomographic technology used in food processing industries for the detection of foreign metals contamination checks, used in clinical diagnostics for lung imaging, used in two-phase flow process imaging<sup>[14]</sup> and also used for metallic mine detection<sup>[13]</sup>. However this research seeks not only to detect metals but to distinguish between the various metals as the area of deployment comprises a variety of metals such as; the mechanical equipment, the magnesium sludge and any other metal objects within the silo. Magnetic Induction Tomography works best where there is a high conductivity contrast between the investigated object and the background medium. Hence this is not a viable solution to this research.

#### 5. Acoustic Tomography

Acoustic Tomography involves the use of sonar transducers for transmission and reception of sound waves. When sound waves approach an acoustic boundary of acoustic impedances  $Z_1$  and  $Z_2$ , the degree of acoustic impedance mismatch dictates the percentage of reflected Intensity ( $R$ ) and transmitted Intensity ( $T = 1 - R$ ) scattered at that boundary as governed by Equation 1<sup>[11]</sup>.

$$R = \left( \frac{Z_2 - Z_1}{Z_2 + Z_1} \right)^2 \quad - \quad (1)$$

Because every material has a unique acoustic impedance, analysing the acoustic backscattered signal's intensity and time data allows for identification of the obstacle's material and position. The frequency of the acoustic signal however affects its spatial resolution and its depth of travel as attenuation increase with frequency. A number of studies have been made on the application of acoustic tomography to underwater obstacle detection for unmanned vehicles<sup>[10]</sup>, settling suspension investigation, flow velocity profiling within a storage pond<sup>[12]</sup> and mine detection<sup>[9]</sup>. These studies have confirmed the suitability of acoustics for underwater sensing. A

challenge faced in acoustics tomography is the low signal to noise ratio caused by multiple scattering. This can be resolved by improving the sensitivity of the transducer used. In order to apply acoustic tomography to this research, a reflection mode known as acoustic backscattering will be adopted. The following section discusses the method of deployment of an acoustic backscattering system in-situ.

#### **Deployment of an In-Situ Acoustic Backscattering System**

Acoustic Backscattering is considered to be the most viable solution for this research and will be investigated further.

A sonar transducer will be mounted on a servo system which will coordinate the scanning process at intervals over a spherical angle covering the investigated volume. In each scanning cycle, a pulse will be transmitted across the region and backscattered intensities would be observed at the transducer. The focus angle and frequency to be used will be determined by experiments to be conducted.

A time – Intensity data will be obtained for use by a reconstruction algorithm in the development of a 3D characterisation map showing the physical composition of the sludge.

As acoustic signals encounter barriers, they will reflect in proportions governed by equation 1. Encountering further acoustic boundaries will result in further attenuation, coupled with absorption, attenuation and spread losses which all have to be taken into account.

Towards designing a robust acoustic backscattering characterisation system, other factors to be considered are:

- **Signal to Noise Ratio (SNR):** To reduce the effect of noise in acoustic tomography three factors must be considered – the sensitivity of the transducer, the start-up incident intensity and the choice of an efficient reconstruction algorithm.
- **Spatial Resolution:** The frequency of the incident acoustic beam, the focus angle and the scanning angle interval must be carefully chosen to meet the 3 mm spatial resolution. Because the investigated volume is to a 15cm depth, the angles mentioned above would be chosen to ensure that the resolution is achieved throughout the volume.
- **The Worst Case Scenario:** The wider the acoustic impedance margin in an acoustic boundary, the higher the reflection coefficient. A worst case boundary scenario could occur involving a 99% reflection effect. This is sufficient to prevent further penetration. Increasing the start-up incident intensity as a solution comes with limitations; it must be below

cavitation limit of the medium <sup>[11]</sup> and below the capacity of the amplifier system used.

## Conclusions and Future Work

The decision of an acoustic backscattering method most suits the portability and in-depth penetration required. Acoustic systems are safer to use and most suitable for general underwater imaging applications.

Having adopted a methodology for this project, a design of the scanning system and the servo-motor system will be made. To support the development of a prototype system, experiments to be carried out include the study of acoustic attenuation in water, sludge, metals, concrete and air, development of an acoustic backscattering profile for the variety of acoustic boundaries possible and a design of a servo system circuit and reconstruction algorithm.

The final deliverable from this project will be the construction of a demonstrator system that will operate in a 3.6m x 3.6m x 2.4m tank.

## Acknowledgements

The research team would like to acknowledge the funding provided by the Dalton Cumbrian Facility, through the Nuclear Decommissioning Authority and EPSRC - EP/L014041/1.

## References

- [1] Magnox Swarf Storage Silos <http://www.sellafieldsites.com/solution/risk-hazard-reduction/magnox-swarf-storage-silos/>, Date accessed: 18/03/2015 10:37pm.
- [2] Kak, A.C and Slaney, M., 2001, Principles of Computerised Tomographic Imaging, Society for Industrial and Applied Mathematics SIAM, Philadelphia
- [3] Abdul Rahim R., Rahiman, M.H.F, Nyap, N.W and San, C.K., 2004, On Monitoring of Liquid/Gas Flow Using Ultrasonic Tomography, *Jurnal Teknologi*, Malaysia, 40(D): pp.77-88, Jun 2004.
- [4] Mahon, D.F., 2014, Characterising legacy Nuclear Waste using Muon Tomography, TotalDecom™2014 Waste management Session, United Kingdom.
- [5] Greenawald, E.C., Draper, C., Chow, J., Levenberry, L., Poranski, C.F. and Ham, Y.S., 1996, Underwater X-RAY Tomography using Compton Backscatter Imaging, Review of Progress in Quantitative Nondestructive Evaluation, Vol 15, New York.
- [6] Gooneratne, C.P., Mukhopahyay, S.C. and Sen Gupta, G., 2004, A Review of Sensing Technologies For Landmine Detection: Unmanned Vehicle Based Approach, 2<sup>nd</sup> International Conference on Autonomous Robots and Agents, New Zealand.
- [7] Karabchevsky, S., Kahana, D. and Guterman, H., 2010, Acoustic Real-Time, Low-Power FPGA Based Obstacle Detection For AUVs, IEEE 26-th Convention of Electrical and Electronics Engineers, Israel.
- [8] Cadalli, N., Shargo, P.J., Munson, D. C. and Singer, A. C., 3-D Tomographic Imaging of Ocean Mines from Real and Simulated LIDAR Returns, [http://www.ifp.illinois.edu/~singer/pub\\_files/3-D\\_Tomographic\\_Imaging\\_of\\_Ocean\\_Mines\\_from\\_Real\\_and\\_Simulated\\_LIDAR\\_Returns.pdf](http://www.ifp.illinois.edu/~singer/pub_files/3-D_Tomographic_Imaging_of_Ocean_Mines_from_Real_and_Simulated_LIDAR_Returns.pdf) Date accessed: 21/03/2015.
- [9] Soldovieri, F., Crocco, L., Brancaccio, A., Solimene, R. and Persico, R., 2011, Applications of Ground Penetrating Radar and Microwave Tomography in Water Monitoring and Management, International Water Technology Journal, Vol. 1. Issue 1.
- [10] Martin, A., An, E., Neson, K. and Smith, S., 2000, Obstacle Detection by a Forward Looking Sonar Integrated in an Autonomous Underwater Vehicle, OCEANS 2000 MTS/IEEE Conference and Exhibition 337 - 341 Vol.1
- [11] Kinsler, L.E. and Frey, A.R., 1950, Fundamentals of Acoustics (Second Edition), John Wiley & Sons, Inc. USA
- [12] Hunter, T., Simon, B., Young, J., Fairweather, M. and Peakall, J. (2011), Ultrasonic Techniques for the In Situ Characterization of Nuclear Waste Sludges – 11275, WM2011 Conference, Phoenix.
- [13] Robledo, L., Carrasco, M. and Mery, D., 2009, A Survey of Land Mine Detection Technology, International Journal of Remote Sensing Vol. 30 No. 9, 10 May 2009
- [14] Wei, H.-Y. and Soleimani, M., 2013, Electromagnetic Tomography for Medical and Industrial Applications: Challenges and Opportunities, Proceedings of the IEEE Vol.101, No.3, March 2013.
- [15] Niedostatkiewicz, M., Tejchmana, J., Grudzien, K. and Chaniecki, Z., 2010, Application of ECT to Solid Concentration Measurements During Granular Flow in a Rectangular Model Silo, Chemical Engineering Research and Design 88 (2010) 1037–1048

# Novel Nanoparticle Cement for Crack Sealing

Riccardo Maddalena\*<sup>1</sup>, Andrea Hamilton<sup>1</sup>

\*Correspondence: riccardo.maddalena@strath.ac.uk

<sup>1</sup>Department of Civil and Environmental Engineering, University of Strathclyde, Glasgow - UK

## Abstract

Novel cementitious materials are being investigated as crack-healing agents. The cementitious materials used included nanoparticles such as nano-silica, silica fume and metakaolin. Several composites were chemically and mechanically tested, and a comparison was made between the composite and Portland cement characteristics. Continuing work includes an evaluation of the interaction between nanoparticle cement and existing concrete, and the mobilization of nanoparticles into cracks. Experiments will be assembled to simulate electro-migration, electro-deposition or localized injection through cracks. Numerical modelling will be also used to predict the water-flow permeability of the materials and their durability.

## Introduction

Cracking in building materials is a very common phenomenon. In concrete, formation of cracks (micro and nano) can appear straight after casting in the mould or with ageing. It can be attributed to many factors (aggressive environment, temperature, load and construction technique [1]) and can be observed either in the free surface or at the concrete-steel interface [2]. Durability of concrete is related to the presence of cracks since they provide a fast pathway for the transport of liquid and gases that potentially contain hazardous compounds [3]. Healing cracks in concrete is a well-studied research area and many different solutions have been recently proposed. Self-healing concrete is a concrete mixture in which healing agents (i.e. sodium silicate spheres) are encapsulated. These spheres rupture in response to cracking, reacting with calcium hydroxide present to form calcium silicate hydrate gel [4]. Self-healing bacteria have also been proposed as healing agents, which heal by reacting with atmospheric carbon dioxide and precipitating calcium carbonate in the cracks [5], [6]. Regarding any possible application of healing agents in existing structures [7], progress must be made into understanding the microstructural behaviour and relation to impact at the bulk scale. Micro and nanoparticles play an important role in cement and concrete performance: they act as a *filler*, reducing the water penetration content (or other potential contaminants) [8], improving compressive strength [10], and enhancing the long term durability of concrete. As shown in Figure 1, decreasing the particle size increases reactivity and allows the nanoparticle

surface to act as a nucleation site for crystal growth and formation of C-S-H [11].

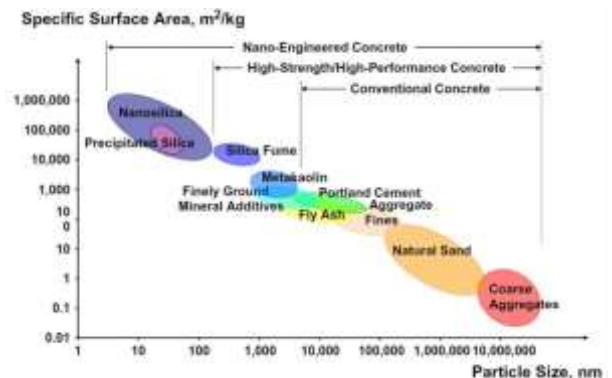


Figure 1 Particle size and specific surface area related to concrete materials. Adapted from [12].

Most research into nanoparticles has focused on the production of self-healing concrete, its mechanical characteristics and its introduction into the market, but less attention has been paid to the restoration of existing structures.

## Aim of the study

This project is focused on developing a nano-particle cement paste, capable of penetrating into micro and nano-size cracks, which reacts chemically with the existing concrete. Part of the project focuses on understanding how nanoparticles react in nano-pores and micro-pores. Filling nano and micro cracks with healing agents could cause localized stress promoting fracture propagation so it is important to understand the chemomechanics of crack filling as the sealant reacts. The focus of this work is to develop a nanoparticle cement capable of being mobilized into

cracks (see Figure 2), which reacts with existing material and consolidates.

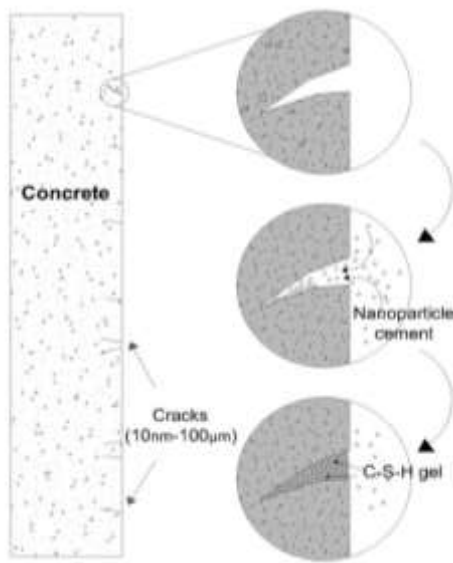


**Figure 2** Layout of nanoparticle cement behaviour into nano-sized cracks. Crack width 10nm - 10µm.

## Methodology Details

### Materials and preparation of specimens

The Portland cements used were CEM I – 42.5 (OPC 425) and CEM I – 52.5 (OPC 525), as classified by the EN 197-1 standard. Silica fume (SF, 920 D, Elkem Microsilica, Norway) and nanosilica particles (NS powder, Sigma Aldrich Ltd.) presented a particle size range of 0.15 µm and 12-25 nm respectively. Metakaolin (MK) was made by heating kaolinite (China clay type) at 750° C over 24 hours [13]. Cement pastes were prepared using a rotary mixer according to EN 196-1 and cast in cubic moulds for 24 hours. After casting, samples were kept at 20° C, RH 95% and placed in a nitrogen environment to prevent carbonation and dehydroxylation prior to testing. OPC 425 and 525 were mixed at liquid/solid (l/s) ratio of 0.3 and used as a reference. Nanoparticle cement pastes were made according to [14], [13], [15] with either deionised water or NaOH solutions. The mixes are summarized in Table 1.

**Table 1** Mix Proportion of cement paste composites.

Sample	OPC	CH	SF	NS	MK	W	NaOH 10 M	NaOH 1 M
	%					l/s ratio		
OPC425	100	-	-	-	-	0.3	-	-
OPC525	100	-	-	-	-	0.3	-	-
CHI	-	75	25	-	-	0.6	-	-
CHI act	-	75	25	-	-	-	0.8	-
MK10	-	-	-	-	100	-	0.8	-
AMK	-	75	-	-	25	-	1	-
BMK	-	66	-	-	33	-	1	-
MK-NS	-	10	-	5	85	-	-	1

### Experimental methodology

Compressive strength test was performed at 1, 3, 7 and 28 days according to the standard EN 196-1, at a constant strain rate of 0.4 mm/min [19]-[20]. Each result was the mean value of 3 samples. The heat of hydration was measured using an isothermal calorimeter (I-Cal 4000 HPC, Calmetrix). Hydrated sample phases were analysed by X-Ray diffraction (XRD) using a Bruker D8 powder diffractometer with Cu-K $\alpha$ . Measurements were made from 2° to 60° 2 $\theta$  at a rate of 1°/min with a step size of 0.02° 2 $\theta$ . Hydraulic properties such as bulk density, open porosity and matrix density were evaluated according to BS 1377-2.

## Results and Discussion

### X-ray diffraction

Hydration of cement phases are mainly CH (portlandite) and C-S-H gel. Other products can form, such as ettringite (E) and calcite (C), as reported in Figure 3. Leftover alite and belite are also shown. These are the phases which react to form CH and C-S-H gel.

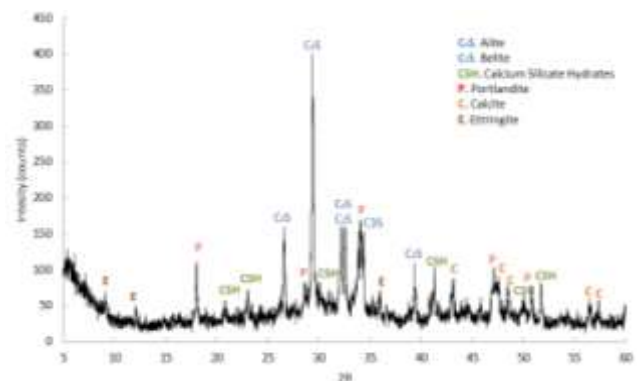


**Figure 3** XRD pattern of 28 days hydrated OPC paste.

The XRD pattern of sample CHI in Figure 4 shows the formation portlandite and an amorphous phase (at 29.4° 2 $\theta$ ) which can be attributed to C-S-H gel[18]–[21]. Hydration of metakaolin and calcium hydroxide powder with 10M aqueous sodium hydroxide (sample BMK) forms an semi-amorphous phase, calcium aluminate hydrate (C-A-H) and its peaks can be found at 11.2°, 22.8° and 31.1° 2 $\theta$  [22]–[24], as shown in Figure 5.

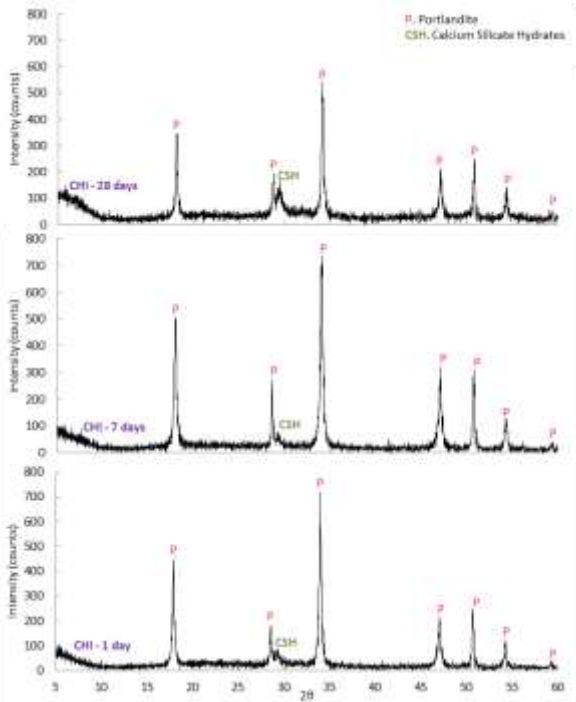


**Figure 4** XRD pattern of CHI paste hydrated at 1, 3 and 28 days. Much greater heat flow is evident in figure 7 for activated CHI and we would expect the XRD results of this material (pending) to show more CSH gel formation than the un-activated CHI presented here.

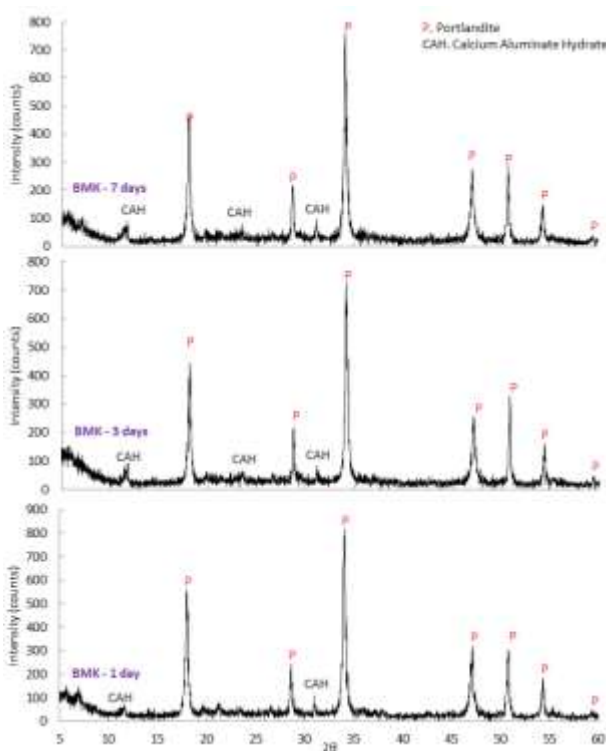


**Figure 5** XRD pattern of BMK paste hydrated at 1, 3 and 7 days.

**Heat of hydration**

The formation of C-S-H gel is an exothermic reaction which takes place in the first few hours of the hydration process, when water (or an activator

solution) comes in contact with the cement powder. As shown in Figure 6, heat flow of nanoparticle cement does not present the same behaviour as OPC, however the SF can be alkali-activated and react with CH, providing an exothermic reaction which develops a total heat of 43 J/g (CHI) and 208 J/g (CHI act.) as shown in Figure 7. The MK sample shows stronger exothermic behaviour compared with OPC samples, with a total heat developed of 455 J/g.

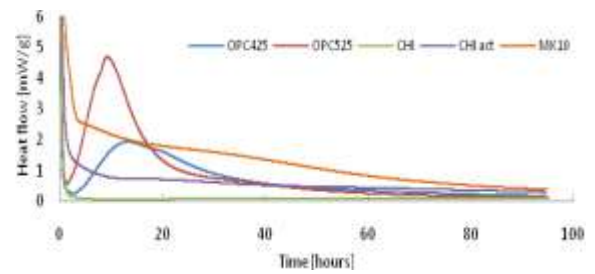


**Figure 6** Heat flow of nanoparticle cement compared with Portland cement.

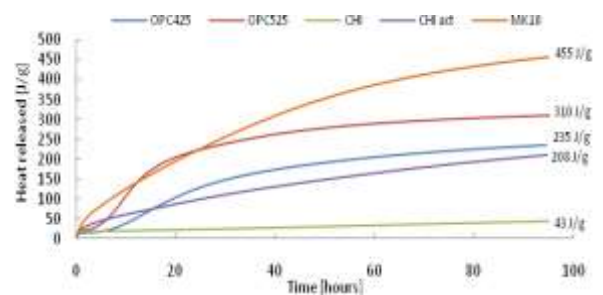


**Figure 7** Heat released during the hydration process in nanoparticle cement compared with Portland cement.

**Compressive strength**

Compressive strength results are shown in Figure 8. Strength developed by samples OPC 425 and OPC 525 are in accordance with the standard for Portland cement. The nanoparticle cement samples do not show strength comparable with Portland cement. However, between a curing time of 3 days and 28 days, an increased resistance can be seen. The low strength can be attributed to the physical effect of space filling from the nanoparticles[25]. Although it has been found that nanoparticle pozzolanic material commences reaction between 3 and 7 days, a considerable amount of CH and nanoparticles remain unreacted after 91 days [26]. Results are in accordance with the work of Lam et al., nanoparticles contribute to strength development better in concrete than in pastes. This is due to the active role that micro-silica plays at the interface between the cement matrix and aggregates [27]. High compressive strength is not necessarily desirable for crack filling but is measured for comparison with the industry standard, OPC. Tailoring hydraulic properties

is more important for long term durability and wide applicability which will be the focus of future work. At a given age of 28 days, values of open porosity ( $\psi$ ), dry bulk density and matrix density were determined and compared with Portland cement. Each value was calculated as a mean number on three measurements, summarized in table 2.

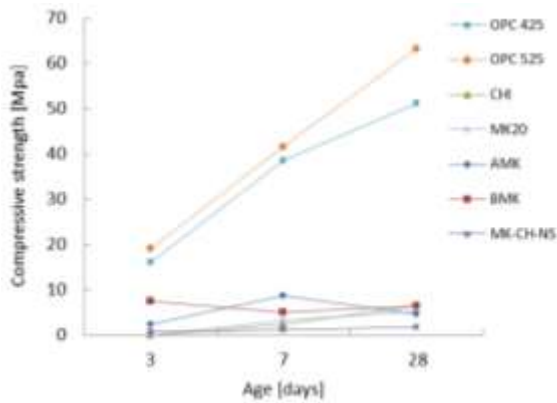


**Figure 8** Compressive strength of nanoparticle cement samples at different ages, compared with Portland cement samples.

Nanoparticle cement pastes present a porosity value in the range 0.5-0.7, which is much higher than Portland cement and a lower density. The next step is to determine the optimal range of permeability values for crack sealing and tailor porosity and sorptivity accordingly.

**Table 2** Results of tests per each mixing.

Sample	Compressive strength [Mpa]			Heat released [J/g]	Bulk density [g/cm <sup>3</sup> ]	Matrix density [g/cm <sup>3</sup> ]	$\psi$	XRD phases
	Age [days]							
	3	7	28					
OPC425	16.1	38.4	51.2	235	1.9	2.4	0.21	E, P, CSH, C, C3S, C2S
OPC525	19.2	41.6	63.2	310	1.6	2.4	0.35	E, P, CSH, C, C3S, C2S
CHI	0	2.4	6.4	43	0.9	2.3	0.61	P, CSH
CHI act	n/a	n/a	n/a	208	1.2	1.5	0.22	n/a
MK	0	3.2	5.1	455	1.0	2.2	0.53	n/a
AMK	2.8	8.7	4.6	n/a	0.9	2.2	0.59	P, CAH
BMK	7.5	5.1	6.6	n/a	0.9	2.1	0.58	P, CAH
MK-NS	0.8	1.2	1.8	n/a	0.6	2.3	0.72	n/a

## Conclusions

Early results show significant heat flow from samples (MK and CHI) activated with very strong alkaline solutions (NaOH 10M) which indicates a vigorous reaction and high production of C-S-H gel. Confirmation by XRD analysis is pending. Figure 4 shows slow development of C-S-H gel over 28 days which fits with the low and slow release heat flow shown in figure 7. Figures 6 and 7 indicate the alkali activated nanoparticle cements could be very fast setting and have high compressive strength. Analytical results are required to confirm.

## References

[1] A. . Harris, M. . Manning, W. . Tearle, and C. . Tweed, "Testing of models of the dissolution of cements—leaching of synthetic CSH gels," *Cem. Concr. Res.*, vol. 32, no. 5, pp. 731–746, 2002.

[2] J. Pacheco, B. Šavija, E. Schlangen, and R. B. Polder, "Assessment of cracks in reinforced concrete by means of electrical resistance and image analysis," *Constr. Build. Mater.*, vol. 65, pp. 417–426, 2014.

[3] K. Van Tittelboom, N. De Belie, W. De Muynck, and W. Verstraete, "Use of bacteria to repair cracks in concrete," *Cem. Concr. Res.*, vol. 40, no. 1, pp. 157–166, 2010.

[4] H. Huang and G. Ye, "Application of sodium silicate solution as self-healing agent in cementitious materials," *Int. RILEM Conf. Adv. Constr. Mater. Through Sci. Eng.*, pp. 530–536, 2011.

[5] W. De Muynck, K. Cox, N. De Belie, and W. Verstraete, "Bacterial carbonate precipitation as an alternative surface treatment for concrete," *Constr. Build. Mater.*, vol. 22, pp. 875–885, 2008.

[6] R. Pei, J. Liu, S. Wang, and M. Yang, "Use of bacterial cell walls to improve the mechanical performance of concrete," *Cem. Concr. Compos.*, vol. 39, pp. 122–130, 2013.

[7] H. E. Cardenas and L. J. Struble, "Modeling Electrokinetic Nanoparticle Penetration for Permeability Reduction of Hardened Cement Paste," 2008.

[8] H. Du, S. Du, and X. Liu, "Durability performances of concrete with nano-silica," *Constr. Build. Mater.*, vol. 73, pp. 705–712, 2014.

[9] P. Hou, S. Kawashima, K. Wang, D. J. Corr, J. Qian, and S. P. Shah, "Effects of colloidal nanosilica on rheological and mechanical properties of fly ash-cement mortar," *Cem. Concr. Compos.*, vol. 35, no. 1, pp. 12–22, 2013.

[10] J.-Y. Shih, T.-P. Chang, and T.-C. Hsiao, "Effect of nanosilica on characterization of Portland cement composite," *Mater. Sci. Eng. A*, vol. 424, no. 1–2, pp. 266–274, 2006.

[11] H. F. W. Taylor, *Cement chemistry*, 2nd ed., vol. 20, 1998.

[12] K. Sobolev and M. F. Gutiérrez, "How nanotechnology can change the concrete world," *Am. Ceram. Soc. Bull.*, vol. 84, no. October, pp. 14–18, 2005.

[13] S. Alonso and A. Palomo, "Alkaline activation of metakaolin and calcium hydroxide mixtures: influence of temperature, activator concentration and solids ratio," *Mater. Lett.*, vol. 47, no. 1–2, pp. 55–62, Jan. 2001.

[14] Y. Qing, Z. Zenan, S. Li, and C. Rongshen, "A Comparative Study on the Pozzolanic Activity between Nano-SiO<sub>2</sub> and Silica Fume 1 Introduction 2 Experimental," *J. Wuhan Univ. Technol.*, vol. 21, no. 3, pp. 0–4, 2006.

[15] Q. Lin, X. Lan, Y. Li, Y. Ni, C. Lu, Y. Chen, and Z. Xu, "Preparation and characterization of novel alkali-activated nano silica cements for biomedical application," *J. Biomed. Mater. Res. B. Appl. Biomater.*, vol. 95, no. 2, pp. 347–356, Nov. 2010.

[16] F. Sanchez and C. Ince, "Microstructure and macroscopic properties of hybrid carbon nanofiber/silica fume cement composites," *Compos. Sci. Technol.*, vol. 69, no. 7–8, pp. 1310–1318, Jun. 2009.

[17] M. S. Morsy, S. H. Alsayed, and M. Aqel, "Hybrid effect of carbon nanotube and nano-clay on physico-mechanical properties of cement mortar," *Constr. Build. Mater.*, vol. 25, no. 1, pp. 145–149, Jan. 2011.

[18] F. Kontoleontos, P. Tsakiridis, A. Marinou, N. Katsiotis, V. Kaloidas, and M. Katsioti, "Dry-grinded ultrafine cements hydration. physicochemical and microstructural characterization," *Mater. Res.*, vol. 16, no. 2, pp. 404–416, Apr. 2013.

[19] E. M. Foley, J. J. Kim, and M. M. Reda Taha, "Synthesis and nano-mechanical characterization of calcium-silicate-hydrate (C-S-H) made with 1.5 CaO/SiO<sub>2</sub> mixture," *Cem. Concr. Res.*, vol. 42, no. 9, pp. 1225–1232, Sep. 2012.

[20] S. T. Bergold, F. Goetz-Neunhoeffer, and J. Neubauer, "Quantitative analysis of C-S-H in hydrating alite pastes by in-situ XRD," *Cem. Concr. Res.*, vol. 53, pp. 119–126, Nov. 2013.

[21] R. Snellings, A. Salze, and K. L. Scrivener, "Use of X-ray diffraction to quantify amorphous supplementary cementitious materials in anhydrous and hydrated blended cements," *Cem. Concr. Res.*, vol. 64, pp. 89–98, Oct. 2014.

[22] C. K. Yip, G. C. Lukey, and J. S. J. van Deventer, "The coexistence of geopolymeric gel and calcium silicate hydrate at the early stage of alkaline activation," *Cem. Concr. Res.*, vol. 35, no. 9, pp. 1688–1697, Sep. 2005.

[23] D. Torr ns-Mart n, L. Fern ndez-Carrasco, and S. Mart nez-Ram rez, "Hydration of calcium aluminates and calcium sulfoaluminate studied by Raman spectroscopy," *Cem. Concr. Res.*, vol. 47, pp. 43–50, May 2013.

[24] M. A. Chavda, S. A. Bernal, D. C. Apperley, H. Kinoshita, and J. L. Provis, "Identification of the hydrate gel phases present in phosphate-modified calcium aluminate binders," *Cem. Concr. Res.*, vol. 70, pp. 21–28, Apr. 2015.

[25] E. E. Berry, R. T. Hemmings, and B. J. Cornelius, "Mechanisms of hydration reactions in high volume fly ash pastes and mortars," *Cem. Concr. Compos.*, vol. 12, no. 4, pp. 253–261, Jan. 1990.

[26] R. F. Feldman, G. G. Carrette, and V. M. Malhotra, "Studies on mechanics of development of physical and mechanical properties of high-volume fly ash-cement pastes," *Cem. Concr. Compos.*, vol. 12, no. 4, pp. 245–251, Jan. 1990.

[27] L. Lam, Y. . Wong, and C. . Poon, "Degree of hydration and gel/space ratio of high-volume fly ash/cement systems," *Cem. Concr. Res.*, vol. 30, no. 5, pp. 747–756, May 2000.

# Use of Colloidal Silica Ground Barriers in Decommissioning

M. Pedrotti\*<sup>1</sup>, C. Wong<sup>1</sup>, G. El Mountassir<sup>1</sup> and R. Lunn<sup>1</sup>

\*matteo.pedrotti@strath.ac.uk

<sup>1</sup>Department of Civil and Environmental Engineering (University of Strathclyde, Glasgow, UK)

## Abstract

Hydraulic ground barriers are an established technology for use on contaminated sites, as a method of pollutant migration control. However traditional techniques of cement based grouts, soil-bentonite slurries and chemical grouts pose several limitations for use at in sites sensitive locations such as excavation requirements, high pH leachates and presence of toxic components. Colloidal silica has been proposed as new material grout for the creation of hydraulic barrier. Colloidal silica is being considered as performance material because it has an initial low viscosity, small particle size and chemically and biologically inert. Colloidal silica can be destabilised by the addition of a salt accelerator compound and a change to pH, resulting in a rapid increase in viscosity (i.e. gelation) and formation of a rigid solid gel. This behaviour allows for low injection pressures to be used during the grouting process due to the initial low viscosity; with the resulting gel forming the contaminant ground barrier. This study aims to investigate the use of colloidal silica based grouts with applications taking into consideration existing challenges at the Sellafield site e.g. to inject horizontal barriers under unlined waste disposal trenches. The overall aim of this research is therefore the completion of a large scale laboratory experiment and field trials in order to design a suitable colloidal silica grout for horizontal barriers in situ, as required at Sellafield site.

## Introduction

The creation of hydraulic barriers by means of soil-bentonite slurries or grouting techniques are generally required i) to control and/or suppress the release of contaminants from buried sources, ii) to prevent the spread of existing plumes, and iii) due to the inability to effectively remove contaminants from the subsurface [1]. Such barriers can be a practical alternative to other options, such as physical extraction methods, excavation and disposal of contaminated soils or pump and treat methods.

There are multiple types of grouts and emplacements techniques that have been developed and demonstrated [2]. Jet grouting and permeation grouting are two general categories usually suitable for hydraulic barriers. Jet grouting uses high-energy emplacement of cement or chemical grouts whereby the sediment is displaced and mixed with the grouting material. Permeation grouting is the injection of a liquid grout (low viscosity) that fills the natural porosity and then gels to form a solid void-filling material [3]. In general grout materials are split into two families: cement-based grouts and chemical grouts. Chemical grouts are easier to inject since they are generally stable and have an initial low viscosity. As result they can be injected using permeation techniques into soil having a smaller pore size (ie. fine sand).

## Soil-bentonite slurry trenches

Soil-bentonite cut-off walls are constructed by excavating a continuous narrow trench under a bentonite slurry that stabilizes the excavation. The trench is backfilled subsequently with a blend of natural soil and bentonite, thereby displacing the slurry [4]. The completed wall acts as a barrier to lateral flow of water and most fluid pollutants. The main issues with such technique usually relate to workers exposure or the impossibility of accessing or digging into the contaminated area.

## Cement-based grouts

Cement grouts use Portland cement as the primary component. The particle size distribution of solids in cement grouts controls the ability of the grout to penetrate fine formation openings. For cement grouts, emplacement is often an issue for finely textured regions (in Figure 1 the dimension of a cement grain is compared with a silica particle). Microfine or ultrafine cement grouts incorporate micron-scale solids in the mix. However grout penetration for cement grouts would only be appropriate for coarse sand or gravel layers, with no fine sediments less than about 0.1 mm diameter [3].

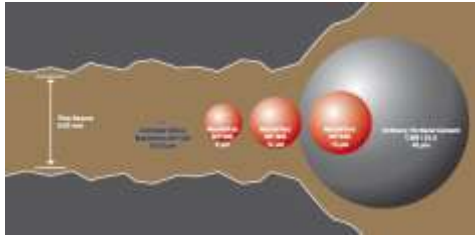


**Figure 1** Illustration of size comparison of Colloidal Silica to ordinary Portland cement [5].

Moreover cement based grouts have the potential to release high pH (12-13) leachates which may cause adverse effects on the groundwater chemistry. Furthermore, cement injection near surface can contribute to heave.

### Chemical grouts

Chemical grouts are easier to inject than cement grouts because they are stable solutions, they have lower viscosity and can be injected into smaller pore sizes. Such grouts consist of a solution comprised of a binder (other than Portland) that reacts in place to form a gel or a solid after the injection into a porous subsurface. Particles in chemical grouts are on the orders of nanometres and therefore their delivery into a porous media is not limited by particle filtration. There are varieties of materials that have been used for in situ grouting. These include: sodium silicate formulations, acrylic/acrylamides, urethanes, lignosulfates, phenoplasts, aminoplasts and colloidal silica [3]. Chemical grouts are often expensive, exhibit syneresis and may contain toxic components [6], colloidal silica represents an exception.

### Colloidal silica

The potential of colloidal silica as a favourable grouting material exists due to its: i) initial low viscosity (close to water), ii) low permeability after gelling (of the order of  $10^{-7}$  cm/s), iii) not requiring excessive injection pressure, iv) controllable set/gel times (from minutes to several days), v) environmental inert nature once formed into a rigid gel state, vi) smaller particle size when compared with cement grouts (Figure 1) and lower costs than chemical grouts.

Colloidal silica is a stable aqueous suspension of microscopic silica particles ( $\text{SiO}_2$ ). Particles are approximately uniform in size, and are obtainable typically with particle sizes from 2 to 150nm [7].

In alkaline solutions and low electrolyte concentration colloidal silica is stable (Figure 2a). Destabilization of the solution and subsequent gelation can be induced by destabilization of the particle repulsive forces through the addition of an accelerator electrolyte compound. This process will result in a rapid viscosity increase after a given period of time (Figure 2b).



(a) Stable colloidal silica



(b) Gelled colloidal silica

**Figure 2** Stages of colloidal silica viscosity evolution

According to Iler [7], gelling occurs as silica particles approach each other closely enough to link together forming three-dimensional branched chains of siloxane bonds (Si-O-Si) (Figure 3).

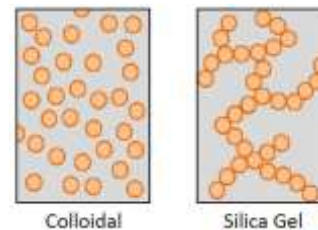


**Figure 3** Colloidal suspension and silica gel.

### Review of the previous works and application of silica grouts

The application of colloidal silica has historically been used within the petroleum industry for the enhancement of oil recovery by controlling fluid flow in porous media. Consolidated core plugs of fully cured colloidal silica were observed to withstand applied pressure gradients of more than (56 MPa/m) before exhibiting permeability change [8].

Passive site remediation proposed by Gallagher [9] studied the application of colloidal silica as a non-disruptive mitigation technique to sites susceptible to liquefaction risks by densification of soils. Desirable characteristics were long injection periods up to 100 days for low concentration solutions of approximately 10 to 20% colloidal silica concentration. The concept of treatment technique involved slow injection of colloidal silica the up gradient edge of a site, utilizing groundwater flow as the transport medium (Figure 4).

Du Pont Chemicals R & D initiated work examining the feasibility of colloidal silica grout as a soil remediation technique through a series of bench-scale laboratory studies. Gelled colloidal silica was seen to prevent leaching of fluids containing metals through permeability reduction. Secondly, high affinities for the adsorption of metals from solution were seen by the colloidal silica gel itself [10].

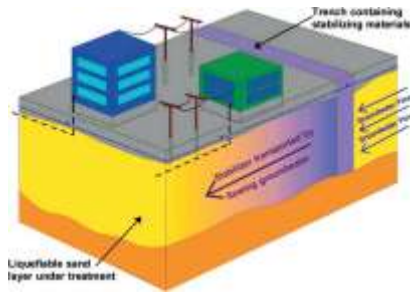


Figure 4 Passive site remediation delivery concept [9].

In-situ tests were carried out by Lawrence Berkley National Laboratory to demonstrate the use of silica colloids as permeation grouting for containment technology. Post-grouting excavation allowed visual inspection of the grouted plume which confirmed the uniformity of the grouting despite the heterogeneity of the soil (sand, silt and gravel).

**.Existing gaps in the literature**

Although some in-situ trials have been accomplished so far, further studies are still required in order to gain an acceptable control of silica grouting. Existing gaps are: i) understanding and control the influence of the chemistry of the in-situ water on silica gelling time, ii) understanding the interaction between different kinds of soil and the silica gel, iii) understanding the interaction between silica and in-situ contaminants or radionuclides and iv) understanding how the grouting conditions (injection rate, pressure, soil and so on) can affect silica gelation.

**Trenches at Sellafield site**

This research is focused on the potential use of colloidal silica to form horizontal barriers at Sellafield site. The site presents many different scenarios where this technology could be applied. The first considered scenario is the one at the Windscale Trenches (Figure 5). It was the site of a series of 6 unlined trenches which were progressively filled during the period 1955 to 1959 with uncontained low activity waste and with some more highly contaminated items that were too large to go into transport flasks to the waste silo.

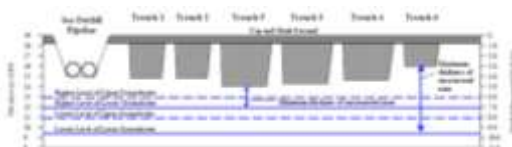


Figure 5 About 70m cross section through the trenches illustrating ground water level [11]

These trenches are now covered over with soil and surfaced with tarmac. Intrusive investigations carried out in the area around the trenches have generally encountered an initial shallow layer of made ground (generally less than 1.0m in thickness but recorded to a maximum depth of 2.1mbgl) underlain by natural superficial deposits predominantly comprising medium dense to very dense inter-bedded coarse grained sands and gravels with varying proportions of silt, clay and cobbles and occasional clay dominated, fine grained layers. Groundwater levels are recorded at between 6 to 9 mbgl. The hydraulic conductivity of the superficial deposits over the majority of the site is in the range of 1-10 m/day [11].

**Laboratory grout injection set up**

The next stage of the investigation study to be conducted will investigate grouting penetrability of various colloidal silica grout mixtures in a large scale tank (1825 by 265 mm, depth 400 mm) experiment shown in Figure 6 and Figure 7. Following this experiment a larger test (about 10 m<sup>2</sup>) is being planned which will enable the injection strategy for horizontal barriers to be investigated.



Figure 6 Experimental tank

In conjunction with a numerical model of the system, several soil and groundwater conditions shall be investigated in the laboratory set-up to simulate various environmental factors alongside saturated and unsaturated conditions.

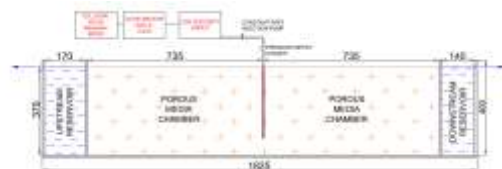


Figure 7 Test setup of experimental test

**Conclusions**

In order to design a silica based grout suitable for potential use for Sellafield site, a multi-stages laboratory campaign has been designed. The stages involve small scale laboratory experiments on silica gelation (see companion paper) in order to develop a

theoretical model able to predict the gelation time for different boundary conditions. Large and larger laboratory scale grouting experiment in order to simulate the in-situ conditions and test the reliability of the model are being constructed. Field tests will be conducted within the DISTINCTIVE program.

### Acknowledgements

This work was funded by a UK EPSRC research grant (EP/L0140441/1). The authors also thank Nick Atherton for the collaboration

### References

1. Moridis, G.J., et al. *New barrier fluids for subsurface containment of contaminants*. 1993.
2. Bolisetti, T., *Experimental and numerical investigations of chemical grouting in heterogeneous porous media*, 2005, University of Windsor (Canada): Ann Arbor. p. 151-151 p.
3. Truex, M.J., et al., *Evaluation of In Situ Grouting as a Potential Remediation Method for the Hanford Central Plateau Deep Vadose Zone*. Pacific Northwest National Laboratory, 2011.
4. Tallard, G., *Slurry trenches for containing hazardous wastes*. Civil Engineering—ASCE, 1984. **54**(2): p. 41-45.
5. BASF, *Injection Solutions for Underground Construction*, 2013: Germany.
6. Gallagher, P.M., S. Spatari, and J. Cucura, *Hybrid life cycle assessment comparison of colloidal silica and cement grouted soil barrier remediation technologies*. Journal of Hazardous Materials, 2013. **250**: p. 421-430.
7. Iler, R.K., *The Chemistry of Silica: Solubility, Polymerization, Colloid and Surface Properties, and Biochemistry*. 1979: John Wiley & Sons.
8. Jurinak, J.J. and L.E. Summers, *Oilfield applications of colloidal silica gel*. SPE Production Engineering, 1991. **6**(4): p. 406-412.
9. Gallagher, P.M., *Passive Site Remediation for Mitigation of Liquefaction Risk*, in *Civil and Environmental Engineering 2000*, Virginia Polytechnic Institute and State University.
10. Noll, M.R., C.L. Bartlett, and T.M. Dochat. *In situ permeability reduction and chemical fixation using colloidal silica*. in *Proceedings of the Sixth National Outdoor Action Conference*. 1992.
11. Atherton, S.L.-N., *Sellafield report - Info on trenches*, 2012.

# An Electro-chemical Model and Experimental Validation of Silica Gelling

C. Wong\*<sup>1</sup>, M. Pedrotti<sup>1</sup>, G. El Mountassir<sup>1</sup>, and R. Lunn<sup>1</sup>

\*Correspondence: christopher.wong@strath.ac.uk

<sup>1</sup>Department of Civil and Environmental Engineering (University of Strathclyde, Glasgow, UK)

## Abstract

Hydraulic ground barriers are an established technology for use on contaminated sites, as a method of controlling contaminant migration. However traditional techniques of cement based grouts, soil-bentonite slurries and chemical grouts pose several limitations for use at sensitive locations for example due to excavation requirements, high pH leachates and presence of toxic components. Colloidal silica based grouts are increasingly being considered as a potential grouting technology. Colloidal silica is being considered because it has initial low viscosity, small particle size and it is chemically and biologically inert. Colloidal silica can be destabilised by the addition of a salt accelerator compound and or changes to pH, resulting in a rapid increase in viscosity (i.e. gelation) and formation of a rigid solid gel. This behaviour allows for low injection pressures to be used during the grouting process due to the initial low viscosity; with the resulting gel forming the contaminant ground barrier. Predicting the change in viscosity over time for given variables (pH and electrolyte concentration) is considered to be a necessary requirement in order to design colloidal silica based grouts. This study aims to investigate the dependency of silica gelation time on electrolyte concentration and pH. A series of laboratory tests were conducted to explore the influence of accelerator concentration, ion valence and pH on gel time. An electro-chemically inferred model that can predict silica gel time has been developed and is presented in this paper.

## Introduction

Traditional hydraulic barriers formed from soil-bentonite slurries, cement based grout and chemical grouts pose several limitations in the case of sensitive sites e.g. nuclear decommissioning sites. Trench methods are unsuitable due to the requirement of soil excavation that could increase worker exposure to radionuclides. Likewise, cement based grouts have the potential to release high pH (12-13) leachates causing adverse effects on groundwater chemistry. Furthermore, cement injection near surface can contribute to heave. In heavily congested sites where structures and infrastructure remain operational heave is undesirable. On the other hand chemical grouts are easier to inject than cement grouts because they are stable solutions, they have lower viscosity and can be injected in smaller pore sizes. However chemical grouts are often expansive and may contain toxic components [1].

The potential of colloidal silica as a favourable grouting material exists due to its [2]: i) initial low viscosity, ii) low permeability after gelling, iii) minimal injection pressure iv) controllable set/gel times from minutes to several days, v) environmental inert nature once formed into a rigid gel state, and vi) smaller particle size when compared with cement grouts (figure 1).

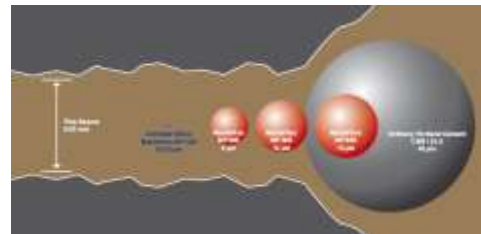


**Figure 1** Illustration of size comparison of Colloidal Silica particles to ordinary Portland cement particles [3]

Viscosity evolution and rigid gel state testing was conducted to determine the impact on the gelation process considering three main categories of variables: colloidal silica solutions, accelerator, and background conditions. An electro-chemically inferred model has been developed to predict silica gel time and it is compared with experimental data.

## Theory of gelling of colloidal silica

The theory of gelling of colloidal silica has been first discussed by Iler [4].

### Colloidal silica stability

Colloidal silica is an aqueous dispersion of silica particles, which are generally uniform in size (ranging from several to hundreds of nanometres). A silica particle surface has a negative electrical charge that is

dependent on the pH of the aqueous suspension. The more alkaline the suspension, the higher the electrical charge is. Generally the point of zero charge lies around pH 2 for silica. The electrical repulsion generated by particles having the same negative electrical charge stabilises the suspension and prevents particles from colliding and gelling. There are two possible ways of destabilising the suspension: i) adding an electrolyte (accelerator) to the suspension or 2) lowering the pH. In the former case the electrolyte affects the double layer created around the particles reducing the repulsion potential. In the latter case a lower pH causes protonation of the particle surface, lowering the net negative charge. In either case the probability of particle collision is increased and thus the likelihood of gelation.

### Aim of study

Predicting the change in viscosity over time for given variables (pH and electrolyte concentration) is considered to be a necessary requirement in order to design silica based grouts. Therefore, this study aims to investigate the dependency of silica gelation time on electrolyte concentration and pH. A series of laboratory tests were conducted to explore the impact on gel time as a result of accelerator concentration, ion valence and pH. In this paper an electro-chemically inferred model which can predict silica gel time is presented.

### Material and specimen preparation

#### Colloidal silica

MasterRoc MP 320 (formerly Meyco MP 320) colloidal silica solution was used in this study. According to BASF [5] product information, MP320 has a SiO<sub>2</sub> concentration 40±1%, an average particle size of 0.015µm, and density of 1.3 kg/l. Before dilution at 20°C, the solution has a dynamic viscosity of ~10mPa.s and a pH of 9.5-9.8. For gel time control, accelerator solutions of sodium chloride and calcium chloride were used.

#### Sample preparation and experimental procedure

For the experimental tests a mixing ratio of 5:1 colloidal silica to accelerator by volume was used.

Gel-time batch assessment tests were carried out based upon a 12 gel state code developed by Sydansk [6] and further expanded Persoff, et al [7] and Gallagher [8].

Gel-time batch tests were run at varying accelerator concentrations of NaCl and a pH range of 8 to 2. For batch tests, the time taken to achieve gel state 9 is regarded to be an accurate gauge for the time at which the hydraulic barrier in the ground has become rigid.

Samples	Gel state descriptions
1	No detectable gel formed. Gel appears to have same viscosity (fluidity) as original polymer solution and no gel is visually detectable.
2	Highly flowing gel. Gel appears to be only slightly more viscous than initial polymer solution.
3	Flowing gel. Most of obviously detectable gel flows to bottle cap upon inversion.
4	Moderately flowing gel. Small portion (<5-15%) of gel does not readily flow to bottle cap upon inversion—usually characterized as “trailing” gel [i.e., after hanging out of bottle, gel can be made to flow back into bottle by closely (lighting) it.
5	Barely flowing gel. Gel slowly flows to bottle cap and/or significant portion (>15%) of gel does not flow upon inversion.
6	Highly deformable nonflowing gel. Gel does not flow to bottle cap upon inversion (gel flows to just short of reaching bottle cap).
7	Moderately deformable nonflowing gel. Gel flows about halfway down bottle upon inversion.
8	Slightly deformable nonflowing gel. Only gel surface deforms slightly upon inversion.
9	Rigid gel. There is no gel surface deformation upon inversion.
10	Flexing rigid gel. Tuning fork-like mechanical vibration can be felt or tone can be heard after bottle is tapped.
11	Rigid gel no longer flexing. No tone or vibration can be felt or heard, because natural frequency of gel has increased.

Figure 2 Gel-time jar test assessment code [7].

The testing campaign considered a range of acidic conditions beyond presumable suitable grouting mixtures. Despite this, the lower pH spectrum inclusion in the batch tests enables the capture of acidic effects on grout mixtures that may exist due to extreme in-situ groundwater conditions.

Measurements of the increase in dynamic viscosity as a result of gelling were captured using a Brookfield LVT DV-II digital viscometer in accordance with ASTM D4016 [9]. In the viscosity tests, 200 ml of colloidal silica solution to 40 ml of accelerator were used.

### Experimental results and discussion

Laboratory experiments were carried out in order to investigate the influence of concentration and valence (monovalent vs divalent cation) of the accelerator.

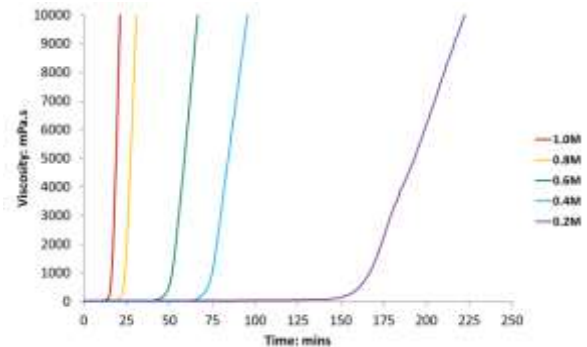
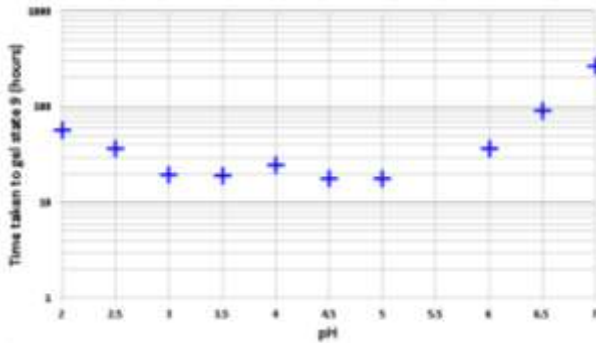


Figure 3 Viscosity evolution of colloidal silica mixed with CaCl<sub>2</sub>.

Viscosity evolution of colloidal silica mixtures with varying concentrations of CaCl<sub>2</sub> for the same pH 6.50 is shown in figure 3. The time taken to achieve the given viscosity of 10,000mPa.s is shown to decrease for solutions with higher calcium chloride concentration. Comparisons between colloidal silica mixtures with same concentration of CaCl<sub>2</sub> and NaCl (results are not reported) showed shorter gelling times for the divalent accelerator i.e (CaCl<sub>2</sub>).

For a 0.1M NaCl accelerator concentration solution as shown in figure 4, the pH region of reaching the rigid gel state within the shortest time was observed to occur between pH 3.5 to 5.5.

This trend was noted to shift with the minimum time region occurring at varying pH ranges for different accelerator concentrations.



**Figure 4** Gel state assessment results for colloidal silica mixed with 0.1M NaCl accelerator at varying pH.

Gelling tests carried out to study the influence of clay on the gelling time results not included here showed that gelling occurs in shorter time when the colloidal silica solution is mixed with clay. Further investigations are needed in order to understand the involved mechanisms.

### Chemistry of gelation

When particles in suspensions collide it is assumed that Van der Waals adhesion can occur, but in the case of silica particles attachment is enhanced by the formation of Si-O-Si bonds.

The chemistry that controls such bond formation is of the same nature of the chemistry that controls polymerization of silica in aqueous systems. Silica in an aqueous system keeps dissolving and condensing. Such dynamic equilibrium is controlled by the temperature, the curvature radius of the particles and the suspension pH. The solubility of silica is proportional to the radius of curvature of the particle. The smaller the positive radius the smaller the solubility is. When two spherical particles come into contact there is at that point an infinitely small negative radius of curvature and solubility is zero. Monomers (that are dispersed in solutions) will therefore be instantly deposited around that point, forming a cementing bond. On the other hand, the presence of  $\text{OH}^-$  anions in the suspension acts as a catalyser of the polymerization. Therefore the higher the pH of the solution the faster the chemical reaction is that leads to the Si-O-Si bonds.

Figure 5 presents the trend of the gel time at different pH. It is possible to see the gel is more stable at about pH 2 and pH 9. These points of stability are however due to different mechanisms: i) at pH 9 the high negative electrical charge prevents particle coming into contact and therefore creating the Si-O-Si bonds, on the other hand, ii) at pH 2 the particle charge is almost zero but the lack of  $\text{OH}^-$  anions slows down the chemical reaction required to form the Si-O-Si bonds.

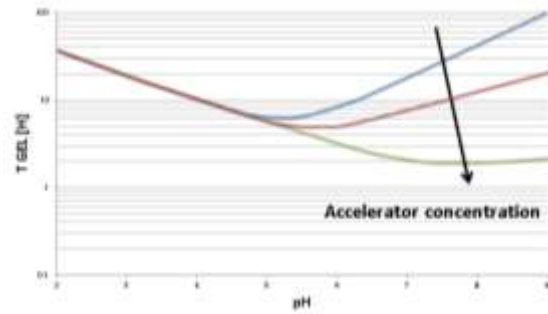


**Figure 5** Gel time vs pH.

When the pH is increased from pH 2, the rate of collision remains high and the concentration of  $\text{OH}^-$  increases. This leads to a reduction of the gel time. On the other hand, when the pH is decreased from pH 9, the electrical charge of the particles is reduced, allowing more particle collisions, so the gel time decreases as well.

The minimum generally occurs between pH 5 and 7 (depending on the electrolyte type and concentration). When the electrolyte concentration is increased the suspension becomes instable also for alkaline solutions, while for pH next to 2 remains unaffected.

### Modelling gel time

Time of gelation in silica colloids is a function of pH, electrolyte concentration, silica concentration and silica particle dimensions. A model able to predict the gel time of silica suspensions at different pH and electrolyte concentrations for given silica particle dimensions and concentration is proposed. The gel time is assumed to be controlled by two different mechanisms: i) particle collision rate and ii) likelihood of forming Si-O-Si bond at each collision.

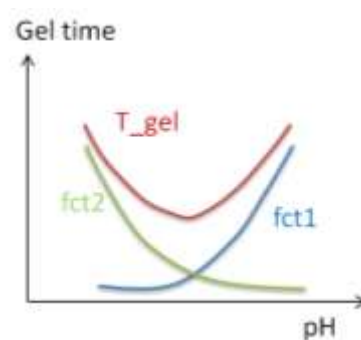


**Figure 6** Conceptual of gel time function

The former mechanism is controlled by the electrical repulsion of the particle. Electrical repulsion depends on pH in terms of particle electrical charge and on the electrolyte concentration in terms of double layer extension. (fct1 in figure 6)

The latter is controlled by the presence of  $\text{OH}^-$  anions and therefore it depends on the pH of the solution (fct 2 in figure 6)

Each of the mechanisms has been modelled using an exponential function with three parameters and two variables (pH and electrolyte concentration).

As reported in figure 6, the gel time is considered to be the sum of the two functions (equation 1).

$$t_{gel} = fct_1(\text{particle collision}) + fct_2(\text{Si-O-Si bonds}) \quad 1$$

## Model validation

The model has been validated using the experimental data of the gel solid state reported in figure 4.

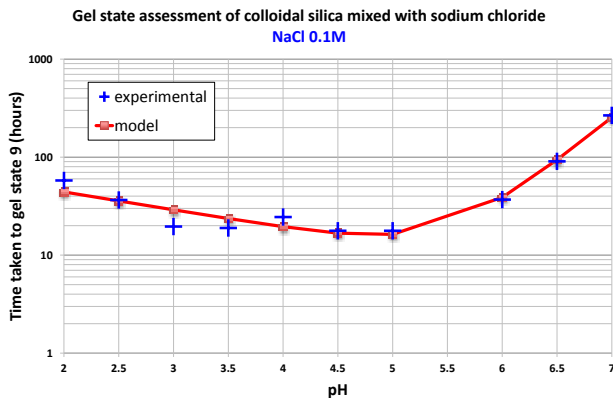


Figure 7 Model interpolations of experimental data

In figure 7 it is possible to see that the model was able to catch the non-monotonic behaviour of the gel time. The interpolation shows an average error of about 14% and a standard deviation of about 2 hours.

## Conclusion

A series of laboratory tests to explore the impact on gelling time as a result of accelerator concentration, ion valence and pH was showed. An electro-chemically inferred model to predict silica gel time was presented and validated with experimental results.

## Acknowledgements

This work was funded by a UK EPSRC research grant (EP/L0140441/1). The authors also thank Nick Atherton for the collaboration.

## References

1. Gallagher, P.M., S. Spatari, and J. Cucura, *Hybrid life cycle assessment comparison of colloidal silica and cement grouted soil barrier remediation technologies*. Journal of Hazardous Materials, 2013. 250: p. 421-430.
2. Noll, M.R., C.L. Bartlett, and T.M. Dochat. *In situ permeability reduction*

*and chemical fixation using colloidal silica*. in *Proceedings of the Sixth National Outdoor Action Conference*. 1992.

3. BASF, *Injection Solutions for Underground Construction*. 2013: Germany.
4. Iler, R.K., *The Chemistry of Silica: Solubility, Polymerization, Colloid and Surface Properties, and Biochemistry*. 1979: John Wiley & Sons.
5. BASF, *MasterRoc MP 320*. 2014: Zurich, Switzerland. p. 257-259.
6. Sydansk, R.D., *A Newly Developed Chromium(III) Gel Technology*. SPE, 1990: p. 346-352.
7. Persoff, P., et al., *Effect of dilution and contaminants on sand grouted with colloidal silica*. Journal of Geotechnical and Geoenvironmental Engineering, 1999. 125(6): p. 461-469.
8. Gallagher, P.M., *Passive Site Remediation for Mitigation of Liquefaction Risk*, in *Civil and Environmental Engineering*. 2000, Virginia Polytechnic Institute and State University.
9. Standards, A., *D4016 - Standard Test Method for Viscosity of Chemical Grouts by Brookfield Viscometer (Laboratory Method)* 2014. p. 11-13.